The University of Nottingham

UNITED KINGDOM · CHINA · MALAYSIA

Hijacking Bacterial Electron Transfer for Iron - Mediated Polymerisations

Mechelle Rebecca Bennett

M. Chem. (Hons)

School of Pharmacy

Divisions: Regenerative Medicine & Cellular Therapies,

Molecular Therapeutics & Formulation

Thesis submitted to The University of Nottingham for the degree of

Doctor of Philosophy, 12th February 2021

Regenerative Medicine & Cellular Therapies

MOLECULAR THERAPEUTICS & FORMULATION

BBSRC bioscience for the future

SynBio SBRC Nottingham a BBSRC/EPSRC Synthetic Biology Research Centre

“Data! Data! Data!” he cried impatiently. “I can’t make bricks without clay.”

Sherlock Holmes *(Arthur Conan Doyle: The Adventure of the Copper Beeches)*

~

“Equipped with his five senses, man explores the universe around him and calls the adventure Science.”

Edwin Powell Hubble

~

“We are mirrors whose brightness is wholly derived from the sun that shines upon us.”

C.S Lewis

Abstract

Polymer synthesis offers a plethora of methods and techniques to develop diverse and functional materials for a variety of applications. Reversible Deactivation Radical Polymerisation (RDRP) methods are the most versatile methods of which, Atom Transfer Radical Polymerisation (ATRP) and Reversible Addition Fragmentation chain-Transfer (RAFT) are highly promising for applications which require control over polymer structure, whilst sustaining mild reaction conditions. In the emerging areas of bioenergy harvesting and self-healing systems, methods to generate engineered living materials (ELM)s and hybrid synthetic/natural superstructures are being considered. These might have applications in microbial fuel cells (MFC), biological sensing, bioreactors, bioremediation, or as implantable synthetic microbiomes.

Cell mediated polymerisation reactions have been carried out to generate these hybrid superstructures, but most require conditions which affect cell metabolism, and the methods of biological redox initiation are not well understood. The research carried out in this thesis aims to utilise bacterial extracellular electron transfer (EET) systems to create novel hybrid bio-polymerisations, and to investigate the mechanisms by which they operate. The first chapter of this thesis examines ATRP and RAFT techniques that could be utilised for such experiments, and bacterial EET, quorum sensing (QS) and MFCs are discussed to provide context for the study. Prior literature surrounding biocatalysts and living materials

are reviewed and a proposal for each results chapter in this thesis is given.

In the second chapter of this thesis a novel Fe ATRP polymerisation technique initiated by living bacteria is presented. The method can be carried out whilst maintaining bacterial viability under biological conditions (room temperature (RT), 37 °C, phosphate buffered saline (PBS)), to produce polymers, whereas chemically killed bacteria are unable to initiate the polymerisation. Different parameters including bacteria concentration, catalyst concentration, bacteria type, initiator type, degree of polymerisation (DP) and monomer type are explored. The 'livingness' of the bacterial initiated Fe ATRP methods are shown to be somewhat compromised, likely due to biological interference with the Fe catalyst which is essential for maintaining polymerisation control. Although difficulty in molecular weight (M_n) control of the resulting polymers is displayed, the findings point towards a future platform technology for the manipulation of cells via a synthetic extracellular matrix (ECM) environment.

The third chapter of this thesis offers an alternative novel Fenton Glucose Oxidase - RAFT (FG-RAFT) technique that could be carried out in the presence of air without the need for prior degassing. This bacterial initiated polymerisation method introduces a less time-consuming and more economically viable technique than that of bacterial initiated Fe ATRP. Furthermore, the resulting polymers of FG-RAFT display lower dispersities ($Đ$ ~ 1.12) with somewhat predictable M_ns. The initial radical flux in these reactions is explored by altering component concentrations

(Glucose, GOx, $FeCl_3$), revealing that the catalyst concentration ($FeCl_3$) can be tailored to generate polymers with lower *Đ*s in the case of N-acryloylmorpholine (NAM), but in turn the M_n control is slightly compromised. The polymerisations can be carried out maintaining bacterial viability, whilst heat killed bacteria is shown to be unable to initiate the polymerisations, indicating the necessity of bacterial metabolism to the redox initiation. The quality of the resulting polymers are shown to differ depending on monomer type, with dimethylacrylamide (DMA) producing the most well-defined polymers, even with Fe concentrations as low as 7 µM.

The fourth chapter of this thesis investigates the Cytochrome C (C-Cyt) protein NapC of *E. coli* as an EET component in the reduction of Fe^{3+} by bacteria. Cloning techniques are used to upregulate the protein in *E. coli* of which the inducible promoter P_{BAD} is successful. Sodium dodecyl sulphate – polyacrylamide gel electrophoresis (SDS-PAGE) reveals greater NapC production for higher induced cultures. These are subsequently utilised in Fe ATRP polymerisations, showing higher reaction rates than those initiated by wild type cultures. Linear sweep voltammetry (LSV) is finally used to probe the Fe reduction capabilities of the clones, and although further research is necessary, the results suggest that Fe reduction is upregulated by the bacteria in times of environmental stress.

Overall, the development of 2 new synthetic polymerisation methods utilising bacterial redox chemistry as an initiation stimulus are presented, and cloning methods are used to investigate the involvement of NapC in

bacterial EET. The methods presented contribute to advances in the fields of hybrid biosynthetic technologies, improved EET knowledge and innovations to sustainable polymerisation chemistry.

Publications and Conferences

Papers accepted

- **Bennett, M. R**., Gurnani, P., Hill, P. J., Alexander, C., & Rawson, F. J. (2020). Iron-Catalysed Radical Polymerisation by Living Bacteria. *Angewandte Chemie (International ed. in English)*, *59*(12), 4750–4755. https://doi.org/10.1002/anie.201915084

Oral Presentations

- Nov 2019: 37th Australasian Polymer Symposium (37APS), sunshine Coast, Australia.
- Oct 2019: School of Pharmacy Postgraduate Seminar
- May 2018, RMCT Divisional Seminar
- Nov 2017, MTF Divisional Seminar

Poster Presentations

- 2019: EPSRC Biomaterials Discovery workshop
- 2018: Royal Society of Chemistry (RSC) Analytical Biosciences Group (ABG) – ***Award for Best Poster***
- 2018: School of Pharmacy Poster Day, ***Award for Best Poster***
- 2018: RSC Biomaterials – ***Award for Best Poster***
- 2017: Macro-group Young Researchers Meeting (YRM)

Acknowledgements

Firstly, I would like to thank my supervisors, Frankie Rawson, Cameron Alexander and Phil Hill, for their great support and guidance throughout my PhD. Thank you for inspiring me with enthusiasm throughout the project and always being available to give feedback and encouragement when I most needed it. I would also like to acknowledge the funding bodies; Engineering and Physical Sciences Research Council (EPSRC) (Grant numbers EP/R004072/1, EP/N03371X/1) and Biotechnology and Biological Sciences Research Council (BBSRC) (Grant number BB/L013940/1) for funding this project.

I would like to thank all members, past and present, of the Boots Science Building and CBS/BDI for their support and friendship throughout the years. Thank you also all those in the labs who were kind and helpful during my time here. I would like to thank Pratik Gurnani for his support, encouragement, and guidance through this project. Thank you to both Pratik and Cara Moloney for taking interest in this work and contributing to the final experiments during difficult COVID-19 times. Thank you also to Federico Turco and Francesco Catrambone for all your help with bacterial culture and molecular biology advice. I also want to thank Katalin Kovacs, Rajan Patel, Josh Gascoyne and Christian Arenas-Lopez for their assistance in the CBS labs and helping me with molecular biology techniques. A big thank you to Michaella Whittle and Maria Zygouropoulou for being amazing teachers of molecular cloning and showing me so much kindness and patience.

Thanks to Lucy Li, Akosua Anane-Adjei and Catherine Vasey and Andie Robinson for their encouragement in this battle together. Thanks to Jacqueline Hicks, Paola Sanjuanalberte, Harry Sherman, the rest of the Rawson group and the members of the Alexander group for their warm welcome and support during my studies, as well as all the CDT members for adopting me.

Thanks to Lorna and Abigail for being wonderful friends the past few years! Thank you to my amazing siblings, In-laws, nieces, and nephews who have been so supportive and helped me during times of need. Thank you to my partner Calum France for making me laugh in all the hard times and helping me through this PhD. I would also like to thank the Frances for adopting me into their home during the pandemic and being so supportive.

Last but by no means least, I would like to thank my incredible mother who gave me continuous encouragement and support to be able to complete this work. She has always taken an interest in my work and her curious mind has always inspired mine. I am so grateful to God for all the things I have been blessed to learn during this time, and for the wonderful support I have received.

Contents

List of Figures

CHAPTER 1

CHAPTER 2

CHAPTER 3

CHAPTER 4

CHAPTER 5

List of Tables

CHAPTER 2

CHAPTER 3

CHAPTER 4

Abbreviations

Abbreviation	Description
3-oxo-C12-AHL	N-(3-Oxododecanoyl)-l-homoserine
AC	Articular chondrocyte
ACAC	Acetylacetonate
AMPS	2-Acrylamido-2-methyl-1-propanesulfonic
ARGET/AGET	Activator (regenerated) electron transfer
AscA	Ascorbic acid
ATP	Adenosine triphosphate
ATRP	Atom transfer radical polymerisation
BCA	Bicinchoninic acid
b-FG-RAFT	Bacterial initiated FG-RAFT
Bpy	2, 2 – Bipyridine
BSA	Bovine serum albumin
C. met	*Cupriavidus metallidurans*
C. spor	*Clostridium sporogenes*
CCT	Catalytic chain transfer
C-Cyt	Cytochrome C
CE	Counter electrode
CFU	Colony forming unit
Cm	Chloramphenicol
CNT	Carbon nanotube
COE	Conjugated oligo-electrolyte
CRP	Controlled radical polymerisation
CSLM	Confocal scanning laser microscopy
CTA	Chain transfer agent
CTX	Cholera toxin
CV	Cyclic voltammetry
DG	D-glucose
DGA	D-glucanolactate
DHBP	2,3-dihydroxypropyl 2-bromo-2-methylpropanoate
DIRB	Dissimilatory Iron reducing bacteria
DMA	Dimethylacrylamide
DMAEMA	N,N-dimethylaminoethyl methacrylate
DMRB	Dissimilatory metal reducing bacteria
DNA	Deoxyribonucleic acid
DP	Degree of Polymerisation
DPBS	Dulbecco’s phosphate buffer saline
DSSN+	4,4’ – bis (4’ - (N,N-bis(6’-(N,N,N-trimethylammonium) - hexyl) amino) -styryl) stilbene tetraiodide
E. coli	*Escherichia coli*
EC	Endothelial cells

ECM	Extracellular matrix
EDGMA	Ethylene glycol dimethylacrylate
EDTA	Ethylenediaminetetraacetic acid
EET	Extracellular electron transfer
ELM	Engineered living material
EPM	Extracellular polymer matrix
EPS	Extracellular Polymeric substances
ET	Electron transfer
FG	Fenton Glucose Oxidase (GOx)
FG-RAFT	Fenton GOx-RAFT
FRP	Free radical polymerisation
GOx	Glucose Oxidase
HEA	Hydroxyethyl acrylate
HEBIB	2-hydroxyethyl 2-bromoisobutyrate
HEMA	Hydroxyethyl methacrylate
HPMA	2-hydroxypropyl methacrylate
HRP	Horseradish peroxidase
IPA	Isopropyl alcohol
KATRP	ATRP equilibrium constant
LAM	Less activated monomer
LB	Lysogeny broth
LSV	Linear sweep voltammetry
LTV	Laccase from Trametes versicolor
MA	Methacrylates
MAA	Methacrylamides
MAM	More activated monomer
MCS	Multiple cloning site
Me_3TREN	Tris(N-methyl-2-aminoethyl)amine
Me_6TREN	Tris(2-dimethylaminoethyl)amine
MEDSA	2-(Methacryloyloxy) ethyl dimethyl-(3-sulfopropyl) ammonium hydroxide
MES	Microbial Electrochemical system
MFC	Microbial fuel cell
MIC	Minimum inhibitory concentration
MIP	Molecularly imprinted polymer
MMA	Methyl methacrylate
MPC	2-methacryloyloxyethyl phosphorylcholine
MWCO	Molecular weight cut off
NAM	N-acryloylmorpholine
NHEA	N-Hydroxyethyl acrylamide
NIP	Non-imprinted polymer
NIPAM	N-isopropylacrylamide
NMP	Nitroxide mediated polymerisation
NMR	Nuclear magenetic resonance
NMR	Nuclear magenetic resonance
NVIm	N-vinylimidazole

OD_{600}	Optical density (600 nm)
OEOMA	Oligo(ethylene oxide) methyl ether methacrylate
OMRP	Organometallic mediated radical polymerisation
P_{BAD}	Arabinose-inducible promoter
PBS	Phosphate buffered saline
PCR	Polymerase chain reaction
PDm	Polydopamine
PEG	Polyethylene glycol
PEGA	Polyethylene glycol acrylate
PEGMA	Poly(ethylene glycol) methyl ether methacrylate
PEM	Proton exchange membrane
PET	Photo-induced electron
PI	Propidium iodide
PISA	Polymerisation induced self-assembly
PMF	Poly(MPC-co-VF)
P_{Nat}	Native promoter
PNVIm	Poly(NVIm)
Ppy	Polypyrrole
PRE	Persistent radical effect
PSBEDOT	Poly(sulfobetaine-3,4-ethylenedioxythiophene)
Py	Pyrrole
QS	Quorum sensing
RAFT	Reversible activation chain transfer
RDRP	Reversible deactivation radical polymerisation
RE	Restriction enzyme
RI	Refractive index
ROS	Reactive oxygen species
RS	Restriction site
RT	Room temperature
SDS-PAGE	Sodium dodecyl sulphate – polyacrylamide gel electrophoresis
SEC	Size exclusion chromatography
SI	Surface initiated
SMA	Sodium methacrylate
STP	Strongly templated polymers
TAE	Tris acetate EDTA
TDA-1	Tris[2-(2-methoxyethoxy)ethyl]amine
THS	Thermosome
tPMET	Trans plasma membrane electron transport
TPP	Triphenylphosphine
UV	Ultraviolet
VF	Vinyl ferrocene
WE	Working electrode
WTP	Weakly templated polymers

Chapter 1. Exploring the Combination of Redox Controlled Polymer Techniques with Biological Systems

Introduction

The combination of synthetic polymer chemistries with biological components offers possibilities to make new bio-catalysts,[1-3] hybrid 'living materials',[4] cell surface modifiers,[5] cell binding agents,[6, 7] and opportunities to contribute better to probiotics,[8] engineered metabolic products,[9] microbial fuel cells (MFC)s,[10, 11] and conducting materials.[12, 13] Atom Transfer Radical Polymerisation (ATRP) and Reversible Addition-Fragmentation Chain Transfer (RAFT) polymerisations provide tools for creating a range of synthetic materials whilst controlling their architecture, composition, chemical and physical properties, making them highly attractive for a range of applications.[14-16] Combining such techniques with biological processes may enable new biomedical materials to be prepared, and also to help understand more regarding important electron transfer processes in biology.

Various groups have sought to develop engineered living materials (ELM)s as hybrid 'bio-machines',[4] and the use of whole living cells to initiate polymer synthesis via electron transfer has recently been reported.[13, 17-21] However, the complex bio-electrochemical processes that exist in biology vary widely across different organisms and the way that these systems interact with abiotic chemistries is not fully understood. The purpose of this thesis is to explore reversible deactivation radical polymerisation (RDRP) reactions and how they might interface with bacterial redox systems. The generation of synthetic polymer materials via bacterial redox chemistries is largely novel and so

the work in this thesis explores various optimisation processes for bacterial-mediated polymer synthesis. Overall, this work aims to expand the scope of RDRP chemistries with a range of microorganisms and to explore the biological mechanisms underlying the polymerisations.

Polymer Synthesis

Polymeric materials and the diverse range of applications they may deliver are crucially important for the development and sustainability of today's world.[22] Polymers are appealing for use in many academic and industrial sectors due to the range of synthetic methods available, the wide variety of possible structures and ability to alter the functionalities of the resulting materials.[23, 24] Controlled radical polymerisation (CRP) or Reversible Deactivation Radical Polymerisation (RDRP) is one of the most used polymer synthesis techniques in academic laboratories due to its ability to create well defined polymers of complex architectures and functionalities.[25] These polymerisation methods have facilitated the preparation of complex materials for use in areas such as drug delivery, regenerative medicine, diagnostic sensors and anti-infectives.[26, 27]

RDRP is a widespread method for the regulation of radical polymerisation reactions, providing well defined polymers (Dispersity Index ($Đ$) <1.2) of targeted molecular weights (M_n).[28-30] Such RDRP methods include ATRP, RAFT polymerisation and Nitroxide Mediated Polymerisation (NMP). The success of RDRP methods can be attributed to the fast and dynamic equilibrium present between reactive propagating polymer species and dormant species, in which a shift towards the latter prevents termination reactions.[28]

1.1.1 Atom Transfer Radical Polymerisation (ATRP)

The reaction now described as ATRP was first reported in 1995,[31] and can be applied to a wide variety of monomers. ATRP is tolerant to many functional groups and can be performed both in polar and aqueous solvents.[29, 32, 33] This versatility provides the means to carry out reactions under a range of conditions, with tailored polymer properties or functionalities and makes ATRP a great contender towards a variety of applications, particularly drug delivery, tissue engineering and diagnostics.[16, 34, 35] ATRP relies on the persistent radical effect (PRE) to generate growing polymer chains (P*) in a controlled and effective manner.[36] In this way, the total concentration of P* ([P*]) is minimised by abstracting a halogen (X) from a metal catalyst (Mt-X) to become temporarily dormant species (P-X). By lowering the [P*] present at one time, this process reduces the rate of radical termination (R_t) which is proportional to $[P^*]^2$. ATRP has become one of the most effective and widely used RDRPs, with commercially available initiators and a variety of accessible catalysts.

The redox chemistry of the transition metal catalyst (commonly Cu, Ru, Fe, Mo, Os) is exploited in a halide exchange reaction to form an equilibrium between active and dormant polymer chains (Figure 1. 1).[25, 28, 34] Initiation takes place by the reaction between an active alkyl halide initiator (R-X) and the catalyst in its' lower oxidation state (Figure 1. 2, i) The radicals formed can attack monomer units (Figure 1. 2, ii) to become propagating radical species (P*). These continue to grow into polymer chains (Figure 1. 2, iii) with a rate of propagation (k_p) dependent on

deactivation efficiency (k_{deac}) of the metal catalyst and the position of the ATRP equilibrium (K_{ATRP}). The radical reaction is controlled by this fast and dynamic equilibrium between a low concentration of growing radical species (P*) and a large concentration of dormant species (P_n-X) which are temporarily deactivated by halide X (Figure 1. 1).

K_{ATRP} can be influenced by various components, including ligand type, solvent, monomer, and metal.[37] It is defined as the rate of activation (k_{act}) divided by k_{deact} of growing polymer chains (Figure 1. 1). For a polymerisation to remain 'controlled,' radicals must be efficiently deactivated by the higher oxidation state metal (X-Mt^{n+1}/L), with k_{deact} >> k_{act}. This influences K_{ATRP} to shift to the left (K_{ATRP} <<1), minimising the propagating radical species in the system and thereby reducing the rate of radical-radical termination or side reactions. Radical termination events irreversibly stop the growth of a polymer chain which is referred to as 'dead'. Examples include termination by radical coupling (Figure 1. 2, iv) and termination by the simultaneous reduction and oxidation of two radicals, disproportionation (Figure 1. 2, v).

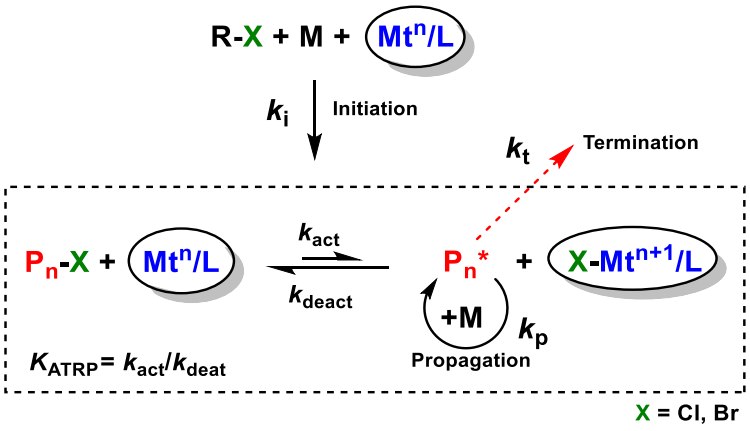

Figure 1. 1 Conventional ATRP Equilibrium Reaction Between Dormant Halogen Capped Polymer Species (Left) and Propagating Radical Species (Right).

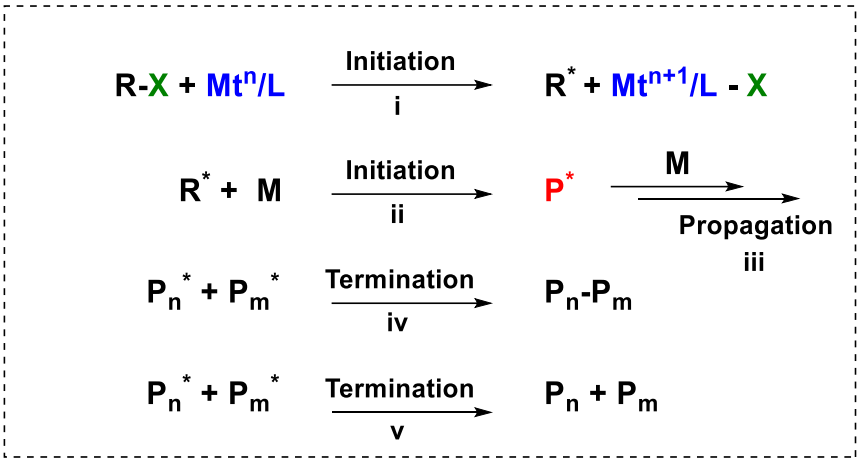

Figure 1. 2 Mechanisms of ATRP. Initiation (i and ii); Propagation (ii); Termination by Radical Coupling (iv) and Termination by Disproportionation (v).

1.1.1.1 Aqueous ATRP

Aqueous environments are crucial in most biomedical applications, [35, 37] making ATRP in aqueous solvents a requirement to explore for our biological systems. Challenges arise in aqueous solvent systems because K_{ATRP} increases with the polarity of the solvent, leading to an increase in activated propagating radicals and an increased likelihood of termination events.[29, 38] During which, the speed of the polymerisation (k_{act}) is increased, causing the concentration of deactivated polymer chains (X-Mt^{n+1}/L) to be lowered due to the equilibrium shift, which results in a less controlled reaction.[25, 29] These systems may also suffer from; i) partial dissociation of the halide from the deactivator complex (X-Mt^{n+1}/L) and subsequent replacement with water ligands, causing further loss of control,[39] ii) binding of hydrophilic monomer and polymer groups to the catalyst, leading to inefficient deactivation of propagating radical chains (P_n*) and increased radical-radical termination events,[40, 41] iii) disproportionation of the metal, resulting in catalyst dissociation.[29]

The addition of excess halide salts in aqueous ATRP environments have been shown to increase the degree of control by suppressing the loss of halide ligand from the deactivator, $X\text{-}Mt^{n+1}/L$.[39] Another important feature of ATRP is that the reagent mixture should be homogeneous to maintain the availability of reactive centres.[28] This means that when conducting aqueous ATRP reagents with sufficient water solubility must be used for optimum results, and reactions should be carried out with continuous stirring.

1.1.1.2 Iron Catalysed ATRP

The activity of most commonly used Cu catalysts in ATRP has been enhanced considerably due to the discovery of complexes with extremely high K_{ATRP}.[42] However, Cu catalysts are difficult to remove from reactions and concerns still arise surrounding the toxicity residual copper especially when used in biomedical applications.[34, 43-45] Fe is an attractive alternative to Cu due to its abundance in the earth's crust, low cost and ease of removal from reactions.[46] Like, Cu, Fe is a cofactor in many metalloproteins that catalyse biological functions, making it an interesting and important contender as an ATRP catalyst, particularly towards biomedical applications.[47, 48]

Research surrounding Fe ATRP has become of interest and numerous literature exists for organic solvent synthesis, including ATRP with ligands based on nitrogen, phosphines, carbonyl complexes, onium salts, solvents and porphyrins.[46, 49-51] For example, Gibson and O'Reilly *et al* showed that the donor capacity of tridentate nitrogen donor ligands

in 5 coordinate Fe catalyst complexes correlated with the corresponding redox potentials.[52] They showed that modifying the ligand can have a dramatic effect on the redox potential and the ATRP reaction kinetics.

The mechanistic paths of ATRP have also been explored, for example, Shaver *et al* studied the mechanistic interplay between catalytic chain transfer (CCT) organometallic radical polymerisation (OMRP) and ATRP (Figure 1.3). The polymers resulting from CCT are vinyl products and so a CCT mechanism can be easily inferred from ^{1}H NMR analysis of the resulting polymers.[53] The reaction mechanisms of ATRP or OMP seem to be more difficult to decipher in a polymerisation because the resulting polymers have the same structures. It is likely that these exist in parallel as theoretical models suggest the mechanism is influenced by solvent, pressure and the spin state of the catalyst (Figure 1.4).[54]

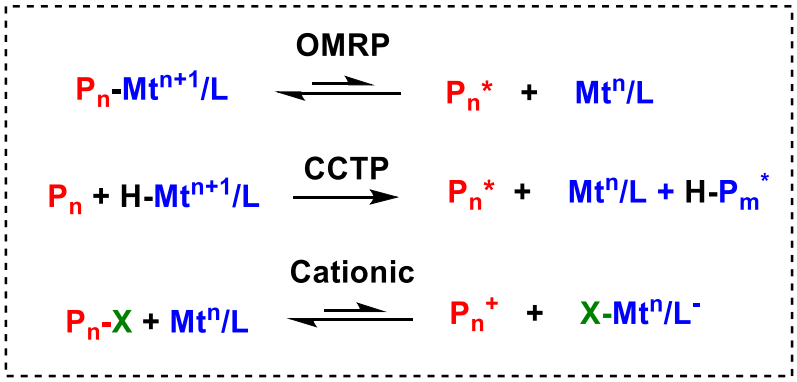

Figure 1. 3 Various pathways for Fe catalysed polymerisations.

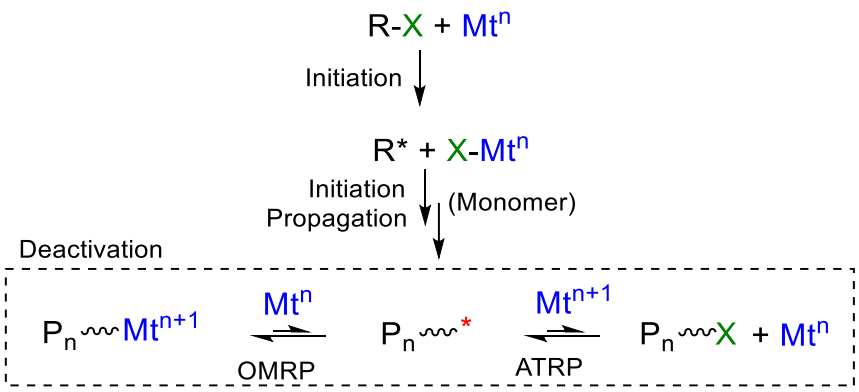

Figure 1. 4 Organometallic radical polymerisation (OMRP) and Atom transfer radical polymerisation (ATRP) mechanism pathways.

An ideal ATRP catalyst would facilitate the formation of polymers with low *Đ*s of targeted molecular weights, and good chain end fidelity. These well controlled reactions are often catalysed by metals with low standard redox potentials and high halidophilicity.[55] Coordinated ligands are employed to solubilise the metal, but also directly affect the catalyst activity due to withdrawal or donation of electron density. The activity of the catalyst strongly influences the position of the equilibrium and can be correlated to the standard reduction potential ($E_{1/2}$).[25] The more negative the $E_{1/2}$, for the higher oxidation state catalyst, the more reducing the complex, increasing K_{ATRP}.

In general, a more reducing complex will be more active for ATRP as the electron density is concentrated largely on the metal, and so the donation of an electron (k_{act}) is easier. For example, several 1,4,8,11-tetraazacyclotetradecane (Me_4cylam) derivatives were shown to give highly negative redox potentials and fast polymerisation reactions, however, poor control was obtained due to insufficient deactivation by the Cu(II)X_2/Me_4Cylam complex.[56] This indicates that whilst high

activation is necessary, a balance is required for control to be maintained in the reaction.

Most Fe ATRP catalysts are only well studied in organic solvents and for limited monomers (styrene (St) and methyl methacrylate (MMA)). Indeed, during photo-initiated Fe ATRP of MMA in anisole, Anastasaki *et al* revealed that the Fe catalyst concentration had a direct effect on the dispersity of resulting polymers.[57] However, most of the ligands studied in such organic solvents (e.g. carbenes) are incompatible with water and so they cannot be applied to aqueous environments. Whilst other ligands require elevated temperatures to overcome high activation barriers, which is not ideal for biological environments.[46, 58, 59] Phosphine ligands, such as triphenylphosphine (TTP) and substituted TPPs,[60-64] have shown some promise towards Fe ATRP in aqueous conditions.[65] These types of ligands spontaneously reduce Fe^{3+} catalysts to the active Fe^{2+} catalyst without the presence of additional species.[66] The use of phosphine ligands in our studies would therefore complicate the future bacterial studies in which Fe^{3+} reduction by bacterial redox mechanisms is to be inspected. The bacterial reduction of the Fe could be carried out directly by surface proteins or by mediator molecules released by the bacteria. For this reason, we have chosen highly complexing, commercially available nitrogen and oxygen donor ligands which are less likely to interfere with the Fe reduction.

1.1.1.3 Activator Regenerated Electron Transfer (ARGET) ATRP

Conventional ATRP is air sensitive and requires a complex set up to prevent oxygen contamination or catalyst oxidation.[41] To overcome this problem, the ARGET ATRP method was developed, using a redox process to produce the active catalyst *in situ* (Figure 1.5).[67] Although ARGET ATRP was first reported for Cu catalysts which enabled lower catalyst concentrations to be used, studies have also extended to Fe catalyst systems. In these reactions, air stable metal Fe^{3+}/L is reduced *in situ*, forming the active catalyst Fe^{2+}/L which instigates the initiation of the system. Newly generated active catalyst Fe^{2+}/L and alkyl halide (R-X) react to generate the initiating radical species (R*) which can initiate and grow monomer units (M) into propagating polymer chains (P*). The ATRP equilibrium proceeds as usual but the reaction is more tolerant to O_2 contamination due to the presence of the reducing agent which acts as a radical scavenger. Existing literature concerning ARGET ATRP is limited to hydrophobic monomers like styrene (St) and methyl methacrylate (MMA), and most reactions are carried out in bulk or organic solvents.[63, 68-72] To further improve the biocompatibility of Fe ATRP, several groups have expanded research to ARGET ATRP in aqueous solutions,[73-75] but the literature is not extensive. A better understanding of aqueous Fe ATRP systems with different ligands is needed.

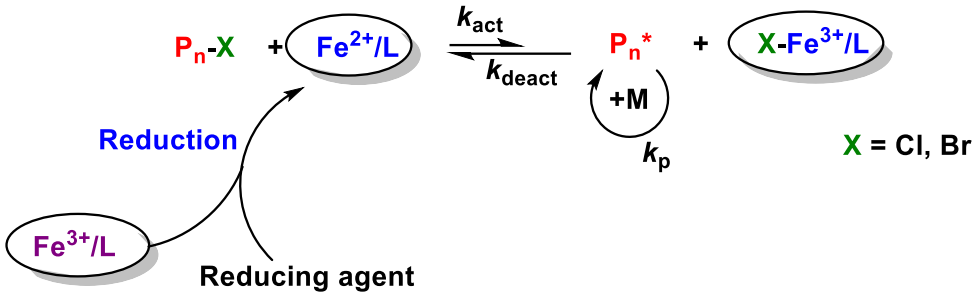

Figure 1. 5 ARGET ATRP of Fe^{2+} and Fe^{3+} Redox Couple.

Additionally, the application of Fe ARGET ATRP to biology, i.e., bacterial initiation of the system, requires modification to the standard set up and reaction conditions. For example, using water as the solvent may cause an osmotic shock to bacterial cells causing unwanted cell death, and some ATRP reagents may also be toxic to the cells. Together with other biological polymerisation systems (Section Reversible Addition Fragmentation Chain -Transfer (RAFT) Polymerisation), this thesis strives to enhance the knowledge in the research area towards synergistic biological-polymer systems.

1.1.2 Reversible Addition Fragmentation Chain - Transfer (RAFT) Polymerisation

Reversible Addition-Fragmentation Chain transfer (RAFT) polymerisation was first reported in 1998,[76] and since then over 8000 RAFT papers have been published.[77] RAFT, like ATRP, is a form of RDRP (or CRP) and is a great tool for creating polymers with predictable molecular weights, low dispersity and high-end fidelity. RAFT polymerisation can be used to create polymers of different architectures including and characteristics including block, star, branched, hyperbranched, grafted to/from, and stimuli-responsive polymers.[78-80] The versatility of RAFT has encouraged its use in several medical and biological applications,[15, 81-83] and has inspired us to investigate its compatibility with bacterial redox systems.

The mechanism by which RAFT polymerisation takes place relies on degenerative chain transfer.[84] The initiation of the RAFT process requires an external radical stimuli, such as thermal, redox or light.[85-88] The generated initiating radicals (I·) can then react with monomer species to form a growing polymer chain (P_n·) with *n* monomer units (Figure 1. 6). To control the reaction and prevent termination events, a chain transfer agent (CTA) or RAFT agent is used - often in the form of a tri-thiocarbonate group. The growing polymer chain reversibly reacts with the sulphur group in a pre-equilibrium step, whereby the radical is stabilised by the CTA and a re-initiating molecule (R·) is formed. This molecule can react with monomer units to form another growing polymer chain (P_m·) in the main equilibrium. During this process, polymer chains

(P_n and P_n) are in equilibrium between active and dormant states, allowing uniform chain growth.[77]

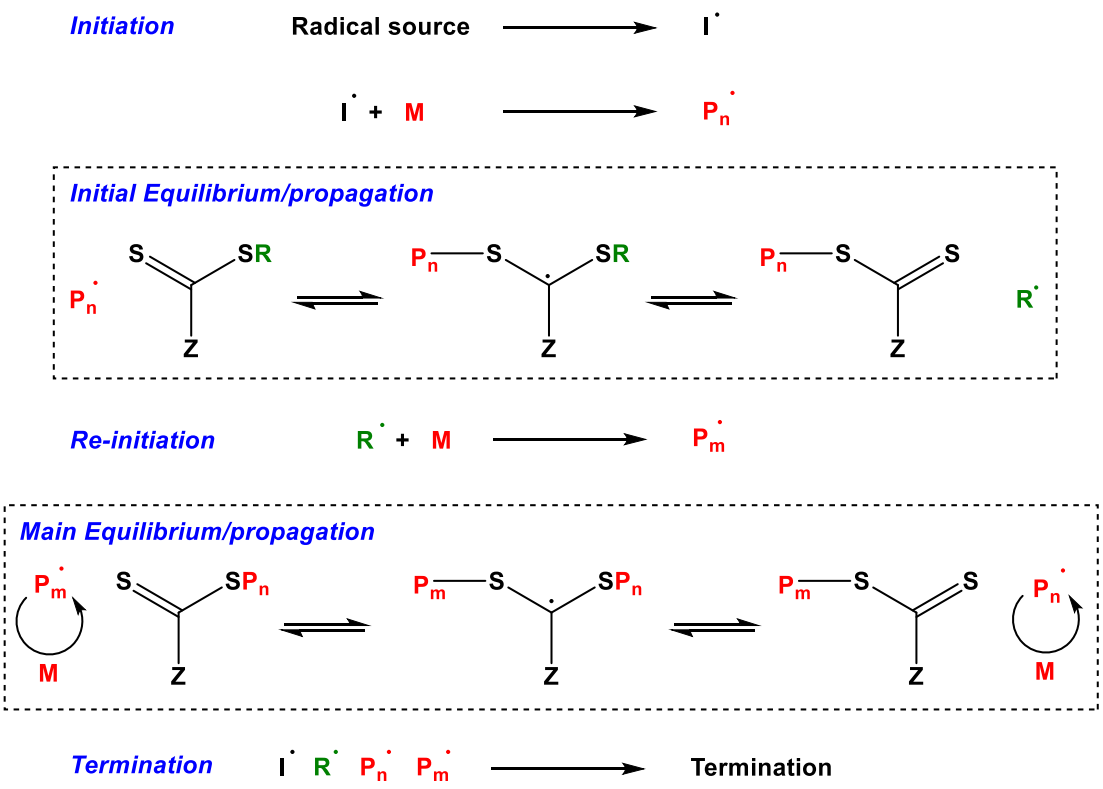

Figure 1. 6 RAFT Polymerisation schematic mechanism including Initiation, propagation and termination events.

1.1.2.1 Monomer Types & CTAs

Living polymerisations are achieved by suitably selecting CTAs with certain Z and R groups according to the monomer (Figure 1. 7). The C=S bond of the CTA must be more reactive to radical addition than the C=C bond of the monomer to encourage the RAFT equilibrium to take place. Monomers are classed as either More Activated Monomers (MAMs) or Less Activated Monomers (LAMs) depending on their reactivity which is defined by their structure and the substituents attached. MAMs contain a

vinyl bond joined by a single bond to another double bond, aromatic ring, a carbonyl group or a nitrile group (e.g., butadiene, St, methacrylates (MA) and methacrylamides (MAA)). LAMs on the other hand contain a vinyl bond joined by a single bond to an electron withdrawing group (O, N, halogen, or S with a lone pair) for example, vinyl acetate, N-vinylpyrrolidone and vinyl chloride.[77, 89]

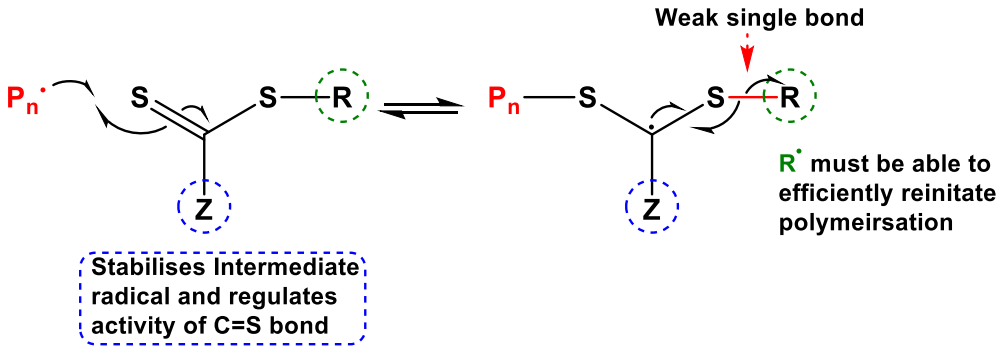

Figure 1. 7 CTA structure showing roles of R and Z groups. Modified from reference.[90]

The Z group of the CTA helps to control the reactivity of the C=S group. MAMs form stabilised propagating radicals ($P_n\cdot$) due to the electron withdrawing groups of their substituents that are not very reactive. This means that the Z group of the CTA will need to stabilise the radical intermediate (P_n-CTA·) to encourage radical addition. In such cases, trithiocarbonates (Z = S-alkyl) and dithiobenzoates (Z = Ph) are typically used.[77] Conversely, LAMs form reactive propagating radicals ($P_n\cdot$) which, once in the (P_n-CTA·) intermediate, makes homolytic cleavage of the P_n group difficult. In this case, a Z group which destabilises the C=S bond is required to make the intermediate radical less stable and encourage fragmentation. Xanthates (Z = O-alkyl) or

dithiocarbamates (Z = *N*-alkyl) can destabilise the C=S bond by delocalisation of the lone pair of O or N respectively.[77] It is also important to mention the R group of the CTA. In the pre-equilibrium stage of the RAFT polymerisation, a balance must be achieved for the R group to be a good leaving group but its radical must be unstable enough to re-initiate monomer chains. Factors such as sterical and electron withdrawing substituents can influence the radical stability of the R group.[81]

The advantage of RAFT polymerisation over other RDRP techniques is that it does not require high temperatures, like NMP, or catalysts that can be sensitive to solvents, like ATRP. Indeed, RAFT can be performed in a variety of solvents, is tolerant to a wide variety of functionalities and can be used to generate many different architectures, which are important in various bio-applications (e.g. drug delivery, nucleic acid delivery, diagnostics, tissue engineering, surface modification).[14, 15, 80-82, 91, 92] Enzyme mediated RAFT polymerisations are particularly useful (Section 1.4.1) as they can be conducted in air, overcoming a challenge to traditional RDRP methods.[92] Furthermore, RAFT polymerisation initiated by the Fenton reaction (Fenton RAFT) provide very fast polymerisation rates with an inexpensive initiating system to generate well defined polymers in benign reaction conditions (RT, H_2O) within minutes.[93-95]

Glucose Oxidase (GOx) is a commercially available enzyme, naturally produced by some fungi and insects. It has relatively high stability and used widely for improving the shelf life of many materials in the food industry, as well as in glucose biosensors.[96] Iwata and co-

workers showed that a cascade reaction combining GOx catalysis of glucose, to produce hydrogen peroxide radicals (H_2O_2), with Fenton RAFT polymerisation (Figure 1. 8) was possible at 37°C in the presence of air (O_2) - but in the absence of O_2 or Fe^{2+} ions there was no polymerisation. The lack of stability toward air is a major drawback to most RDRP methods, so GOx-RAFT is highly attractive, particularly for biocompatible applications. In fact, this method was applied to balloon catheters which were used to treat aneurysms in a clinical setting.[97]

In recent years Reyhani *et al* have exploited the use of Fe^{2+} in haemoglobin (Hb) of Red Blood Cells for Fenton RAFT polymerisations,[98] and others have investigated applications towards hydrogels and nanogel formation.[95, 99] This thesis (Chapter 3) will explore the use of Fenton GOx RAFT (FG-RAFT) reactions in combination with cell-redox behaviour for the synthesis of polymers.

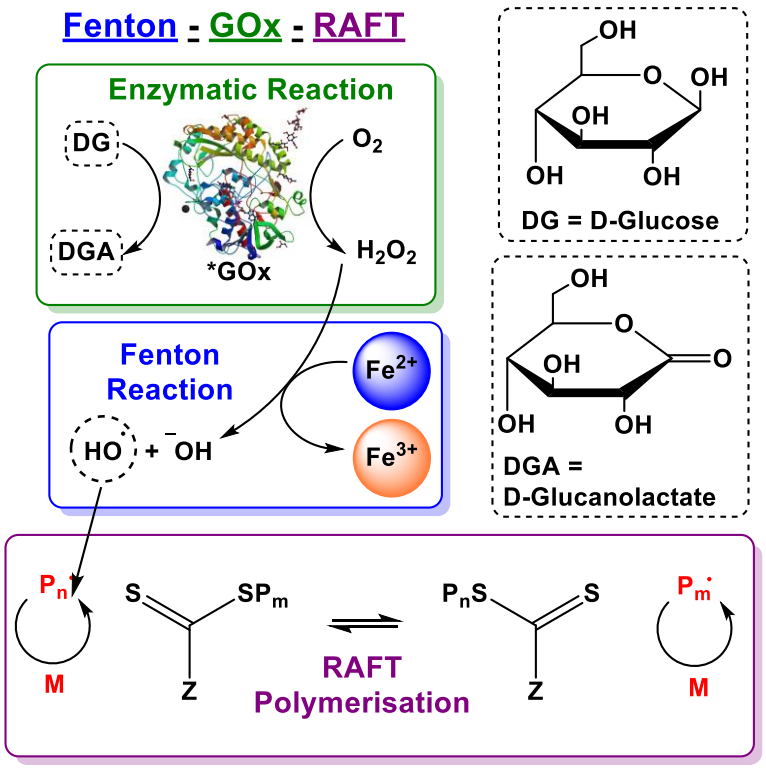

Figure 1. 8 Fenton GOx RAFT reaction scheme modified from literature.[95] *GOx protein image from PBD ID: 3QVP.A.[100]

Bacterial Extracellular Electron Transfer

As discussed, both ATRP and RAFT involve electron transfer radical reactions and can be initiated or controlled by redox processes.[68, 101] Redox reactions are highly abundant in nature and control some of life's most complex reactions.[102, 103] In these, metal containing proteins are often exploited,[104] particularly for respiration and homeostasis, and many of these proteins contain Fe complexes.[105-110] Extracellular electron transfer (EET) is a process by which microorganisms transport electrons from the cytosol to an external substrate, or vice versa, harvesting energy (via ATP) in the process.[111] Mechanisms of EET for anaerobic respiration in bacteria can be facilitated directly by cytochrome C-type redox proteins, extracellular polymeric substances or indirectly by chelating shuttle molecules.[112, 113] [111, 114]

The use of these biologically driven reactions in polymer chemistry might enable faster, more sustainable, dynamic applications whilst shedding insight into important redox mechanisms of biology as shown by several authors.[13, 115-119] Despite some remarkable research, more insights into the synergy between biotic and abiotic systems are required, and new techniques are needed to progress the field. Before exploiting bacterial EET for radical polymerisations, it was first important to understand bacterial EET mechanisms and to review their significance towards current applications, such as biosensors and MFCs.

1.1.3 Exoelectrogenic Bacteria

Exoelectrogenic bacteria are organisms that anaerobically employ EET to capture, store and release energy in the absence of molecular oxygen (O_2). Bacteria of this type can utilise EET to reduce metals (E.g. Fe^{3+}, Co^{3+}, Cr^{6+} Mn^{4+}, U^{6+}) that are often insoluble and would otherwise be inaccessible.[113, 120, 121] Metal reduction by microorganisms is coupled to oxidation of organic compounds (e.g. formate, acetate, volatile fatty acids) and H_2, and has contributed greatly to biogeochemical cycling in the environment for millions of years. These dissimilatory metal reducing bacteria (DMRB) are typically found in aquatic sediments, submerged oils and the terrestrial subsurface.[122-124] DMRB can be both Gram positive (*Thermincola potens*, *Bacillus subtilis*, *Enterococcus faecalis, Listeria monocytogenes*)[125-128] and Gram negative (*Shewanella oneinesis* and *Geobacter sulffureduens)*[129] but also extend to archaea.[130] These microorganisms have evolved mechanisms to transport electrons between the cytoplasmic membrane of the cell and extracellular minerals, for respiration or redox homeostasis.[131] Exoelectrogens can connect these intracellular biocatalytic pathways to redox reactions on an electrode surface, creating a microbial electrochemical system (MES). Decades of electromicrobiological research contribute to applications such as MFC bioelectricity generation, bioremediation, microbial electrosynthesis, biosensing and biocomputing.[112, 129, 132, 133]

Although EET mechanisms of DMRB can be complex and difficult to identify, research shows that outer membrane C-type cytochromes (C-Cyts) play a vital role in the reduction of metals.[112, 134-136] These

cytochromes are a family of heme-containing electron transfer proteins that often catalyse chemical reactions via EET mechanisms.[134, 137, 138] The most well characterised EET pathway is the Mtr pathway of *S. oneidenisis* MR-1, a type of dissimilatory iron reducing bacteria (DIRB). The Mtr pathway is a collection of genes encoding cytochromes involved in extracellular electron transfer (Figure 1.9). DIRB anaerobically conserve energy for metabolism, respiration, and cell growth, using the world's fourth most abundant element, Fe^{3+} (often in the form of crystalline or amorphous iron oxides). The Mtr pathway consists of proteins; CymA, Fcc_3 (also known as FccA), STC (small tetrahaem cytochrome), MtrA-C and OmcA (Figure 1.9).[113, 136, 139] CymA (a member of the NapC/NirT family) is a membrane bound tetraheme C-Cyt which oxidizes quinol in the cytoplasmic membrane and releases the electrons to Fcc_3 and STC.[140-142] Electrons are relayed to the protein complex MtrA MtrB and MtrC where they are shuttled across the outer membrane. On the surface of the bacteria MtrC and OmcA facilitate the transfer of electrons to or from the extracellular substrate by a mixture of mechanisms; i) directly, ii) by flavin mediators and iii) through conductive pili.[113, 136, 143-145]

Many Gram-negative bacteria express pili which are fibrous polymer organelles existing on the cell surface that can mediate cell attachment, DNA exchange, movement, and substrate transport. There are several types of pili classed by their assembly pathways. Nanowires or 'e' pili are conductive and found in many types of *Shewanella* and *Geobacter* bacteria, but also other organisms.[145-147] These bacteria have been

shown to contain outer membrane C-Cyts on the pili extensions and were first assumed to carry out EET by via multistep hopping or tunnelling (Eg. Figure 1. 9, iii).[143] Obstacles in relating pili structure to electric conductivity has, however, caused much debate over the exact mechanism of EET via pili.[148, 149 136, 143] Molecular dynamics simulations have suggested that π-π interactions of electronically functional proteins on the pili may be more likely than C-Cyts, but much more research is needed for full elucidation.[150]

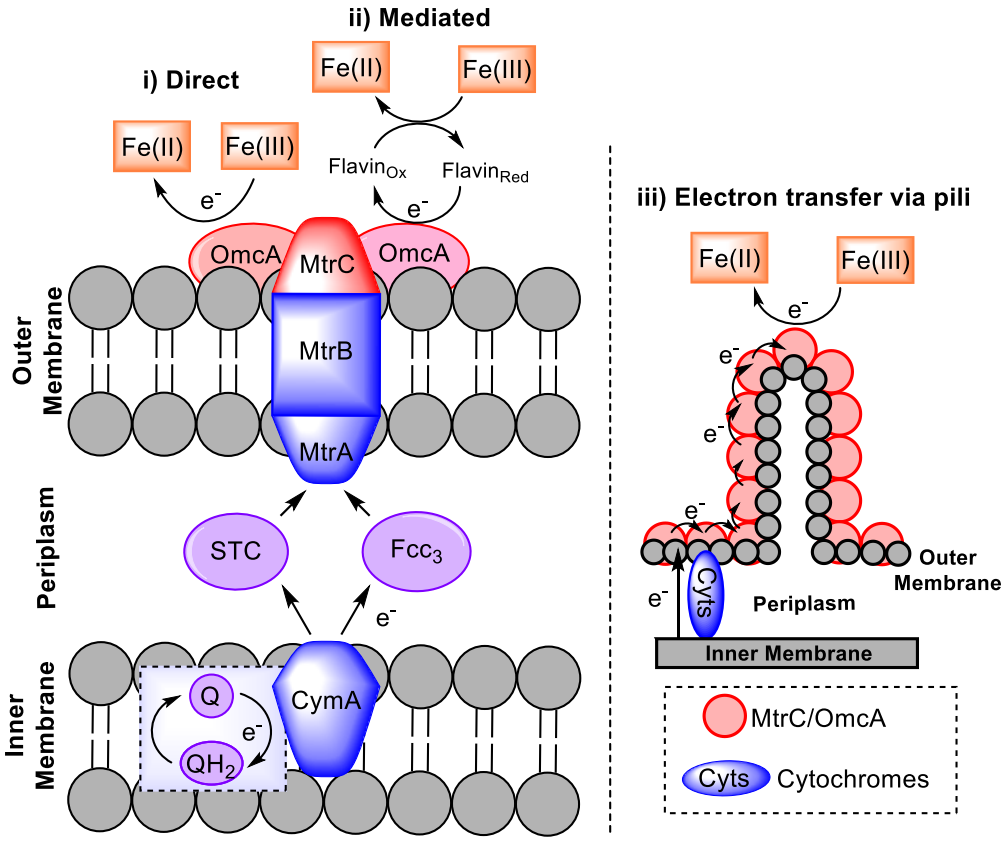

Figure 1. 9. Representation from gathered references of the Mtr pathway of Shewanella Oneidensis involving EET to electron acceptor Fe(III) via i) direct Cyt contact, ii) Mediated transport and iii) pili assisted transport.[136, 142, 145]

As well as these proposed mechanisms there may be many other ways by which bacteria use metals for respiration. Furthermore, all bacteria utilise metal homeostasis to prevent toxicity or to accumulate essential metals for storage or energy production, e.g. siderophores.[109] Although many mechanisms may exist in parallel, it was hypothesised in this thesis that a variety of bacteria types should be able to catalyse the reduction of Fe catalysts in Fe ATRP reactions or FG-RAFT reactions to initiate polymerisations.

Combining bacterial EET redox systems with these polymerisation techniques could expose new capabilities towards bacterial instructed polymerisations (discussed later) for molecularly imprinted polymers (MIP)s, MFCs, cell manipulation and tissue regeneration. For example, MIPs have been utilised for chemical and biological sensing and they mimic the ‘key and lock’ system in nature for molecular recognition. Bacterial mediated polymer synthesis might enable an *in vivo* approach to MIPs, whereby MIPs formed around bacteria could be used for bacterial diagnostics, or for anode materials to improve MFC efficiency through better adsorption of the bacteria to an anode and faster EET.[6, 151 7]

1.1.4 Bacterial Biofilms and Quorum Sensing

Bacteria often aggregate into complex and dynamic biofilms containing extracellular polymeric substances (EPS) vital for intracellular interactions, resource capture, gene exchange and antimicrobial tolerance.[152] The EPS matrix comprises proteins, glycoproteins and extracellular DNA.[153] These organised electroactive microbial communities contribute to EET, sometimes aided by pili entangled in the biofilms.[149] A biofilm also protects microorganisms from UV radiation, extreme temperatures or pH, pressure/force and antibiotics.[154] Research concerning biofilm formation applies to a variety of applications,[155] including areas of food safety,[156] medical safety (e.g. catheters),[157] anti-biofouling,[158-160] bioremediation, fermentation, wastewater treatment[161] and MFCs.[11, 129, 132, 162] For this reason there have been extensive studies surrounding biofilm development, of which findings show that biofilm composition, organism type(s) and the surrounding environment greatly influence the resulting properties, integrity and survival of the biofilm.[161, 163, 164]

Changes in cell density, species composition, or nutrient availability in a biofilm are closely monitored by quorum sensing (QS). QS is a process in which bacteria extracellularly release QS molecules, sometimes known as auto-inducers. Thereafter, the bacteria monitor QS molecule accumulation during specific stages of growth or environmental

changes to regulate the expression of genes and synchronise the behaviour of the whole bacterial population.[165] These QS mechanisms can control processes such as bioluminescence, sporulation, antibiotic resistance, biofilm formation and virulence.[110, 166] Biofilm formation causes huge challenges to treating infectious diseases, particularly since the emergence of antibiotic resistance.[167] As opposed to an individual planktonic state, bacteria in a biofilm show increased tolerance to the antibiotics in the maturation stage, which can arise due to incomplete diffusion of antibiotics to the inner layers of the biofilm, and the release of antibiotic-neutralising enzymes in the biofilm.[168, 169] To interfere with bacterial adhesion and prevent unwanted biofilm formation and subsequent infection, polymer materials have been used to induce antifouling or antimicrobial properties, bacterial sequestration, or to disrupt QS signals.[12, 158, 160, 170-174]

Antifouling polymers can be hydrophilic (e.g., Polyethylene glycol (PEG) derivatives) or zwitterionic (e.g., Betaine derivatives), which resist adsorption of biomolecules, cells, and microorganisms. When these polymers are exposed to an aqueous solution a hydration layer forms on the surface, where the water molecules strongly interact with hydrophilic or zwitterionic polymers, via hydrogen bonding or ionic bonds, respectively.[175] This hydration layer prevents interactions between biomolecules and the polymer surface, reducing fouling for various engineering and biomedical applications.[12, 160, 171, 175] Antifouling polymers used in healthcare applications are extremely important as biomedical devices are inherently exposed to *in vivo* environments and

are likely to malfunction or cause bacterial infection if biofilm accumulation occurs on implanted devices.[160] The prevention of fouling for glucose sensors, for example, was investigated by Wu *et al*. Zwitterionic betaine polymer, poly(sulfobetaine-3,4-ethylenedioxythiophene) (PSBEDOT) polymers were synthesised in the presence of GOx enzyme to create an antifouling, conductive glucose biosensor. Strong hydration of the zwitterionic side chains were effective at stabilising the entrapped GOx, but in the presence of blood, these were able to repel biological entities. The group were able to create a highly sensitive biosensor using the conductive polymer with good stability shown after 14 days stored in the blood (90%) due to the antifouling nature of the polymer.[176]

Although antifouling coatings can be extremely effective at preventing biofilm formation, they may have a short lifetime or become ineffective under high loadings of *in vivo* material. A way to challenge this is to use QS inhibitors to quench QS, block QS signals and prevent biofilm maturation.[177] Preventing these QS signals was shown to improve the susceptibility of bacteria to antibiotics and may provide a better way to fight infections of this sort.[178] For example, *Pseudomonas aeruginosa* (*P. aeruginosa*) biofilm formation is regulated by QS molecules such as *N*-(3-oxododecanoyl)-L-homoserine lactone (3-oxo-C12-AHL). Ma *et al* were able to develop MIPs by ultraviolet (UV) polymerisation of hydroxyethyl methacrylate (HEMA) monomers in the presence of 3-oxo-C12-AHL.[174] During the polymerisation crosslinking with ethylene glycol dimethylacrylate (EDGMA) was used to fix HEMA monomers around the

3-oxo-C12-AHL template. When washed, 3-oxo-C12-AHL recognition site cavities were left in the MIPs. These recognition sites were able to absorb 3-oxo-C12-AHL molecules and prevent QS in the presence of *P. aeruginosa* cultures which significantly reduced biofilm formation by 62% compared to non-imprinted polymers (NIP)s.

Other groups have similarly investigated the use of polymers as an alternative to antibiotic resistance to prevent QS and reduce colonisation by sequestering bacteria away from the infected site.[6, 173, 179, 180] For example, Perez *et al* showed that a cationic polymer with tertiary amine groups (poly(*N*-[3-(dimethylamino)propyl] methacrylamide)) could bind to the negative surface of *Vibrio cholera* bacteria causing clustering. In the presence of Caco-2 cells and zebrafish, colonisation by the polymer-sequestered-*V. cholerae* was greatly reduced compared to colonisation by planktonic-*V. cholera*. A key virulence factor, cholera toxin (CTX) was also shown to be reduced in the presence of clustered bacteria, lowing the toxicity towards Caco-2 cells.[179]

This thesis explores bacterial initiated synthetic polymerisations which could later be developed into such materials for bacterial clustering or antibiofilm formation by adapting the monomer type and composition as previously shown by Magennis *et al*.[6] Further to this, possibilities might also arise where a bacterial extracellular polymer matrix (EPM) could be manipulated using selected synthetic polymers to influence the phenotype of the bacteria.[5, 181]

1.1.5 Microbial Fuel Cells (MFC)s

Microorganisms (e.g. electrogenic bacteria) in MFCs catalyse biochemical reactions via EET to convert organic or inorganic compounds (e.g. wastewater) into electrical energy, simultaneously cleaning the environment and generating renewable bioelectricity.[112, 182] For example, bacteria anaerobically decompose organic matter (e.g. starch, cellulose, organic acids, phenols) to CO_2 (Figure 1. 10).[183-185]

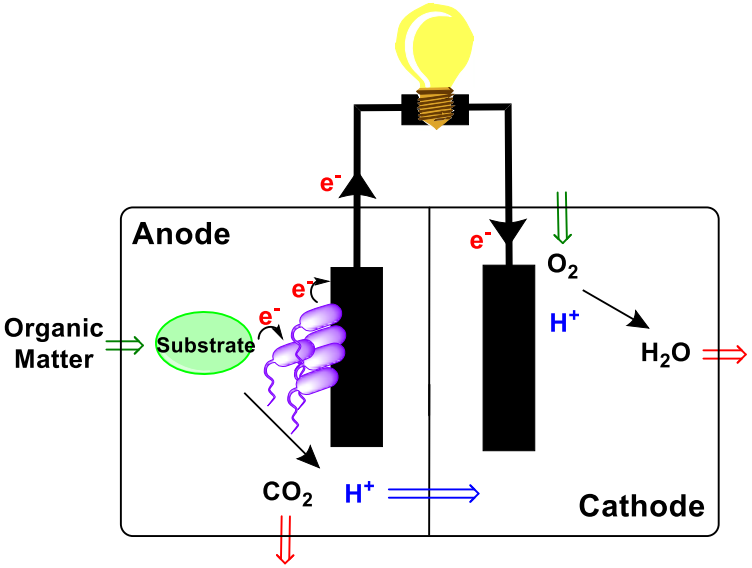

Figure 1. 10. Representation of a typical microbial fuel cell where the substrate from the organic matter is oxidised by bacteria, releasing CO_2 and H^+. The electrons are transferred by EET to the anode and through the electrical circuit to the cathode. H^+ migrates through the PEM and combines with O_2 and the electrons to give water. This whole process generates electricity output which can be harnessed and used as renewable energy.

During oxidation of the electron donor, electrons are transferred from the bacterial respiratory system to the anode, where they flow through the external circuit to reach the cathode. Combining this to an appropriate cathodic reaction, such as O_2 reduction, completes the circuit. This involves the migration of protons, released in the wastewater of the anodic chamber, through a proton exchange membrane (PEM) (preventing O_2 contamination of the anaerobic anodic chamber) to the cathodic chamber where they can combine with O_2 to form H_2O.[182, 186]

Similarly, microbial electrosynthesis can also be used to convert organic matter into important valuable chemicals or fuels by the addition of an external current.[132] Electrogens, therefore, offer sustainable solutions to various environmentally damaging issues, such as pollution, fossil fuels, and harsh chemical synthesis, however, EET rates often limit MES efficiency and its large scale usage.[187] Anode material modifications have been explored in efforts to improve EET rates, as well as the inspection of the bacterial mechanistic pathways, but these are extremely complex and there is still much more to be discovered.[187]

MFCs connect to other bacteria cells and electrodes through an electrically conductive biofilm containing extracellular substances that contribute to ET to the anode.[188] Therefore understanding the biofilm composition may be important in improving electron transfer efficiency. To probe the function of the bacterial biofilm attached to the anode surface, confocal scanning laser microscopy (CSLM) and protein measurements were carried out by Reguera *et al*. It was found that current production increased linearly with the amount of biomass on the

anode as the *G.sulfurreducens* biofilm developed. Cells at a distance from the anode were found to be viable and metabolically active during biofilm formation and are thought to contribute to EET to the anode by pili-pili interaction.[189] The effectiveness of electron transfer from organism to the anode is limited by the natural metabolic rate of the organism and EET rates. These pose challenges towards maximising MFC fuel output and increasing its potential for large scale industrial use, and so new ways to increase the current density at the anode are necessary.[188] To tackle challenges surrounding bacterial attachment and poor electron transfer rates, several improvements including anode modification and genetic or chemical modification of organisms have been attempted.[182, 185]

1.1.5.1 Anode Modification

The choice of anode material of a MFC is important for ensuring effective adherence of cells. Graphite is commonly used due to its non-toxic, inexpensive and chemically stable properties, however, several metals (Au, Ag, Cu, Ni) have also shown to be promising anode materials due to their increased conductivity.[190] Many investigations into anode modifications have been carried out,[182] including the use of carbon nanotube (CNT),[191, 192] metal oxides,[193] and conductive polymers.[194, 195] Heavy metal ion addition to media has also been found to increase energy output by enhancing electron shuttle mediators (Ribo-flavins) and increasing anodic bacterial attachment.[196]

1.1.5.2 Genetic Modification

Genetic modifications of bacteria have also been utilised to improve fuel cell efficiency. For example, the overexpression of the electron shuttle synthesis pathway (methyltransferase encoding gene) of *P. aeruginosa* enhanced the energy output of a MFC by 4 times than that of the unmodified organism.[197] Overexpression of both flavin and metal reducing biosynthesis gene clusters in *S. oneidenesis* were also able to enhance EET capacity in MFCs and showed that a synergy between mediated and direct electron transport is likely to exist.[198]

1.1.5.3 Chemical Modification

The cell membrane and cell wall(s) of bacteria are insulators, hindering electron transfer to the electrode. Chemical modification of the cell membrane has therefore been explored to enable better conductivity. For example, an improved power output of MFCs was achieved by chemically perforating the pores and channels in the cell membranes of several types of bacteria such as *P. aeruginosa,*[199] and *Tolumonas osonensis*.[200] This chemical treatment facilitated the diffusion of electron transfer mediators through the channels and pores but also increased cell surface roughness, which enhanced cell adherence to the anode.[185] Interestingly, conjugated oligo-electrolytes (COEs) have been found to improve current generation in both yeast and *E. coli* cells by incorporation into the biological membrane.[201, 202] COE molecule, 4,4' – bis (4' - (*N,N*-bis(6'-(*N,N,N*-trimethylammonium) - hexyl) amino) -styryl) stilbene tetraiodide (DSSN+) (Figure 1. 11) was inserted into the membranes of *S. oneidenesis* MR1 bacteria and found to increase electrode

colonisation, cytochrome based EET and flavin mediated electron transfer. Although the exact mechanism is not known, it is suggested that the contact of the COEs with membrane bound proteins may facilitate the direct electron transfer and result in the rise in redox current that is seen.[203]

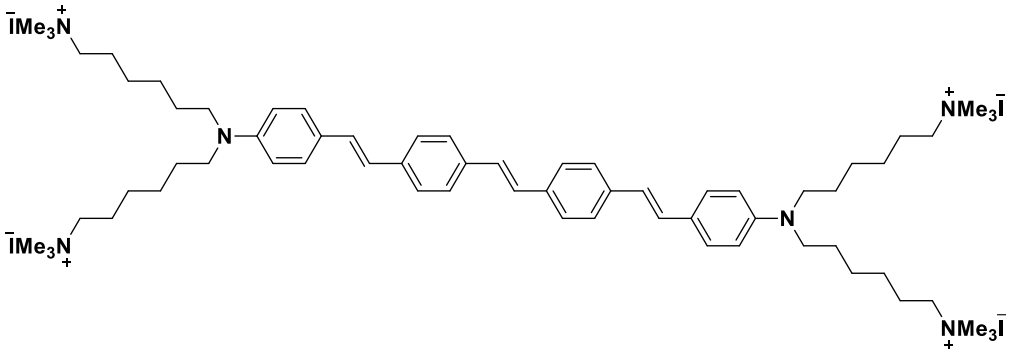

Figure 1. 11 Structure of COE, 4,4' – bis (4' - (*N,N*-bis(6'-(*N,N,N*-trimethylammonium) -hexyl) amino) -styryl) stilbene tetraiodide (DSSN+).

1.1.5.4 Polymer Mediators

A variety of conductive or redox active polymers have been developed to aid EET efficiency between microbes and an electrode. One class of these, Type 1 mediators, facilitate electron hopping between the bacteria and the electrode by forming a 3D polymer matrix around the cells.[204] For example, polypyrrole (discussed later),[10, 13, 17, 205] osmium-containing polymers,[125, 195, 206] and ferrocene-containing polymers. In comparison, type 2 mediators are polymers that can diffuse through a cell membrane to intracellularly extract electrons and shuttle them to the anode. For example, Nishio *et al* created phospholipid polymers containing 2-methacryloyloxyethyl phosphorylcholine (MPC) and vinyl ferrocene (VF) chains, poly(MPC-co-VF) (PMF). The MPC unit

allows diffusion through the bacterial membrane whilst he VF unit facilitates electron transfer due to its redox properties (Figure 1. 12).

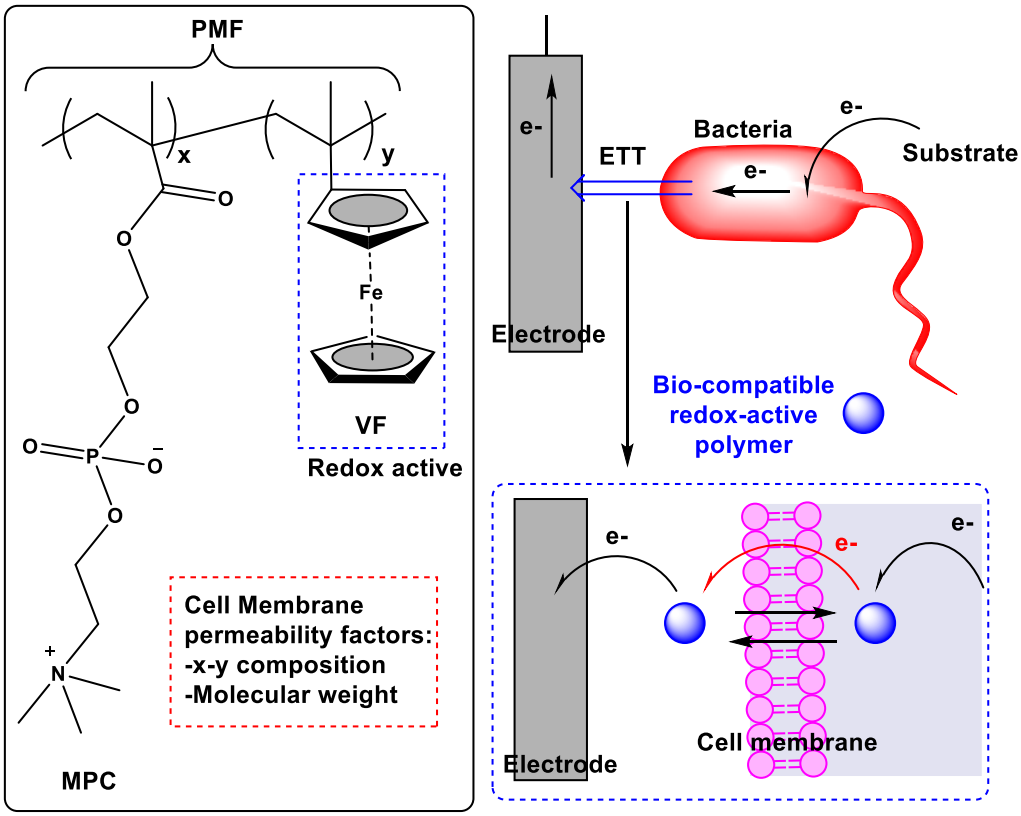

Figure 1. 12 Phospholipid polymer structure (left) containing 2-methacryloyloxyethyl phosphorylcholine (MPC) and vinyl ferrocene (VF) chains, poly(MPC-co-VF) (PMF). And the application of PMF to assist (extracellular electron transfer) EET in bacteria by shuttling intracellular electrons to the anode. Modified from reference.[204]

Incubation of PMF with Gram negative (*E. coli)* and Gram positive (*Lactobacillus plantarum*) cultures showed an increase in the anodic current compared to cultures in absence of PMF. The viability of the cells was maintained in both cases, showing that PMF membrane diffusion did not cause cytotoxic effects whilst effectively shuttling electrons.[207] The design of PMF polymers was shown to regulate EET which changed when altering the molecular weights and copolymer ratios.[208] The design

of redox-active polymers can therefore easily be tailored to change the desired properties for potential applications, like metabolism regulation and intracellular redox sensing.[204, 209, 210] This design could be applicable to Fe ATRP or FG RAFT RDRP methods designed in this thesis. The formation of redox active polymers in response to EET might enable sensing of bacterial metabolism or combination with MIPs towards signal detection upon binding of redox active MIPs to a specific bacteria type. These polymers may also provide great potential for increasing fuel cell efficiency by aiding EET rates. Furthermore, encapsulation of bacteria with synthetic ECMs formed via Fe ATRP or FG RAFT methods might aid the preservation of bacterial metabolism and in turn increase the efficiency of MFCs.

1.1.6 Iron Reduction by *C. metallidurans* and *E. coli*

Inorganic matter can also be metabolised by bacteria to produce energy and for bioremediation (e.g. of toxic metals).[122, 211] *Cupriadivus metallidurans* (*C. met*) are extremophiles, highly adapted to metal-contaminated environments, with resistance to many toxic metals.[212, 213] *C. met* have the ability to reduce toxic gold (Au^{3+}) complexes forming extremely pure gold biomineralised precipitates.[214, 215] Au/Cu resistance has shown to be induced synergistically by pre-incubation with Cu-ions via periplasmic oxidoreductases.[216, 217] Anaerobic Au reduction by *C. met* was also shown to result in pili structures, often used by Gram negative bacteria to transfer electrons to electron acceptors.[214] Although *C. met* is less well studied than the organisms discussed above and the exact

modes of metal reduction are debated, several modes of metal homeostasis/resistance may work in parallel, including EET and metal efflux systems. This facultative anaerobe was used in our studies for anaerobic Fe ATRP polymerisation studies (Chapter 2) due to its metal resistance, ability to reduce various metals, tolerance to deoxygenated environments and its fast growing nature. After success in Chapter 2 with *C. met*, the bacteria were also used in Chapter 3 towards Fenton GOx RAFT polymeirsations.

E. coli were previously used as a means of Cu^{2+} reduction for ATRP polymerisation synthesis,[6] and are also facultative anaerobes, making them a reasoned candidate for our bacteria initiated Fe ATRP polymerisations. *E. coli* can reduce Fe/metals via excretion of flavin molecules,[218] extracellular enzymes or siderophores for Fe homeostasis.[109, 219] Other studies suggest Fe reduction can be used for anaerobic respiration in *E. coli*.[220] *E. coli* contains C-Cyts such as NapC which are homologues of Fe reducing CymA of *Shewanella oneidensis*,[221] and other ferric reductases also exist in *E. coli*.[108] It is likely that there are several synergistic Fe reducing processes involved in assimilatory and dissimilatory respiration, and further research is essential to understand the exact mechanisms.[108] The cloning of *E. coli* was carried out in the 4th Chapter of this thesis as a means to evaluate the role of NapC in Fe reduction.

1.1.7 Enzyme Catalysed Polymerisations

Enzymes are complex proteins that exist in all living things and catalyse life's most vital reactions including respiration and DNA synthesis.[103, 222] They offer a sustainable alternative to industrial catalysts, particularly for 'green chemistry' as they are derived from natural resources, highly selective, biodegradable, non-toxic and work under mild reaction conditions.[3, 223] Biocatalysts and enzyme-mimics have been used for a variety of RDRP reactions including NMP, ATRP and RAFT.[92, 223-226]

1.1.7.1 ATRPases and BioATRP

Enzymes that contain metal ion centres offer biologically friendly alternatives to ATRP catalysts, for example, cytochromes and oxidoreductases. Such enzymes, typically Fe and Cu centred-proteins, have been implemented in a variety of ATRP reactions, known as ATRPases.[116, 227-229] Nico Bruns *et al* and di Lena *et al* showed that ATRP could be driven by the catalytic activity of horseradish peroxidase (HRP), haemoglobin (Hb), Hb in red blood cells, catalases and laccases.[73, 115, 230-233] After establishing biorelevant conditions for grafting polymers from proteins,[234] Matyjaszewski *et al* also created synthetic analogues of Fe containing enzymes based on hematin (Figure 1. 13).[47] These contained PEG chains to make them more water soluble and were found to be effective in both organic and aqueous media making them suitable protein alternatives.

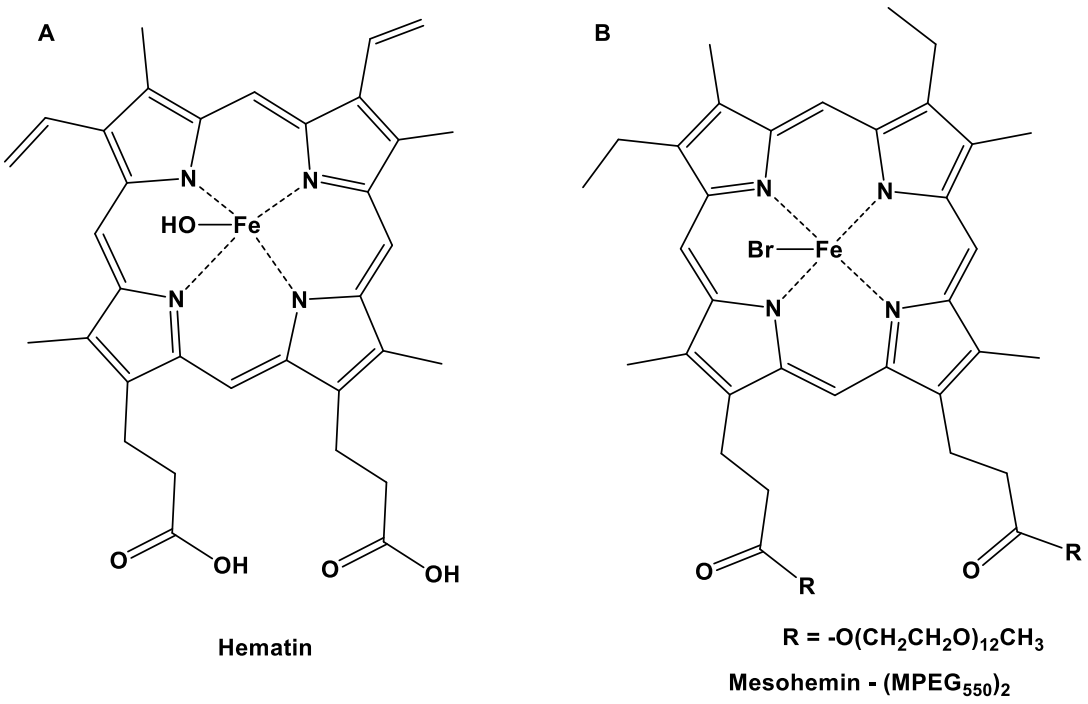

Figure 1. 13 Structures of (A) Hematin and (B) Mesohemin – $(MPEG_{550})_2$ - water soluble, Br bearing derivative of hematin.[47]

Polymersomes, protein cages and inorganic structures can be used to create nanoreactors and microreactors and have been exploited for enzyme-initiated polymerisations.[2, 235-239] Such structures allow the components of a reaction to be held in a closed compartment, speeding up the reaction rates and reducing side reactions from contaminants. They are also useful mimics for cell compartmentalisation which support the integrity of organelles, cell signalling and enzyme cascades for vital processes (e.g. homeostasis, respiration, digestion, repair and function).[160] Bruns *et al* demonstrated that HRP bound nanoreactors could be used to polymerise polyethylene glycol acrylate (PEGA), by enzyme initiated ARGET ATRP.[238] Modified HRP was covalently bound to the cavities of modified thermosome (THS) protein cages and incubated with ATRP reagents. Polymers formed by the nanoreactors were found to be lower molecular weights and narrower dispersities (M_n

= 4400, *Đ* = 1.08) than for analogous solution-based polymerisations (M_n= 43700, *Đ* = 1.23). Advances in permeable polymersomes have allowed successful cascade reactions of enzymes which may in the future be applied to polymerisation reactions.[235]

1.1.7.2 BioRAFT

HRP was able to facilitate a BioRAFT polymerisation by catalysing acetylacetonate (ACAC) radical generation using H_2O_2 for the RAFT initiation step (Figure 1. 14).[240] [241, 242] The ACAC radical could then effectively react with monomers to create a propagating radical chain to begin the RAFT polymerisation.[243] HRP has also been exploited for aqueous RAFT dispersion polymerisation, resulting in polymerisation induced self-assembly (PISA).[78, 240] Zhang *et al* reported the formation of AB Block copolymer nano-objects mediated by a PEG based macro-CTA by HRP initiated PISA RAFT of HPMA monomers. Near quantitative conversion (>99% in 20 minutes) was achieved in water under mild reaction conditions which also allowed the loading of SiO_2 nanoparticles and BSA biomolecules into the vesicles.

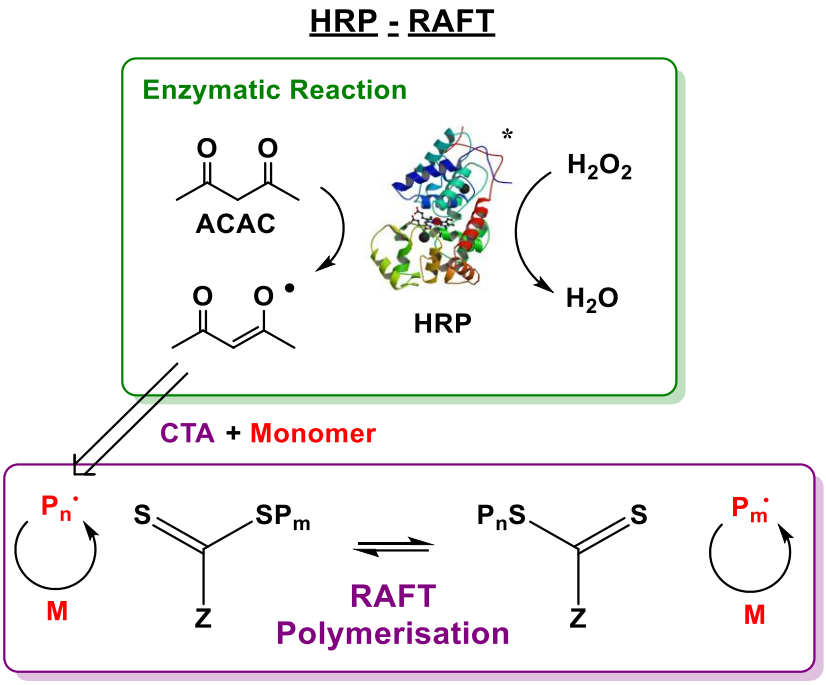

Figure 1. 14 BioRAFT mechanism using catalysis of ACAC by horseradish peroxidase with H_2O_2 to generate ACAC radicals for initiation of a RAFT polymerisation.[223]*HRP protein structure from PDB ID: 1GWU.A.[244]

1.1.7.3 Oxygen Tolerance

Oxygen contamination in RDRP can be detrimental to many polymerisations by acting as a radical scavenger, radical inhibitor or deactivating ATRP catalysts.[245] Methods to limit oxygen sensitivity during RDRP would enable an easier reaction set up and improve the control of the resulting polymerisations.[86, 245, 246] The GOx-HRP enzyme cascade has been utilised to initiated RAFT reactions in the presence of oxygen for; a variety of copolymers and conditions,[1, 86] in PISA dispersion RAFT,[78] and in conjunction with red blood cells.[98] During the cascade reaction, GOx oxidises glucose using oxygen which generates H_2O_2. (Figure 1. 15). H_2O_2 is a substrate for HRP and is used to generate

ACAC radicals which can initiate a RAFT polymerisation in the presence of the correct reagents (Monomer and CTA).[1]

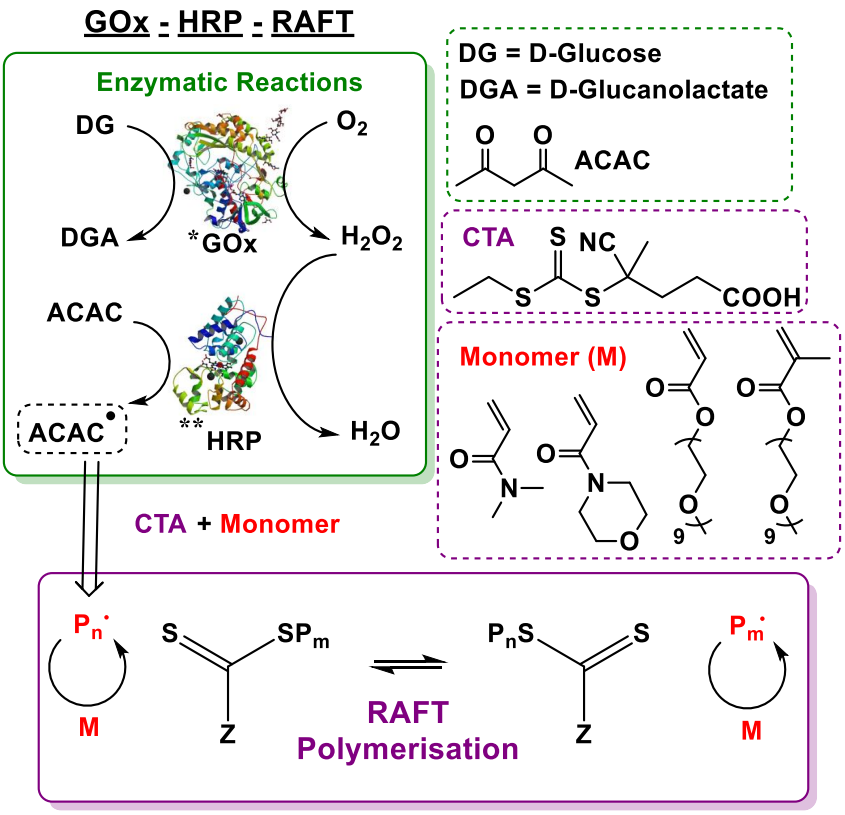

Figure 1. 15 GOx - HRP enzymatic catalysis in air forming active radicals for RAFT polymerisation of various monomers.[1]*GOx protein structure from PBD ID: 3QVP.A.[100] **HRP protein structure from PDB ID: 1GWU.A.[244]

These reactions are not just limited to RAFT polymerisations. Indeed, such enzyme cascades have been implemented into ATRP methods, to impart oxygen tolerance, in which the ACAC radical generated reacts with the monomer to begin the polymeriation.[75, 247] Matyjaszewski *et al* discovered the ability of GOX/HRP ATRP reactions to be turned on and off using an aerobic/anaerobic switch and were also able to form DNA-Polymer bioconjugates using this technique.[247] The utilisation of these cascades are likely to transform applications that require oxgen presence and widely broaden the scope of RDRP methods in function.

1.1.7.4 Progress in Enzyme RDRP

Although proteins cause some limitations in reaction conditions, and poor control, they offer progress towards 'green chemistry' and have the potential to widen the perspective on biotechnological applications. 'Green Chemistry' is defined as a method of fabricating chemical products and processes that can reduce or eliminate the use or generation of hazardous substances. Green chemistry is applicable throughout a products' life cycle concerning its design, manufacture, use and disposal.[248] Catalysts are an important part of green chemistry as they improve the efficiency of chemical reactions by lowering the activation energy and therefore reducing the required energy input. Biocatalysts such as enzymes often have improved selectivity than conventional catalysts, increasing the yields of desired products and decreasing waste. Biocatalysts are also sourced naturally and can provide solutions to chemical challenges that might otherwise require harsh conditions. Enzymes are therefore a promising tool to support sustainability for green sourcing, manufacturing, and reducing waste.[3, 237]

An example is given for the case of chemically challenging *N*-vinylimidazole (NVIm), which is an extremely difficult monomer to polymerise in a controlled manner using conventional RDRP methods.[249] This difficulty arises due to the absence of resonance stabilisation of the propagating radical and because the polymer P(NVIm) strongly complexes Cu ions, depleting the catalyst concentration in the solution.[223] To overcome this, the multi-copper-containing

oxidoreductase, laccase from *Trametes versicolor* (LTV) was effectively used to catalyse NVIm polymerisation under aqueous conditions, achieving *Đ* as low at 1.07 (Figure 1. 16).[233] These results show promise for providing cationic PNVIm polymers capable of drug and gene delivery, as uniform polymers with predictable properties are highly desirable for these applications.[250]

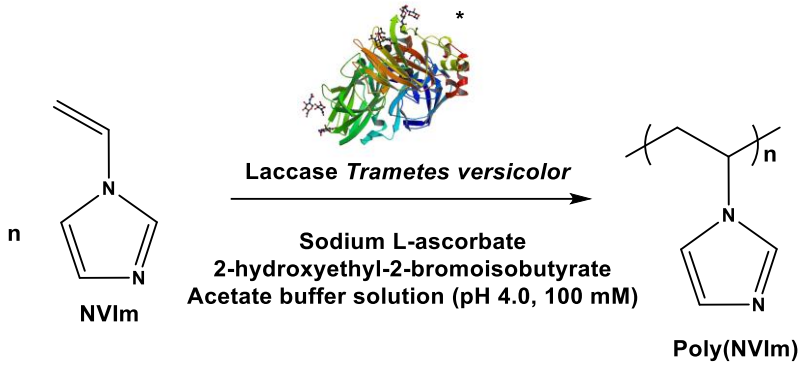

Figure 1. 16 Polymerisation of *N*-vinylimidazole (NVIm) using laccase from *Trametes versicolor* in mild conditions.[233] *Laccase structure from PDB ID: 1GYC.A.[251]

Other examples where enzymes are useful as catalysts include, the utilisation of GOx for RAFT polymerisations of hydroxy ethyl acrylate (HEA) in a variety of solvents including, beer, wine, various liquors and fermentation broth.[252] In nearly all cases polymers were formed in high conversion, attained good control and narrow molecular weight dispersities. This example highlights the robustness of enzyme mediated polymerisations and the tolerance of GOx to impurities.

Biocatalysts also offer interesting biosensing and diagnostics tools, for example, enzyme-MIPs made for identifying infectious bacterial species. In this example, electrochemically mediated ATRP (eATRP) catalysed by Hb was used to generate Hb-MIPs on the surface of a gold electrode (Figure 1. 17).[253] Hb acted as both the template and the

catalyst which, once removed, provided a MIP-modified electrode for Hb detection. Sun *et al* also used this technique to prepare MIPs on 3D nano-dendrites to increase the number of imprinting receptors and enhancing electrode surface area which gave a Hb detection limit of 7.8 x 10^{-11} mg/ml.[254] Another interesting example of enzymatic catalysis are BSA hybrid inorganic nano flowers. BSA-$Cu_3(PO_4)_2.3H_2O$ biocatalysts were found to display enhanced activity and stability, able to catalyse RAFT polymerisation of DMAEMA and $PEMGA_{500}$.[255] This hybrid catalyst was much easier to remove from the resulting polymers (centrifugation) than traditional free enzymes which often to adhere to the polymers, making them easier to reuse and generate purer polymers.

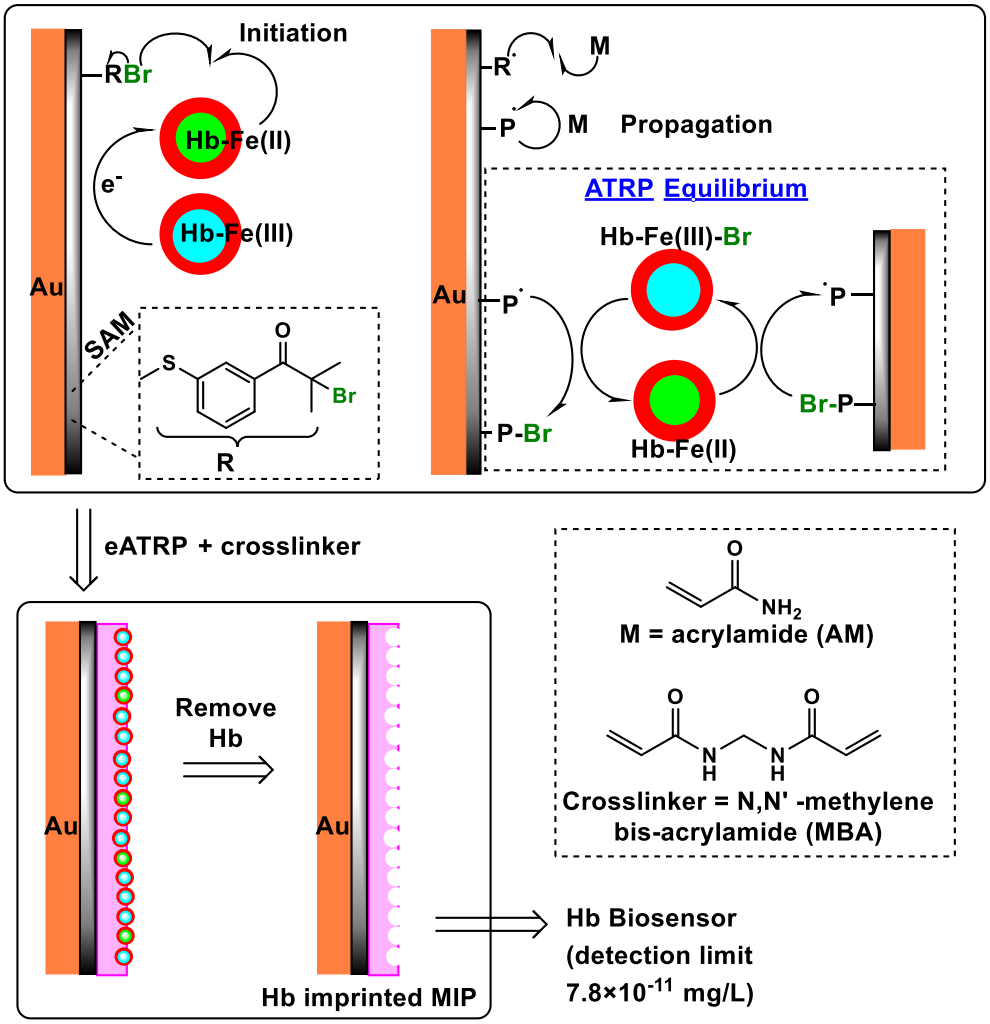

Figure 1. 17 Electrochemically mediated ATRP (eATRP) catalysed by Hb-Fe. Hb-Fe acted as both catalyst and template for MIPs. The MIPs on the anode surface could then be used as a biosensor for Hb. Modified from reference.[253]

1.1.8 Whole Cells as Biocatalysts and Living Materials

Although examples of catalysis using whole blood cells have been discussed, more complicated cells for polymerisation catalysis exist in literature. Drawbacks associated with using enzymes, such as high cost, enzyme isolation and purification can be overcome by using whole living cells as biomolecular machines. Cell-bound enzymes are protected by the cells' natural defences making them less sensitive to environmental pressures or contaminants. Although the membrane barrier can cause poor diffusion of substrates, reagents and products and side reactions may occur.[256] Research has been implemented to develop and improve whole cell - polymer hybrids for cell manipulation, biosensors and fuel cells.

1.1.8.1 Conducting Polymers

As discussed previously, EET in organisms can be harnessed by electrodes in MFCs to produce electricity. MFC efficiency is however, limited by the poor attachment of bacteria to the anode, biofilm build up, and cell death, but modification with conducting materials might facilitate ET rates. Conducting polymers such as polyaniline, polydopamine and polypyrrole (PPy) exhibit good conductivity, biocompatibility and stability, making them suitable materials for biosensors or MFCs.[118, 257-259] Ramanavicius *et al* sought to increase the conductivity of electrons through yeast (*Saccharomyces cerevisiae*) cells by the synthesis of

PPy.[260] The proposed mechanism of this polymerisation is by the oxidation of the mediator complex, $[Fe(CN)_6]^{4-}$, via oxidoreductases in the yeast cell membrane to $[Fe(CN_6)]^{3-}$ which reacts with Py to begin the reaction, and subsequently form conductive polymer chains. The localisation of the resulting PPy was tracked using ^{15}N isotope labelling of the Py monomer, revealing that PPy was evenly distributed across the cells which did not change in size after the polymerisation.[261] Further to this, fluorescent mannose binding molecules were used to evaluate the surface binding affinity of unmodified yeast cells compared to those 'modified' with PPy, showing similar fluorescence intensities in both cases. These findings suggest that PPy is likely to be localised in the cell wall rather than encapsulated around the cell surface.

Other groups have utilised similar approaches to coat microorganisms with PPy for use in MFCs.[10, 205, 262] *S. oneidensis* MR-1, *E. coli*, *Ochrobacterium anthropic* and *Streptococcus thermophilus*, were modified with PPy showing an enhanced conductivity in all cases. *S. oneidensis* coated PPy was effectively used as an anode in an MFC, generating an increased EET, increased cell viability, and 14.1-fold increase in power output compared to the native bacteria.[10]

Trans plasma membrane electron transport (tPMET) systems, which are equatable to bacterial periplasmic membrane proteins (C-Cyts), have also been of interest for their involvement in Fe homeostasis and oncogenic Fe reduction.[263, 264] Indeed, it was hypothesised that tPMETs in cancer cell lines might be capable of Py oxidisation polymerisation.[17] However, in these experiments the mammalian cells were shown to be

extremely sensitive to the reagents, particularly Py, causing instead a ROS induced polymerisation. Although these findings might be useful towards biosensors that detect and signal cell damage via polymer formation. The complexity of living cells remains a challenge in the identification and prediction of redox mechanisms that drive polymerisations. This necessitates the need for continued studies into the scope of what can be achieved in order to both push boundaries and ellucidate the mechanistic pathways involved. This thesis soughts to build novel polymer synthesis techniques and shed light on the possible bacterial mechanisms involved.

1.1.8.2 Bacterial Instructed - RDRP

Increasing the selectivity of cell binding agents (MIPs) for diagnostic pathogen detection might be advantageous for identifying specific types of bacteria, particularly within mixed cultures. To this cause Magennis *et al* exploited bacterial homeostasis to initiate Cu-ATRP, producing polymers that displayed cell binding and entrapped bacteria in a synthetic ECM.[6] The mechanism was suggested to be driven by EET of C-Cyts or oxidoreductases in a redox reaction with the Cu ATRP catalyst. Polymers that were formed in solution (weakly templated polymers (WTPs)) were shown to be structurally different from polymers grown at the bacterial surface (strongly templated polymers (STPs)). The STPs had higher specificity to the bacteria that they had grown around, causing an increased clustering which could be used for specific bacterial identification or sequestration of bacteria away from an infected site.

Bacterial-instructed Cu catalysed 'click chemistry' (b-click) was further utilised to demonstrate the diagnostic potential of the method. Bacterial cells remained in a dispersed suspension in the presence of a pro-fluorescent marker, whilst the addition of a bacterial binding cationic polymer (STP) with a terminal-alkyne chain caused bacterial clustering (Figure 1. 18). The clustering could be fluorescently imaged due to the b-click reaction between the azide group of the fluorescent marker and the alkyne functionalised polymer, which was demonstrated for several types of bacteria: *E. coli, Clostridium difficile, Yersinia pseudotuberculosis, Helicobacter pylori* and *Campylobacter jejuni*. As well as this ability to combine synthetic methods with biological flux, b-ATRP was found to provide good control over the polymerisation kinetics and an extremely low amount of Cu catalyst was needed (4.42 ng/mL).

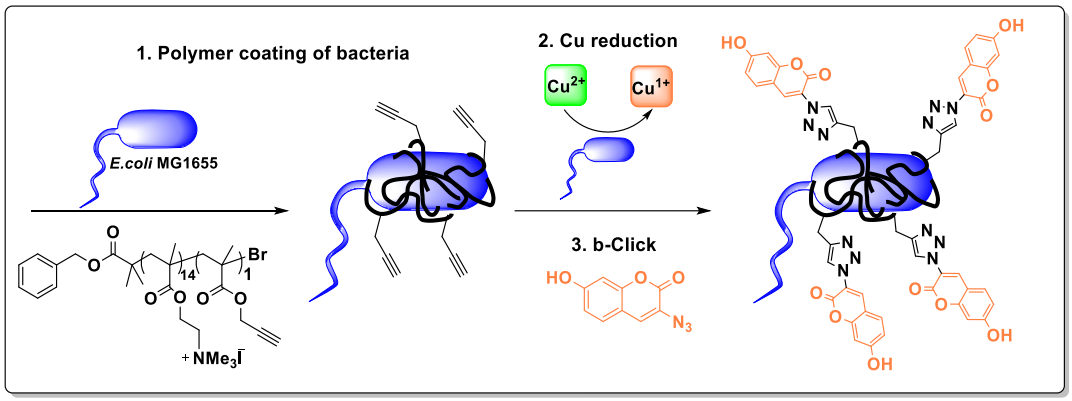

Figure 1. 18 Polymerisation induced by *E. coli*, leading to the coating of bacteria by alkyne terminated polymer (1). Cu^{2+} reduction to Cu^{1+} (2), which catalyses b-click chemistry of azide molecule resulting in fluorescently labelled bacteria (3).[6]

Building from these studies, Luo and Haddleton *et al* used sugar containing monomers to form glycopolymers by *E. coli* facilitated Cu

AGET ATRP.[18] Similar results to Magennis *et al* were seen, polymers obtained in solution (WTPs) and bound to the bacterial surface (STPs). The STPs were found to specifically cluster the bacteria that templated them, even when mixtures of templated and non-templated bacteria were present. STPs were found to inhibit infection of endothelial cells (ECs) in the presence of bacteria compared to WTPs and no polymer. It was suspected that STPs prevented bacterial adherence to the ECs by occupying the binding sites on the bacteria surface. Similarly, in the presence of a gold surface competition between bacteria and ECs for adherence was reduced in the presence of STPs. These results show promise towards reducing bacterial adhesion which often leads to infection, particularly with medical implants and devices.

Another example of bacteria-induced polymerisations was shown by Fan *et al* who carried out b-ATRP initiated by *S. oneidensis* MR-1. Low levels of Cu catalyst (0.2 μM) were required to form $OEOMA_{500}$ and NIPAM polymers with narrow dispersities and good control over the molecular weights.[218] The mechanism of catalyst activation by bacteria was investigated by testing the supernatant of viable *S. oneidensis* in b-ATRP, revealing minimal polymerisation. This suggested that the polymerisations shown were unlikely to be caused by the release of secreted reducing agents, suggesting that C-Cyts were involved in the *S. oneidensis* initiated b-ATRP.

Interestingly, *E. coli* was found to be ineffective at initiating these polymerisations when viable, but when lysed both *E. coli* and MR-1 activated the b-ATRP. Fan *et al* hypothesised that this was due to the

release of redox molecules by lysed *E. coli,* like glutathione and flavins, causing ATRP initiation rather than direct reduction of the catalyst by C-Cyts. Whilst, when both bacterial strains were metabolically inactivated no polymerisation activity occurred, suggesting that metabolism was a key factor in the initiation pathway. Fenton – associated catalysis from cell lysis/stress was ruled out by experiments with *S. oneidensis* MR-1 in the presence of Cu^{2+} (5 μM), which revealed only minimal grown inhibition. A variety of carbon sources were also added to assist the metabolism of *S. oneidensis* MR-1 in the study, which increased the polymerisation rate compared to starved cells. However, the lack of control experiments with carbon sources omitting bacteria, suggest these observations may be due to direct interaction between the carbon source and Cu complex (e.g. redox or ligand displacement reactions).[265] Lastly, studies involving mutant strains of *S. oneidensis* MR-1 which lacked ΔmtrC and ΔomcA genes showed decreased polymerisation activity, suggesting that C-Cyt proteins contributed to the initiation of the polymerisation.

Since the data in the second chapter of this thesis was published,[266] more groups have incorporated bacterial EET into redox initiated polymerisations.[21] A Bac-RAFT polymerisation was achieved by Qiao *et al*, showing that *E. coli* and *Salmonella enterica* were able to facilitate radical generation by EET redox interactions with a aryldiazonium salt, generating polymers in a controlled manner (*Đ*=1.3). This research area concerned with exploiting whole cells for polymerisation methods, although in its infancy, is rapidly growing and further studies will help to

expand the mechanistic reasoning of bacterial redox behaviour concerning materials synthesis.

1.1.8.3 Cell Modification and Manipulation

Engineering the surface of cells can be a useful tool to modify adhesion and cell-cell interactions which are abundant in bacterial infections. Furthermore, cell surface modification could be useful for the development of whole-cell biosensors, biocatalysts, cell therapy and towards modulating cell stability, viability and chemical activity.[20, 155, 267-273] Due to the dynamic and complex nature of the cells' microenvironment, modification can be extremely challenging or detrimental to the viability of the modified cells.[274] Despite these challenges, polymer-cell hybrid materials have been generated by Kim *et al*, exploiting aqueous surface initiated (SI) ARGET ATRP.[275] Yeast cells were coated with polydopamine macroinitiators (PDm) before SI ARGET ATRP of sodium methacrylate (SMA) monomer was performed with ascorbic acid to activate the Cu catalyst. The PDm layer acted as a radical scavenger, effectively protecting the yeast cells from any ROS generated during the reaction. The yeast cells retained 66.7 % viability after the polymerisation was complete, whereas the non-PDm coated yeast cells only retained 31.7 % viability. Native yeast cells aggregate rapidly in the presence of bacteria due to the strong mannose binding sites on the bacteria cell surface. However, yeast cells coated with Poly(SMA) effectively blocked these binding sites and anti-agglutination was observed in the presence of bacteria, showing affective manipulation

of the cells. Furthermore, ascorbic acid regenerated inactivated Cu (II) catalyst in the polymerisation, allowing some level of oxygen tolerance without affecting the reaction rate.

Further to this, Hawker *et al.* demonstrated photo-induced electron transfer (PET) RAFT to implement polymer grafting from the surface of yeast and Jurkat cells.[5] A RAFT initiator (CTA) was covalently attached to yeast cell surfaces by initial amidation of the cell surface and azide alkyne cycloaddition chemistry, followed by SI RAFT polymerisation. The viability of the resulting polymer-cell hybrids was retained (>90%) as measured by flow cytometry. Jurkat mammalian cells were also modified by the same method, but poor viability was observed due to their increased sensitivity compared to yeast. To overcome this sensitivity, a CTA-lipid analogue was created and non-covalently anchored into the cell membrane of Jurkat cells, where subsequent SI RAFT polymerisation was carried out. The resulting polymer-modified-Jurkat cells showed 90 % viability by flow cytometry.

The above examples show successes in grafting to or from a cell surface, however, Bradley *et al* investigated the modification of cells from the inside.[19] Natural polymers, such as polyphosphates, polyesters and polysaccharides, are synthesized by cells and are important in mediating cellular functions such as storage and stress responses.[276-278] To investigate how synthetic polymers affect cellular functions and to create a means for long term tracking, intracellular photo-initiated free radical polymerisation was carried out inside living HeLa cells. Mixtures of photo-initiator (Irgacure 2959) and monomer (HPMA) were incubated with cells

in medium for 4 hours before the cells were washed and irradiated with light (365 nm). Cell lysis allowed the polymerisation conversion (68 %) to be calculated based on the remaining HPMA concentration in cells after illumination, whilst no HPMA consumption was detected in either cells that were not exposed to illumination or in the absence of photo-initiator. Monitoring the cells after the polymerisation by flow cytometry showed no significant DNA damage and no increase in apoptosis. It was discovered that the intracellular polymerisation could manipulate cell migration by altering monomer and initiator ratios. F-actin staining revealed that polymerised HeLa cells altered cytoskeleton organisation and phenotype which could be useful for wound healing applications. They also demonstrated that a variety of intracellular fluorescent polymers could be used to track cells that retained high fluorescence after several passages. This is particularly important for regenerative medicine applications as a non-invasive, long lived method to monitor tissue regeneration, however limitations still exist for larger imaging depths.[279]

Surface functionalisation has also been used to alter adhesion, wettability, antifouling and biocompatibility of abiotic-biotic interfaces, towards applications such a tissue regeneration, modulation of cell behaviour and anti-bacterial activity.[280] Benetti *et al* demonstrated the growth of polymer brushes from a surface modified with an ATRP-initiator using SI-ATRP in organic solvents, aqueous solvents and cell media.[281] In these polymerisations an Fe^0 coated plate acted both as a biocompatible catalyst and reducing agent whilst deoxygenating the

system by generating Fe_xO_x species. These species diffused through the solution to form an ATRP catalyst couple Fe^{2+}/Fe^{3+}. The addition of deactivating species ($FeCl_3$/Ligand or $FeBr_3$/ligand) was found to speed up the reaction and increase grafting thickness by comproportionation (Reaction 1) with Fe^0 to generate active Fe^{2+}/L catalyst. This addition of deactivator also inhibited radical recombination termination reactions of propagating grafting chains, but beyond 10 mM slowed down the grafting process due to a high level of deactivated chains.

$$Fe^0 + 2Fe^{3+} \rightarrow 3Fe^{2+} \qquad \text{(Reaction 1)}$$

Switching from organic solvents to aqueous solvents resulted in faster polymer growth and increased grafting thickness due to the large K_{ATRP} associated with aqueous conditions. However large concentrations (3 M) of monomer can be harmful to cells, therefore the concentration of 2-methacryloyloxyethyl phosphorylcholine (MPC) was decreased to 0.3 M, resulting in a decrease in reaction rate. Controlled growth of Poly(MPC) brushes was achieved from initiator bearing surfaces in the presence of primary articular chondrocyte (AC) cells. These ACs were cultured on the surface before polymerisation and their settlement was altered by the *in-situ* formation of polymer grafts whilst maintaining reasonable viability. This oxygen tolerant, biocompatible SI-ATRP system can be used to modify the physicochemical properties of cells without altering their viability which could be used in tissue engineering for manipulating the biological affinity of scaffolds towards a particular cell type. These methods also provide applications towards living materials, where-by an entanglement of polymer grafted brushes and cultured cells on a surface

could be influenced depending on the material, functionalities, environment, and cell type.

Engineered living material (ELM)s encompass biological engineering and material synthesis to create biohybrid devices or systems towards self-healing, bio responsive, self-growing or dynamic materials.[4] Examples include, living hydrogels loaded with engineered curli nanofibers which were able to grow and self-renew for applications towards gastrointestinal tissue repair.[119] Biological engineering of *E. coli* was also used to sense cobalt and Nickel contamination based on cellular uptake by triggering metal sequestering biofilm formation.[282] Many biological mechanisms are complex and still unknown which is a challenge for ELM development. Research into these mechanisms is therefore extremely important for advancing these technologies. In this thesis hypotheses are explored to evaluate the use of whole bacterial cells in polymer synthesis towards a variety of ELM applications. This thesis will explore possible mechanisms behind these and evaluate the challenges still present.

Conclusions and Motivations for Thesis

RDRP is an extremely useful tool for synthesizing complex materials for various applications in diagnostics, biosensors, antifouling, drug delivery and more. ATRP and RAFT are the most widely used methods and exploring the use of biological entities in these polymerisations may open a variety of applications towards biotic-abiotic interfaces like MIPS, cell surface modification, MFCs, ELMs etc. Various groups have used enzymes to catalyse polymerisation reactions in biologically benign conditions. As enzymes can be expensive and difficult to extract, whole cells might be a more convenient way to progress the field. Several examples have shown that cells are capable of metal reduction to catalyse ATRP and RAFT reactions.

The main aim of this thesis is to:

'Explore the application of bacterial redox processes to RDRP systems'

The thesis is comprised of 3 results chapters - Chapters 2, 3 and 4:

Chapter 2: Iron Catalysed Radical Polymerisation by Living Bacteria

Iron is a necessary nutrient of bacteria, present in many enzymes and displays relatively low toxicity to cells compared to other metals. Few studies have been conducted with Fe ATRP in biological conditions, necessitating the need for further development. After which, it would then be possible to test bacterial redox processes with Fe catalysts to drive a polymerisation, and to probe the parameters of the bacteria-instructed polymerisation. The aims of this chapter are therefore to:

- Develop a novel strategy to synthesise polymers using Fe catalysed ATRP under biological conditions
- Test Bacteria for Fe ATRP initiation
- Probe the parameters of bacterial-instructed Fe ATRP

Chapter 3: Bacterial Driven Fenton - GOx - RAFT Polymerisations

Where anoxic conditions are not available, commercial enzyme, GOx is also proven to tolerate air sensitive reactions. The combination of GOx and whole cells to drive Fenton RAFT polymerisations might enable polymer formation and a basis for future diagnostics in air. The aims of this chapter are to:

- Develop methods to conduct Fenton GOx RAFT polymerisations under biological conditions
- Apply bacteria to initiate Fenton GOx RAFT polymerisations

Chapter 4: Up-Regulation of Cytochrome-C Protein, NapC, in *E. coli*

The bacterium *Shewanella* contains an essential gene (*cymA*) an analogue of *napC* in *E. coli.* The purpose of this chapter was to observe whether *napC* could be cloned into vectors and if the corresponding protein NapC could be upregulated for further studies into NapC Fe reduction. The aims of this chapter are to:

- Clone *napC* into vectors and observe sequencing data
- Up-regulate NapC in *E. coli* and examine protein expression
- Analyse how upregulation of NapC effects Fe Reduction

References

1. Z. Liu, Y. Lv and Z. An, *Angew. Chem. Int. Ed. Engl.*, 2017, **56**, 13852-13856.
2. M. V. Dinu, M. Spulber, K. Renggli, D. Wu, C. A. Monnier, A. Petri-Fink and N. Bruns, *Macromol. Rapid Commun.*, 2015, **36**, 507-514.
3. S. Shoda, H. Uyama, J. Kadokawa, S. Kimura and S. Kobayashi, *Chem Rev*, 2016, **116**, 2307-2413.
4. P. Q. Nguyen, N. D. Courchesne, A. Duraj-Thatte, P. Praveschotinunt and N. S. Joshi, *Adv. Mater.*, 2018, **30**, e1704847.
5. J. Niu, D. J. Lunn, A. Pusuluri, J. I. Yoo, M. A. O'Malley, S. Mitragotri, H. T. Soh and C. J. Hawker, *Nat Chem*, 2017, **9**, 537-545.
6. E. P. Magennis, F. Fernandez-Trillo, C. Sui, S. G. Spain, D. J. Bradshaw, D. Churchley, G. Mantovani, K. Winzer and C. Alexander, *Nat Mater*, 2014, **13**, 748-755.
7. N. Idil and B. Mattiasson, *Sensors (Basel)*, 2017, **17**, 708.
8. A. B. Shori, *HAYATI Journal of Biosciences*, 2017, **24**, 1-5.
9. N. Schuergers, C. Werlang, C. M. Ajo-Franklin and A. A. Boghossian, *Energy Environ Sci*, 2017, **10**, 1102-1115.
10. R. B. Song, Y. Wu, Z. Q. Lin, J. Xie, C. H. Tan, J. S. C. Loo, B. Cao, J. R. Zhang, J. J. Zhu and Q. Zhang, *Angew. Chem. Int. Ed. Engl.*, 2017, **56**, 10516-10520.
11. M. J. Angelaalincy, R. Navanietha Krishnaraj, G. Shakambari, B. Ashokkumar, S. Kathiresan and P. Varalakshmi, *Frontiers in Energy Research*, 2018, **6**.
12. J. G. Wu, J. H. Chen, K. T. Liu and S. C. Luo, *ACS Appl Mater Interfaces*, 2019, **11**, 21294-21307.
13. R. M. Apetrei, G. Carac, A. Ramanaviciene, G. Bahrim, C. Tanase and A. Ramanavicius, *Colloids Surf B Biointerfaces*, 2019, **175**, 671-679.
14. B. D. Fairbanks, P. A. Gunatillake and L. Meagher, *Adv Drug Deliv Rev*, 2015, **91**, 141-152.
15. P. Gurnani and S. Perrier, *Prog. Polym. Sci.*, 2020, **102**, 101209.
16. D. J. Siegwart, J. K. Oh and K. Matyjaszewski, *Prog. Polym. Sci.*, 2012, **37**, 18-37.
17. H. G. Sherman, J. M. Hicks, A. Jain, J. J. Titman, C. Alexander, S. Stolnik and F. J. Rawson, *Chembiochem*, 2019, **20**, 1008-1013.
18. Y. Luo, Y. Gu, R. Feng, J. Brash, A. M. Eissa, D. M. Haddleton, G. Chen and H. Chen, *Chem Sci*, 2019, **10**, 5251-5257.
19. J. Geng, W. Li, Y. Zhang, N. Thottappillil, J. Clavadetscher, A. Lilienkampf and M. Bradley, *Nat Chem*, 2019, **11**, 578-586.
20. C. A. Custodio, R. L. Reis and J. F. Mano, *Adv Healthc Mater*, 2014, **3**, 797-810.
21. M. D. Nothling, H. Cao, T. G. McKenzie, D. M. Hocking, R. A. Strugnell and G. G. Qiao, *J. Am. Chem. Soc.*, 2020, DOI: 10.1021/jacs.0c10673.
22. J. Jagur-Grodzinski, *Polym. Adv. Technol.*, 2006, **17**, 395-418.
23. M. F. Maitz, *Biosurface and Biotribology*, 2015, **1**, 161-176.

24. B. D. Ulery, L. S. Nair and C. T. Laurencin, *J Polym Sci B Polym Phys*, 2011, **49**, 832-864.
25. K. Matyjaszewski, *Macromolecules*, 2012, **45**, 4015-4039.
26. A. George, P. A. Shah and P. S. Shrivastav, *Int. J. Pharm.*, 2019, **561**, 244-264.
27. A. Bordat, T. Boissenot, J. Nicolas and N. Tsapis, *Adv Drug Deliv Rev*, 2019, **138**, 167-192.
28. F. di Lena and K. Matyjaszewski, *Progress in Polymer Science*, 2010, **35**, 959-1021.
29. M. Fantin, A. A. Isse, A. Gennaro and K. Matyjaszewski, *Macromolecules*, 2015, **48**, 6862-6875.
30. R. Whitfield, A. Anastasaki, V. Nikolaou, G. R. Jones, N. G. Engelis, E. H. Discekici, C. Fleischmann, J. Willenbacher, C. J. Hawker and D. M. Haddleton, *J. Am. Chem. Soc.*, 2017, **139**, 1003-1010.
31. J.-S. Wang and K. Matyjaszewski, *Journal of the American Chemical Society*, 1995, **117**, 5614-5615.
32. J. Qiu, B. Charleux and K. Matyjaszewski, *Prog. Polym. Sci.*, 2001, **26**, 2083-2134.
33. V. Coessens, T. Pintauer and K. Matyjaszewski, *Progress in Polymer Science*, 2001, **26**, 337-377.
34. C. Boyer, N. A. Corrigan, K. Jung, D. Nguyen, T. K. Nguyen, N. N. Adnan, S. Oliver, S. Shanmugam and J. Yeow, *Chem Rev*, 2016, **116**, 1803-1949.
35. S. Antonina Alekseyevna, *Development of Aqueous ATRP for Biomedical Applications*, 2015.
36. H. Fischer, *Chem Rev*, 2001, **101**, 3581-3610.
37. C. H. Liao and L. M. Shollenberger, *Lett. Appl. Microbiol.*, 2003, **37**, 45-50.
38. H. Bergenudd, G. Coullerez, M. Jonsson and E. Malmström, *Macromolecules*, 2009, **42**, 3302-3308.
39. N. V. Tsarevsky, T. Pintauer and K. Matyjaszewski, *Macromolecules*, 2004, **37**, 9768-9778.
40. M. Mertoglu, A. Laschewsky, K. Skrabania and C. Wieland, *Macromolecules*, 2005, **38**, 3601-3614.
41. W. Jakubowski and K. Matyjaszewski, *Macromolecules*, 2005, **38**, 4139-4146.
42. T. G. Ribelli, F. Lorandi, M. Fantin and K. Matyjaszewski, *Macromol. Rapid Commun.*, 2019, **40**, e1800616.
43. L. Mueller and K. Matyjaszewski, *Macromolecular Reaction Engineering*, 2010, **4**, 180-185.
44. K. Matyjaszewski, W. Jakubowski, K. Min, W. Tang, J. Huang, W. A. Braunecker and N. V. Tsarevsky, *Proc Natl Acad Sci U S A*, 2006, **103**, 15309-15314.
45. N. V. Tsarevsky and K. Matyjaszewski, *Chem Rev*, 2007, **107**, 2270-2299.
46. Z. Xue, D. He and X. Xie, *Polymer Chemistry*, 2015, **6**, 1660-1687.
47. A. Simakova, M. Mackenzie, S. E. Averick, S. Park and K. Matyjaszewski, *Angew. Chem. Int. Ed. Engl.*, 2013, **52**, 12148-12151.

48. L. Fu, A. Simakova, S. Park, Y. Wang, M. Fantin and K. Matyjaszewski, *Molecules*, 2019, **24**, 3969.
49. S. Dadashi-Silab and K. Matyjaszewski, *Molecules*, 2020, **25**.
50. H. Bergenudd, M. Jonsson and E. Malmström, *J. Mol. Catal. A: Chem.*, 2011, **346**, 20-28.
51. M. Y. Khan, J. Zhou, X. Chen, A. Khan, H. Mudassir, Z. Xue, S. W. Lee and S. K. Noh, *Polymer*, 2016, **90**, 309-316.
52. R. K. O'Reilly, V. C. Gibson, A. J. P. White and D. J. Williams, *Polyhedron*, 2004, **23**, 2921-2928.
53. M. P. Shaver, L. E. N. Allan and V. C. Gibson, *Organometallics*, 2007, **26**, 4725-4730.
54. R. Poli and M. P. Shaver, *Inorg. Chem.*, 2014, **53**, 7580-7590.
55. M. Ouchi and M. Sawamoto, *Macromolecules*, 2017, **50**, 2603-2614.
56. M. Teodorescu and K. Matyjaszewski, *Macromolecules*, 1999, **32**, 4826-4831.
57. M. Rolland, N. P. Truong, R. Whitfield and A. Anastasaki, *ACS Macro Letters*, 2020, **9**, 459-463.
58. G. J. Britovsek, J. England and A. J. White, *Inorg. Chem.*, 2005, **44**, 8125-8134.
59. L. E. N. Allan, J. P. MacDonald, G. S. Nichol and M. P. Shaver, *Macromolecules*, 2014, **47**, 1249-1257.
60. C. Uchiike, T. Terashima, M. Ouchi, T. Ando, M. Kamigaito and M. Sawamoto, *Macromolecules*, 2007, **40**, 8658-8662.
61. J. Miao, W. He, L. Zhang, Y. Wang, Z. Cheng and X. Zhu, *Journal of Polymer Science, Part A: Polymer Chemistry*, 2012, **50**, 2194-2200.
62. Y. Wang, Y. Kwak and K. Matyjaszewski, *Macromolecules*, 2012, **45**, 5911-5915.
63. Z. Xue, B. W. Lee, S. K. Noh and W. S. Lyoo, *Polymer*, 2007, **48**, 4704-4714.
64. Z. Xue, D. He, S. K. Noh and W. S. Lyoo, *Macromolecules*, 2009, **42**, 2949-2957.
65. C. Bian, Y.-N. Zhou, J.-K. Guo and Z.-H. Luo, *Polymer Chemistry*, 2017, **8**, 7360-7368.
66. J. D. Walker and R. Poli, *Inorganic Chemistry*, 1989, **28**, 1793-1801.
67. W. Jakubowski and K. Matyjaszewski, *Angew. Chem. Int. Ed. Engl.*, 2006, **45**, 4482-4486.
68. R. Luo and A. Sen, *Macromolecules*, 2008, **41**, 4514-4518.
69. L. Zhang, Z. Cheng, S. Shi, Q. Li and X. Zhu, *Polymer*, 2008, **49**, 3054-3059.
70. L. Zhang, Z. Cheng, Z. Zhang, D. Xu and X. Zhu, *Polymer Bulletin*, 2009, **64**, 233.
71. T. Guo, L. Zhang, H. Jiang, Z. Zhang, J. Zhu, Z. Cheng and X. Zhu, *Polymer Chemistry*, 2011, **2**, 2385.
72. Y. Wang, L. Bai, W. Chen, L. Chen, Y. Liu, T. Xu and Z. Cheng, *Polymer Bulletin*, 2013, **70**, 631-642.
73. Y. H. Ng, F. di Lena and C. L. Chai, *Chem Commun (Camb)*, 2011, **47**, 6464-6466.

74. W. He, L. Zhang, J. Miao, Z. Cheng and X. Zhu, *Macromol. Rapid Commun.*, 2012, **33**, 1067-1073.
75. A. E. Enciso, L. Fu, A. J. Russell and K. Matyjaszewski, *Angew. Chem. Int. Ed. Engl.*, 2018, **57**, 933-936.
76. J. Chiefari, Y. Chong, F. Ercole, J. Krstina, J. Jeffery, T. P. Le, R. T. Mayadunne, G. F. Meijs, C. L. Moad and G. Moad, *Macromolecules*, 1998, **31**, 5559-5562.
77. S. Perrier, *Macromolecules*, 2017, **50**, 7433-7447.
78. J. Tan, Q. Xu, X. Li, J. He, Y. Zhang, X. Dai, L. Yu, R. Zeng and L. Zhang, *Macromol. Rapid Commun.*, 2018, **39**, e1700871.
79. J. Rieger, *Macromol. Rapid Commun.*, 2015, **36**, 1458-1471.
80. L. Barner, C. Barner-Kowollik, T. P. Davis and M. H. Stenzel, *Aust. J. Chem.*, 2004, **57**, 19-24.
81. C. Boyer, V. Bulmus, T. P. Davis, V. Ladmiral, J. Liu and S. Perrier, *Chem Rev*, 2009, **109**, 5402-5436.
82. C. Xian, Q. Yuan, Z. Bao, G. Liu and J. Wu, *Chin. Chem. Lett.*, 2020, **31**, 19-27.
83. X. Huang, J. Hu, Y. Li, F. Xin, R. Qiao and T. P. Davis, *Biomacromolecules*, 2019, **20**, 4243-4257.
84. K. Matyjaszewski, *Macromolecules*, 2020, **53**, 495-497.
85. L. D. Blackman, K. E. B. Doncom, M. I. Gibson and R. K. O'Reilly, *Polym Chem*, 2017, **8**, 2860-2871.
86. Y. Lv, Z. Liu, A. Zhu and Z. An, *J. Polym. Sci., Part A: Polym. Chem.*, 2017, **55**, 164-174.
87. Y. Shi, H. Gao, L. Lu and Y. Cai, *Chem Commun (Camb)*, 2009, DOI: 10.1039/b821486g, 1368-1370.
88. A. Sanchez-Sanchez, I. Asenjo-Sanz, L. Buruaga and J. A. Pomposo, *Macromol. Rapid Commun.*, 2012, **33**, 1262-1267.
89. D. J. Keddie, G. Moad, E. Rizzardo and S. H. Thang, *Macromolecules*, 2012, **45**, 5321-5342.
90. G. Moad, E. Rizzardo and S. H. Thang, *Chem Asian J*, 2013, **8**, 1634-1644.
91. A. W. York, S. E. Kirkland and C. L. McCormick, *Adv Drug Deliv Rev*, 2008, **60**, 1018-1036.
92. Q. Xiong, X. Zhang, W. Wei, G. Wei and Z. Su, *Polymer Chemistry*, 2020, **11**, 1673-1690.
93. A. Reyhani, T. G. McKenzie, H. Ranji-Burachaloo, Q. Fu and G. G. Qiao, *Chemistry*, 2017, **23**, 7221-7226.
94. A. Reyhani, H. Ranji-Burachaloo, T. G. McKenzie, Q. Fu and G. G. Qiao, *Macromolecules*, 2019, **52**, 3278-3287.
95. A. Reyhani, T. G. McKenzie, Q. Fu and G. G. Qiao, *Macromol. Rapid Commun.*, 2019, **40**, e1900220.
96. C. M. Wong, K. H. Wong and X. D. Chen, *Appl. Microbiol. Biotechnol.*, 2008, **78**, 927-938.
97. H. Iwata, Y. Hata, T. Matsuda, W. Taki, Y. Yonekawa and Y. Ikada, *Biomaterials*, 1992, **13**, 891-896.

98. A. Reyhani, M. D. Nothling, H. Ranji-Burachaloo, T. G. McKenzie, Q. Fu, S. Tan, G. Bryant and G. G. Qiao, *Angew. Chem. Int. Ed. Engl.*, 2018, **57**, 10288-10292.
99. X. Wang, S. Chen, D. Wu, Q. Wu, Q. Wei, B. He, Q. Lu and Q. Wang, *Adv. Mater.*, 2018, **30**, e1705668.
100. P. R. Kommoju, Z. W. Chen, R. C. Bruckner, F. S. Mathews and M. S. Jorns, *Biochemistry*, 2011, **50**, 5521-5534.
101. A. Reyhani, T. G. McKenzie, Q. Fu and G. G. Qiao, *Aust. J. Chem.*, 2019, **72**, 479-489.
102. F. H. Arnold, *Angew. Chem. Int. Ed. Engl.*, 2019, **58**, 14420-14426.
103. G. C. Brown, *Biochem. J*, 1992, **284 (Pt 1)**, 1-13.
104. J. Liu, S. Chakraborty, P. Hosseinzadeh, Y. Yu, S. Tian, I. Petrik, A. Bhagi and Y. Lu, *Chem Rev*, 2014, **114**, 4366-4469.
105. C. Zhang, *Genome Integr*, 2015, **6**, 2.
106. P. Chandrangsu, C. Rensing and J. D. Helmann, *Nat Rev Microbiol*, 2017, **15**, 338-350.
107. A. Pinochet-Barros and J. D. Helmann, *Antioxid Redox Signal*, 2018, **29**, 1858-1871.
108. I. Schroder, E. Johnson and S. de Vries, *FEMS Microbiol. Rev.*, 2003, **27**, 427-447.
109. S. C. Andrews, A. K. Robinson and F. Rodriguez-Quinones, *FEMS Microbiol. Rev.*, 2003, **27**, 215-237.
110. C. M. Waters and B. L. Bassler, *Annu. Rev. Cell Dev. Biol.*, 2005, **21**, 319-346.
111. J. A. Gralnick and D. K. Newman, *Mol. Microbiol.*, 2007, **65**, 1-11.
112. S. Kato, *Microbes Environ*, 2015, **30**, 133-139.
113. Y. Jiang, M. Shi and L. Shi, *Sci China Life Sci*, 2019, **62**, 1275-1286.
114. Y. Xiao, E. Zhang, J. Zhang, Y. Dai, Z. Yang, H. E. M. Christensen, J. Ulstrup and F. Zhao, *Sci Adv*, 2017, **3**, e1700623.
115. J. Pollard, O. Rifaie-Graham, S. Raccio, A. Davey, S. Balog and N. Bruns, *Anal. Chem.*, 2020, **92**, 1162-1170.
116. J. Pollard and N. Bruns, in *Reversible Deactivation Radical Polymerization: Mechanisms and Synthetic Methodologies*, American Chemical Society, 2018, vol. 1284, ch. 19, pp. 379-393.
117. L. C. Recco, I. Tokarev, S. Minko and V. A. Pedrosa, *Chemistry*, 2014, **20**, 1226-1230.
118. R.-B. Song, K. Yan, Z.-Q. Lin, J. S. Chye Loo, L.-J. Pan, Q. Zhang, J.-R. Zhang and J.-J. Zhu, *Journal of Materials Chemistry A*, 2016, **4**, 14555-14559.
119. A. M. Duraj-Thatte, N. D. Courchesne, P. Praveschotinunt, J. Rutledge, Y. Lee, J. M. Karp and N. S. Joshi, *Adv. Mater.*, 2019, **31**, e1901826.
120. D. R. Lovley, *ASM News*, 2002, **68**, 231-237.
121. Y. Roh, S. V. Liu, G. Li, H. Huang, T. J. Phelps and J. Zhou, *Appl. Environ. Microbiol.*, 2002, **68**, 6013-6020.
122. D. R. Lovley, *Annu Rev Microbiol*, 1993, **47**, 263-290.
123. D. R. Lovley and E. J. Phillips, *Appl. Environ. Microbiol.*, 1988, **54**, 1472-1480.

124. J. Buongiorno, L. C. Herbert, L. M. Wehrmann, A. B. Michaud, K. Laufer, H. Roy, B. B. Jorgensen, A. Szynkiewicz, A. Faiia, K. M. Yeager, K. Schindler and K. G. Lloyd, *Appl. Environ. Microbiol.*, 2019, **85**, e00949-00919.
125. V. Coman, T. Gustavsson, A. Finkelsteinas, C. von Wachenfeldt, C. Hagerhall and L. Gorton, *J. Am. Chem. Soc.*, 2009, **131**, 16171-16176.
126. D. Keogh, L. N. Lam, L. E. Doyle, A. Matysik, S. Pavagadhi, S. Umashankar, P. M. Low, J. L. Dale, Y. Song, S. P. Ng, C. B. Boothroyd, G. M. Dunny, S. Swarup, R. B. H. Williams, E. Marsili and K. A. Kline, *mBio*, 2018, **9**, e00626-00617.
127. S. H. Light, L. Su, R. Rivera-Lugo, J. A. Cornejo, A. Louie, A. T. Iavarone, C. M. Ajo-Franklin and D. A. Portnoy, *Nature*, 2018, **562**, 140-144.
128. H. K. Carlson, A. T. Iavarone, A. Gorur, B. S. Yeo, R. Tran, R. A. Melnyk, R. A. Mathies, M. Auer and J. D. Coates, *Proc Natl Acad Sci U S A*, 2012, **109**, 1702-1707.
129. M. Shi, Y. Jiang and L. Shi, *Science China Technological Sciences*, 2019, **62**, 1670-1678.
130. S. T. Lohner, J. S. Deutzmann, B. E. Logan, J. Leigh and A. M. Spormann, *ISME J*, 2014, **8**, 1673-1681.
131. L. J. C. Jeuken, K. Hards and Y. Nakatani, *J. Bacteriol.*, 2020, **202**, e00029-00020.
132. C. Santoro, C. Arbizzani, B. Erable and I. Ieropoulos, *J. Power Sources*, 2017, **356**, 225-244.
133. L. Zou, Y. H. Huang, Z. E. Long and Y. Qiao, *World J. Microbiol. Biotechnol.*, 2018, **35**, 9.
134. T. Mehta, M. V. Coppi, S. E. Childers and D. R. Lovley, *Appl. Environ. Microbiol.*, 2005, **71**, 8634-8641.
135. A. S. Beliaev, D. A. Saffarini, J. L. McLaughlin and D. Hunnicutt, *Mol. Microbiol.*, 2001, **39**, 722-730.
136. L. Shi, H. Dong, G. Reguera, H. Beyenal, A. Lu, J. Liu, H. Q. Yu and J. K. Fredrickson, *Nat Rev Microbiol*, 2016, **14**, 651-662.
137. J. W. Allen, O. Daltrop, J. M. Stevens and S. J. Ferguson, *Philos Trans R Soc Lond B Biol Sci*, 2003, **358**, 255-266.
138. S. T. Gabilly and P. P. Hamel, *Front Plant Sci*, 2017, **8**, 1313.
139. L. Shi, K. M. Rosso, J. M. Zachara and J. K. Fredrickson, *Biochem. Soc. Trans.*, 2012, **40**, 1261-1267.
140. K. Zargar and C. W. Saltikov, *Arch. Microbiol.*, 2009, **191**, 797-806.
141. C. R. Myers and J. M. Myers, *J. Bacteriol.*, 1997, **179**, 1143-1152.
142. L. Shi, K. M. Rosso, T. A. Clarke, D. J. Richardson, J. M. Zachara and J. K. Fredrickson, *Front Microbiol*, 2012, **3**, 50.
143. P. Subramanian, S. Pirbadian, M. Y. El-Naggar and G. J. Jensen, *Proc Natl Acad Sci U S A*, 2018, **115**, E3246-E3255.
144. S. Xu, Y. Jangir and M. Y. El-Naggar, *Electrochim. Acta*, 2016, **198**, 49-55.
145. S. Pirbadian, S. E. Barchinger, K. M. Leung, H. S. Byun, Y. Jangir, R. A. Bouhenni, S. B. Reed, M. F. Romine, D. A. Saffarini, L. Shi, Y. A. Gorby, J. H. Golbeck and M. Y. El-Naggar, *Proc Natl Acad Sci U S A*, 2014, **111**, 12883-12888.

146. D. R. Lovley and D. J. F. Walker, *Front Microbiol*, 2019, **10**, 2078.
147. D. J. Walker, R. Y. Adhikari, D. E. Holmes, J. E. Ward, T. L. Woodard, K. P. Nevin and D. R. Lovley, *ISME J*, 2018, **12**, 48-58.
148. N. S. Malvankar, M. T. Tuominen and D. R. Lovley, *Energy & Environmental Science*, 2012, **5**, 8651-8659.
149. D. R. Lovley, *Annu Rev Microbiol*, 2012, **66**, 391-409.
150. C. Shu, Q. Zhu, K. Xiao, Y. Hou, H. Ma, J. Ma and X. Sun, *Biomed Res Int*, 2019, **2019**, 6151587.
151. S. A. Zaidi, *Crit. Rev. Anal. Chem.*, 2020, DOI: 10.1080/10408347.2020.1755822, 1-10.
152. H. C. Flemming, J. Wingender, U. Szewzyk, P. Steinberg, S. A. Rice and S. Kjelleberg, *Nat Rev Microbiol*, 2016, **14**, 563-575.
153. H. C. Flemming, T. R. Neu and D. J. Wozniak, *J. Bacteriol.*, 2007, **189**, 7945-7947.
154. W. Yin, Y. Wang, L. Liu and J. He, *International Journal of Molecular Sciences*, 2019, **20**, 3423.
155. A. Sarjit, S. Mei Tan and G. A. Dykes, *AIMS Bioengineering*, 2015, **2**, 404-422.
156. Y. Huang, S. Chakraborty and H. Liang, *Analytical Methods*, 2020, **12**, 416-432.
157. S. Hogan, E. Kasotakis, S. Maher, B. Cavanagh, J. P. O'Gara, A. Pandit, T. E. Keyes, M. Devocelle and E. O'Neill, *FEMS Microbiol. Lett.*, 2019, **366**.
158. P. S. Murthy and R. Venkatesan, in *Marine and Industrial Biofouling*, eds. H.-C. Flemming, P. S. Murthy, R. Venkatesan and K. Cooksey, Springer Berlin Heidelberg, Berlin, Heidelberg, 2009, DOI: 10.1007/978-3-540-69796-1_4, ch. Chapter 4, pp. 65-101.
159. T. Bottcher, I. Kolodkin-Gal, R. Kolter, R. Losick and J. Clardy, *J. Am. Chem. Soc.*, 2013, **135**, 2927-2930.
160. V. B. Damodaran and N. S. Murthy, *Biomater Res*, 2016, **20**, 18.
161. B. Gao, X. Zhu, C. Xu, Q. Yue, W. Li and J. Wei, *Journal of Chemical Technology & Biotechnology*, 2008, **83**, 227-232.
162. L. H. Hsu, Y. Zhang, P. Deng, X. Dai and X. Jiang, *Nano Lett.*, 2019, **19**, 8787-8792.
163. S. S. Branda, S. Vik, L. Friedman and R. Kolter, *Trends Microbiol*, 2005, **13**, 20-26.
164. E. S. Gloag, S. Fabbri, D. J. Wozniak and P. Stoodley, *Biofilm*, 2020, **2**, 100017.
165. N. Hoiby, T. Bjarnsholt, M. Givskov, S. Molin and O. Ciofu, *Int J Antimicrob Agents*, 2010, **35**, 322-332.
166. S. T. Rutherford and B. L. Bassler, *Cold Spring Harb Perspect Med*, 2012, **2**.
167. P. K. Singh, A. L. Schaefer, M. R. Parsek, T. O. Moninger, M. J. Welsh and E. P. Greenberg, *Nature*, 2000, **407**, 762-764.
168. M. E. Hernandez and D. K. Newman, *Cell Mol Life Sci*, 2001, **58**, 1562-1571.
169. S. Marić and J. Vranes, *Periodicum Biologorum*, 2007, **109**, 115-121.

170. I. Francolini, G. Donelli, F. Crisante, V. Taresco and A. Piozzi, in *Biofilm-based Healthcare-associated Infections: Volume II*, ed. G. Donelli, Springer International Publishing, Cham, 2015, DOI: 10.1007/978-3-319-09782-4_7, pp. 93-117.
171. A. K. Leonardi and C. K. Ober, *Annu Rev Chem Biomol Eng*, 2019, **10**, 241-264.
172. C. Zhao and J. Zheng, *Biomacromolecules*, 2011, **12**, 4071-4079.
173. L. T. Lui, X. Xue, C. Sui, A. Brown, D. I. Pritchard, N. Halliday, K. Winzer, S. M. Howdle, F. Fernandez-Trillo, N. Krasnogor and C. Alexander, *Nat Chem*, 2013, **5**, 1058-1065.
174. L. Ma, S. Feng, C. Fuente-Nunez, R. E. W. Hancock and X. Lu, *ACS Appl Mater Interfaces*, 2018, **10**, 18450-18457.
175. L. Liu, W. Li and Q. Liu, *Wiley Interdiscip Rev Nanomed Nanobiotechnol*, 2014, **6**, 599-614.
176. H. Wu, C. J. Lee, H. Wang, Y. Hu, M. Young, Y. Han, F. J. Xu, H. Cong and G. Cheng, *Chem Sci*, 2018, **9**, 2540-2546.
177. S. V. V. S. N. P and S. V. V. S. P, *Regenerative Engineering and Translational Medicine*, 2019, **6**, 330-346.
178. G. Brackman, P. Cos, L. Maes, H. J. Nelis and T. Coenye, *Antimicrob. Agents Chemother.*, 2011, **55**, 2655-2661.
179. N. Perez-Soto, L. Moule, D. N. Crisan, I. Insua, L. M. Taylor-Smith, K. Voelz, F. Fernandez-Trillo and A. M. Krachler, *Chem Sci*, 2017, **8**, 5291-5298.
180. X. Xue, G. Pasparakis, N. Halliday, K. Winzer, S. M. Howdle, C. J. Cramphorn, N. R. Cameron, P. M. Gardner, B. G. Davis, F. Fernandez-Trillo and C. Alexander, *Angew. Chem. Int. Ed. Engl.*, 2011, **50**, 9852-9856.
181. J. U. Kreft and J. W. Wimpenny, *Water Sci. Technol.*, 2001, **43**, 135-141.
182. Y. Hindatu, M. S. M. Annuar and A. M. Gumel, *Renewable and Sustainable Energy Reviews*, 2017, **73**, 236-248.
183. L. Hao, B. Zhang, M. Cheng and C. Feng, *Bioresour. Technol.*, 2016, **201**, 105-110.
184. J. Yang, M. Zhou, Y. Zhao, C. Zhang and Y. Hu, *Bioresour. Technol.*, 2013, **150**, 271-277.
185. M. Li, M. Zhou, X. Tian, C. Tan, C. T. McDaniel, D. J. Hassett and T. Gu, *Biotechnol. Adv.*, 2018, **36**, 1316-1327.
186. D. F. Juang, P. C. Yang, H. Y. Chou and L. J. Chiu, *Biotechnol. Lett*, 2011, **33**, 2147-2160.
187. A. J. Slate, K. A. Whitehead, D. A. C. Brownson and C. E. Banks, *Renewable and Sustainable Energy Reviews*, 2019, **101**, 60-81.
188. A. Kumar, L. H.-H. Hsu, P. Kavanagh, F. Barrière, P. N. L. Lens, L. Lapinsonnière, J. H. Lienhard V, U. Schröder, X. Jiang and D. Leech, *Nature Reviews Chemistry*, 2017, **1**, 0024.
189. G. Reguera, K. P. Nevin, J. S. Nicoll, S. F. Covalla, T. L. Woodard and D. R. Lovley, *Appl. Environ. Microbiol.*, 2006, **72**, 7345-7348.
190. A. Baudler, I. Schmidt, M. Langner, A. Greiner and U. Schröder, *Energy & Environmental Science*, 2015, **8**, 2048-2055.

191. H. Ren, S. Pyo, J.-I. Lee, T.-J. Park, F. S. Gittleson, F. C. C. Leung, J. Kim, A. D. Taylor, H.-S. Lee and J. Chae, *J. Power Sources*, 2015, **273**, 823-830.
192. N. Thepsuparungsikul, T. C. Ng, O. Lefebvre and H. Y. Ng, *Water Sci. Technol.*, 2014, **69**, 1900-1910.
193. A. Mehdinia, E. Ziaei and A. Jabbari, *Int. J. Hydrogen Energy*, 2014, **39**, 10724-10730.
194. Y. L. Kang, S. Pichiah and S. Ibrahim, *Int. J. Hydrogen Energy*, 2017, **42**, 1661-1671.
195. Y. Yuan, H. Shin, C. Kang and S. Kim, *Bioelectrochemistry*, 2016, **108**, 8-12.
196. Y. S. Xu, T. Zheng, X. Y. Yong, D. D. Zhai, R. W. Si, B. Li, Y. Y. Yu and Y. C. Yong, *Bioresour. Technol.*, 2016, **211**, 542-547.
197. X. Y. Yong, D. Y. Shi, Y. L. Chen, J. Feng, L. Xu, J. Zhou, S. Y. Wang, Y. C. Yong, Y. M. Sun, P. K. OuYang and T. Zheng, *Bioresour. Technol.*, 2014, **152**, 220-224.
198. D. Min, L. Cheng, F. Zhang, X. N. Huang, D. B. Li, D. F. Liu, T. C. Lau, Y. Mu and H. Q. Yu, *Environ. Sci. Technol.*, 2017, **51**, 5082-5089.
199. J. Liu, Y. Qiao, Z. S. Lu, H. Song and C. M. Li, *Electrochem. Commun.*, 2012, **15**, 50-53.
200. J. Luo, J. Yang, H. He, T. Jin, L. Zhou, M. Wang and M. Zhou, *Bioresour. Technol.*, 2013, **139**, 141-148.
201. H. Hou, X. Chen, A. W. Thomas, C. Catania, N. D. Kirchhofer, L. E. Garner, A. Han and G. C. Bazan, *Adv. Mater.*, 2013, **25**, 1593-1597.
202. L. E. Garner, J. Park, S. M. Dyar, A. Chworos, J. J. Sumner and G. C. Bazan, *J. Am. Chem. Soc.*, 2010, **132**, 10042-10052.
203. N. D. Kirchhofer, X. Chen, E. Marsili, J. J. Sumner, F. W. Dahlquist and G. C. Bazan, *Phys. Chem. Chem. Phys.*, 2014, **16**, 20436-20443.
204. M. Kaneko, K. Ishihara and S. Nakanishi, *Small*, 2020, **16**, e2001849.
205. A. Kisieliute, A. Popov, R.-M. Apetrei, G. Cârâc, I. Morkvenaite-Vilkonciene, A. Ramanaviciene and A. Ramanavicius, *Chem. Eng. J.*, 2019, **356**, 1014-1021.
206. K. Hasan, S. A. Patil, D. Leech, C. Hagerhall and L. Gorton, *Biochem. Soc. Trans.*, 2012, **40**, 1330-1335.
207. K. Nishio, R. Nakamura, X. Lin, T. Konno, K. Ishihara, S. Nakanishi and K. Hashimoto, *Chemphyschem*, 2013, **14**, 2159-2163.
208. M. Kaneko, M. Ishikawa, K. Hashimoto and S. Nakanishi, *Bioelectrochemistry*, 2017, **114**, 8-12.
209. F. J. Rawson, A. J. Downard and K. H. Baronian, *Sci Rep*, 2014, **4**, 5216.
210. Y. Lu, K. Nishio, S. Matsuda, Y. Toshima, H. Ito, T. Konno, K. Ishihara, S. Kato, K. Hashimoto and S. Nakanishi, *Angew. Chem. Int. Ed. Engl.*, 2014, **53**, 2208-2211.
211. T. R. Sandrin and D. R. Hoffman, in *Environmental Bioremediation Technologies*, eds. S. N. Singh and R. D. Tripathi, Springer Berlin Heidelberg, Berlin, Heidelberg, 2007, DOI: 10.1007/978-3-540-34793-4_1, ch. Chapter 1, pp. 1-34.
212. P. Monsieurs, H. Moors, R. Van Houdt, P. J. Janssen, A. Janssen, I. Coninx, M. Mergeay and N. Leys, *Biometals*, 2011, **24**, 1133-1151.

213. I. Llorens, G. Untereiner, D. Jaillard, B. Gouget, V. Chapon and M. Carriere, *PLoS One*, 2012, **7**, e51783.
214. L. Fairbrother, B. Etschmann, J. Brugger, J. Shapter, G. Southam and F. Reith, *Environ. Sci. Technol.*, 2013, **47**, 2628-2635.
215. F. Reith, B. Etschmann, C. Grosse, H. Moors, M. A. Benotmane, P. Monsieurs, G. Grass, C. Doonan, S. Vogt, B. Lai, G. Martinez-Criado, G. N. George, D. H. Nies, M. Mergeay, A. Pring, G. Southam and J. Brugger, *Proc Natl Acad Sci U S A*, 2009, **106**, 17757-17762.
216. N. Wiesemann, L. Butof, M. Herzberg, G. Hause, L. Berthold, B. Etschmann, J. Brugger, G. Martinez-Criado, D. Dobritzsch, S. Baginsky, F. Reith and D. H. Nies, *Appl. Environ. Microbiol.*, 2017, **83**, e01679-01617.
217. L. Butof, N. Wiesemann, M. Herzberg, M. Altzschner, A. Holleitner, F. Reith and D. H. Nies, *Metallomics*, 2018, **10**, 278-286.
218. G. Fan, C. M. Dundas, A. J. Graham, N. A. Lynd and B. K. Keitz, *Shewanella oneidensis as a living electrode for controlled radical polymerization*, 2018.
219. R. E. Cowart, *Arch. Biochem. Biophys.*, 2002, **400**, 273-281.
220. B. M. Appenzeller, C. Yanez, F. Jorand and J. C. Block, *Appl. Environ. Microbiol.*, 2005, **71**, 5621-5623.
221. J. S. Gescher, C. D. Cordova and A. M. Spormann, *Mol. Microbiol.*, 2008, **68**, 706-719.
222. P. M. J. Burgers and T. A. Kunkel, *Annu. Rev. Biochem*, 2017, **86**, 417-438.
223. K. J. Rodriguez, B. Gajewska, J. Pollard, M. M. Pellizzoni, C. Fodor and N. Bruns, *ACS Macro Letters*, 2018, **7**, 1111-1119.
224. H. Zhou, W. Jiang, N. An, Q. Zhang, S. Xiang, L. Wang and J. Tang, *RSC Advances*, 2015, **5**, 42728-42735.
225. Y.-H. Ng, F. di Lena and C. L. L. Chai, *Polymer Chemistry*, 2011, **2**, 589-594.
226. S. Raccio, J. Pollard, A. Djuhadi, S. Balog, M. M. Pellizzoni, K. J. Rodriguez, O. Rifaie-Graham and N. Bruns, *Analyst*, 2020, **145**, 7741-7751.
227. K. Renggli, M. Spulber, J. Pollard, M. Rother and N. Bruns, in *Green Polymer Chemistry: Biocatalysis and Materials II*, American Chemical Society, 2013, vol. 1144, ch. 12, pp. 163-171.
228. G. Kali, T. B. Silva, S. J. Sigg, F. Seidi, K. Renggli and N. Bruns, in *Progress in Controlled Radical Polymerization: Mechanisms and Techniques*, American Chemical Society, 2012, vol. 1100, ch. 11, pp. 171-181.
229. G. Gao, M. A. Karaaslan, J. F. Kadla and F. Ko, *Green Chem.*, 2014, **16**, 3890-3898.
230. S. J. Sigg, F. Seidi, K. Renggli, T. B. Silva, G. Kali and N. Bruns, *Macromol. Rapid Commun.*, 2011, **32**, 1710-1715.
231. T. B. Silva, M. Spulber, M. K. Kocik, F. Seidi, H. Charan, M. Rother, S. J. Sigg, K. Renggli, G. Kali and N. Bruns, *Biomacromolecules*, 2013, **14**, 2703-2712.
232. Y.-H. Ng, F. di Lena and C. L. L. Chai, *Polym. Chem.*, 2011, **2**, 589-594.

233. C. Fodor, B. Gajewska, O. Rifaie-Graham, E. A. Apebende, J. Pollard and N. Bruns, *Polymer Chemistry*, 2016, **7**, 6617-6625.
234. S. Averick, A. Simakova, S. Park, D. Konkolewicz, A. J. D. Magenau, R. A. Mehl and K. Matyjaszewski, *ACS Macro Letters*, 2011, **1**, 6-10.
235. L. D. Blackman, S. Varlas, M. C. Arno, A. Fayter, M. I. Gibson and R. K. O'Reilly, *ACS Macro Lett*, 2017, **6**, 1263-1267.
236. M. Zhang and W. Zhang, *J. Polym. Sci., Part A: Polym. Chem.*, 2010, **48**, 5446-5455.
237. D. M. Scheibel and I. Gitsov, *Biomacromolecules*, 2019, **20**, 927-936.
238. K. Renggli, N. Sauter, M. Rother, M. G. Nussbaumer, R. Urbani, T. Pfohl and N. Bruns, *Polymer Chemistry*, 2017, **8**, 2133-2136.
239. M. Nallani, H. P. de Hoog, J. J. Cornelissen, A. R. Palmans, J. C. van Hest and R. J. Nolte, *Biomacromolecules*, 2007, **8**, 3723-3728.
240. B. Zhang, X. Wang, A. Zhu, K. Ma, Y. Lv, X. Wang and Z. An, *Macromolecules*, 2015, **48**, 7792-7802.
241. A. P. Danielson, D. Bailey-Van Kuren, M. E. Lucius, K. Makaroff, C. Williams, R. C. Page, J. A. Berberich and D. Konkolewicz, *Macromol. Rapid Commun.*, 2016, **37**, 362-367.
242. Z. Liu, Y. Lv, A. Zhu and Z. An, *ACS Macro Letters*, 2017, **7**, 1-6.
243. A. P. Danielson, D. B. Van-Kuren, J. P. Bornstein, C. T. Kozuszek, J. A. Berberich, R. C. Page and D. Konkolewicz, *Polymers*, 2018, **10**, 741.
244. G. I. Berglund, G. H. Carlsson, A. T. Smith, H. Szoke, A. Henriksen and J. Hajdu, *Nature*, 2002, **417**, 463-468.
245. J. Yeow, R. Chapman, A. J. Gormley and C. Boyer, *Chem. Soc. Rev.*, 2018, **47**, 4357-4387.
246. J. Xu, K. Jung, A. Atme, S. Shanmugam and C. Boyer, *J. Am. Chem. Soc.*, 2014, **136**, 5508-5519.
247. A. E. Enciso, L. Fu, S. Lathwal, M. Olszewski, Z. Wang, S. R. Das, A. J. Russell and K. Matyjaszewski, *Angew. Chem. Int. Ed. Engl.*, 2018, **57**, 16157-16161.
248. P. Anastas and N. Eghbali, *Chem. Soc. Rev.*, 2010, **39**, 301-312.
249. M. H. Allen, S. T. Hemp, A. E. Smith and T. E. Long, *Macromolecules*, 2012, **45**, 3669-3676.
250. J. Chen, K. Wang, J. Wu, H. Tian and X. Chen, *Bioconjug Chem*, 2019, **30**, 338-349.
251. K. Piontek, M. Antorini and T. Choinowski, *J. Biol. Chem.*, 2002, **277**, 37663-37669.
252. D. K. Schneiderman, J. M. Ting, A. A. Purchel, R. Miranda, M. V. Tirrell, T. M. Reineke and S. J. Rowan, *ACS Macro Letters*, 2018, **7**, 406-411.
253. Y. Sun, H. Du, Y. Lan, W. Wang, Y. Liang, C. Feng and M. Yang, *Biosens. Bioelectron.*, 2016, **77**, 894-900.
254. Y. Sun, J. Zhang, J. Li, M. Zhao and Y. Liu, *RSC Advances*, 2017, **7**, 28461-28468.
255. X.-H. Wang, M.-X. Wu, W. Jiang, B.-L. Yuan, J. Tang and Y.-W. Yang, *Macromolecules*, 2018, **51**, 716-723.
256. S. F. D'Souza, *Appl. Biochem. Biotechnol.*, 2001, **96**, 225-238.

257. S. H. Yang, S. M. Kang, K. B. Lee, T. D. Chung, H. Lee and I. S. Choi, *J. Am. Chem. Soc.*, 2011, **133**, 2795-2797.
258. W. Wang, S. You, X. Gong, D. Qi, B. K. Chandran, L. Bi, F. Cui and X. Chen, *Adv. Mater.*, 2016, **28**, 270-275.
259. A. Kausaite-Minkstimiene, V. Mazeiko, A. Ramanaviciene and A. Ramanavicius, *Sensors and Actuators B: Chemical*, 2011, **158**, 278-285.
260. A. Ramanavicius, E. Andriukonis, A. Stirke, L. Mikoliunaite, Z. Balevicius and A. Ramanaviciene, *Enzyme Microb. Technol.*, 2016, **83**, 40-47.
261. E. Andriukonis, A. Stirke, A. Garbaras, L. Mikoliunaite, A. Ramanaviciene, V. Remeikis, B. Thornton and A. Ramanavicius, *Colloids Surf B Biointerfaces*, 2018, **164**, 224-231.
262. R.-M. Apetrei, G. Cârâc, G. Bahrim and P. Camurlu, *International Journal of Polymeric Materials and Polymeric Biomaterials*, 2018, **68**, 1058-1067.
263. H. G. Sherman, C. Jovanovic, S. Stolnik, K. Baronian, A. J. Downard and F. J. Rawson, *Front Mol Biosci*, 2018, **5**, 97.
264. H. G. Sherman, C. Jovanovic, S. Stolnik and F. J. Rawson, *Anal. Chem.*, 2018, **90**, 2780-2786.
265. F. Cariati, F. Morazzoni, G. M. Zanderighi, G. Marcotrigiano and G. C. Pellacani, *Inorg. Chim. Acta*, 1977, **21**, 133-140.
266. M. R. Bennett, P. Gurnani, P. J. Hill, C. Alexander and F. J. Rawson, *Angew. Chem. Int. Ed. Engl.*, 2020, **59**, 4750-4755.
267. R. F. Fakhrullin, A. I. Zamaleeva, R. T. Minullina, S. A. Konnova and V. N. Paunov, *Chem. Soc. Rev.*, 2012, **41**, 4189-4206.
268. C. A. Custodio and J. F. Mano, *ChemNanoMat*, 2016, **2**, 376-384.
269. I. Drachuk, M. K. Gupta and V. V. Tsukruk, *Adv. Funct. Mater.*, 2013, **23**, 4437-4453.
270. H. R. Jia, Y. X. Zhu, Z. Chen and F. G. Wu, *ACS Appl Mater Interfaces*, 2017, **9**, 15943-15951.
271. Y. Teramura and H. Iwata, *Soft Matter*, 2010, **6**, 1081-1091.
272. R. F. Fakhrullin and Y. M. Lvov, *ACS Nano*, 2012, **6**, 4557-4564.
273. J. C. Kim and G. Tae, *Bull. Korean Chem. Soc.*, 2015, **36**, 59-65.
274. M. D. Mager, V. LaPointe and M. M. Stevens, *Nat Chem*, 2011, **3**, 582-589.
275. J. Y. Kim, B. S. Lee, J. Choi, B. J. Kim, J. Y. Choi, S. M. Kang, S. H. Yang and I. S. Choi, *Angew. Chem. Int. Ed. Engl.*, 2016, **55**, 15306-15309.
276. Y. Zhu, W. Huang, S. S. Lee and W. Xu, *EMBO Rep*, 2005, **6**, 681-687.
277. B. Kessler and B. Witholt, *J. Biotechnol.*, 2001, **86**, 97-104.
278. B. H. Rehm, *Nat Rev Microbiol*, 2010, **8**, 578-592.
279. E. Sapoznik, G. Niu, Y. Zhou, S. V. Murphy and S. Soker, *Biomed Eng Comput Biol*, 2016, **7**, 29-33.
280. T. Zhou, Y. Zhu, X. Li, X. Liu, K. W. K. Yeung, S. Wu, X. Wang, Z. Cui, X. Yang and P. K. Chu, *Prog. Mater Sci.*, 2016, **83**, 191-235.
281. A. Layadi, B. Kessel, W. Yan, M. Romio, N. D. Spencer, M. Zenobi-Wong, K. Matyjaszewski and E. M. Benetti, *J. Am. Chem. Soc.*, 2020, **142**, 3158-3164.

282. A. Duprey, V. Chansavang, F. Fremion, C. Gonthier, Y. Louis, P. Lejeune, F. Springer, V. Desjardin, A. Rodrigue and C. Dorel, *J Biol Eng*, 2014, **8**, 19.

Chapter 2. Iron Catalysed Radical Polymerisation by Living Bacteria

Abstract

The ability to harness cellular redox processes for abiotic synthesis might allow the preparation of engineered hybrid living systems. Towards this goal, a new bacterial-mediated Iron-catalysed Reversible Deactivation Radical Polymerisation (RDRP) is presented, with a range of metal-chelating agents and monomers that can be used under ambient conditions with a bacterial redox initiation step to generate polymers. Species of bacteria; *Cupriavidus metallidurans*, *Escherichia coli* and *Clostridium sporogenes* were chosen for their redox enzyme systems and evaluated for their ability to induce polymer formation. Parameters including cell and catalyst concentration, initiator species and monomer type were investigated. Water-soluble synthetic polymers were produced in the presence of the bacteria with full preservation of cell viability. This methodology provides a means by which bacterial redox systems can be exploited to generate 'unnatural' polymers in the presence of 'host' cells, thus setting up the possibility of making natural-synthetic hybrid structures and conjugates.

This chapter is expanded from a paper published 02.01.20:

Bennett, M. R., Gurnani, P., Hill, P. J., Alexander, C., & Rawson, F. J. (2020). Iron-Catalysed Radical Polymerisation by Living Bacteria. *Angewandte Chemie (International ed. in English)*, *59*(12), 4750–4755. https://doi.org/10.1002/anie.201915084

Introduction

Nature has evolved a plethora of complex macromolecular materials to generate, sustain and propagate life. However, the rich diversity of biopolymers is derived from a surprisingly small set of monomers, which are combined and repurposed in myriad ways. In recent years, biomimetic polymer synthesis has developed rapidly, with significant advances in methods to generate complex sequence controlled materials.[1-9] These new classes of synthetic polymers offer unprecedented possibilities in applications ranging from information storage and processing[10-12] through to biomedical sensing[13] and therapeutic delivery.[14] The combination therefore of cellular systems with synthetic, or biosynthesized hybrid polymers is now allowing the formation of engineered living materials (ELMs), in which the advantages of natural and artificial systems are combined to generate a whole new domain of 'programmable matter'.[9, 15, 16]

Prokaryotic organisms offer many possibilities for the generation of biohybrid materials, and many bacterial strains are being applied as components of fuel cells,[17-20] bioremediation systems,[21] as well as chasses for synthetic biology.[22-25] Bacteria can synthesise a variety of polymers which generate extracellular matrices (ECM)s, encasing and supporting the cellular communities which produce them. It is possible to alter the ECM biopolymers which bacteria synthesise by genetic engineering, but it would be highly advantageous to expand the range of ECM materials into those available by 'abiotic' chemistry. In particular,

the coupling of bacterial cells to a matrix of synthetic polymers might facilitate electron transfer in fuel cells or aid the application of bacterial cells in bioremediation or fermentation under conditions that would normally degrade or denature natural ECM components.

Many research groups have been interested in utilising cells for polymerisation reactions to possibly extend extracellular matrices beyond the existing types of biopolymers.[26, 27] A key goal has been to generate polymers *in situ* at, or near, bio-interfaces such that the cells 'select' which monomers to form materials in their immediate environments.[26, 28] Growing synthetic polymers in the presence of bacteria might provide not only novel ECM mimics,[29] but also bacteria-specific sequestrants and sensors.[30] The data shown in this chapter describes (Figure 2. 1) the initial steps in bacterial-mediated synthesis of wholly synthetic polymers under 'bio-benign' conditions.

To date, there have been several examples of cell-mediated polymerisations,[9, 27, 28, 31-36] but most have required catalysts or conditions which are toxic to biology or difficult to control. These include the production of polypyrrole that led to increased charge transfer from fungi.[37, 38] The attention of this chapter was focused on whether cellular-Fe mediated atom transfer radical polymerization (ATRP) might be possible, as Fe is ubiquitous in nature and essential to many bacterial strains, for example, *Cupriavidus metallidurans (C. met)*. Furthermore, focus on membrane redox systems capable of modulating the oxidation states of Fe and other metals have been of great interest.[20, 39-41] As discussed in the first chapter of this thesis, ATRP is a commonly used

RDRP method, which employs a metal catalyst to control an equilibrium reaction between activated and deactivated growing polymer chains. ATRP has been utilised for a variety of biomedical applications and can be used to synthesise polymers of complex architectures, block copolymers and it is tolerant to many functionalities.[42-48] It was sought to combine the use of bacterial reducing EET with Fe ATRP to drive a polymerisation. However, whilst Fe-mediated ATRP has been previously used to form polymers in organic solvents,[49, 50] there had been little work on Fe-catalysed ATRP under biologically benign conditions before the work published in this chapter.[51]

The results presented include the use of Fe-reducing systems in three different bacteria types to initiate ATRP-type reactions (Figure 2. 1A) of a variety of monomers (Figure 2. 1B), to generate abiotic polymers under conditions which allowed retention of bacterial viability for up to 24 hours. Live cells were essential to the polymerisation, indicating that viable cellular processes were required for polymer-forming reactions to take place.

***Aim*:** To use bacterial EET to initiate Fe-ATRP polymerisations under biological conditions and to probe the limitations of the method.

Objectives:

(I) Design and develop a biocompatible Fe ATRP system

(II) Explore the use of bacteria as initiating species for these systems

(III) Identify how the viability of the bacteria is affected

(IV) Explore the limitations of bacteria mediated Fe ATRP

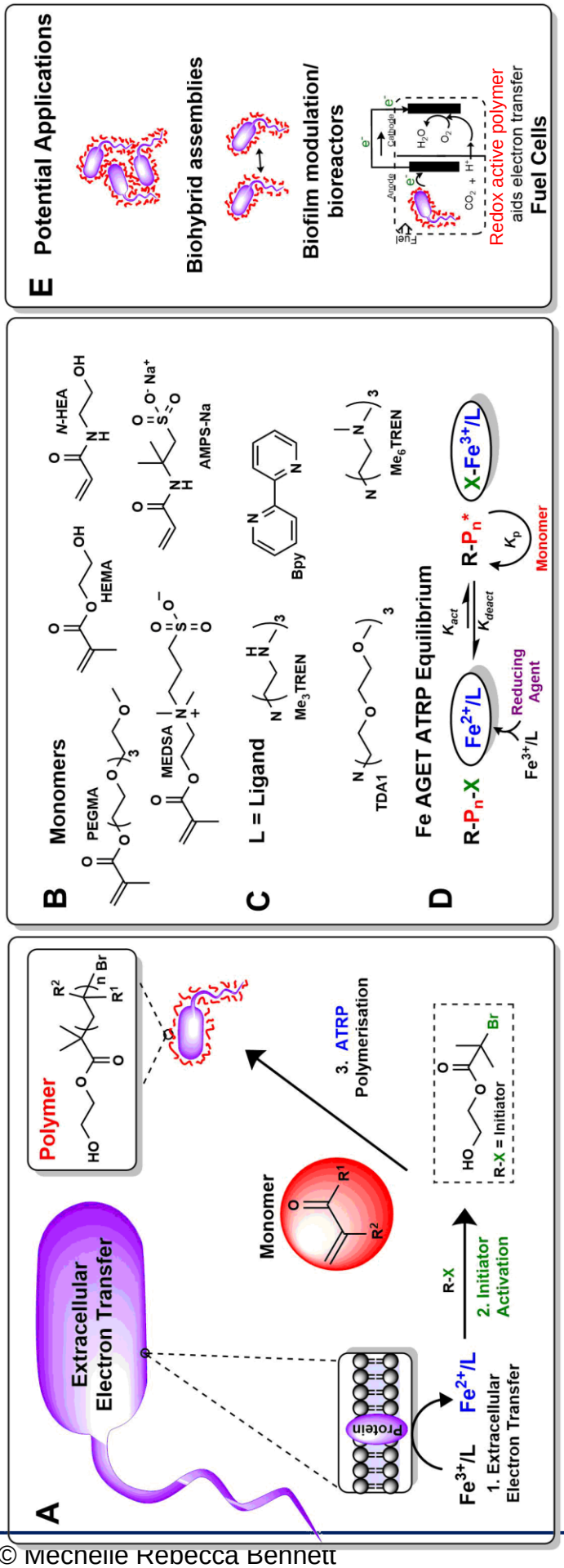

Figure 2. 1 A; Representation of Iron catalysed RDRP using bacteria to initiate redox transformation of catalyst in the reaction. B; Structures of different monomers. C; Ligands for Fe catalyst. D; Representation of AGET ATRP equilibrium with Fe/Ligand catalyst. E; Potential applications.

Results and Discussion

2.1.1 Establishing Biological Conditions for Fe ATRP

Conventional ATRP, as discussed in chapter 1, requires an active metal catalyst which is sensitive to air and must be handled with care, meaning that oxygen contamination is detrimental and complicates the reaction set up. Activators generated by electron transfer (AGET) ATRP on the other hand allows the use of an inactive catalyst which is reduced *in situ* by a reducing agent to form the active metal complex.[52] Ascorbic acid (AscA) is commonly used as a reducing agent and can also scavenge small amounts of O_2 in the reaction, making the reaction less sensitive to air and easier to set up. For the system to be successful with cells, this work first begins with the design and development of a biocompatible Fe ATRP system. Preliminary studies were carried out using AscA as a reducing agent in place of bacteria for ease of better understanding of the Fe catalysed AGET ATRP system during optimisation. The final aims of the project require an environment suitable for sufficient growth and viability of bacteria cells that will also allow for ample ATRP to be possible. Phosphate-Buffered Saline (PBS), containing various salts, was therefore considered as a more suitable solvent than water.[53] The halide salts present in PBS have been shown to prevent dissociation of the catalyst in aqueous Cu ATRP reactions, which might promote control in the polymerisations.[44, 54]

An Fe-catalysed AGET ATRP of the water-soluble biocompatible monomer poly(ethylene glycol methyl ether methacrylate) (PEGMA, M_n

= 300 g mol^{-1})[55] was carried out with the ligand tris(2-dimethylaminoethyl)amine (Me_6TREN, Figure 2. 1C) and AscA for Fe^{3+} reduction. Although phosphine species are particularly effective ligands for Fe ATRP,[56] they are not suitable in this study as they can reduce the Fe catalyst to the active form. This would prevent us from distinguishing between polymer formation as a result of ligand or bacterial activation of the active catalyst (Fe^{2+}). Nitrogen-containing ligands are less likely to display these characteristics and so highly active Me_6TREN was chosen to maximize the rates of reaction at low temperatures. The temperature was set to 37 °C, the optimum temperature at which most biological organisms grow, and commercially available water-soluble initiator 2-hydroxyethyl 2-bromoisobutyrate (HEBIB) was used. An inert atmosphere was maintained (purging with nitrogen gas) to prevent the termination of radicals by oxygen, a well-known radical scavenger.[57] After 5 hours the reaction reached 79% monomer conversion (Table 2.1, Figure 2. 2) and spectroscopy revealed the expected polymer structure (Figure 2. 3 and Figure S2. 1). SEC data (Figure 2. 4, Table 2. 1) indicated a broad molar mass distribution (*Đ* = 1.6), likely due to low initiation efficiency.[44, 58]

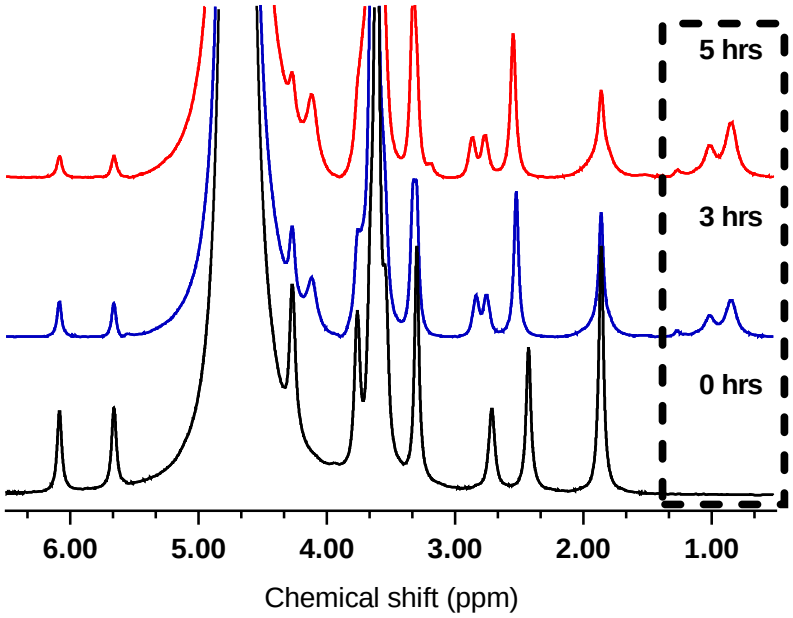

Figure 2. 2 ^{1}H NMR (400 MHz, D_2O) spectra revealing an increase in polymer formation in Fe ATRP (PPEGMA, Me_6TREN, AscA at 37 °C, PBS, HEBIB), with time.

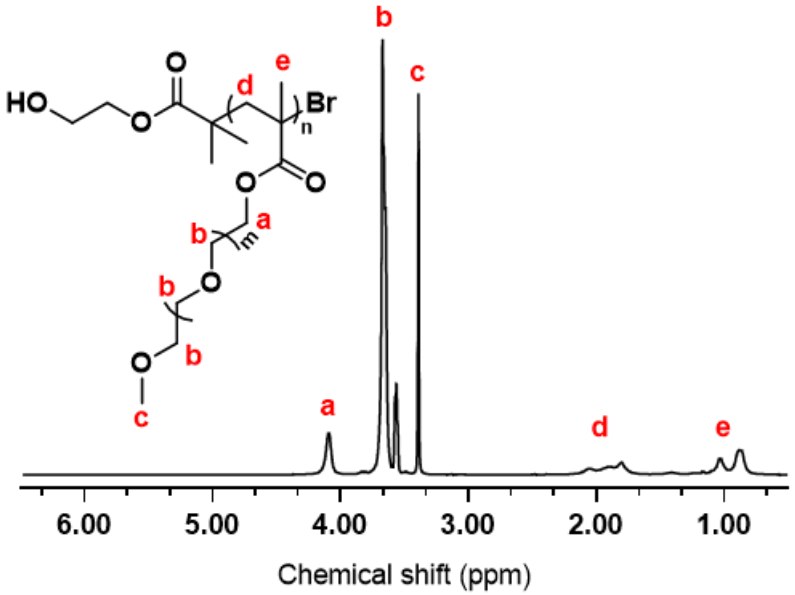

Figure 2. 3 ^{1}H NMR (400 MHz, $CDCl_3$) of purified PPEGMA. Polymer resulting from Fe ATRP initiated by Asc acid using Me_6TREN as a ligand at 37 °C in PBS with HEBIB initiator.

As discussed previously, phosphine ligands have been shown to reduce Fe^{3+} *in situ*. To ensure that activation of the Fe^{3+} catalyst could not be caused by Me_6TREN reduction, a control experiment omitting AscA (Table S2. 2) was carried out, revealing inhibition of polymer growth, and confirming that Me_6TREN is suitable for these investigations. To examine retention of chain end functionality (Br), the polymer was chain extended utilizing similar conditions, (Me_6TREN, PBS 37 °C, Figure S2. 3, Figure S2. 4, Figure S2. 5). An increase in M_n (109 kDa mol^{-1}, Figure 2. 4) was observed, but also a decrease in control of polymer dispersity ($Đ$=2.0).

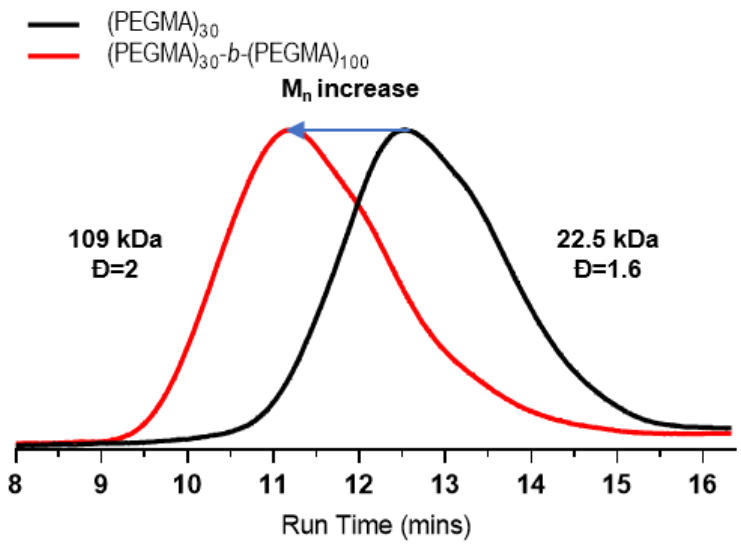

Figure 2. 4 SEC (DMF) graph of Fe ATRP synthesized PPEGMA (Black) and chain extended PPEGMA (Red) carried out with conditions: AscA at 37 °C, PBS, HEBIB, Me_6TREN.

2.1.2 Biologically Benign Fe ATRP with Different Ligands

Experiments were carried out to explore the use of different ligands in the system. Ligands are required to solubilise Fe^{3+} ions, but also affect the redox potential of the resulting catalyst complex and subsequently the ATRP reactivity. The apparent rate constant (k_{app}) represents an estimate of the ATRP equilibrium constant (K_{ATRP}) and is calculated by k_{act}/k_{deact} (Scheme 2.1). k_{app} can be extracted using the gradient of the plot $\ln([M]_0/[M])$ against time (where $[M]_0$= monomer concentration at the start of reaction and [M] = monomer concentration at a specific time).

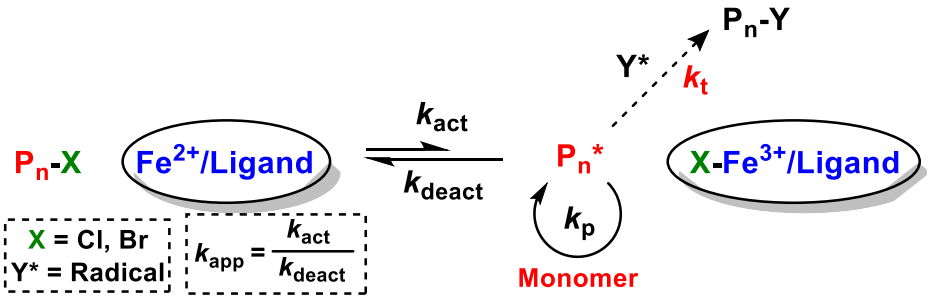

Scheme 2. 1 Fe ATRP equilibrium showing halogen capped polymer chain (P_nX), active catalyst (Fe^{2+}), deactivated catalyst (Fe^{3+}) and propagating radical chain (P_n*).

Kinetic plots using a range of chelating ligands (Table 2. 1, Figure 2. 5) were explored. Firstly, the ligand tris[2-(2-methoxyethoxy)ethyl]amine (TDA-1, Figure 2. 1B), used in prior literature to demonstrated activity with $FeCl_3$ and water at 90 °C, was unsuccessful in mediating the polymerisation at low temperatures (37 °C) in PBS.[50] In contrast, bidentate ligand 2, 2 – Bipyridine (Bpy) induced fast polymerisation (k_{app}

Table 2. 1: Iron AGET ATRP of PEGMA with AscA at 37 °C in PBS using different ligands, Ratio [PEGMA]: [$FeCl_3$]:[Ligand]: [HEBIB]: [AscA] = [30]:[1]:[X]:[1]:[1].

Entry	Ligand[a]	Time (h)	Conv.[b]	K_{app} (s^{-1})[c]	M_n^{th} (kDa)[d]	M_n^{SEC} (kDa)[e]	$Đ$[e]
1	Me_6TREN	5	79%	0.0037	7.2	22.5	1.6
2	TDA-1	24	0%	-	-	-	-
3	Bpy[f]	2.15	93%	0.036	8.6	17.8	1.6
4	Me_3TREN	4.5	36 %	0.0021	3.3	32.7	1.5

[a] All ligand to metal ratios 3:1 (X=3) except Bpy (1:6; X=6). [b] Estimated using of ^{1}H NMR from comparison of monomer: polymer integrals [c] Calculated using gradient of plot Ln[M_0]/[M] vs time from estimated conversions. [d] M_n^{th} = (9.0 * conversion) + 0.211 (kDa). [e] Calculated using SEC (DMF). [f] Bpy was dissolved in 100 µL DMSO before mixing with $FeCl_3.6H_2O$.

~ 0.036 s^{-1}), likely due to a less constrained coordination structure at the Fe center and a fast, efficient, halogen exchange to the metal (high k_{act}).

However, in the reduced form, the transition of Br to the polymer chains (k_{deact}) may be more difficult, making the reaction less controlled ($Đ$=1.6). Ligand or halogen dissociation also affect the control of all aqueous ATRP reactions due to substitution of water or hydroxide ions, intensified by monomer coordination to the catalyst.[59]

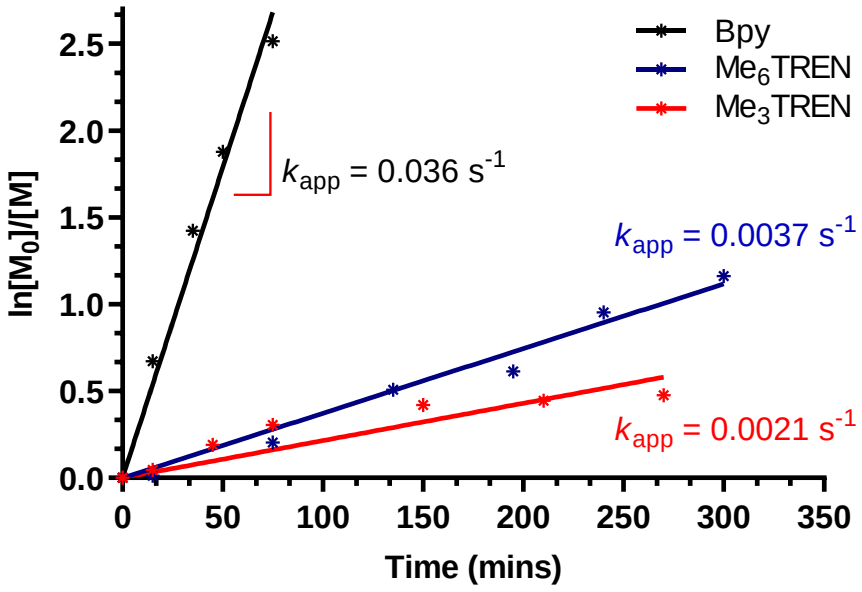

Figure 2. 5 First order kinetics (Ln[M_0]/[M] vs time) comparing different ligands of Fe catalysts for Fe AGET ATRP polymerisations of PEGMA (AscA, 37 °C, PBS, HEBIB). Bpy (black), Me_6TREN (Blue) and Me_3TREN (Red) (Table 2. 1).

The Fe catalyst complexed to Me_6TREN ligand gave rise to a k_{app} (~0.0037 s^{-1}) value 10 times slower than for Bpy (~0.036 s^{-1}), but the dispersity control was comparable (both $Đ$ ~1.6). Although polymers resulting from Fe/Me_3TREN catalysed ATRP provided lower dispersity control ($Đ$ = 1.5), the molecular weight control proved to be inefficient with M_n values 10 times higher than predicted. Furthermore, the lower k_{app} (~0.0021 s^{-1}) value reflected the reduced catalytic activity of Fe/Me_3TREN complexes and the curved kinetic graph (Figure 2. 5, red) indicated significant termination, deviating from linear kinetics after 1 hour. The bpy ligand seemed the most efficient for Fe ATRP in these initial studies, however, they have a high associated toxicity so may not be advantageous when moving to biological experiments,[60] therefore Me_6TREN was used in the remainder of the polymerisations.

2.1.3 Biologically Benign Fe ATRP with Different Monomers

It is an advantage to be able to create polymers of different chain lengths and different monomer materials for versatility in future applications. To explore these features, the degree of polymerisation (DP) was first increased to 100 and 200 (Table 2. 2, entry 2 and 3). Both polymerisations resulted in polymers with similar dispersities, however, the reaction targeting DP200 was slower and M_n^{SEC} results were closer to theoretical values (M_n^{th}) for the reaction targeting DP100. The faster rate of reaction for lower DPs can be rationalized by equation 2.1.[61]

Table 2. 2. Fe AGET ATRP of PEGMA with ascorbic acid at 37 °C in PBS. Ratio: [Monomer]: [$FeCl_3$]:[Ligand]: [Initiator]: [AscA] = [X]:[1]:[3]:[1]:[1] unless stated.

Entry	Monomer	DP (X)	Monomer (mmol)	Time (h)	Conv. [a]	M_n^{th} (kDa)	M_n^{SEC} (kDa)[b]	$Đ$[b]
1	PEGMA	30	1	5	78%	7.2	22.5	1.6
2	PEGMA	100[c]	1	4	78%	23.6	25.4	1.4
3	PEGMA	200[c]	1	5.5	57%	34.4	33.9	1.5
4	HEMA	50	0.97	5	50%	3.5	12.5	1.2
5	*N*HEA	50	0.96	17	54%	3.3	16.5	1.4
6	AMPS-Na	30*	0.93	4.5	36%	6.4	25.2	1.7[d]
7	MEDSA	30*	1	5	33%	3.0	2.8	2.4[e]
8	MEDSA	30*	1	24	>99%	8.6	7.5	2.0[f]

[a] Estimated using of ^{1}H NMR from comparison of monomer: polymer integrals [b] Calculated using SEC (DMF unless stated)) [c]: [Monomer]: [$FeCl_3$] : [Me_6TREN]: [HEBIB] : [AscA] = [X]:[4.65]:[13.95]:[1]:[2.3]. THF SEC - dn/dc = 0.0527 L/g (Figure S2. 7). *Aqueous SEC; [d]; dn/dc = 0.1405 L/g; [e]; dn/dc = 0.1433 L/g; [f]; dn/dc = 0.1381 L/g (Figure S2. 6).

$$R_p = k_p K_{ATRP} \frac{[RX][Fe^{2+}L]}{[Fe^{3+}]}[M] \qquad \text{(Equation 2.1)*}$$

**Where R_p= Rate of propagation, k_p= propagation rate constant, K_{ATRP} = ATRP equilibrium rate constant, [RX] = Initiator (RX) concentration, [M] = monomer concentration.*

A polymerisation with a lower targeted DP (DP= [M]/[RX]) would have a higher concentration of initiator ([RX]). According to equation 2.1, a higher initiator concentration ([RX]) leads to a greater R_p, and therefore increases the reaction rate.

Several monomers were then tested for compatibility with this new biocompatible Fe AGET ATRP technique. Polymerisations (Table 2. 2) were established with monomers including, hydroxyethyl methacrylate (HEMA), *N*-Hydroxyethyl acrylamide (*N*HEA), 2-Acrylamido-2-methyl-1-propanesulfonic sodium (AMPS-Na) and 2-(Methacryloyloxy) ethyl dimethyl-(3-sulfopropyl) ammonium hydroxide (MEDSA) (Figure 2.1B). Of these, the original monomer PEGMA resulted in the fastest polymerisation (~78% conversion in 5 hours for DP30 and ~78% in 4 hours for DP100). The polymerisation with PEGMA targeting DP100 had the best molecular weight control, close to theoretical values. Whilst the polymerisation with HEMA showed the highest dispersity control (*Đ* = 1.2). The results show that this method can be applied to a variety of monomers and targeted DPs, expanding the scope for future applications.

2.1.4 Biologically Benign Fe ATRP - Catalyst Complexes

All biological reactions occur in aqueous media, however, Fe ATRP reactions are mostly reported in organic solvents. As discussed, side reactions can be detrimental to the M_n control or $Đ$ control in an ATRP polymerisation, and these are more common under aqueous media conditions. The stability of the halide bond to the deactivator (Fe-X, for $Fe^{3+}(L)_nX$) is reduced significantly in protic media which often leads to insufficient deactivation and fast, uncontrolled reactions.[62] Adding halide salts or increasing catalyst concentration can help to prevent halide dissociation.[54] Matyjaszewski *et al* also discovered that a mixed halide system of alkyl-bromide initiator (R-Br) and Metal-chloride catalyst were most efficient at controlling the polymerisations for Cu based ATRP.[63] Although other reports suggest that differing systems might be necessary to improve the control of particular monomers or specific reaction conditions.[62] There is, however, no known analogous research for Fe catalysed systems. To investigate the effect of altering the catalyst halide, different Fe salts were employed.

Fe ATRP in biologically benign conditions, catalysed by $FeCl_3$ and $FeBr_3$ catalysts was carried out and the kinetics were compared (Figure 2. 6). The kinetic plots of the polymerisations are both linear but reactions catalysed by $FeBr_3$ had a faster rate of reaction ($k_{app} = 0.007s^{-1}$). This is likely due to the less stable Fe-Br deactivator catalyst bond compared to Fe-Cl, in which Br can dissociate more readily, causing loss of deactivator species. This causes an increase in the rate of activation

(k_{act}) in the ATRP equilibrium according to Le Chatelier's principle, resulting in a much faster but less controlled reaction. As seen in Table 2. 3, molecular weights and dispersities were much higher and broader, respectively, than for polymerisations catalysed by $FeCl_3$. This is reflective of the ATRP equilibrium shift towards uncapped radicals which can cause more side reactions. Catalyst complexes for aqueous Fe ATRP systems are therefore more controlled with chloride-based catalysts.

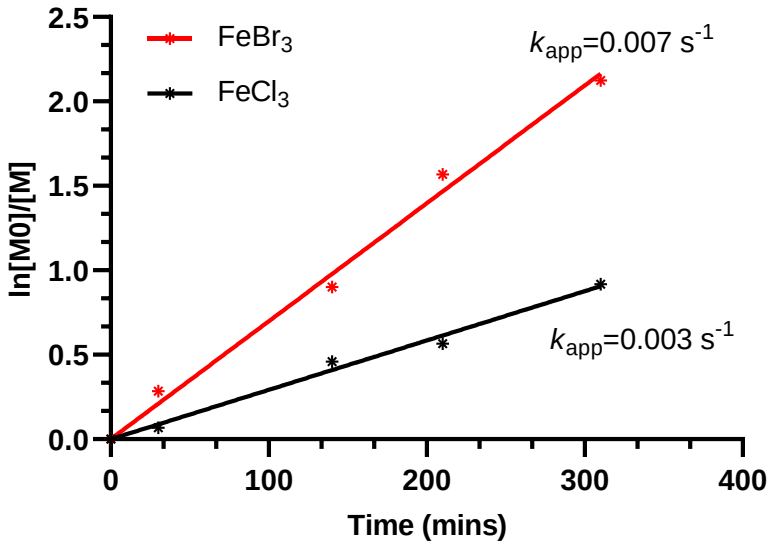

Figure 2. 6 First order kinetics (Ln[M0]/[M] vs time) comparing different $FeCl_3$ (Black) and $FeBr_3$ (Red) catalysts with Me_6TREN ligand for biologically benign Fe AGET ATRP polymerisations of PEGMA (AscA, 37 °C, PBS, Me_6TREN, HEBIB).

Table 2. 3 Fe ATRP under biological conditions (37 °C, PBS) with ligand Me_6TREN. Initiated by HEBIB and activated by AscA.

Catalyst Halide	Conv.[a]	k_{app} (s^{-1})[b]	M_n^{th} (kDa)[c]	M_n^{SEC} (kDa)[d]	$Đ$[d]
$FeCl_3$	56%	0.003	5.3	22	1.68
$FeBr_3$	84%	0.007	9.4	31	3.00

[a] Estimated from ^{1}H NMR monomer: polymer integrals. [b] Calculated using gradient of plot from Figure 2.6 [c] M_n^{th} = (300 * DP* conversion) + 211 Da. [d] From SEC (THF).

The first aim (I) set out at the beginning of this chapter to ‘Design and develop a biocompatible Fe ATRP system’ had been met. At this stage, the goal was to only indicate that Fe AGET ATRP was possible under ambient conditions, and so attempts to optimize the cell-free polymerization reactions were not pursued further. Beyond the scope of this thesis, there is however room for improvement and further studies into improving control will hugely benefit the progression of Fe ATRP in biological conditions.

2.1.5 Bacteria Driven Iron-Catalysed Radical Polymerisation

2.1.5.1 Fe ATRP Activated by *Cupriavidus metallidurans*

Bacterial redox mechanisms were next employed to activate the Fe^{3+} catalyst in Fe ATRP systems. The incubation of PEGMA (0.2 M) with *C. met* bacteria, Fe^{3+}/Me_6TREN and HEBIB under anoxic conditions, successfully generated polymers (Section 2.6.7, Figure 2. 7). Although the molecular weight control (M_n= 650 kDa) was poor, likely due to poor initiation efficiency, the dispersity ($Đ$ = 1.4) was relatively low considering the polymerisation conditions (aqueous Fe ATRP).

To investigate whether a true 'ATRP' type polymerisation reaction had occurred, typical control reactions; omitting the bacteria, Fe catalyst, ATRP initiator or utilising lysed bacteria were performed. These experiments revealed that i) bacteria were solely responsible for the activation of $FeCl_3$ catalyst and ii) the catalyst had a significant role in the ATRP polymerization (Figure 2. 7 and Figure 2. 8). It was anticipated that metallic proteins, such as ferritin,[64] acted as catalysts for the small 28% conversion seen in 24 hours (Bottom, Red Figure 2. 7).

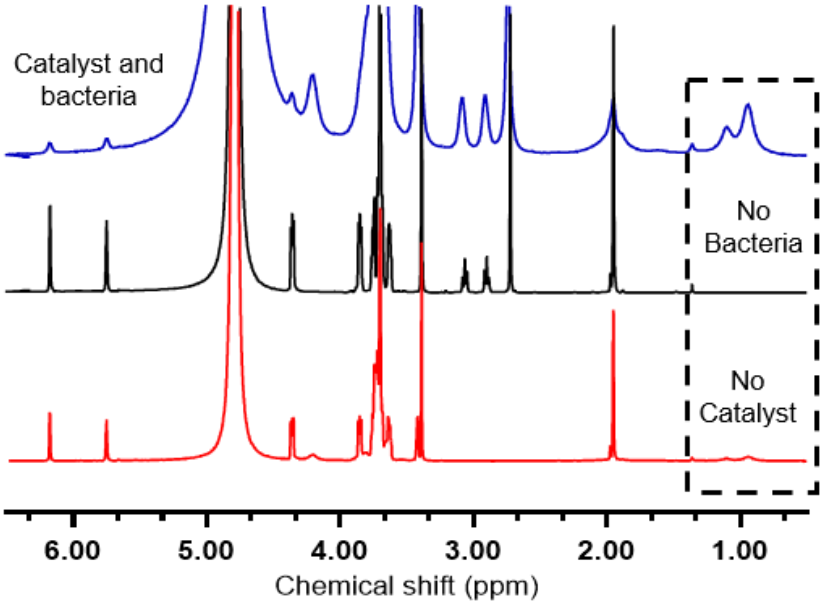

Figure 2. 7. ^{1}H NMR (400 MHz, D_2O) at T = 6 h of the following reactions: *C. met* initiated Fe ATRP of PEGMA (Blue, top). Controls shown without bacteria (Black, middle) and without $FeCl_3$ catalyst (Red, bottom). All carried out at 37 °C in PBS using Me6TREN as a ligand and HEBIB as an initiator.

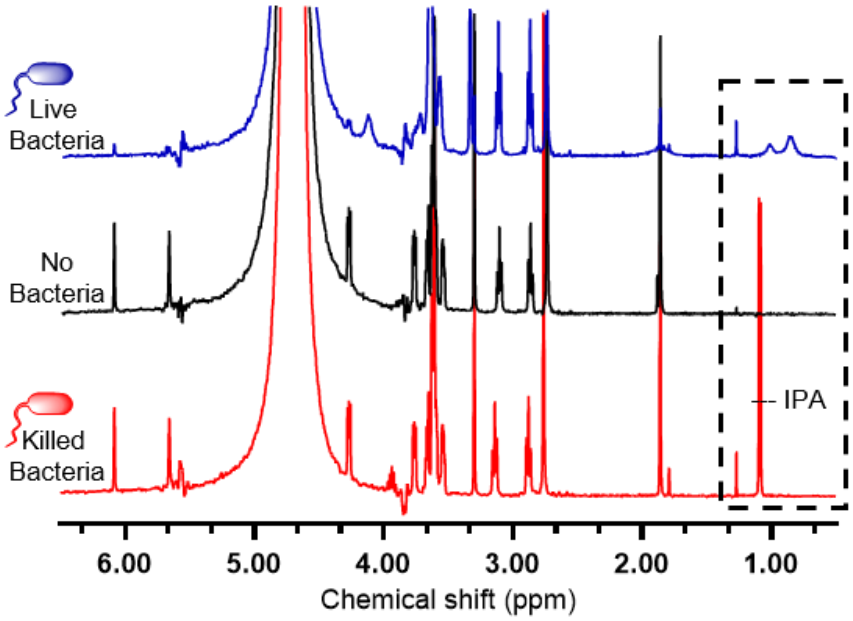

Figure 2. 8. ^{1}H NMR spectra (400 MHz, D_2O) at T=24 h for the following reactions: Reaction A (top, blue) Fe ATRP of PEGMA initiated by *C. met*. Reaction B (middle, black) Fe ATRP of PEGMA without bacteria and Reaction A* (bottom, red) Fe ATRP of PEGMA

with inactivated bacteria. All carried out at 37 °C in PBS using Me6TREN as a ligand and HEBIB as an initiator.

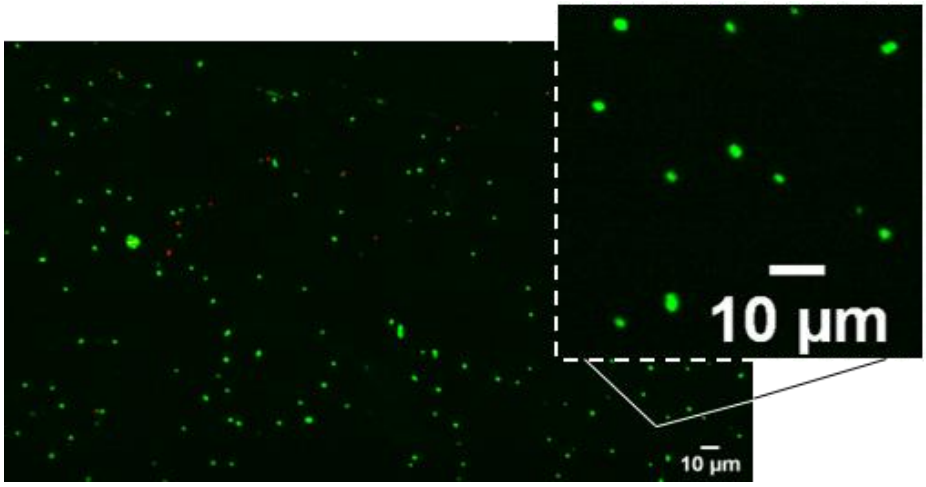

Figure 2. 9. Live/Dead image corresponding to live bacteria instructed Fe ATRP of PEGMA using ligand Me_6TREN in PBS at 37 °C in PBS with HEBIB as an initiator (Reaction A).

When no ATRP initiator (Figure S2. 12) or when killed bacteria (Figure 2. 8) were present, negligible monomer conversion was observed indicating that live bacteria and ATRP halide initiators are essential to promote polymerisation. Importantly this also suggests that no external radicals, such as ROS, produced through cell stress initiated the polymerisation observed. Live/dead staining (Figure 2. 9) and colony forming units (CFU)s counts were performed immediately after the polymerization (Table 2. 4). Approximately 85% of *C. met* bacteria remained metabolically active (Live/Dead assay) after polymerization, a value that matched that of the control culture (80%) not exposed to the polymerisation. The overall reduced viability for both the experimental conditions was a function of performing the polymerisations in an

aqueous buffer without typical amino acids and other growth supplements used for *C. met* cultures.

Table 2. 4. Results of live/ dead study and bacterial growth assays. Live bacterai (A) and killed bacteria (A*) were exposed to Fe ATRP reagents (PEGMA, $FeCl_3$, Me_6TREN and HEBIB in PBS at 37°C) afterwhich the viability was assessed against live (C1) and dead (C2) control cutures that were not exposed to ATRP reagents .

Sample	% Live*	CFU (mL^{-1})
A (ATRP Live Bacteria)	85	1.4×10^9
A* (ATRP Dead Bacteria)	<1	0
C1 (Live control)	81	2.4×10^9
C2 (Dead Control)	13	0

* Determined using Live/Dead calibration curve asymmetric least squares fitting (SI)

The next experiments evaluated the effects of the ATRP components on the growth efficiency of bacterial strains intended to catalyse the polymerisations, to expand its uses in future applications. Growth inhibition experiments (Section 2.6.6; Figure S2. 8, Figure S2. 9, Figure S2. 10 and Table S2. 3) were performed using bacterial species of known metal reducing capability, i.e., *C. met.*[65] Minimum inhibitory concentration (MIC) measurements indicated that bacteria were able to tolerate concentrations of ~14 mM for the water-soluble monomers, while Bpy was toxic from low levels (0.25 mM) as anticipated. Me_6TREN and Me_3TREN caused no adverse effects at 2.5 mM but due to the slow reactions with Me_3TREN, we adopted Me_6TREN for all subsequent biological ATRP studies.

When using a lower monomer concentration (14 mM) polymerization occurred, but again, SEC analysis (Table 2. 5, entry 1) revealed a significantly higher $M_{n,}^{SEC}$ (200 kDa) than $M_{n,}^{th}$ (9.4 kDa) due to a continued low initiator efficiency and relatively poor control ($Đ$ = 2.1). The reduced molecular weight control implies that the initiator may be lost in the reaction, possibly due to bacteria consumption of the small molecule, or poor availability of initiator molecules diffused into the ECM. The poor dispersity control indicates inefficient halogen exchange between the catalyst and the growing polymer chains, as well as an increased halide dissociation resulting from the low reagent concentrations in aqueous media. Differences observed compared to cell-free ATRP, which had better molecular weight control, could also be explained for bacteria catalysed ATRP by; i) catalyst site obstruction by bacteria cell ECM polymeric components,[66] or ii) bacterial uptake of the active catalyst which would disturb the equilibrium.[67, 68]

Despite the poor molar mass distribution control, the data reported demonstrates that bacterial – mediated Fe-catalysed ATRP could take place under ambient conditions.[39] Therefore the chapter aims; (II) ‘Explore the use of Bacteria as initiating species for these systems’ and (III) ‘Identify how the viability of the bacteria is affected’ had been achieved.

2.1.5.2 *Escherichia coli* and *Clostridium sporogenes* Catalysed Fe ATRP

To fulfill the next aim (iv) of this thesis ('Explore the limitations of bacteria mediated polymerisations with an Fe ATRP system'), different bacteria were applied to the initiation system (Table 2. 5, entries 2 and 3). *Escherichia coli* (*E. coli*) top 10 and *Clostridium sporogenes* (*C. spor*) were used in these experiments. The Gram-negative facultative anaerobes, *E. coli* and *C. met* induced a similar polymer yield, whereas the Gram-positive, obligate anaerobe *C*. *spor* initiated a much slower polymerisation (34% yield). These observations suggest that the reducing capability of bacteria for $FeCl_3$ is dependent on bacteria type. Fe reducing bacteria are known to use membrane bound proteins, for example, the cytochrome C (C-Cyts) family, for redox activity.[69] It is suspected that these ferrireductase membrane enzymes might utilise EET mechanisms to reduce the Fe catalyst in the bacterial initiated Fe

Table 2. 5. Fe AGET ATRP of PEGMA ($FeCl_3$, Me_6TREN, HEBIB, in PBS) with different bacteria as reducing agents.

Entry	Bacteria	OD_{600nm}	DP	Time (h)	Conv.[a] (%)	M_n^{th} (kDa)[b]	M_n^{SEC} (kDa)[c]	$Đ$[c]
1	*C. met*	1.1	50	24	61	9.4	200	2.1
2	*E. coli*	1.1	50	24	78	11.9	369	2.0
3	*C. spor*	1.1	50	24	34	5.3	102	2.2

[a] Estimated from ^{1}H NMR monomer: polymer integrals [b] (DP 50); M_n^{th} = (300 * DP* conversion) + 211 Da. [c] From SEC (THF) dn/dc=0.0527 L/g.

ATRP polymerisations described in this chapter.[34, 70] *E. coli* contain C-Cyts such as NapC which are homologues of Fe reducing CymA of *Shewanella oneidensis*,[40] and other ferric reductases also exist in *E. coli*.[71] Some groups have however suggested that *E. coli* may reduce Fe

via excretion of flavin molecules,[36] extracellular enzymes or siderophores for Fe homeostasis.[72] [73] It is therefore likely that several synergistic Fe reducing processes are involved in assimilatory and dissimilatory respiration, and additional research is essential to understand these mechanisms further but is beyond the scope of this chapter.[71]

Control reactions (Figure S2. 16, Figure S2. 17 and Table S2. 4) showed that without bacteria no polymer formation occurs, therefore bacteria are essential to the polymerisations. Secondly, Fe was shown to be necessary to the reaction, although a small amount of polymerisation can be seen for *E. coli* or *C. met* instructed reactions without Fe catalyst. This observation is likely to be due to exogenously released Fe containing bacterial proteins mentioned previously. [68]

2.1.6 Exploring Parameters of Bacterial Catalysed Fe ATRP

2.1.6.1 Bacteria Concentration

Experiments thereafter were conducted to investigate several important parameters that can affect the bacterial driven polymerisation. These were performed to explore the efficiency and control of the polymerisation, which is of importance for future exploitation of this technology. Increasing the bacterial concentration effectively increased the rate of reaction (Figure 2. 10, Table 2. 6) whilst decreasing $M_{n,}^{SEC}$ (Figure 2. 11) slightly closer to M_n^{th}. An extremely high molecular weight was observed when a low concentration of bacteria was used to catalyse the reaction, with exceptionally low yields. This is characteristic of radical-radical termination reactions which may be caused by slow regeneration of Fe^{2+} catalyst causing a slow k_{deact} and increasing the presence of P_n* species, enhancing termination events.

Table 2. 6 Results of bacteria catalysed Fe ATRP (PEGMA, $FeCl_3$, Me_6TREN and HEBIB in PBS at 37°C) using different *C. met* concentrations.

Reaction	Cell Count (CFU mL^{-1})*	Conversion[a]	M_n^{th} (kDa)[b]	M_n^{SEC} (kDa)[c]	$Đ$[c]
1 Low	1 x 10^9	1%	0.2	1200	1.2
2 Medium	6.5 x 10^9	13%	0.4	116	4.0
3 High	1.35 x 10^{10}	61%	9.4	110	2.4

*In final reaction volume [a] Estimated from ^{1}H NMR monomer: polymer integrals. [b] M_n^{th} = (300 * DP* conversion) + 211 Da. [c] From SEC (THF).

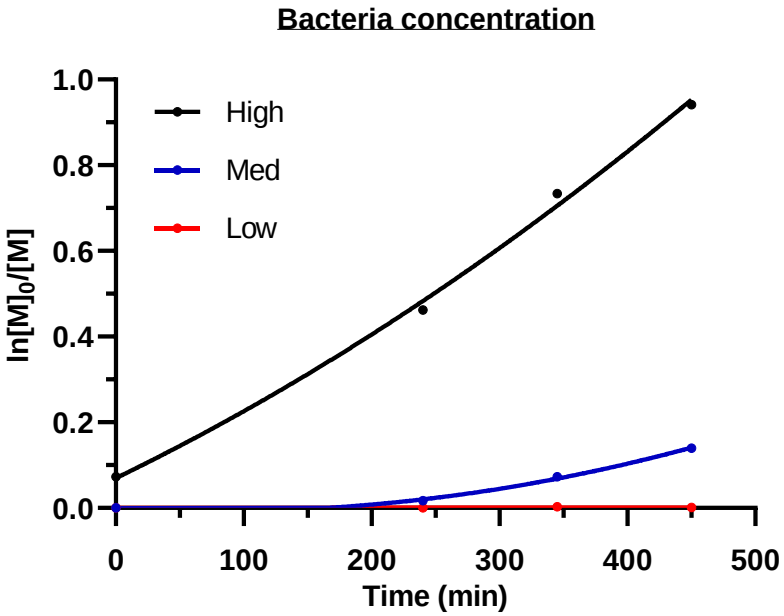

Figure 2. 10 ^{1}H NMR (400 MHz, D_2O) kinetic graph of bacteria catalysed Fe ATRP (PEGMA, $FeCl_3$, Me_6TREN and HEBIB in PBS at 37°C) using different bacterial concentrations.

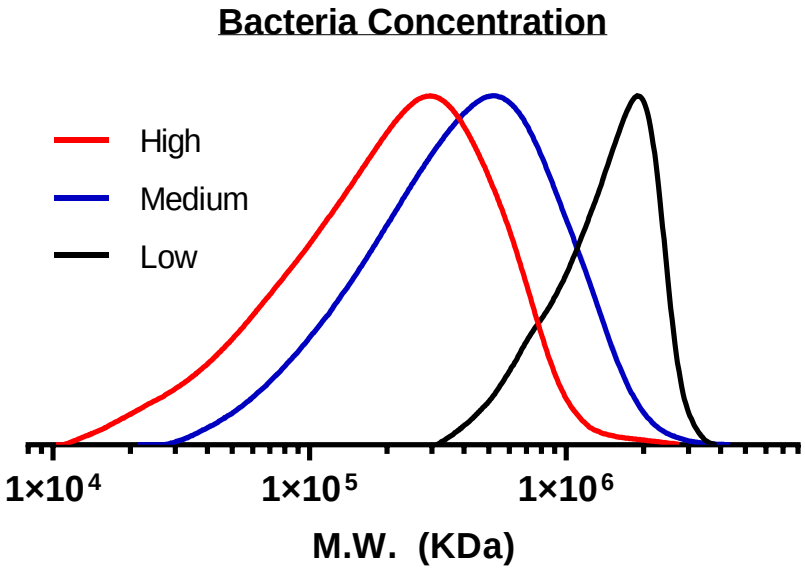

Figure 2. 11 SEC (THF) overlay of polymers bacteria catalysed Fe ATRP (PEGMA, $FeCl_3$, Me_6TREN and HEBIB in PBS at 37°C) using different bacterial concentrations.

Bacterial populations contain an ECM which protects the bacteria and contains various proteins and glycopolymers. Indeed, bacterial

polymer or protein substances (10^4 kDa, $Đ$ ~ 1.05) were identified by SEC of the bacteria solution alone (Figure S2. 21A). Substances in the ECM could interfere with the polymerisation due to polymer chain entanglement, hindering halogen exchange at the polymer chain ends (halide-capped or radical form). This may interfere with the ATRP equilibrium and broaden the dispersity of the polymerisation as demonstrated for the bacterial driven Fe ATRP reactions.

An increase in reaction rate is observed for the high concentration bacteria driven Fe ATRP reactions. For this reason, these conditions were used to investigate other parameters of the reaction. To prove that the initiator is required for the reaction and ensure that bacteria ROS were not contributing to the polymerisation, a control was carried out omitting initiator species (Figure S2. 20) for 24 hours. No polymer formation was observed, highlighting the requirement of the ATRP initiator.

2.1.6.2 Catalyst Concentration

The concentration of Fe catalyst in recent literature for photo-initiated Fe ATRP was shown to affect the resulting polymers,[74] and so the Fe concentration for bacterial initiated Fe ATRP was therefore explored in this section. An increase in reaction rate, better M_n control and more linear kinetics (Figure 2. 12, Table 2. 7) were observed upon increasing the concentration of catalyst. This could be attributed to the excess catalyst which prevents halide dissociation, as discussed in previous sections. The SEC chromatogram (Figure 2. 13) reveals 2 polymer

distributions for reactions catalysed by 6.8 mM Fe which is characteristic of a high amount of combination termination events. However, at the highest catalyst concentration only one polymer species is apparent with lower molecular weights, indicating better initiation efficiency. The small peak in the graphs arising at ~10^4 kDa corresponds to residual bacterial proteins (See S2.21A) mentioned previously.

Various bacterial pathways can control internal Fe regulation for homeostasis, such as extracellularly released siderophores, in *E. coli* these are known as Fur-regulated genes.[75] The faster and more linear kinetics observed for Reaction 5 could be attributed to; i) a genetic response of the bacteria to an overload of catalyst increasing the rate of Fe^{3+} reduction and Fe^{2+} regeneration, affecting the polymerisation equilibrium rates, and/or ii) more available catalyst, reducing potential problems of bacterial Fe uptake for homeostasis or monomer/solvent complexation to the catalyst.

Table 2. 7 Results obtained whilst changing the catalyst concentrations ($FeCl_3$/Me_6TREN) for bacterial instructed Fe - ATRP of PEGMA in PBS at 37°C.

Reaction*	Conversion[a]	M_n^{th} (kDa)[b]	M_n^{SEC} (kDa)[c]	$Đ$[c]
1 (Lowest)	16%	2.6	417.9	1.8
2	17%	2.8	399.6	1.8
3	39%	6.1	140.6	2.9
4	81%	12.4	130.6	3.3
5 (Highest)	84%	12.8	103.2	1.7

*See Table 2S.9 for concentration details [a] Estimated from ^{1}H NMR monomer: polymer integrals. [b] M_n^{th} = (300 * DP* conversion) + 211 Da. [c] From SEC (THF).

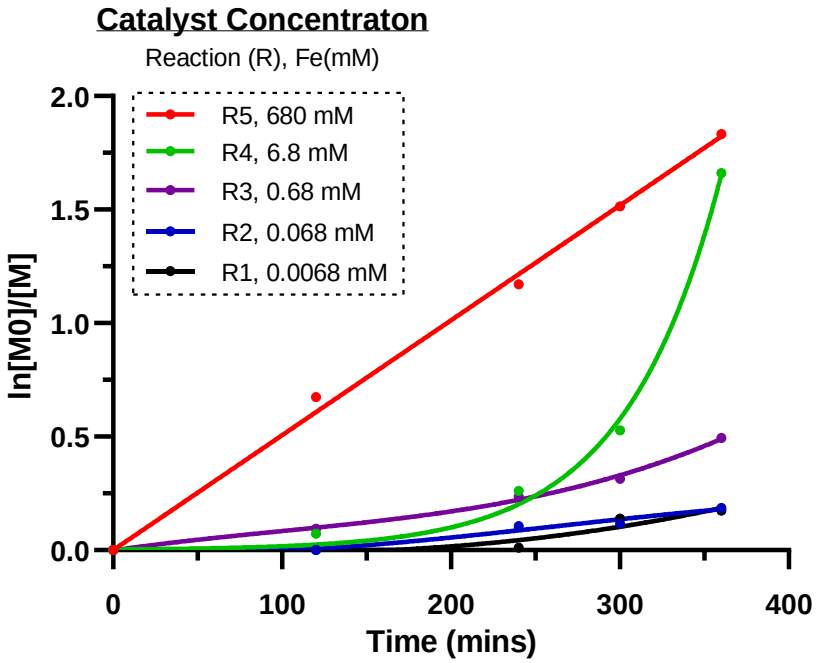

Figure 2. 12. ^{1}H NMR (400 MHz, D_2O) kinetic graph of b-ATRP of PEGMA in PBS at 37 °C using different concentrations of $FeCl_3Me_6TREN$ catalyst from reactions (R)s 1-5 shown in Table 2. 7.

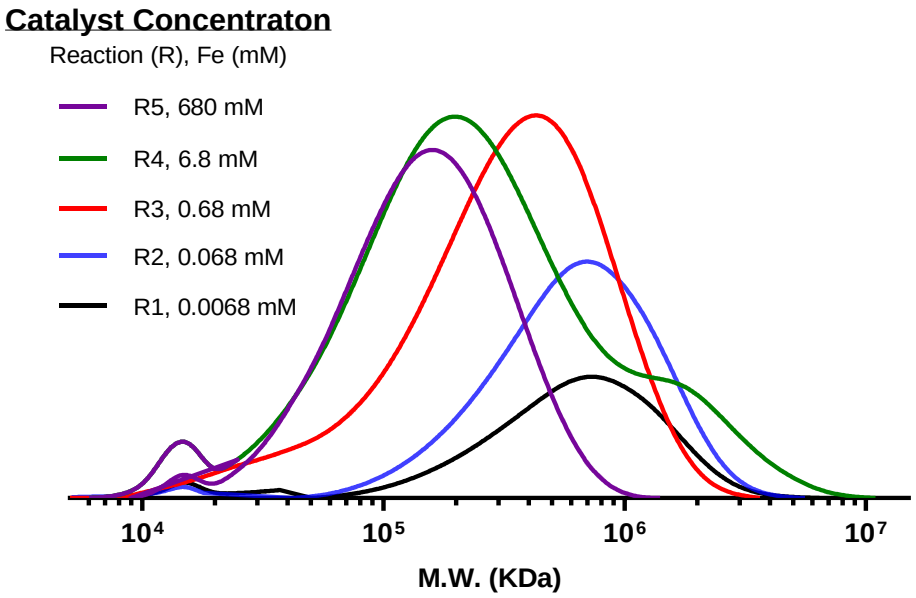

Figure 2. 13 SEC (THF) results of polymers produced during *C. met* initiated Fe ATRP of PEGMA (HEBIB in PBS at 37°C) using different concentrations of $FeCl_3$/Me_6TREN catalyst from reactions (R)s 1-5, Table 2. 7.

2.1.6.3 Degrees of Polymerisation (DP) and Initiator Type

Different degrees of polymerisation (DP) were targeted, DP 50, 25 and 10, to observe any effect on the control of the system (Figure 2. 14), whilst the ratio of initiator to catalyst ($FeCl_3$ and Me_6TREN) was kept constant. The rate of reaction was found to increase for polymerisations targeting DP10 which can be rationalised by equation 2.1, whereby the increased initiator concentration results in a faster R_p. Little effect, however, was seen in M_n or $Đ$ (Table 2. 8, Figure S2. 21A).

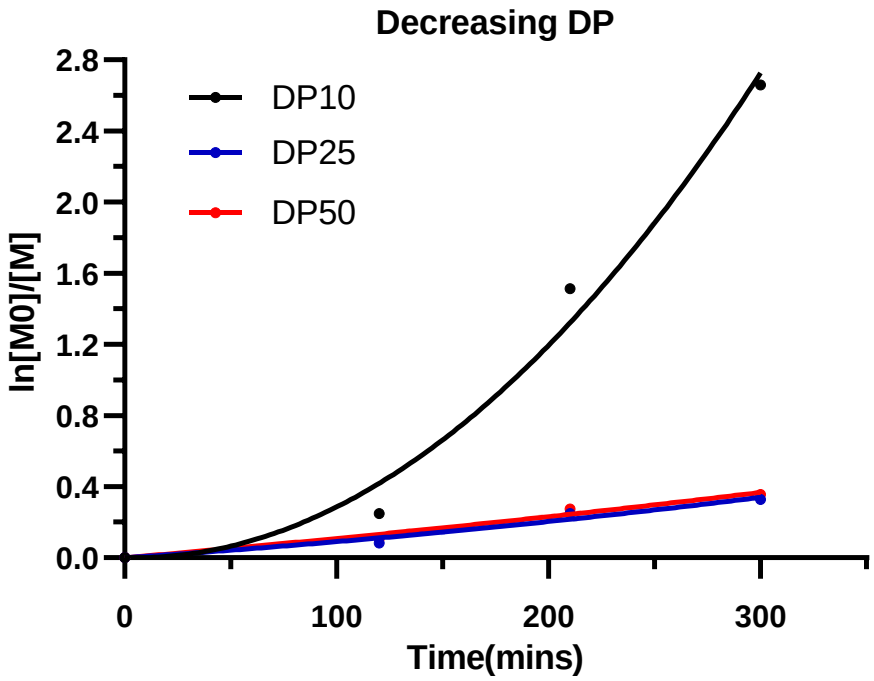

Figure 2. 14 ^{1}H NMR (400 MHz, D_2O) kinetic graph of b-ATRP (PEGMA in PBS at 37 °C) using different DPs; 10, 25 and 50.

Table 2. 8 Results obtained from bacterial initiated Fe ATRP polymerisations of PEGMA whilst varying DP; 10, 25 and 50.

Reaction DP	Conv.[a]	M_n^{th} (kDa)[b]	M_n^{SEC} (kDa)[c]	$Đ$[c]
50	30%	4.7	179	2.5
25	27%	2.2	145.6	2.3
10	78%	2.5	151.6	2.6

[a] Estimated from ^{1}H NMR monomer: polymer integrals. [b] M_n^{th} = (300 * DP* conversion) + 211 Da. [c] From SEC (THF).

The initiator type was also changed to a more water-soluble initiator, 2,3-dihydroxypropyl 2-bromo-2-methylpropanoate (DHBP) (Figure 2. 15, Figure S2. 9) in attempts to improve initiation efficiency. Reactions with this initiator were slower and generated polymers of a lower molar mass dispersity but the reaction was relatively uncontrolled (Figure S2. 21B). Poor initiation efficiency and non-linear second order plots in these studies (Figure S2. 21C) suggests that the initiator may have been partially absorbed/up-taken by the bacteria, or caught in the bacterial ECM, causing an imbalance in catalyst-initiator ratio and therefore polymers with larger M_n were observed.

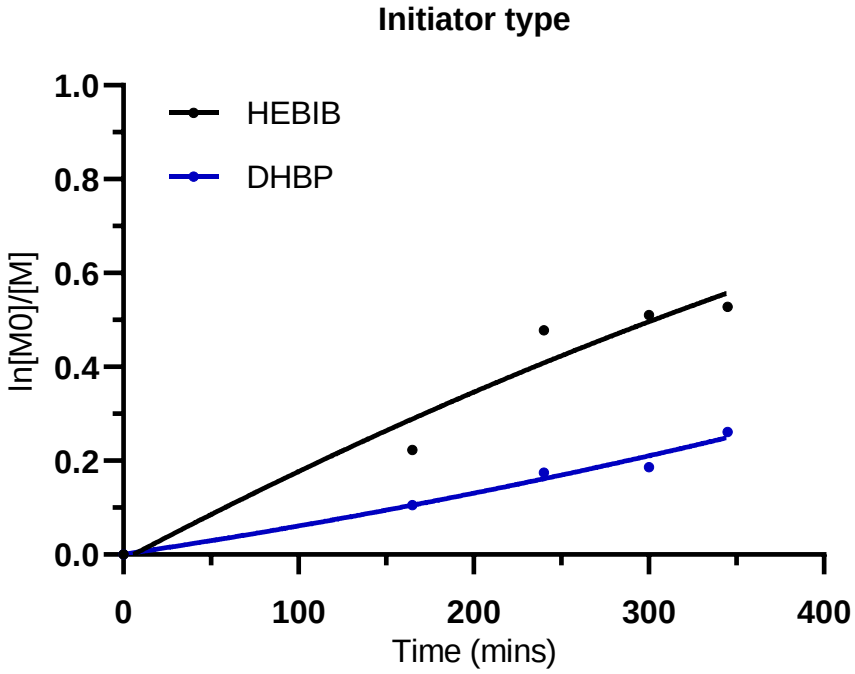

Figure 2. 15; ^{1}H NMR (400 MHz, D_2O) kinetic graph of b-ATRP (PEGMA in PBS at 37 °C) using different initiator types; HEBIB and DHBP.

2.1.6.4 Different Monomer Types

To investigate different chemical tolerances, monomers with charged and hydrophilic sidechains (MEDSA, *N*HEA, *N*IPAM and HEMA) were polymerised in the presence of bacteria (Figures Figure S2. 22, Figure S2. 23, Figure S2. 24, Figure S2. 25). *N*IPAM was found to be the fastest reacting monomer followed by MEDSA and *N*HEA. The results overall (Table 2. 9) showed a reduced polydispersity and better molecular weight control for PMEDSA and suggested that the system was tolerant to a range of monomer functionalities.

Table 2. 9 Polymerisation results for different monomers using bacterial Fe ATRP (PEGMA in PBS at 37 °C) initiated by HEBIB.

Monomer	Conv. (%)[a]	M_n^{th} (kDa) [b]	M_n^{SEC} (kDa) [c]	$Đ$[c]
MEDSA	80	11.4	42.5	1.8
*N*HEA	80	4.8	76.6	2.2
*N*IPAM	90	5.3	317	1.2
HEMA	50	3.5	167.5	2.1

[a] Estimated using of ^{1}H NMR from a comparison of monomer: polymer integral. [b] (DP 50); M_n^{th} = ($Mr_{monomer}$)* DP* conversion) + 211 Da. [c] Calculated using SEC (Aqueous – PBS, using RI detector only).

Conclusions

In summary, a new biocompatible Fe AGET ATRP method has been developed, exploring different ligand-iron combinations and DPs for optimisation. Of these, Me_6TREN was found to be efficient for the polymerisation of the hydrophilic monomer PEGMA. Good control and predictable molecular weights were achieved for targeted DP values of 100 and 200. The system was compatible with a variety of water-soluble monomers, demonstrating its potential to create multi-component materials. Different types of bacteria; *C. met*, *E. coli*, and *C. spor* were successfully able to initiate the polymerisations, further indicating the versatility of the polymerisation processes. The viability of *C. met* cells was retained throughout the reactions. Changing the Fe catalyst concentration was shown to alter the conversion and molecular weight control of the resulting polymers. Although better control of molar mass dispersity might be required, for example, if polymer-cell conjugates of highly specific dimensions were an objective, nevertheless, the results to date suggest a future platform technology that might be used to create a variety of synthetic-natural hybrid materials *in vivo*. These could include bacteria interconnected by redox-active polymers for multiplexed sensing, artificial ECM-bacteria colonies for bioreactor or bioremediation applications, or even implantable synthetic microbiomes. Future work will be directed towards these applications.

Materials and Methods

Materials

All chemicals were purchased from the supplier and used without further purification unless stated. Tris[2-(dimethylamino)ethyl]amine (Me_6TREN) 97%, Tris[2-(methylamino)ethyl]amine 97% (Me_3TREN) Tris[2-(2-methoxyethoxy)ethyl]amine (TDA-1) 95%, 2-2-bipyridine (Bpy) ≥99%, Ethylenediaminetetraacetic acid (EDTA) ≥99%, 2-Hydroxyethyl 2-bromoisobutyrate (HEBIB) 95%, Poly (ethylene gycol) methyl ether metacrylate (PEGMA-300) M_n average 300 (100 ppm MEHQ and 300 ppm BHT inhibitors), 2-Hydroxyethyl methacrylate (HEMA) >99% (<50 ppm MEHQ), *N*-Hydroxyethyl acrylamide (*N*HEA) 97% (1000 ppm MEHQ), 2-acrylamido-2-methyl-1-propanesulfonic acid (AMPS) 99%, 2-(Methacryloyloxy)ethyl dimethyl-(3-sulfopropyl)ammonium hydroxide (MEDSA) 97%, *N*-Isopropylacrylamide (*N*IPAM) 99%, and Dulbecco's Phosphate Buffer Saline (DPBS) (without $CaCl_2$ and $MgCl_2$, filtered, suitable for cell culture) were purchased from Sigma Aldrich. Iron(III)chloride hexahydrate ($FeCl_3.6H_2O$) ≥98% was purchased from scientific laboratory supplies. Ascorbic acid (AscA) >99% was purchased from Alfa Aesar. AMPS was converted to AMPS-Na form via the method detailed in the text. For bacteria growth Lysogeny broth (LB) was used.

Methods

^{1}H and ^{13}C NMR spectra were recorded at room temperature on a 400 MHz (Bruker DPX400 Ultrashield) using deuterated solvents (D_2O, $CDCl_3$ or DMSO). NMR spectra were analysed using MestReNova

11.0.0-17609 2016 Mestrelab Research S.L. Refractive Index (RI) measurements were measured using Anton Paar Abbemat 200 refractometer (25° C, PBS solvent (1X)) used to calculate dn/dc values.

Size Exclusion Chromatography (SEC)

DMF Size Exclusion Chromatography (SEC) was performed on Polymer Laboratories GPC 50 system fitted with refractive index (RI) detector, Agilent PLgel Mixed-D column and DMF + 1% LiBr eluent. Molecular weight (M_n) and polydispersity ($Đ$) were calculated according to PMMA narrow standards (1.5-1,000 kDa). Polymer samples were made by dissolving 3 mg/mL pure polymer in 1 mL DMF + 1% LiBr.

Aqueous SEC was performed on a Shimadzu Prominence UPLC system fitted with a DGU-20A5 degasser, LC-20AD, CBM-20A LITE system controller, SIL-20A auto-sampler, CTO-20A oven and RID-10A refractive index detector. Separations were performed on a series of Aquagel 30-40-50 (300 x 7.8 mm, 5 mm bead size, Agilent UK) columns fitted with a matching guard column (50 x 7.8 mm). The mobile phase was Dulbecco PBS buffer pH 7.4 at a flow rate of 1 mL/min and analysis was carried out at 35 °C. Column calibration was achieved using Polyethylene oxide/glycol EasiVials (2 mL) standards (196 Da–498 kDa, Agilent UK) and M_n and $Đ$ were calculated by LS or using calibrated RIS detectors.

THF SEC was performed on Agilent 1260 infinity system fitted with HPLC with an online vacuum degasser, an Agilent online differential refractometer (DRI) and a Wyatt Helios Dawn 8 multi-angle light scattering detector (MALS). Separations were performed on Agilent 3 µm

PLgel Mixed E columns (7.5 x 300 mm) connected in series with an Agilent PLgel 3 µm Guard column (7.5 x 50 mm). Injection volume was set to 100 uL analysis was carried out at 35 °C using THF (flow rate 1mL/min) at 35 °C. M_n and $Đ$ were calculated by LS (dn/dc= 0.1850 L/g).

Polymerisations carried out using AscA as a reducing agent were degassed using high purity nitrogen gas N_2 gas. Polymerisations carried out using bacteria were purged by storing in an anaerobic cabinet where presence of a small amount of oxygen may exist. Optical density (OD) measurements were carried out using BioMate 3S UV-Visible spectrophotometer at 600 nm.

Toxicity experiments

MICs of ATRP reagents were carried out using microplate reader (Infinite M Nano, TECAN) with 96-Well standard microplates (Costar 3363), measuring the $OD_{600\ nm}$ every 30 minutes for up to 24 hours.

Live/Dead staining and analysis of *C. met* was carried out using Live/Dead Backlight bacterial viability kit containing SYTO9 ($Excitation^{max}$/Emission = 535/617 nm) and Propidium iodide ($Excitation^{max}$/Emission = 483/503 nm) dyes. Live/Dead analysis was carried out using microplate reader with monochromatic fluorescence. Microscope images were taken using Nikon microscope (Japan, TIDH) with optimMOS scMos camera, analysed using NIS elements Advanced Research 4.00 (red and green filters).

Experimental and Supplementary

2.1.7 Synthesis of Poly(Poly ethylene glycol methyl ether methacrylate): AscA Initiated Fe ATRP

Iron(III)chloride hexahydrate ($FeCl_3.6H_2O$) and (Ligand) in (1:**X** ratio) were dissolved in phosphate buffered saline (PBS) (1.5 mL) in a 10 mL reaction vessel with rubber stopper; the solution was degassed for 20 minutes. Meanwhile, ascorbic acid (AscA) was dissolved in PBS (0.5 mL) and degassed separately for 20 minutes before it was transferred under nitrogen via degassed syringe to the iron and ligand mixture. The mixture was degassed for a further 20 minutes during Fe (III) to Fe (II) activation.

Simultaneously polyethylene glycol methyl ether methacrylate (PEGMA) (0.1 mmol) and 2-hydroxyethyl 2-bromoisobutyrate (HEBIB) were dissolved in 1.5 mL PBS in a 5 mL reaction vessel with rubber stopper and degassed for 20 minutes. The degassed monomer/initiator solution was then transferred to the degassed reaction mixture via degassed syringe and reaction vessel placed in a heating block (37 °C) and stirred. The reaction progress was monitored by taking ^{1}H NMR samples at various time intervals, until being terminated on exposure to air. The mixture was then dialysed against de-ionised water with ethylenediaminetetraacetic acid (EDTA) using dialysis membrane (MWCO = 3.5 kDa) for two days and subsequently freeze-dried to obtain polymer. All experiments made to 0.26 M (monomer concentration)

Conversion calculation. The estimated conversion was calculated by ^{1}H NMR using the ratio of integrals for monomer: polymer peaks. For PPEGMA, the first monomer CH from the CH_2 acrylate peak (~6.085 ppm) and CH_3 polymer backbone peak (0.418 – 1.341 ppm) were compared (Equation 1).

$$\text{Conversion} = \frac{\frac{\int Polymer}{protons}}{\frac{\int polymer}{protons} + \frac{\int monomer}{protons}} * 100 \qquad \text{(Equation 1)}$$

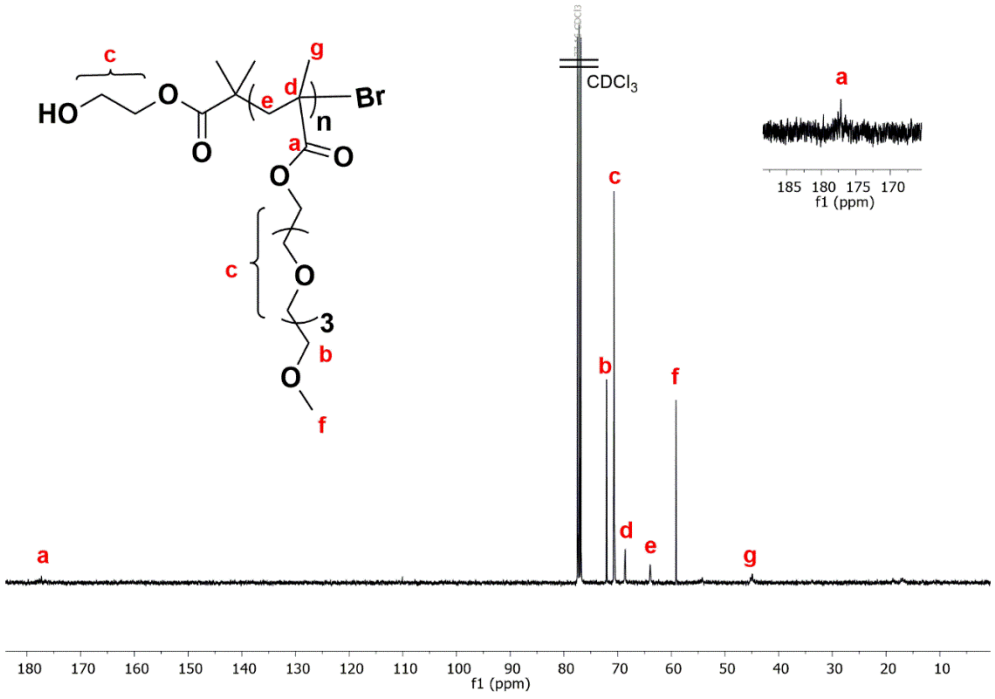

Figure S2. 1. ^{13}C NMR (100 MHz, $CDCl_3$) structure of purified PPEGMA resulting from AscA initiated Fe ATRP (PEGMA, $FeCl_3$, Me_6TREN and HEBIB in PBS at 37°C).

2.1.8 Control Experiment to show that Me_6TREN does not Activate the Polymerisation Reaction

$FeCl_3.6H_2O$ (9 mg, 0.033 mmol) and Me_6TREN (26.7 µL, 0.099 mmol, 1:3 ratio) were dissolved in phosphate buffer solution (PBS) (1.5 mL) in a 10 mL reaction vessel with rubber stopper; the solution was degassed for 20 minutes. AscA was omitted from the reaction. The mixture continued to degas for a further 20 minutes. Meanwhile, PEGMA (285.7 µL, 0.1 mmol) and HEBIB (4.81 µL, 0.033 mmol) were dissolved in 2 mL PBS in a 5 mL reaction vessel with stopper and degassed for 20 minutes. The degassed Monomer/initiator solution was then transferred to the degassed reaction mixture via syringe, and reaction vessel placed in a heating block (37 °C) for 5.5 hours. ^{1}H NMR samples were taken at time 0 and after 5.5 hours to monitor the reaction.

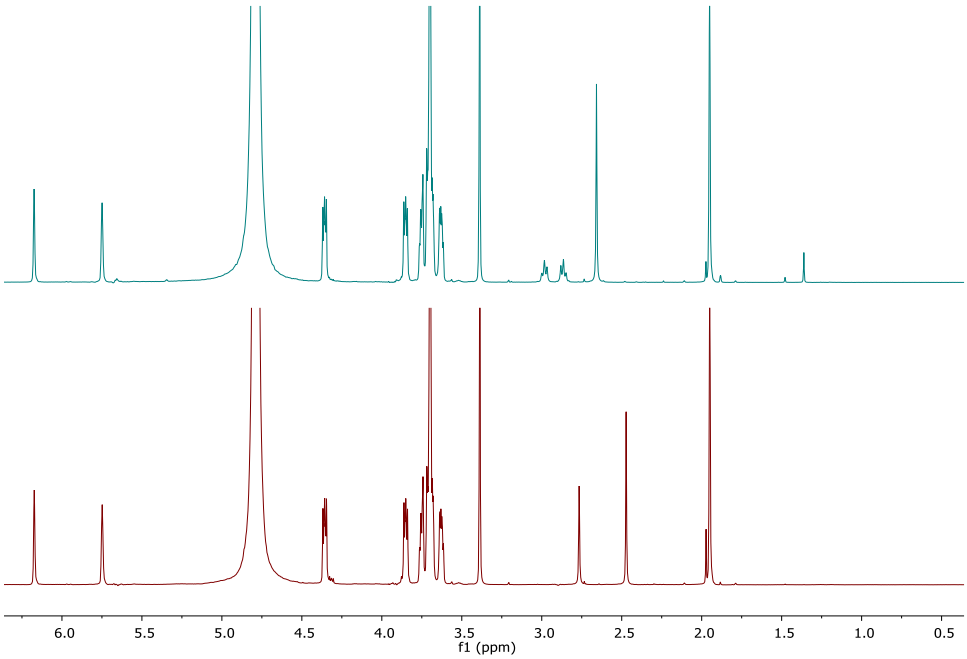

Figure S2. 2. Control Fe ATRP experiment (PEGMA, $FeCl_3$, Me_6TREN and HEBIB in PBS at 37°C) to show polymerisation inhibition without a reducing agent (AscA). ^{1}H NMR (400 MHz, D_2O) overlay at time 0 (bottom) and end, 5.5 hours (top) - absence of broad polymer backbone peaks ~0.4-1.3 ppm reveal no polymer formation.

2.1.9 Chain Extension Polymerisation (Targeted DP 100)

The reaction procedure was carried out as described previously for PPEGMA synthesis, but the chain extension of PPEGMA. Macro-initiator $PPEGMA_{30}$ (Table 1, entry 1) was used in place of the initiator.

Reagent ratio:

[Monomer]:[$FeCl_3$]:[Ligand]:[macro-initiator]:[AscA] =

[100]:[2]:[4]:[1]:[4].

The reaction proceeded for 26 hours resulting in <14% conversion. After purification by dialysis against water (3.5 kDa membrane) polymer was analysed by SEC and ^{1}H NMR.

Conversion calculation. The estimated conversion was calculated by ^{1}H NMR using the ratio of integrals for monomer: polymer peaks. For PPEGMA, the first monomer CH from the CH_2 acrylate peak (~6.085 ppm) and CH_3 polymer backbone peak (0.418 – 1.341 ppm) were compared as follows. The polymer integration from the macro-initiator was then deducted from the calculation of conversion after the chain extension using equation 1.

Before chain extension: Integration for macro-initiator

Monomer (CH): 1/1 proton = 1; Polymer (CH_3): 2.23/3 protons = 0.74

Original macro-initiator backbone peak = (0.74/1.74)*100 = **43%**

After chain extension: Integration for chain extended polymer (Figure S2.3)

Monomer (CH): 1/1 proton = 1; Polymer (CH_3): 3.92/3 protons = 1.31

Conversion + Original macro-initiator peak = (1.31/2.31)*100 = 57%

Conversion = 57% - 43% = **14%**

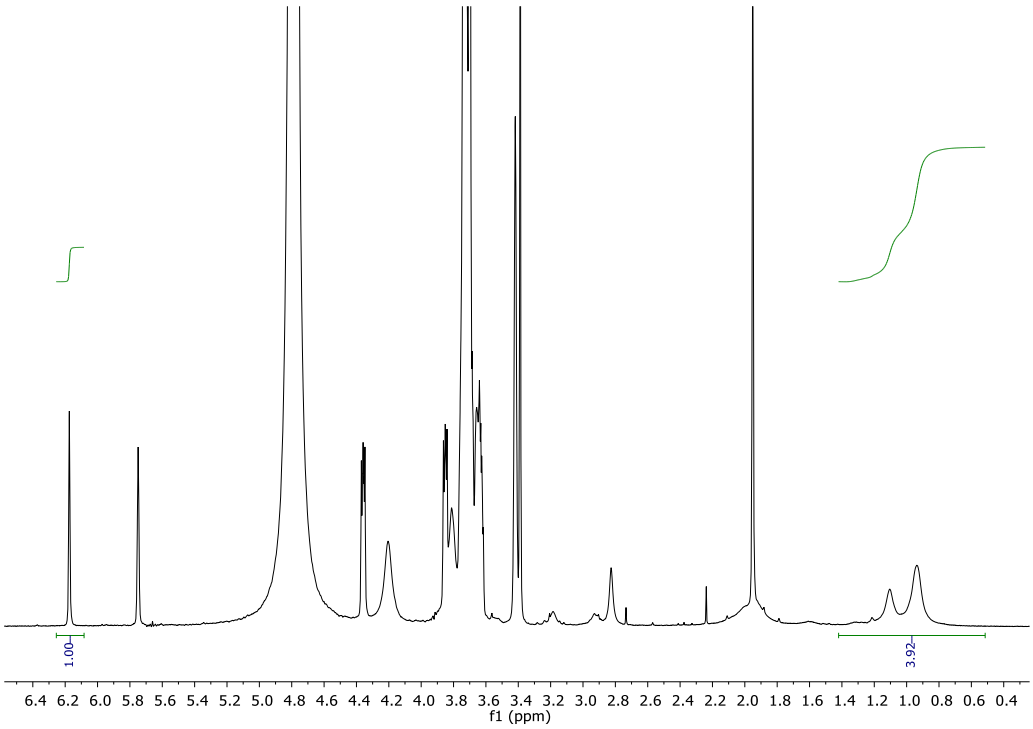

Figure S2. 3. Example ^{1}H NMR (400 MHz, D_2O) spectra after chain extension of PPEGMA macro-initiator. Integration comparison of CH from the CH_2 monomer acrylate and CH_3 polymer backbone peaks shown. Polymer resulting from AscA initiated Fe ATRP (PEGMA, $FeCl_3$, Me_6TREN and HEBIB in PBS at 37°C).

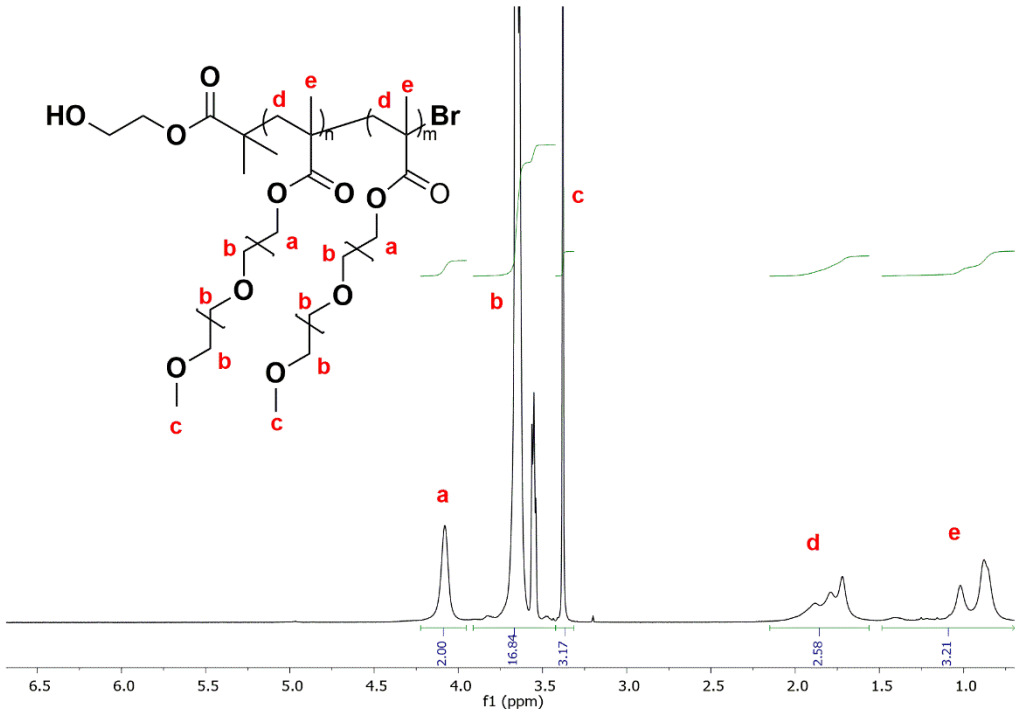

Figure S2. 4. ^{1}H NMR (400 MHz, $CDCl_3$) spectra of pure chain extended PPEGMA with assigned structure. Polymer resulting from AscA initiated Fe ATRP (PEGMA, $FeCl_3$, Me_6TREN and HEBIB in PBS at 37°C).

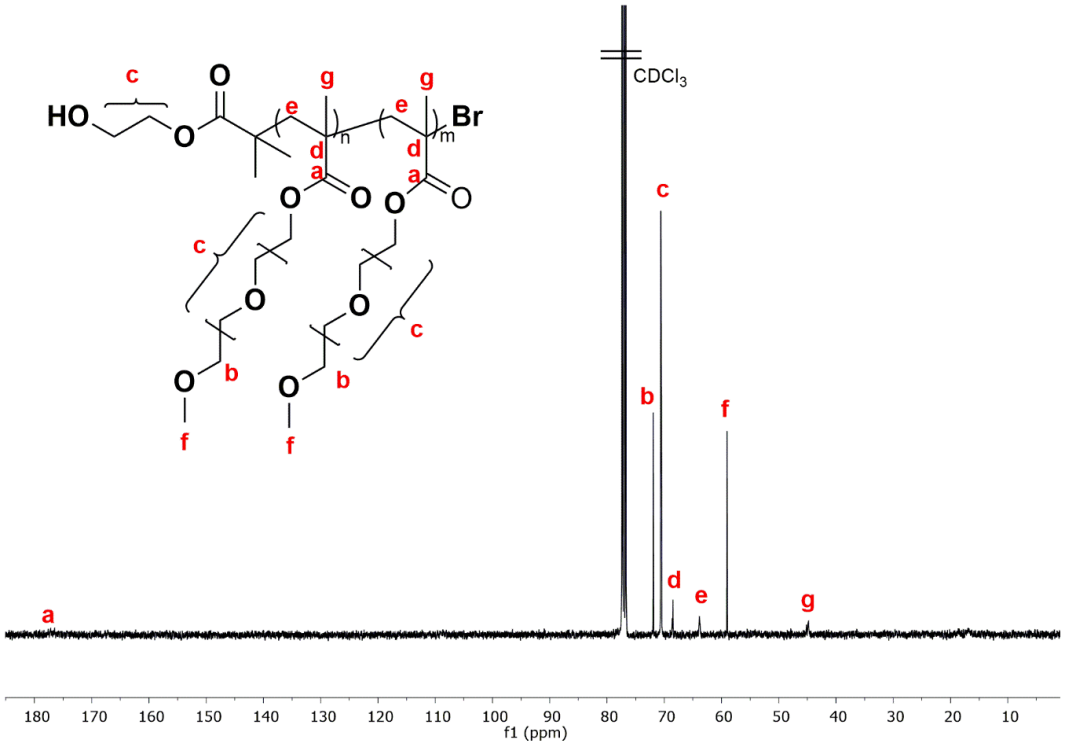

Figure S2. 5. ^{13}C NMR (100 MHz, $CDCl_3$) spectra of pure chain extended PPEGMA with assigned structure. Polymer resulting from AscA initiated Fe ATRP (PEGMA, $FeCl_3$, Me_6TREN and HEBIB in PBS at 37°C).

2.1.10 AscA initiated Fe ATRP: Differing the Monomer Types

The reaction procedure was carried out as described previously for PPEGMA synthesis, substituting different monomers for PEGMA. The concentration of the reaction (monomer concentration/total volume) was kept between 0.26 – 0.27 mol dm^{-3}.

$FeCl_3.6H_2O$ and Me_6TREN (1:3 ratio) were dissolved in PBS (1.5 mL) in a 10 mL reaction vessel with rubber stopper; the solution was degassed for 20 minutes. Meanwhile, AscA was dissolved in PBS (0.5 mL) and degassed separately for 20 minutes before it was transferred under nitrogen via degassed syringe to the Iron and ligand mixture. The mixture was degassed for a further 20 minutes during Fe^{3+} to Fe^{2+} activation.

Simultaneously (Monomer) (~0.1 mmol) and HEBIB (~0.033 mmol) were dissolved in 1.5 mL PBS in a 5 mL reaction vessel with rubber stopper and degassed for 20 minutes. The degassed monomer/initiator solution was then transferred to the degassed reaction mixture via degassed syringe and reaction vessel placed in a heating block (37 °C). The reaction progress was monitored by taking ^1H NMR samples at various time intervals, until being terminated on exposure to air. The mixture was then dialysed against de-ionised water with EDTA using dialysis membrane (MWCO = 3.5 kDa) for two days and subsequently freeze-dried to obtain polymer.

2.5.4.1 Determination of dn/dc for aqueous SEC of polymers

Refractive index increment (dn/dc) was calculated for polymers analysed by aqueous SEC. Several concentrations were measured and plotted against resulting RI measurement (Figure S26). The gradient of the line for each polymer was recorded as the dn/dc value (Table S3).

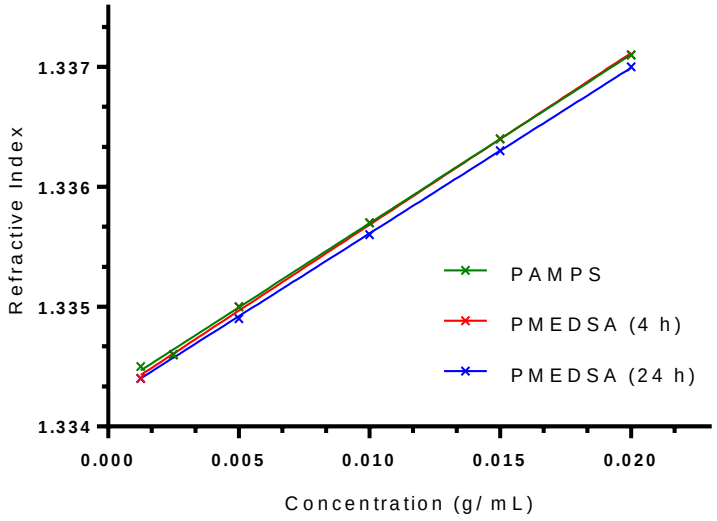

Figure S2. 6. A plot of RI measurements at different concentrations of polymer (PMEDSA – 4 h reaction. PMEDSA, - 24 h reaction and PAMPS) in PBS (1X).

Table S2. 1 Refractive index increment (dn/dc) values of different polymers; calculated using the gradient of RI measurement against concentrations of polymer (Solvent PBS).

Entry from table 2.2	Polymer	Dn/dc (mL/g)
6	PAMPS	0.1405
7	PMEDSA – 4 h reaction	0.1433
8	PMEDSA – 25 h reaction	0.1381

2.5.4.2 Determination of dn/dc for PEGMA for THF SEC

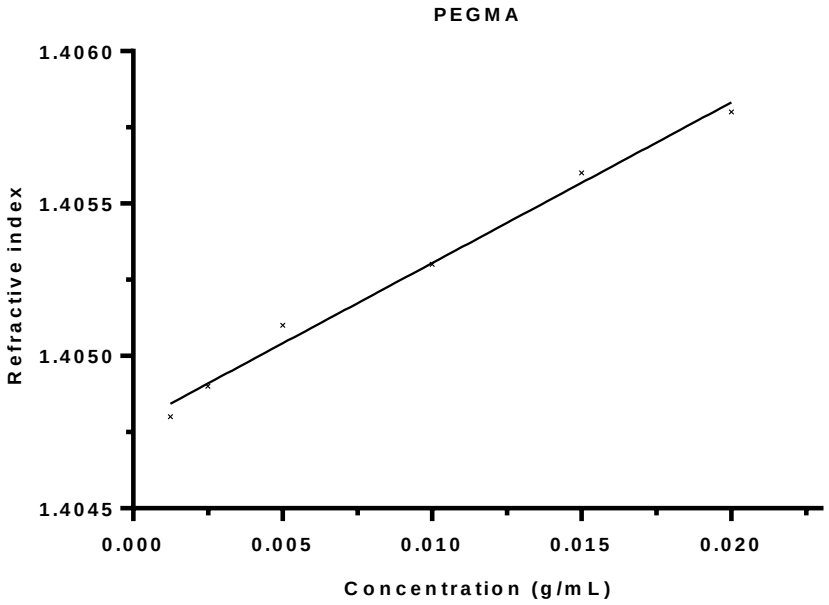

Figure S2. 7 Plot of RI measurements at different concentrations of PPEGMA (DP100) in THF.

Table S2. 2 Refractive index increment (dn/dc) values of PPEGMA; calculated using the gradient of RI measurement against concentrations of polymer (Solvent THF).

Polymer	Dn/dc (mL/g)
PEGMA	0.0527

2.1.11 Investigation of Catalyst Type: AscA Initiated Fe ATRP

$FeCl_3.6H_2O$ (9 mg, 0.033 mmol) **OR** $FeBr_3.6H_2O$ (9.9 mg, 0.033 mmol) was dissolved in phosphate buffer solution (PBS) (1.5 mL) with Me_6TREN (26.7 µL, 0.099 mmol, 1:3 ratio) in a 10 mL reaction vessel with rubber stopper; the solution was degassed for 20 minutes. After which a solution of simultaneously degassed AscA (0.5 mL of stock containing 5.9 mg, 0.033 mmol) was added to the Fe/Ligand solution to premix for 20 minutes. Meanwhile, PEGMA (285.7 µL, 1 mmol) and HEBIB (4.81 µL, 0.033 mmol) were dissolved in 1.5 mL PBS in a 5 mL reaction vessel with stopper and degassed for 20 minutes. The degassed Monomer/initiator solution was then transferred to the degassed reaction mixture via syringe, and the reaction vessel placed in a heating block (37 °C) for 5.1 hours. ^{1}H NMR samples were taken at time points throughout.

2.1.12 Minimum Inhibitory Concentrations (MIC)s of ATRP reagents towards *C. met* cultures

An overnight culture (18 hours growth from pellet) of *C. met* was grown at 30 °C. The culture was adjusted to an OD_{600} 0.2 and 100 µL placed in relevant wells of a 96-well plate. Dilutions of reagents were made in double concentrate in LB solution. 100 µL of each reagent was added to a relevant well containing 100 µL bacteria, diluting both bacteria and reagent by half to the required concentrations. The plate was covered with a lid and placed in a microplate reader with shaking at 30 °C for 24 hours where the OD_{600} was measured continuously. Results for the maximum concentration without affecting log growth rate are displayed in table S2.2.

Table S2. 3. MIC concentrations of ATRP reagents at which *C. met* growth at exponential phase was not significantly affected.

Reagent	Concentration (mM)
PEGMA	14
HEMA	14
*N*IPAM	14
MEDSA	50
*N*HEA	50
Me_6TREN	2.5
Bpy	0.025
Me_3TREN	2.5
HEBIB	2.5
DHBP	5
$FeCl_3.6H_2O$	70

Monomers

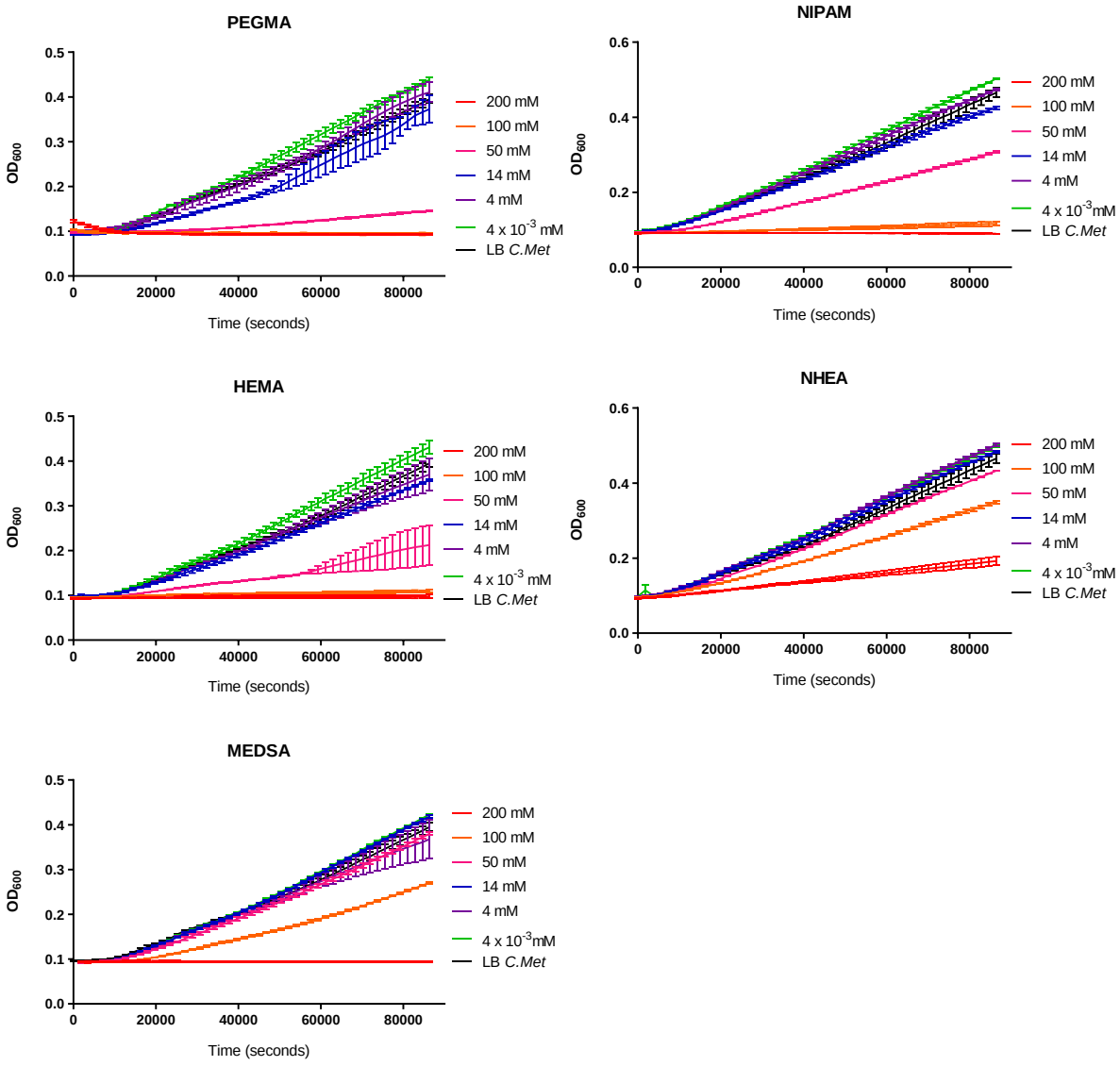

Figure S2. 8. MIC Experiments of different monomers at different concentrations with *C. met* to assay toxicity limits.

Ligands and Iron

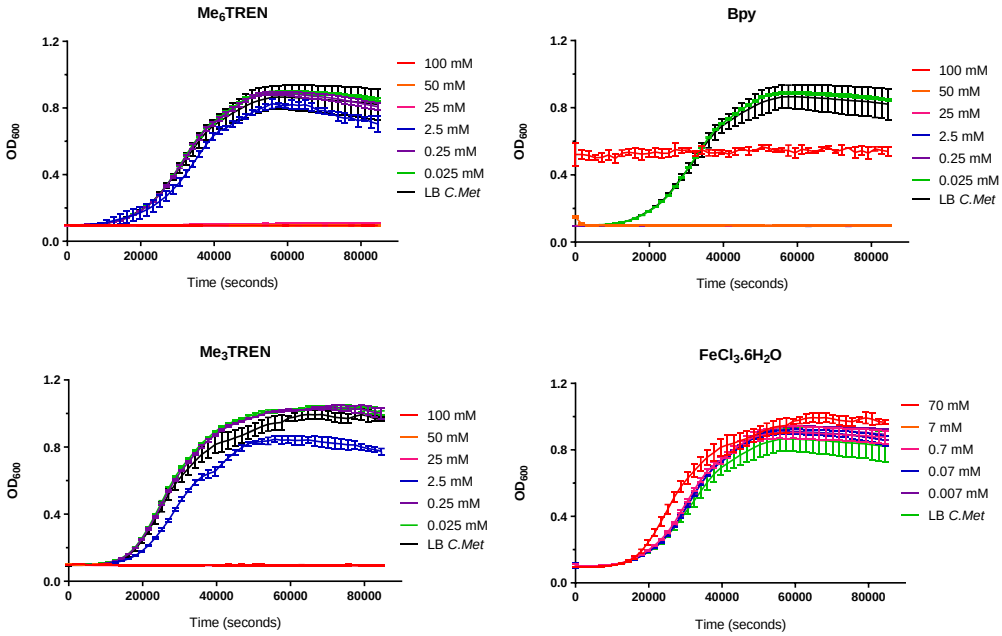

Figure S2. 9. MIC Experiments of different Ligands, iron sources and ligand/catalyst mixtures at different concentrations with *C. met* to assay toxicity limits.

Note: In the case of Bpy, the reagent precipitated out at high concentrations due to its poor solubility.

Initiators

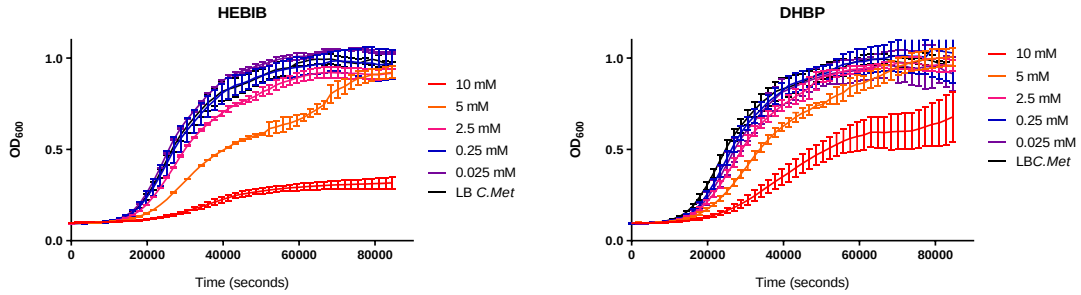

Figure S2. 10. MIC Experiments of different initiators at different concentrations with *C. met* to assay toxicity limits.

2.1.13 Synthesis of Poly(Poly ethylene glycol methyl ether methacrylate) using *C. met* – Catalyst Controls

Bacteria Preparation

C. met were inoculated in 2 x 20 mL LB media and shaken at 30 °C overnight. In preparation for the polymerisation the bacteria were washed with PBS (2 x 10 mL) using centrifugation (8000 rpm, 10 mins). In anaerobic conditions, the pellet was re-suspended in 4 mL PBS solution of which 1 mL was taken for OD_{600} reading. The OD_{600} of the original 20 mL solution was taken and recorded to be 1 – 1.2 for each experiment (~6.5 x 10^9 CFU/mL in total reaction volume). 1.5 mL of the bacteria in PBS were used in the polymerisation. The pellet was suspended in 4 mL PBS solution of which 1 mL was taken for OD_{600} reading.

Polymerisation Procedure

Reagents were weighed out in sterile microfuge tubes (Eppendorf) and placed in the anaerobic cabinet (CO_2:H_2:N_2 = 10:10:80%) for 1 hour before the reaction to remove oxygen traces. The following reactions were carried out inside the anaerobic cabinet at 30 °C.

S2.6.7A; Reaction A – with bacteria

$FeCl_3.6H_2O$ (9 mg, 0.033 mmol) and Me_6TREN (26.7 µL, 0.99 mmol) were added to a 5 mL microfuge tube with small stir bar and 1 mL PBS (degassed). 1.5 mL *C. met* solution was then added to the mixture and left to stir for 20 minutes. PEGMA (204.8 µL, 0.71 mmol) and HEBIB (1.04 µL, 0.007 mmol) in 1 mL PBS (degassed) were lastly added to the

mixture and stirred using a magnetic stir bar and stir plate in an anaerobic cabinet at 30 °C for 6 hours. Time points were taken for ^{1}H NMR analysis; each sample (50 µL) was centrifuged (5,000 g, 2 min) in a microcentrifuge tube (Eppendorf), to remove iron and bacteria residue for clearer spectra, and the supernatant was taken for analysis. The reaction was terminated by exposure to air and the reaction mixture was centrifuged to remove iron and bacteria residue. The supernatant was purified by dialysis (3.5 kDa, MWCO) for two days with EDTA to remove traces of iron catalyst before freeze drying.

S2.6.7B; Control Reaction B – without bacteria

$FeCl_3.6H_2O$ and Me_6TREN were added to a 5 mL microfuge tube and 1 mL PBS (degassed) was added. Bacteria were omitted from the reaction. PEGMA and HEBIB in 1.75 mL PBS (degassed) were lastly added to the mixture and stirred in an anaerobic cabinet at 30 °C for 6 hours. Time points were taken for ^{1}H NMR analysis; each sample (50 - 100 µL) was spun in an microcentrifuge tube (4000 rpm, 1 min) and the supernatant was taken for analysis to remove iron and bacteria residue for clearer spectra.

S2.6.7C; Control Reaction C – without catalyst

PEGMA and HEBIB were added to a 5 mL microfuge tube with small stir bar and 2 mL PBS (degassed) was added. 1.5 mL *C. met* bacteria in PBS was then added to the mixture and left to stir in an anaerobic cabinet at 30 °C for 6 hours. Time points were taken for ^{1}H NMR analysis; each sample (50 - 100 µL) was spun in a microcentrifuge tube (4000 rpm, 1

min) and supernatant taken for analysis to remove iron and bacteria residue for clearer spectra.

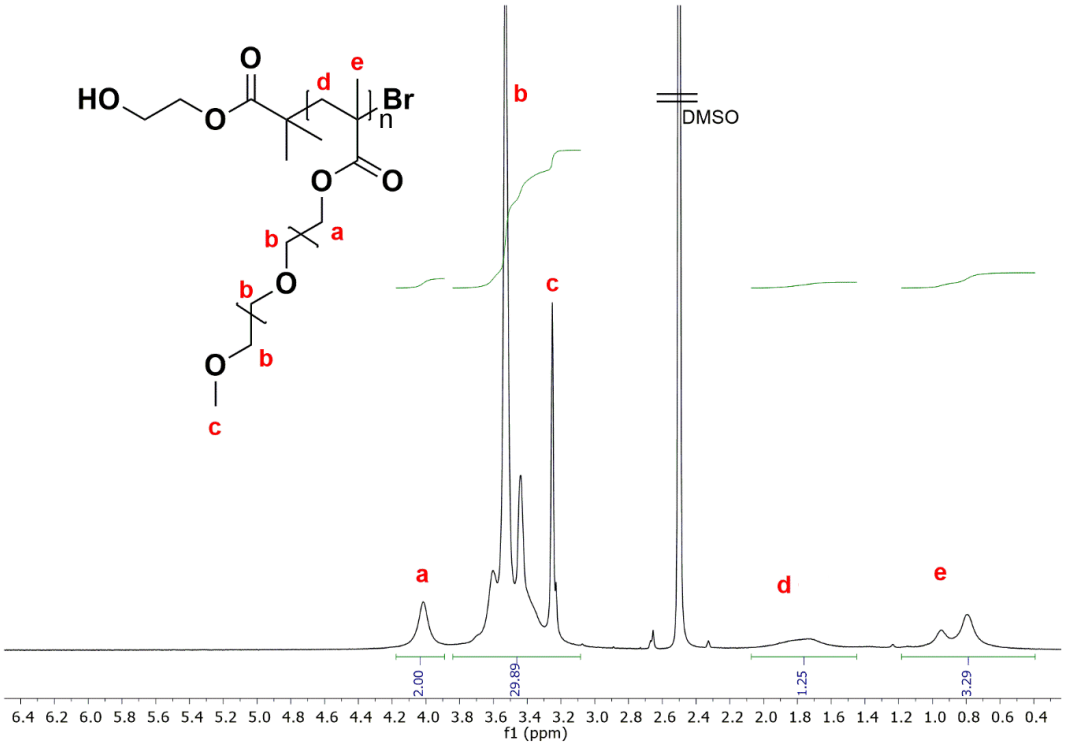

Figure S2. 11. ^{1}H NMR (400 MHz, DMSO) Spectrum of PPEGMA formed via Fe ATRP polymerisation initiated by *C. met* ($FeCl_3$, Me_6TREN and HEBIB in PBS at 37°C) with corresponding structure and assignment.

2.1.14 *C. met* initiated Fe ATRP of PEGMA (14 mM) without HEBIB

An experiment was carried out as written in Section 2.6.7A but without initiator added to the reaction. After 24 hours, unsubstantial amount of polymer was formed.

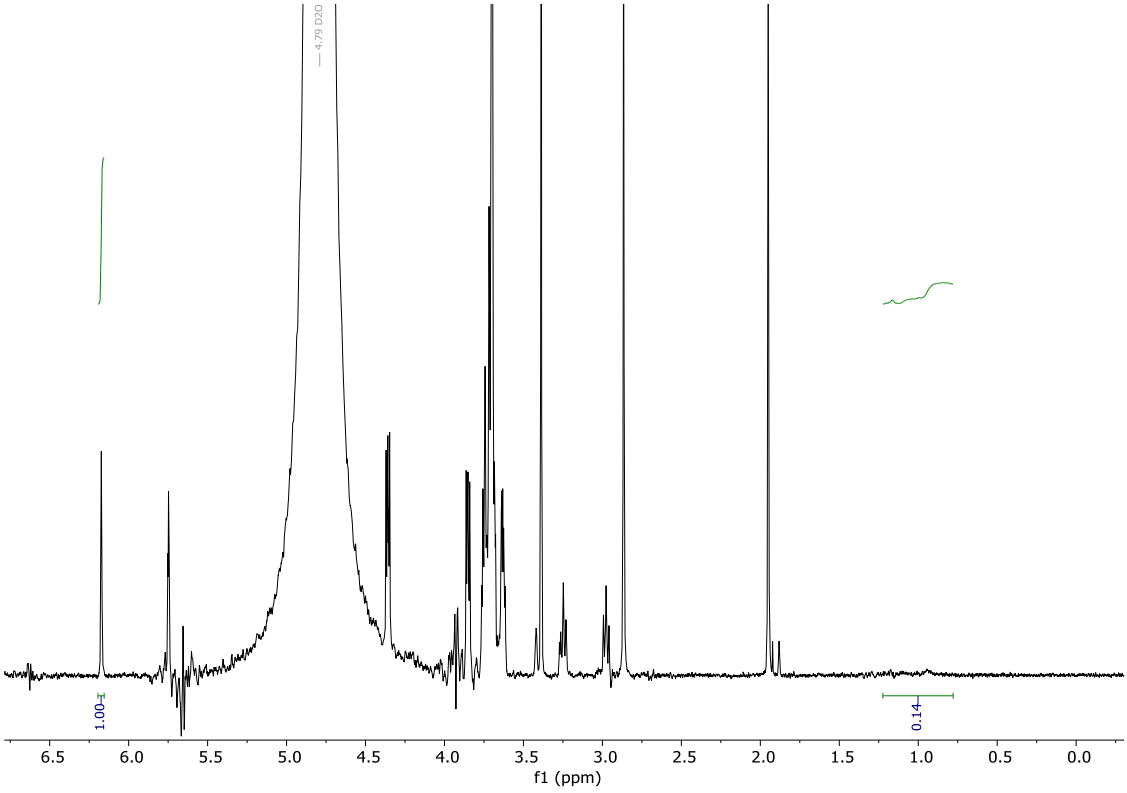

Figure S2. 12 ^{1}H NMR (400 MHz, D_2O) at T = 24 h for bacterial initiated Fe ATRP ($FeCl_3$/Me_6TREN) of PEGMA (14 mM) - control polymerisation reaction using *C. met* without ATRP initiator, HEBIB.

2.1.15 Live/dead Viability Assays and Imaging for *C. met*

Method for the Calibration curve

C. met cultures (3 biological replicates) were grown from a bead stock solution in 5 mL LB at 30°C overnight. These were adjusted to OD_{600} of 0.1. These were subsequently centrifuged (5,000 g, 15 mins) and re-suspended in 1 mL LB. 0.5 mL was added to 10 mL isopropyl alcohol (IPA) and 0.5 mL added to 10 mL LB. These were left for 1 hour at room temperature and on ice, respectively. They were then centrifuged (15 mins), washed with 5 mL PBS (10 mins) and re-suspended in 2 mL PBS each. 1.5 mL of each was added to a further 2.2 mL PBS to dilute to a bacteria concentration which reflects that of the ATRP reactions.

Mixtures of live and dead bacteria were made to obtain different percentages of live bacteria (100%, 90%, 70%, 50%, 30%, 10%, 0%). 100 µL of each sample was transferred to a black bottomed 96-well plate and 100 µL dye mixture added (2 replicas). The dye mixture (1mL:6µL; distilled water:dye mix (Syto9+PI)) was made according to manual (Live/Dead backlight viability assay kit). The plate was incubated for 15 mins before microplate analysis via monochromatic fluorescence. The TECAN reader was set to excitation and emission ranges of; SYTO 9: 483-503 nm and PI: 535-617 nm. Results were plotted in graphpad prism and asymmetric line of best fit was plotted (Figure S2.11). Values above 90% live bacteria are less reliable.

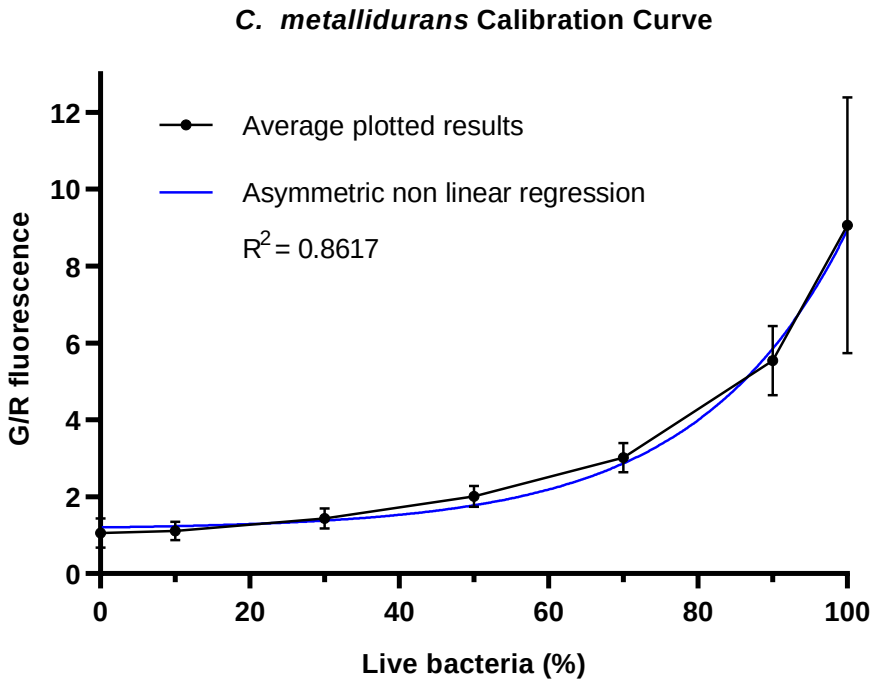

Figure S2. 13. *C. met* calibration curve (live/dead) for determining % live bacteria using fluorescence assay.

C. met instructed ATRP live dead analysis

Method

This method was used for the analysis of samples A, A*, C1, and C2 (Section 2.6.7). 100 µL of each sample was transferred to a black bottomed 96-well plate and 100 µL dye mixture was added (2 replicas). The dye mixture (1 mL:6 µL; distilled water:dye mix (Syto9+PI)) was made according to the manual (Live/Dead backlight viability assay kit). The plate was incubated for 15 mins before TECAN analysis via monochromatic fluorescence. The TECAN reader was set to excitation and emission ranges of; Syto 9: 483-503 nm and PI: 535-617 nm. Fluorescence measurements were converted to percent live bacteria

using the above calibration curve (Figure S2.11) via graphpad prism interpolation analysis.

Fluorescence microscopy imaging for *C. met* instructed ATRP

Method

This method was used for the analysis of samples A, A*, C1, and C2 (Section 2.6.7). Dye mix (Live/Dead backlight viability assay kit) of propidium iodide and SYTO9 (1:1) was made. Distilled water was added to this mix (ratio 1 mL: 3 µL). To each sample (100 µL), 0.3 µL dye solution was added and incubated in the dark for 15 minutes. 5 µL of each sample was pipetted onto a microscope slide and covered with a cover slip, then imaged using Nikon microscope. Images were analysed by Image J, and live/dead filtered combined to overlay fluorescence of SYTO 9 and propidium iodide.

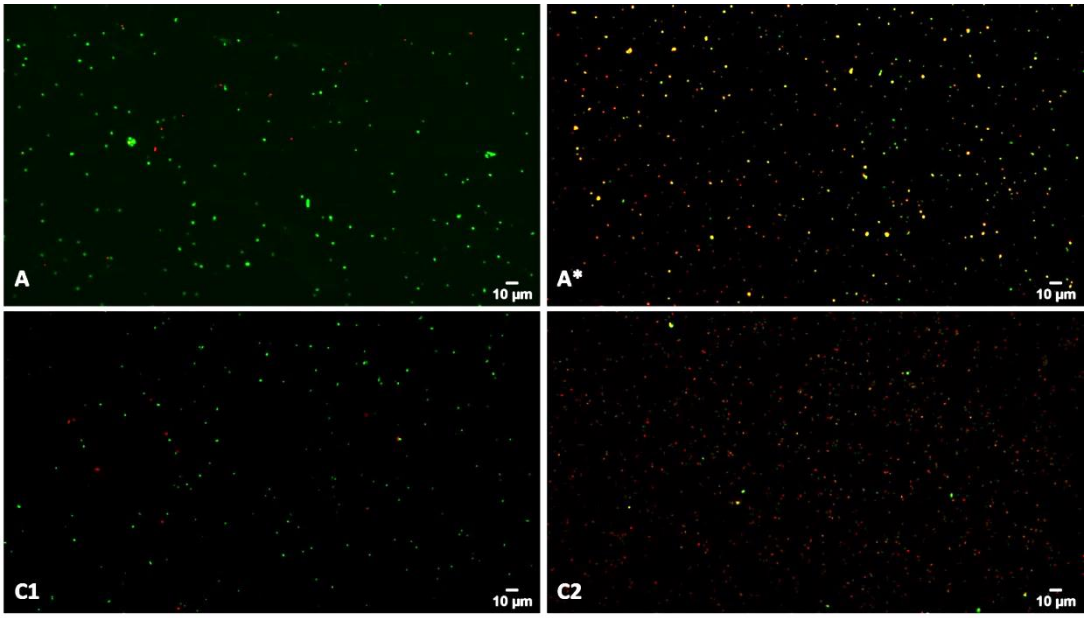

Figure S2. 14 Typical fluorescence microscopy images of A (top left)- ATRP reaction with live cells; A*(Top right) - ATRP reaction with dead cells; C1 (Bottom left) Control of live bacteria incubated in PBS in an anaerobic cabinet; and C2 (Bottom right) - Control of dead bacteria.

Colony Forming Unit (CFU) analysis

Method

This method was used for the analysis of samples A, A*, C1, and C2 (Section 2.6.7). 100 µL of each sample was diluted in 900 µL PBS and vortexed. These serial dilutions were continued appropriately for each sample. 20 µL of selected dilution factors were plated onto an LB agar plate and stored at room temperature for 4 days. After which colonies were counted and cell numbers calculated.

$$CFU = colonies * \frac{1}{dilution\ factor} * \frac{1}{volume(mL)}$$

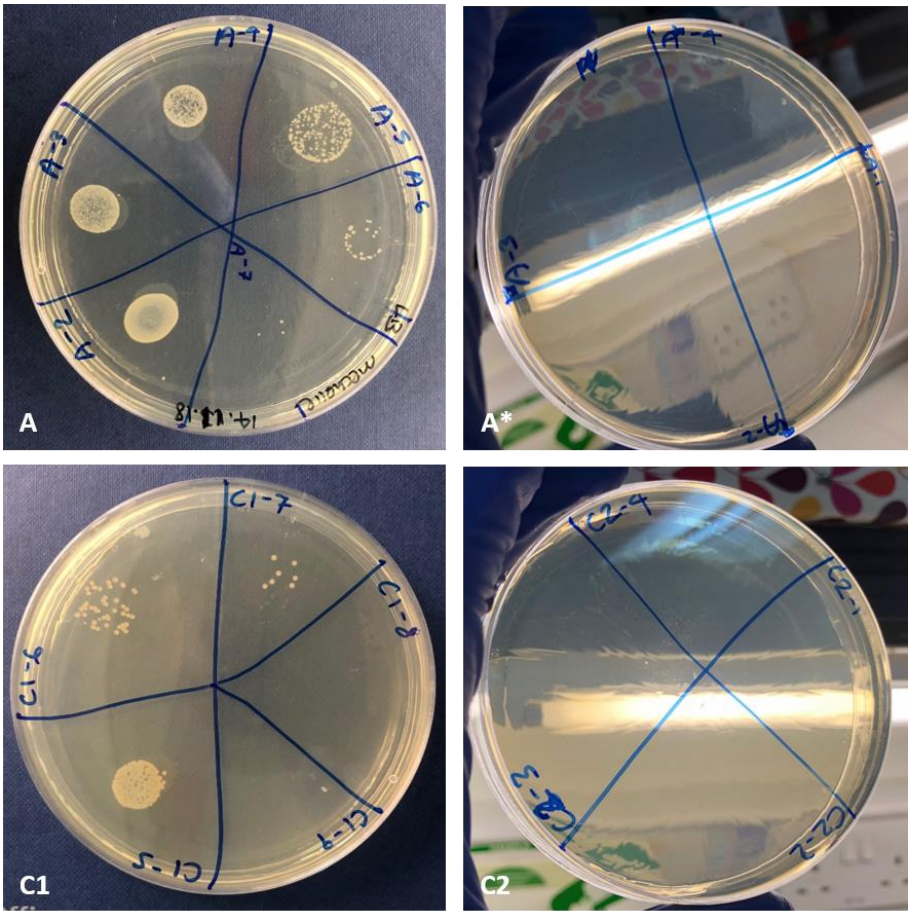

Figure S2. 15. Plates of *C. met* on LB agar after initiating Fe ATRP of PEGMA (FeCl3, Me_6TREN, HEBIB, in PBS at 37 °C). A= live bacteria, A*= pre-killed bacteria. Control bacteria which were not exposed to polymerisation reagents: C1= Live bacteria, C2: pre-killed bacteria.

2.1.16 Synthesis of Poly(Poly ethylene glycol methyl ether methacrylate) Initiated by *C. met., E. coli* and *C. spor.*

In the following Polymerisations 14 mM monomer concentration was used to maintain bacterial viability.

Bacteria Preparation

A cryo-stock bead (stored at -80 °C) of *C. met* CH34, *E. coli* top 10 or *C. spor** wild type were inoculated in 5 mL LB media and shaken at 30 °C and 37.5 °C, respectively overnight. The culture was then adjusted to OD_{600} 0.1 in 20 mL LB and grown for a further 16-18 hours until the OD_{600} of the culture reached 1.1 - 1.2 (~6.5 x 10^9 CFU/mL in final reaction volume). The culture was centrifuged (5,000 g, 15 mins) and the supernatant was washed with PBS twice (10 mL for 15 mins, and 5 mL for 10 mins). The pellet was re-suspended in 4 mL degassed PBS in the anaerobic cabinet and further deoxygenated for 45 mins.

For each reaction 1.5 mL of bacteria was used (total 40% bacteria solution): **A**: Bacteria instructed ATRP reaction; **B**: No bacteria and **C**: No $FeCl_3.6H_2O$.**

**In the case of C. spor care was taken to eliminate contact of culture with air; culture was grown in an anaerobic cabinet (37.5 °C) and all washes took place in anaerobic conditions due to extreme sensitively of the bacteria to the outside air. Polymerisations of this organism took place in an anaerobic 37.5 °C cabinet.*

For C. met just Reaction A was carried out as the previous section includes similar controls to B and C. Additionally the **reaction A was carried out to observe the effect of using killed bacteria in the polymerisation.*

2.6.10A; Reaction A

E. coli and C. met

In an anaerobic cabinet (30 °C), $FeCl_3.6H_2O$ (100 µL of 7.49 mM stock solution, $2.63x10^{-3}$ mmol) and Me_6TREN (100 µL of 22.2 mM stock solution, $7.91x10^{-3}$ mmol) were added to a 5 mL microfuge tube with a small stir bar and 1 mL PBS (degassed) was added. 1.5 mL bacteria culture was then added to the mixture and left to stir for 20 minutes. PEGMA (16.2 µL, 0.0567 mmol) and HEBIB (100 µL of 3.22 mM stock solution, $1.13\ x10^{-3}$ mmol) in 1 mL degassed PBS were lastly added to the mixture and stirred using a magnetic stir bar and stir plate in an anaerobic cabinet at 30 °C for 24 hours. Time points were taken before and after the reaction for ^1H NMR analysis; each sample (50 µL) was spun in an microcentrifuge tube (5,000 g, 2 min) to remove iron and bacteria residue for clearer spectra, and the supernatant was taken for analysis. The reaction was terminated after 24 hours by exposure to air and the reaction mixture was centrifuged to remove iron and bacteria residue. The supernatant was purified by dialysis (3.5 kDa, MWCO membrane) for two days with EDTA to remove traces of iron catalyst before freeze-drying.

C. spor

In an anaerobic cabinet (37.5 °C), $FeCl_3.6H_2O$ (100 µL of 7.49 mM stock solution, $2.63x10^{-3}$ mmol) and Me_6TREN (100 µL of 22.2 mM stock solution, $7.91x10^{-3}$ mmol) were added to a 5 mL microfuge tube with a small stir bar and 1 mL PBS (degassed) was added. 1.5 mL bacteria culture was then added to the mixture and left to stir for 20 minutes. PEGMA (16.2 µL, 0.0567 mmol) and HEBIB (100 µL of 3.22 mM stock solution, $1.13\ x10^{-3}$ mmol) in 1 mL degassed PBS were lastly added to the mixture and stirred using magnetic stir bar and stir plate in an anaerobic cabinet at 37.5 °C for 24 hours. Time points were taken before and after the reaction for ^1H NMR analysis; each sample (50 µL) was spun in a microcentrifuge tube (5,000 g, 2 min) to remove iron and bacteria residue for clearer spectra, and the supernatant was taken for analysis. The reaction was terminated after 24 hours by exposure to air and the reaction mixture was centrifuged to remove iron and bacteria residue. The supernatant was purified by dialysis (3.5 kDa, MWCO membrane) for two days with EDTA to remove traces of iron catalyst before freeze drying.

2.6.10A*; Reaction A* (C.met)

This procedure was carried out as written in 2.6.10 (Reaction A) but before washing, the *C. met* pellet was re-suspended in isopropyl alcohol (IPA) (70%) for 1 hour. The bacteria were washed using centrifugation (5000 g, 15 mins, PBS (10 mL)) before resuspending in PBS (4 mL), degassing in an anaerobic cabinet (1 hour) and 1.5 mL was added to the reaction mixture.

2.6.10B; Reaction B

The reaction was carried out using the method from Reaction A (S2.5.10A) but omitting bacteria.

Briefly, $FeCl_3.6H_2O$ and Me_6TREN were added to a 5 mL microfuge tube with a small stir bar and 1 mL PBS (degassed) was added. 1.5 mL PBS was then added to the mixture and left to stir for 20 minutes. PEGMA and HEBIB in 1 mL degassed PBS were lastly added to the mixture and stirred using a magnetic stir bar and stir plate in an anaerobic cabinet (30 °C for *E. coli* and *C. met*, **OR** 37.5°C for *C.s por*) for 24 hours. The reaction was terminated after 24 hours by exposure to air and the reaction mixture was centrifuged to remove iron and bacteria residue. The supernatant was purified by dialysis (3.5 kDa, MWCO membrane) for two days with EDTA to remove traces of iron catalyst before freeze-drying.

2.6.10C; Reaction C

The reaction was carried out using the method from Reaction A (2.6.10A) but omitting catalyst ($FeCl_3$ and Me_6TREN).

Briefly, 1.2 mL PBS (degassed) was added to a 5 mL microfuge tube with a small stir bar. 1.5 mL bacteria were then added to the mixture and left to stir for 20 minutes. PEGMA and HEBIB in 1 mL degassed PBS were lastly added to the mixture and stirred using a magnetic stir bar and stir plate in an anaerobic cabinet (30 °C for *E. coli* and *C. met*, **OR** 37.5°C for *C. spor*) for 24 hours. The reaction was terminated after 24 hours by exposure to air and the reaction mixture was centrifuged to remove iron and bacteria residue. The supernatant was purified by dialysis (3.5 kDa,

MWCO membrane) for two days with EDTA to remove traces of iron catalyst before freeze-drying.

Table S2. 4 Conversions of reactions and controls using *E. coli* and *C. spor* to initiate Fe ATRP of PEGMA ($FeCl_3$, Me_6TREN, HEBIB, 37 °C, in PBS).

	Conversion calculated by ^{1}H NMR monomer:polymer integral ratio	
	E. coli top 10	***C. spor.***
A	78%	36%
B	0%	0%
C	20%	0%

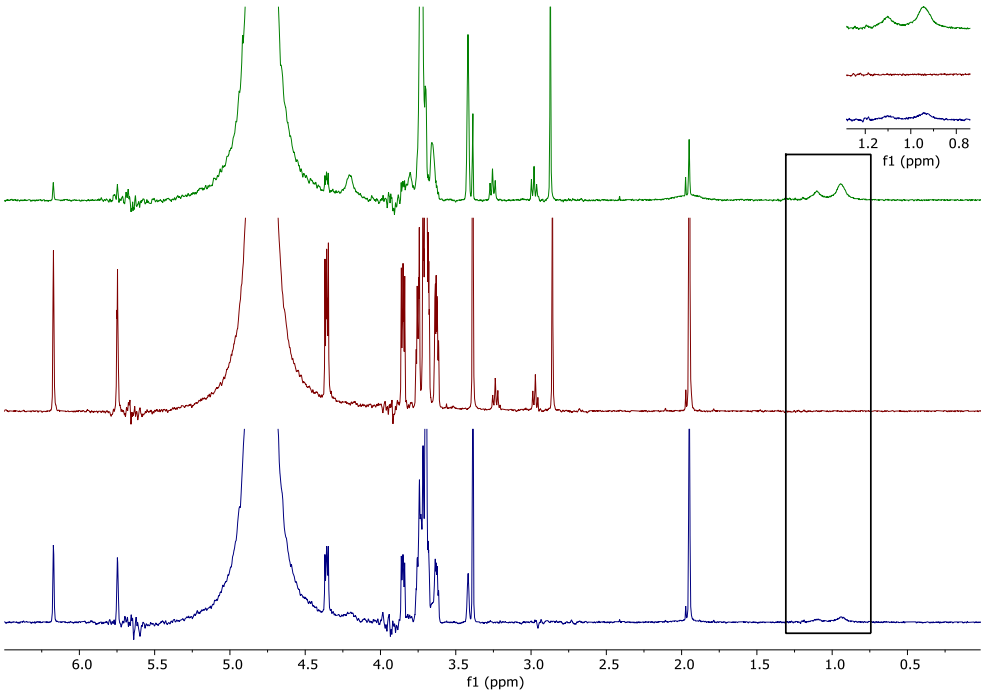

Figure S2. 16. ^{1}H NMR Spectra (400 mHz; D_2O) time 24 hours for *E. coli* instructed Polymerisation A (Top green) and controls B (Middle red) and C (Bottom, Blue). Resulting from Fe ATRP reactions of PEGMA using $FeCl_3$/Me_6TREN and HEBIB at 37 °C, in PBS.

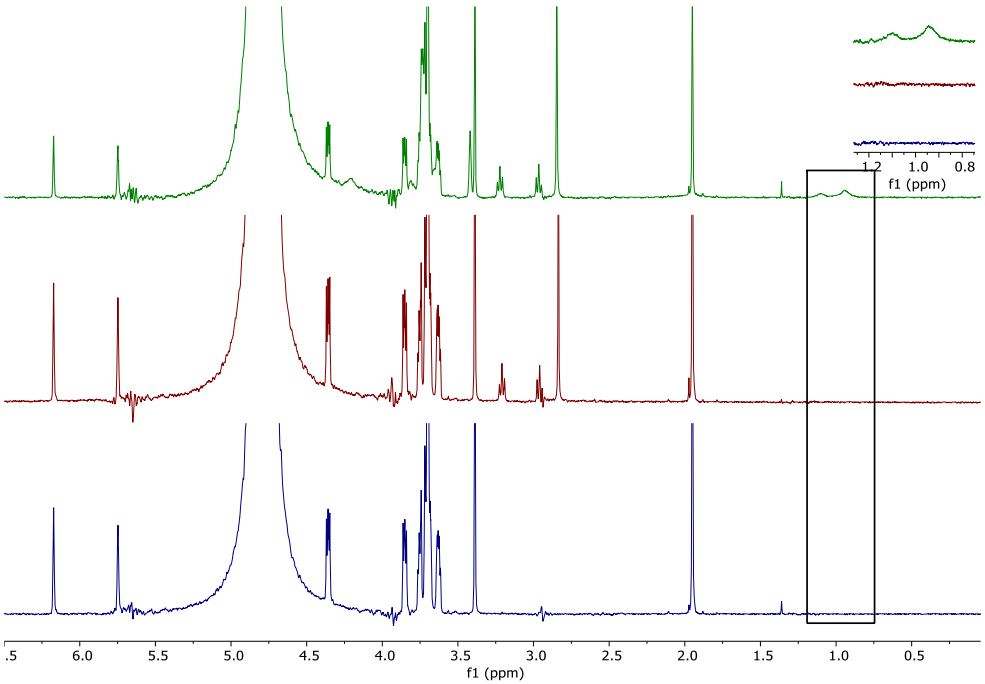

Figure S2. 17. ^{1}H NMR Spectra (400 MHz; D_2O) time 24 hours for *C. spor* instructed polymerisation A (Top green) and controls B (Middle red) and C (Bottom, Blue). Resulting from Fe ATRP reactions of PEGMA using $FeCl_3$/Me_6TREN and HEBIB at 30 °C, in PBS.

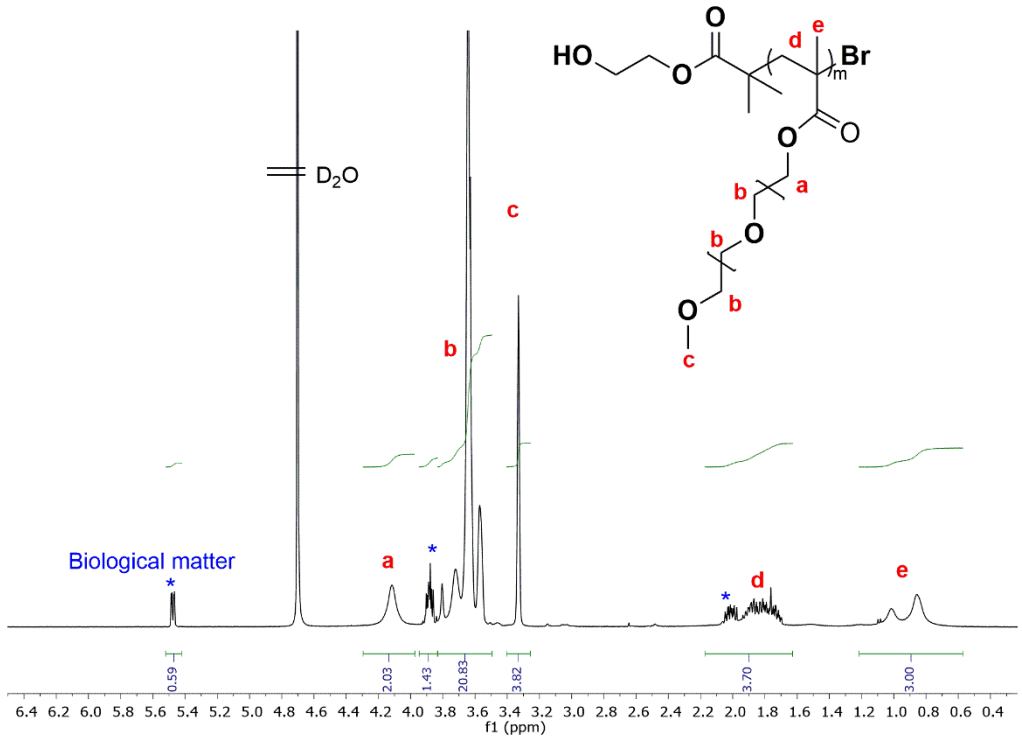

Figure S2. 18. ^{1}H NMR (400 MHz, DMSO) Spectra of PPEGMA formed via reduced concentration ATRP polymerisation, initiated *by E. coli with* corresponding structure and assignment.

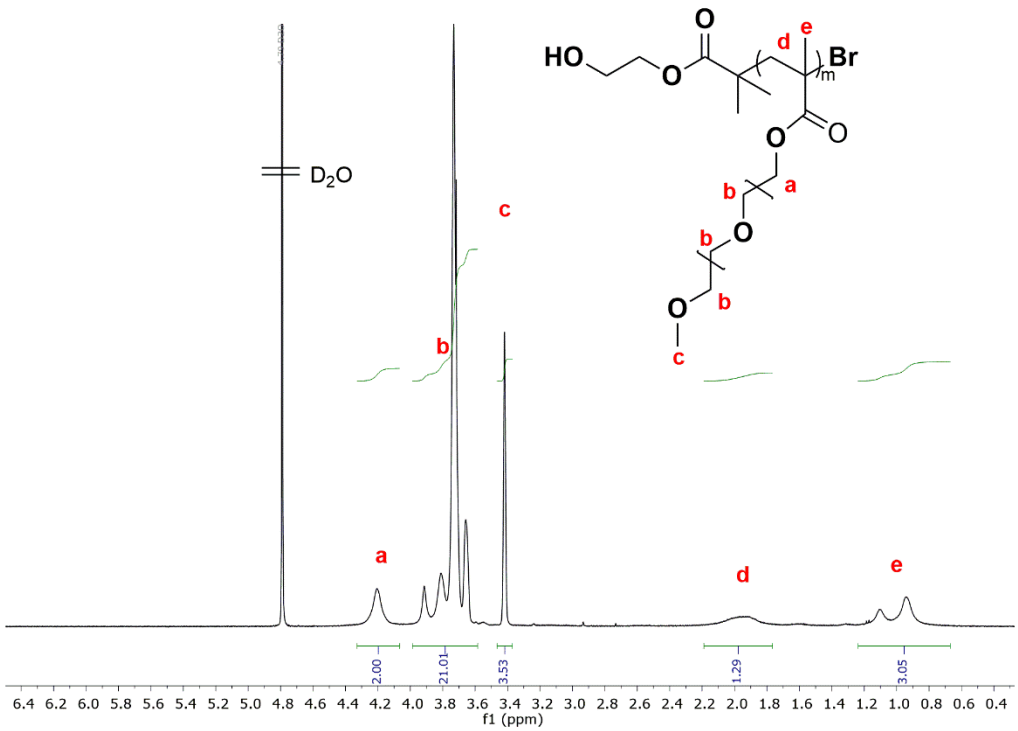

Figure S2. 19 ^{1}H NMR (400 MHz, DMSO) Spectra of PPEGMA formed via reduced concentration ATRP polymerisation, initiated *by C. spor* with corresponding structure and assignment.

2.1.17 Exploring Bacterial Assisted Fe ATRP Parameters

2.1.17.1 Synthesis of PPEGMA using different bacteria concentrations

C. met cultures were grown from cryo-bead stocks (2 x 5mL in LB) at 30°C overnight. Each were adjusted to OD_{600} 0.1 in 20 ml LB and grown further overnight. They were centrifuged (15 mins, 5,000 g) and washed with PBS (10 mL and 5 mL) before achieving final pellets. One pellet was re-suspended in 1.5 mL degassed PBS to be used in high concentration bacteria ATRP (**Reaction 1**). The second culture was re-suspended in 4 mL degassed PBS of which 1.5 mL was used for medium concentration bacterial ATRP (**Reaction 2**) and 150 µL used for a low

concentration bacterial ATRP (**Reaction 3**). Stock solutions were made for $FeCl_3.6H_2O$ and HEBIB. Appropriate volume $FeCl_3.6H_2O$ stock and Me_6TREN were added to a 5 mL microcentrifuge tube for each reaction along with stir bar and PBS. In separate tubes Monomer and HEBIB were dissolved in PBS. These were placed in the anaerobic cabinet for a minimum 1 hour to degas. Total amount PBS (including bacteria) equalled 4 mL in each reaction and reagent quantities are given in table S2.5. After degassing, bacteria were added to $FeCl_3$/Me_6TREN mix and pre-mixed for 15 minutes before adding monomer/initiator mixture where the reaction began. The reaction was terminated after 7.5 hours by exposure to air, with time point taken in between.

Table S2. 5 Reagent ratios for Bacterial assisted Fe ATRP study with different *C. met* concentrations.

Reagent	Ratio	mmol	Mass (mg)	Vol (µL)
PEGMA	100	0.052	17	16.2
$FeCl_3.6H_20$	4.65	0.0024	0.65	0.36
Me_6TREN	13.95	0.0072	1.66	1.9
HEBIB	2	0.0010	0.22	0.15

2.1.17.2 High concentration Bacteria control

The reaction was set up as described previously (2.6.11.1, Reaction 1) with the highest concentration of bacteria (1.35×10^{10} CFU ml^{-1} in final reaction volume), however no initiator was added to the reaction and it was left for 24 hours.

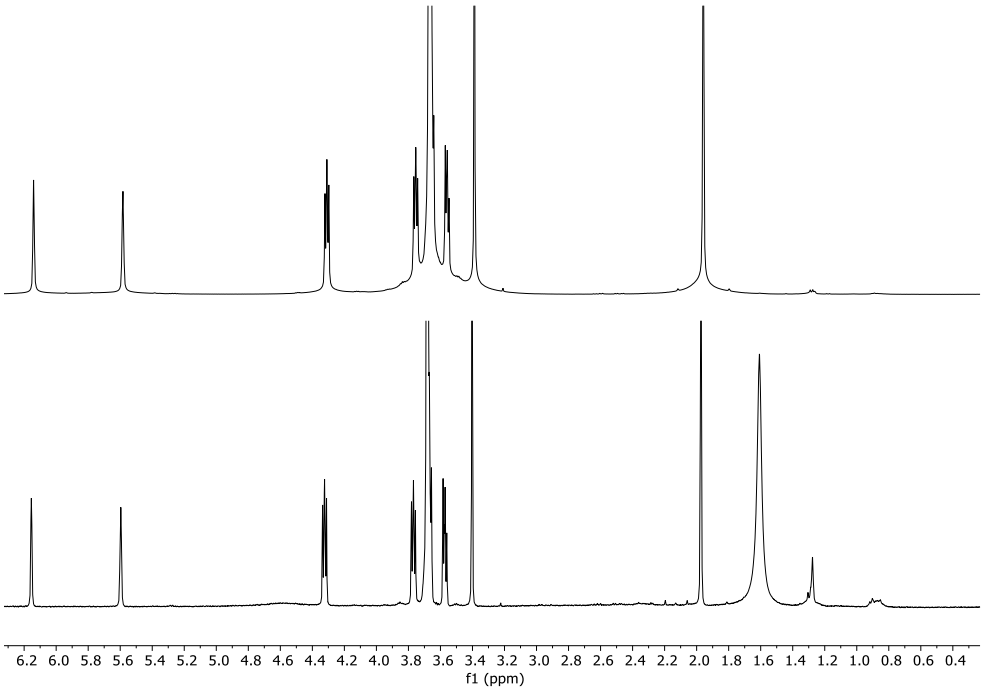

Figure S2. 20 ^{1}H NMR (400 MHz, $CDCl_3$) of Fe ATRP (PEGMA in PBS at 37 °C) control polymerisation with no-initiator for high concentration bacteria reactions: Bottom; Time 0 of the reaction and top; 24 hours after the reaction.

2.1.17.3 Synthesis of PPEGMA using different catalyst concentrations

C. met cultures were grown from bead cryo-stocks (5 x 5 mL in LB) at 30°C overnight. These were adjusted to OD_{600} 0.1 in 20 ml LB and grown further overnight. They were centrifuged (15 mins, 5,000 g) and washed with PBS (10 mL and 5 mL) before achieving final pellets which were re-suspended in 1.5 mL degassed PBS. 1.5 mL of this was used in each reaction (1.35 x 10^{10} CFU ml^{-1} in final reaction volume). Stock solutions were made for $FeCl_3.6H_2O$ and HEBIB. Appropriate volume $FeCl_3.6H_2O$ stock and Me_6TREN were added to a 5 mL Microcentrifuge tube for each reaction along with stir bar and PBS. In separate tubes Monomer and HEBIB were dissolved in PBS. These were placed in the

anaerobic cabinet for minimum 1 hour to degas. Total amount PBS (including bacteria) equalled 4 mL in each reaction, reagent quantities are given in table S2.5 with $FeCl_3.6H_2O$ and Me_6TREN values varying for each reaction as shown in Table S2.6. After degassing, bacteria were added to $FeCl_3$/Me_6TREN mix and pre-mixed for 15 minutes before adding monomer/initiator mixture where the reaction began. The reaction was terminated after 6 hours by exposure to air, with time point taken in between.

Table S2. 6 Varying amounts of catalyst ($FeCl_3$/Me_6TREN) in moles for bacterial initiated Fe ATRP polymerisations (PEGMA in PBS at 37 °C).

Sample	Concentrations	
	$FeCl_3.6H_2O$ (mg)	**Me_6TREN (uL)**
1	0.0068	0.02
2	0.068	0.2
3	0.68	2
4	6.8	20
5	68	200

2.1.17.4 Synthesis of PPEGMA targeting different DPs

C. met cultures were grown from cryo-stock beads (3 x 5 mL in LB) at 30°C overnight. These were adjusted to OD_{600} 0.1 in 20 ml LB and grown further overnight. They were centrifuged (15 mins, 5,000 g) and washed with PBS (10 mL and 5 mL) before achieving final pellets which were re-suspended in 1.5 mL degassed PBS. 1.5 mL of this was used in each reaction (1.35 x 10^{10} CFU ml^{-1} in final reaction volume). Stock solutions were made for $FeCl_3.6H_2O$ and HEBIB. Appropriate volume

$FeCl_3.6H_2O$ stock and Me_6TREN were added to a 5 mL Microcentrifuge tube for each reaction along with stir bar and PBS. In separate tubes appropriate amount of monomer and HEBIB were dissolved in PBS. These were placed in the anaerobic cabinet for minimum 1 hour to degas. Total amount PBS (including bacteria) equalled 4 mL in each reaction, reagent quantities are given in table S2.7. After degassing, bacteria were added to $FeCl_3$/Me_6TREN mix and pre-mixed for 15 minutes before adding monomer/initiator mixture where the reaction began. The reaction was terminated after 5 hours by exposure to air, with time point taken in between.

Table S2. 7 Varying DP of bacterial induced Fe ATRP polymerisations (PEGMA in PBS at 37 °C) by changing initiator:monomer (HEBIB:PEGMA) ratio.

DP	50	25	10
PEGMA (µL)	16.1	16.1	16.1
$FeCl_3$ (mg)	0.65	1.3	3.25
Me_6TREN (µL)	1.9	3.8	9.7
HEBIB (µL)	0.14	0.28	0.7

2.1.17.5 Synthesis of PPEGMA using different initiators

C. met cultures grown from cryo-stock beads (2 x 5 mL in LB) at 30°C overnight. These adjusted to OD_{600} 0.1 in 20 ml LB and grown further overnight. They were centrifuged (15 mins, 5,000 g) and washed with PBS (10 mL and 5 mL) before achieving final pellets which were re-suspended in 1.5 mL degassed PBS. 1.5 mL of this was used in each reaction (1.35 x 10^{10} CFU ml^{-1} in final reaction volume). Stock solutions

were made for $FeCl_3.6H_2O$ and HEBIB. Appropriate volume $FeCl_3.6H_2O$ stock and Me_6TREN were added to a 5 mL Microcentrifuge tube for each reaction along with stir bar and PBS. In separate tubes Monomer and HEBIB were dissolved in PBS. These were placed in the anaerobic cabinet for minimum 1 hour to degas. Total amount PBS (including bacteria equalled 4 mL in each reaction), reagent quantities are given in table S2.5 but initiator type varies as in table S2.8. After degassing, bacteria were added to $FeCl_3$/Me_6TREN mix and pre-mixed for 15 minutes before adding monomer/initiator mixture where the reaction began. The reaction was terminated after 5.75 hours by exposure to air, with time point taken in between.

Table S2. 8 Different initiator types used in bacterial initiated Fe ATRP polymerisations (PEGMA in PBS at 37 °C).

Initiator	Mass/Volume
HEBIB	0.149 µL
DHBP	0.240 mg

Table S2. 9 Results for varying Initiator types used in bacterial initiated Fe ATRP polymerisations (PEGMA in PBS at 37 °C)

Initiator	**Conversion**	***Mn* (kDa)**	***Đ***
HEBIB	41%	188.8	2.4
DHBP	21%	450	1.9

2.1.17.6 Additional SEC traces for *C.met* catalysed Fe ATRP of PEGMA with altering parameters (DP and initiator type)

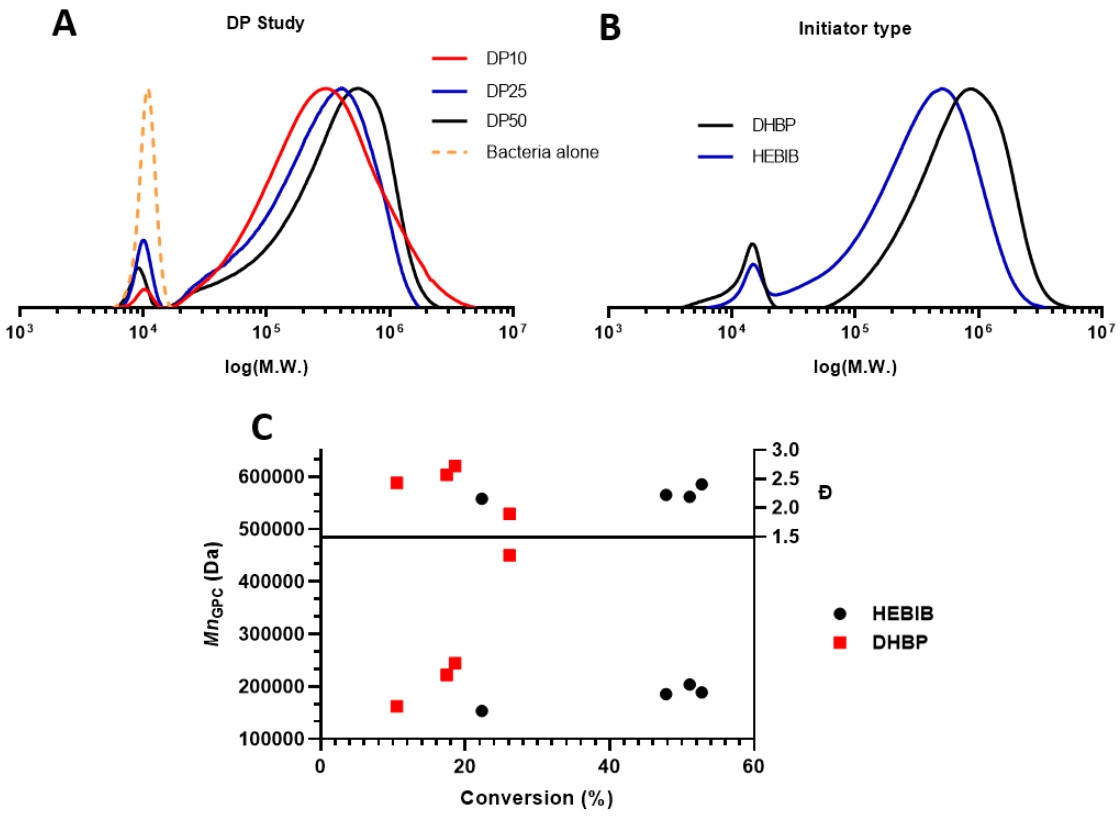

Figure S2. 21. SEC (THF) traces of *C. met* catalysed Fe ATRP of PEGMA in different conditions; A - Degree of polymerisation (DP) was altered to 10, 25 and 50, and B - Different initiators were used, HEBIB (Blue) and DHBP (Black). A second order plot (C) of M_n^{SEC} and conversion (^{1}H NMR) is displayed, comparing the characteristics of Fe ATRP polymerisations with different initiators.

Note: Small peak at 10^4 Da corresponds to protein component of bacteria *Đ*~1.05 (Overlay seen for comparison in A)

2.1.17.7 Synthesis of other polymers using high concentration of bacteria

C. met cultures grown from cryo-stock beads (5 x 5 mL in LB) at 30°C overnight. These adjusted to OD_{600} 0.1 in 20 ml LB (to ~OD_{600} 1-1.5) and grown further overnight. They were centrifuged (15 mins, 5,000 g) and washed with PBS (10 mL and 5 mL) before achieving final pellets which were re-suspended in 1.5 mL degassed PBS. 1.5 mL of this was used in each reaction (1.35 x 10^{10} CFU ml^{-1} in final reaction volume; 4 mL). Stock solutions were made for $FeCl_3.6H_2O$ and HEBIB. Appropriate volume $FeCl_3.6H_2O$ stock and Me_6TREN were added to a 5 mL Microcentrifuge tube for each reaction along with stir bar and PBS. In separate tubes Monomer and HEBIB were dissolved in PBS. These were placed in the anaerobic cabinet for minimum 1 hour to degas. Total amount PBS (including bacteria equalled 4 mL) in each reaction, reagent quantities are given in table S2.5 with Monomer values varying for each reaction as shown in Table S2.10. After degassing, bacteria were added to $FeCl_3$/Me_6TREN mix and pre-mixed for 15 minutes before adding monomer/initiator mixture where the reaction began. The reaction was left overnight and terminated by exposure to air.

Table S2. 10 Different monomer types (14 mM) used in Fe ATRP (PEGMA in PBS at 37 °C) initiated by bacteria.

Monomer	Mass (mg)
MEDSA	14 mg
*N*HEA	5.7 mg
*N*IPAM	5.7 mg
HEMA	6.5 mg

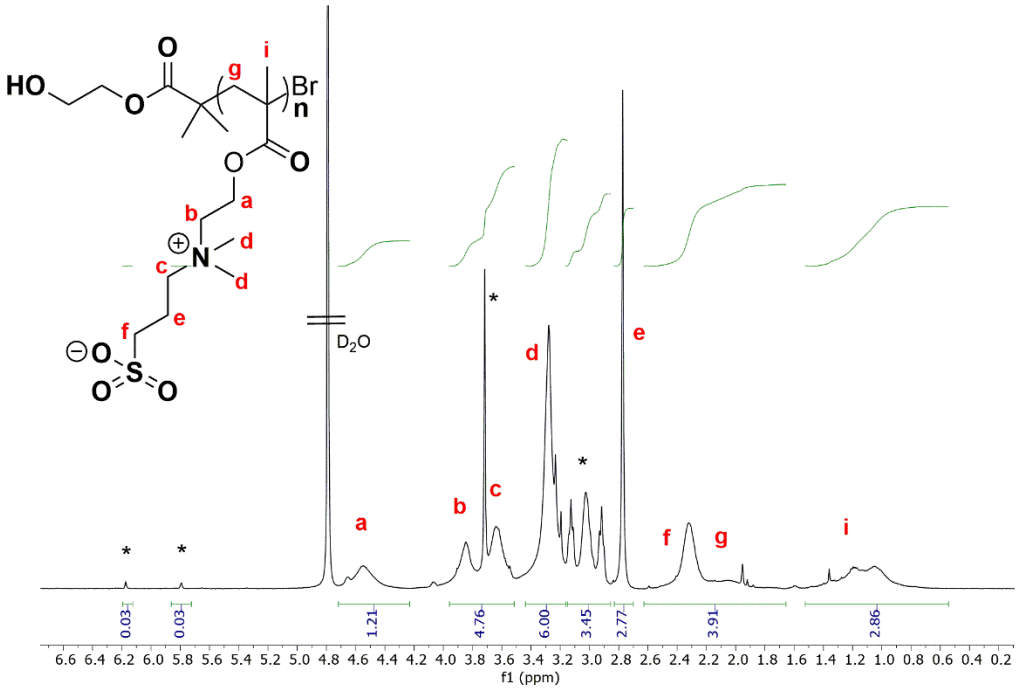

Figure S2. 22 ^{1}H NMR (400 MHz, D_2O) of polymer resulting from b-ATRP ($FeCl_3$/Me_6TREN) of MEDSA at 37 °C in PBS. *residual monomer or biological matter.

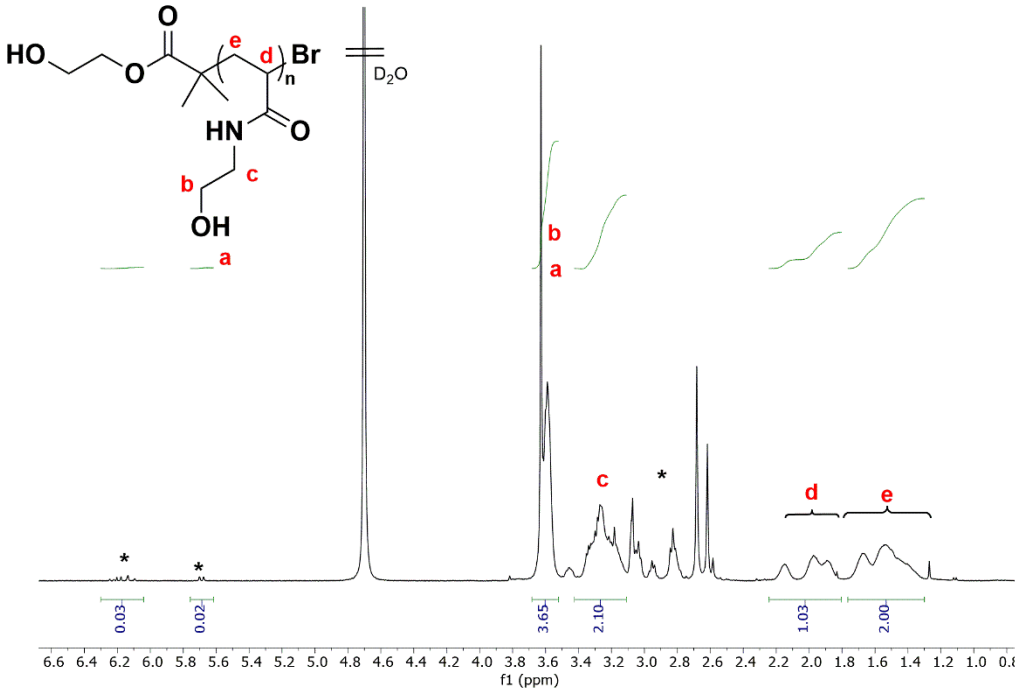

Figure S2. 23 ^{1}H NMR (400 MHz, D_2O) of polymer resulting from b-ATRP ($FeCl_3$/Me_6TREN) of *N*HEA at 37 °C in PBS. *residual monomer/ $FeCl_3Me_6$TREN or biological matter.

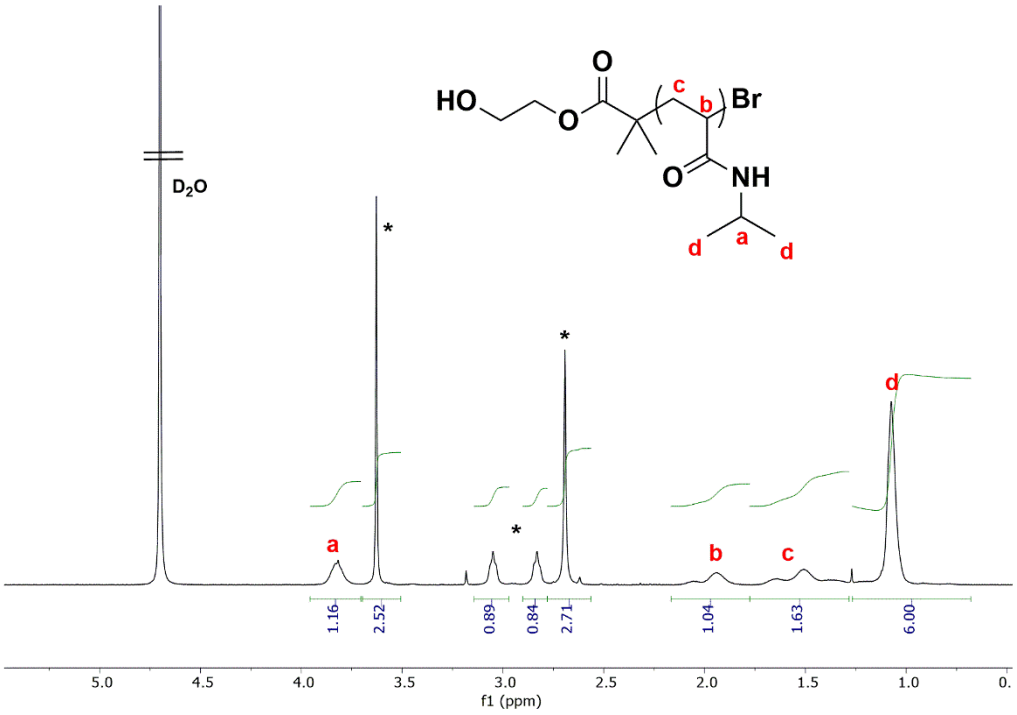

Figure S2. 24 ^{1}H NMR (400 MHz, D_2O) of polymer resulting from b-ATRP ($FeCl_3$/Me_6TREN) of *N*IPAM at 37 °C in PBS. *residual monomer/ $FeCl_3Me_6$TREN or biological matter.

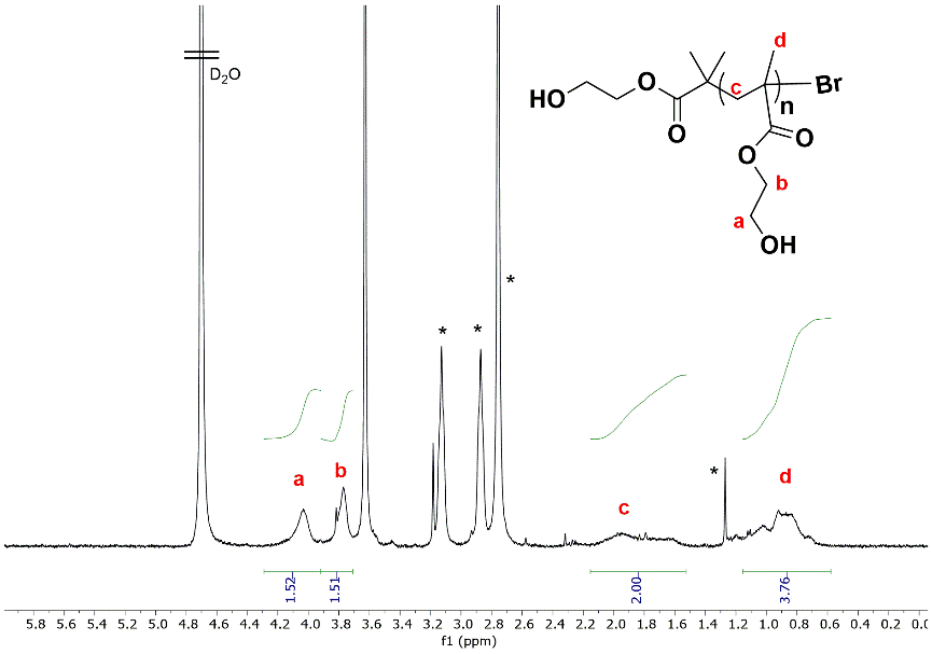

Figure S2. 25 ^{1}H NMR (400 MHz, D_2O) of polymer resulting from b-ATRP ($FeCl_3$/Me_6TREN) of HEMA at 37 °C in PBS. *residual monomer/ $FeCl_3Me_6$TREN or biological matter.

References

1. J. F. Lutz, *Macromol. Rapid Commun.*, 2017, **38**.
2. S. Celasun, D. Remmler, T. Schwaar, M. G. Weller, F. Du Prez and H. G. Borner, *Angew. Chem. Int. Ed. Engl.*, 2019, **58**, 1960-1964.
3. J. O. Holloway, C. Mertens, F. E. Du Prez and N. Badi, *Macromol. Rapid Commun.*, 2019, **40**, e1800685.
4. Y. Kametani, M. Sawamoto and M. Ouchi, *Angew. Chem. Int. Ed. Engl.*, 2018, **57**, 10905-10909.
5. M. Ouchi and M. Sawamoto, *Polym. J.*, 2017, **50**, 83-94.
6. G. Gody, P. B. Zetterlund, S. Perrier and S. Harrisson, *Nat Commun*, 2016, **7**, 10514.
7. N. G. Engelis, A. Anastasaki, G. Nurumbetov, N. P. Truong, V. Nikolaou, A. Shegiwal, M. R. Whittaker, T. P. Davis and D. M. Haddleton, *Nat Chem*, 2017, **9**, 171-178.
8. J. F. Lutz, M. Ouchi, D. R. Liu and M. Sawamoto, *Science*, 2013, **341**, 1238149.
9. M. D. Nothling, H. Cao, T. G. McKenzie, D. M. Hocking, R. A. Strugnell and G. G. Qiao, *J. Am. Chem. Soc.*, 2020, DOI: 10.1021/jacs.0c10673.
10. R. Szweda, M. Tschopp, O. Felix, G. Decher and J. F. Lutz, *Angew. Chem. Int. Ed. Engl.*, 2018, **57**, 15817-15821.
11. G. Cavallo, S. Poyer, J. A. Amalian, F. Dufour, A. Burel, C. Carapito, L. Charles and J. F. Lutz, *Angew. Chem. Int. Ed. Engl.*, 2018, **57**, 6266-6269.
12. S. Martens, A. Landuyt, P. Espeel, B. Devreese, P. Dawyndt and F. Du Prez, *Nat Commun*, 2018, **9**, 4451.
13. D. Karamessini, T. Simon-Yarza, S. Poyer, E. Konishcheva, L. Charles, D. Letourneur and J. F. Lutz, *Angew. Chem. Int. Ed. Engl.*, 2018, **57**, 10574-10578.
14. A. Kuroki, P. Sangwan, Y. Qu, R. Peltier, C. Sanchez-Cano, J. Moat, C. G. Dowson, E. G. L. Williams, K. E. S. Locock, M. Hartlieb and S. Perrier, *ACS Appl Mater Interfaces*, 2017, **9**, 40117-40126.
15. P. Q. Nguyen, N. D. Courchesne, A. Duraj-Thatte, P. Praveschotinunt and N. S. Joshi, *Adv. Mater.*, 2018, **30**, e1704847.
16. K. Pardee, S. Slomovic, P. Q. Nguyen, J. W. Lee, N. Donghia, D. Burrill, T. Ferrante, F. R. McSorley, Y. Furuta, A. Vernet, M. Lewandowski, C. N. Boddy, N. S. Joshi and J. J. Collins, *Cell*, 2016, **167**, 248-259 e212.
17. C. Santoro, C. Arbizzani, B. Erable and I. Ieropoulos, *J. Power Sources*, 2017, **356**, 225-244.
18. I. Llorens, G. Untereiner, D. Jaillard, B. Gouget, V. Chapon and M. Carriere, *PLoS One*, 2012, **7**, e51783.
19. H. Yokoyama, M. Ishida and T. Yamashita, *J. Microbiol. Biotechnol.*, 2016, **26**, 757-762.
20. O. Choi and B. I. Sang, *Biotechnol Biofuels*, 2016, **9**, 11.

21. N. Bansal, J. J. Coetzee and E. M. N. Chirwa, *Ecotoxicol. Environ. Saf.*, 2019, **172**, 281-289.
22. X. Yun, Q. Zhang, M. Lv, H. Deng, Z. Deng and Y. Yu, *Org Biomol Chem*, 2019, **17**, 454-460.
23. Y. Wang, Y. Tashiro and K. Sonomoto, *J Biosci Bioeng*, 2015, **119**, 10-18.
24. S. Slomovic, K. Pardee and J. J. Collins, *Proc Natl Acad Sci U S A*, 2015, **112**, 14429-14435.
25. G. M. Church, M. B. Elowitz, C. D. Smolke, C. A. Voigt and R. Weiss, *Nat Rev Mol Cell Biol*, 2014, **15**, 289-294.
26. E. P. Magennis, F. Fernandez-Trillo, C. Sui, S. G. Spain, D. J. Bradshaw, D. Churchley, G. Mantovani, K. Winzer and C. Alexander, *Nature Materials*, 2014, **13**, 748-755.
27. J. Geng, W. Li, Y. Zhang, N. Thottappillil, J. Clavadetscher, A. Lilienkampf and M. Bradley, *Nat. Chem.*, 2019, DOI: 10.1038/s41557-019-0240-y.
28. J. Niu, D. J. Lunn, A. Pusuluri, J. I. Yoo, M. A. O'Malley, S. Mitragotri, H. T. Soh and C. J. Hawker, *Nat Chem*, 2017, **9**, 537-545.
29. Y. Zhao, X. Zhang, Y. Wang, Z. Wu, J. An, Z. Lu, L. Mei and C. Li, *Carbohydr. Polym.*, 2014, **105**, 63-69.
30. N. Idil and B. Mattiasson, *Sensors (Basel)*, 2017, **17**, 708.
31. R. B. Song, Y. Wu, Z. Q. Lin, J. Xie, C. H. Tan, J. S. C. Loo, B. Cao, J. R. Zhang, J. J. Zhu and Q. Zhang, *Angew. Chem. Int. Ed. Engl.*, 2017, **56**, 10516-10520.
32. A. Ramanavicius, E. Andriukonis, A. Stirke, L. Mikoliunaite, Z. Balevicius and A. Ramanaviciene, *Enzyme Microb. Technol.*, 2016, **83**, 40-47.
33. E. Andriukonis, A. Stirke, A. Garbaras, L. Mikoliunaite, A. Ramanaviciene, V. Remeikis, B. Thornton and A. Ramanavicius, *Colloids Surf B Biointerfaces*, 2018, **164**, 224-231.
34. H. G. Sherman, J. M. Hicks, A. Jain, J. J. Titman, C. Alexander, S. Stolnik and F. J. Rawson, *ChemBioChem*, 2019, **20**, 1008-1013.
35. Y. Luo, Y. Gu, R. Feng, J. Brash, A. M. Eissa, D. M. Haddleton, G. Chen and H. Chen, *Chem Sci*, 2019, **10**, 5251-5257.
36. G. Fan, C. M. Dundas, A. J. Graham, N. A. Lynd and B. K. Keitz, *Shewanella oneidensis as a living electrode for controlled radical polymerization*, 2018.
37. R. M. Apetrei, G. Carac, A. Ramanaviciene, G. Bahrim, C. Tanase and A. Ramanavicius, *Colloids Surf B Biointerfaces*, 2019, **175**, 671-679.
38. R. M. Apetrei, G. Carac, G. Bahrim, A. Ramanaviciene and A. Ramanavicius, *Bioelectrochemistry*, 2018, **121**, 46-55.
39. H. F. Downie, J. P. Standerwick, L. Burgess, L. S. Natrajan and J. R. Lloyd, *Res. Microbiol.*, 2018, **169**, 582-589.
40. J. S. Gescher, C. D. Cordova and A. M. Spormann, *Mol. Microbiol.*, 2008, **68**, 706-719.
41. M. J. Colombo, J. Ha, J. R. Reinfelder, T. Barkay and N. Yee, *Chem. Geol.*, 2014, **363**, 334-340.
42. S. Antonina Alekseyevna, *Development of Aqueous ATRP for Biomedical Applications*, 2015.

43. D. J. Siegwart, J. K. Oh and K. Matyjaszewski, *Prog. Polym. Sci.*, 2012, **37**, 18-37.
44. S. Averick, A. Simakova, S. Park, D. Konkolewicz, A. J. D. Magenau, R. A. Mehl and K. Matyjaszewski, *ACS Macro Letters*, 2011, **1**, 6-10.
45. T. Zhou, Y. Zhu, X. Li, X. Liu, K. W. K. Yeung, S. Wu, X. Wang, Z. Cui, X. Yang and P. K. Chu, *Prog. Mater Sci.*, 2016, **83**, 191-235.
46. A. E. Enciso, L. Fu, S. Lathwal, M. Olszewski, Z. Wang, S. R. Das, A. J. Russell and K. Matyjaszewski, *Angew. Chem. Int. Ed. Engl.*, 2018, **57**, 16157-16161.
47. H. Zhou, W. Jiang, N. An, Q. Zhang, S. Xiang, L. Wang and J. Tang, *RSC Advances*, 2015, **5**, 42728-42735.
48. J. Pollard, O. Rifaie-Graham, S. Raccio, A. Davey, S. Balog and N. Bruns, *Anal. Chem.*, 2020, **92**, 1162-1170.
49. Z. Xue, D. He and X. Xie, *Polymer Chemistry*, 2015, **6**, 1660-1687.
50. W. He, L. Zhang, J. Miao, Z. Cheng and X. Zhu, *Macromol. Rapid Commun.*, 2012, **33**, 1067-1073.
51. M. R. Bennett, P. Gurnani, P. J. Hill, C. Alexander and F. J. Rawson, *Angew. Chem. Int. Ed. Engl.*, 2020, **59**, 4750-4755.
52. A. Simakova, S. E. Averick, D. Konkolewicz and K. Matyjaszewski, *Macromolecules*, 2012, **45**, 6371-6379.
53. C. H. Liao and L. M. Shollenberger, *Lett. Appl. Microbiol.*, 2003, **37**, 45-50.
54. N. V. Tsarevsky, T. Pintauer and K. Matyjaszewski, *Macromolecules*, 2004, **37**, 9768-9778.
55. D. Hutanu, M. D. Frishberg, L. Guo and C. C. Darie, *Mod. Chem. Appl*, 2014, **2**, 1-6.
56. Z. Xue, B. W. Lee, S. K. Noh and W. S. Lyoo, *Polymer*, 2007, **48**, 4704-4714.
57. C. Boyer, N. A. Corrigan, K. Jung, D. Nguyen, T. K. Nguyen, N. N. Adnan, S. Oliver, S. Shanmugam and J. Yeow, *Chem Rev*, 2016, **116**, 1803-1949.
58. W. Tang, Y. Kwak, W. Braunecker, N. V. Tsarevsky, M. L. Coote and K. Matyjaszewski, *J. Am. Chem. Soc.*, 2008, **130**, 10702-10713.
59. N. Kadayıfçıoğlu and H. Y. Acar, *Eur. Polym. J.*, 2013, **49**, 3366-3376.
60. S. Li, P. A. Crooks, X. Wei and J. de Leon, *Crit. Rev. Toxicol.*, 2004, **34**, 447-460.
61. D. A. Shipp and K. Matyjaszewski, *Macromolecules*, 1999, **32**, 2948-2955.
62. N. V. Tsarevsky, W. A. Braunecker, S. J. Brooks and K. Matyjaszewski, *Macromolecules*, 2006, **39**, 6817-6824.
63. K. Matyjaszewski, D. A. Shipp, J.-L. Wang, T. Grimaud and T. E. Patten, *Macromolecules*, 1998, **31**, 6836-6840.
64. P. Arosio, L. Elia and M. Poli, *IUBMB Life*, 2017, **69**, 414-422.
65. P. Monsieurs, H. Moors, R. Van Houdt, P. J. Janssen, A. Janssen, I. Coninx, M. Mergeay and N. Leys, *Biometals*, 2011, **24**, 1133-1151.
66. L. Gao, X. Lu, H. Liu, J. Li, W. Li, R. Song, R. Wang, D. Zhang and J. Zhu, *Front Microbiol*, 2019, **10**, 575.

67. A. Pinochet-Barros and J. D. Helmann, *Antioxid Redox Signal*, 2018, **29**, 1858-1871.
68. K. D. Krewulak and H. J. Vogel, *Biochim. Biophys. Acta*, 2008, **1778**, 1781-1804.
69. T. S. Magnuson, N. Isoyama, A. L. Hodges-Myerson, G. Davidson, M. J. Maroney, G. G. Geesey and D. R. Lovley, *Biochem. J*, 2001, **359**, 147-152.
70. M. L. Guerinot, *Annu Rev Microbiol*, 1994, **48**, 743-772.
71. I. Schroder, E. Johnson and S. de Vries, *FEMS Microbiol. Rev.*, 2003, **27**, 427-447.
72. R. E. Cowart, *Arch. Biochem. Biophys.*, 2002, **400**, 273-281.
73. B. M. Appenzeller, C. Yanez, F. Jorand and J. C. Block, *Appl. Environ. Microbiol.*, 2005, **71**, 5621-5623.
74. M. Rolland, N. P. Truong, R. Whitfield and A. Anastasaki, *ACS Macro Letters*, 2020, **9**, 459-463.
75. S. C. Andrews, A. K. Robinson and F. Rodriguez-Quinones, *FEMS Microbiol. Rev.*, 2003, **27**, 215-237.

Chapter 3. Bacteria Driven Fenton Glucose Oxidase-RAFT (FG-RAFT) Polymerisations

Abstract

The ability to utilise bacterial redox mechanisms for synthetic chemistry has grown in interest as a potential means to create new forms of engineered living materials (ELM),[1-3] to manipulate cell properties or phenotype,[4-6] and to probe the mechanistics of cellular machinery.[7, 8] It is also an advantage to be able to perform such experiments in the presence of air which might expand the scope for future applications and avoid the need for degassing air sensitive reagents. Enzyme cascade reactions involving Glucose Oxidase (GOx) were employed in this research to facilitate an air stable Reversible Addition Fragmentation chain-Transfer (RAFT) polymerisation driven by the Fenton reaction. An *in situ* reducing activation step (Fe^{3+} to Fe^{2+}) was introduced to protect the air sensitive reagent Fe^{2+}, via a reaction with ascorbic acid (AscA). These methods were adapted towards biocompatible conditions with a variety of monomers, and investigations were carried out to inspect how reagents associated with the initial radical flux (Glucose, GOx, $FeCl_3$, AscA) would affect the reaction. Altering $FeCl_3$ and AscA concentrations were found to influence the dispersity (***Đ***)s and molecular weight (M_n) distributions of the resulting polymers. The application of bacterial (*Cupriavidus metallidurans* (*C. met*)) redox catalysis in place of AscA successfully generated polymers of dimethyl acrylamide (DMA) in a controlled manner (***Đ*** ~ 1.12), advancing bacterial mediated polymerisation techniques compared to previous methods.[9] Concentrations of $FeCl_3$ as low as 7 μM were effective at producing

polymers in a relatively controlled manner. Heat-killed bacteria were unable to catalyse the reaction, highlighting the necessity of active bacterial metabolism to instigate the Fenton GOx (FG) cascade reaction. Other monomers, *N*-Hydroxyethyl acrylamide (NHEA) and *N*-acryloylmorpholine (NAM) were also polymerised by *C. met* activated FG-RAFT, revealing that the *Đ* and M_n of the resulting polymers was monomer dependant. In the case of polymerisation with NAM, decreasing the concentration of $FeCl_3$ significantly aided smaller *Đ*s but at a compromise of slightly poorer M_n control.

Introduction

The previous chapter of this thesis explored the use of bacteria to initiate ATRP. It was shown that an Fe^{3+} catalyst could be activated by the presence of bacteria to polymerise a range of vinyl monomers, and various ATRP parameters such as cell and catalyst concentration and initiator species were investigated. The Fe catalyst played a vital role in mediating the control of ATRP polymerisations by influencing the equilibrium between dormant and active growing polymer species. As discussed previously, there were several unknowns concerning possible Fe catalyst uptake by the bacteria or entanglement in the bacterial extracellular matrix (ECM) during these Fe ATRP polymerisations, which somewhat compromised the molecular weight (M_n) control of the polymers. Secondly, a complex reaction set-up was required as typical ATRP experiments are conducted under inert conditions to avoid oxidation of the catalyst and inhibition of the polymerisation process, which confined the method to anaerobic bacteria and limited future applications to anoxic conditions.

In contrast, RAFT polymerisations do not rely on the oxidation state of a metal catalyst to control the equilibrium but are instead controlled by the reactivities of the chain transfer agent (CTA), monomer and external radical/electron source (e.g. azoinitiator[10, 11], redox couple,[12-14] electricity,[15] electromagnetic irradiation[16-18]) . As the RAFT CTA mediates a conventional radical polymerisation to enable M_n control, low *Đ,* and because RAFT is more compatible with aqueous

environments,[19] it was envisioned that RAFT polymerisation might better facilitate the synthesis of uniform polymers with controllable M_n under biocompatible conditions, compared to Fe ATRP.

Furthermore, the ability to conduct Reversible Deactivation Radical Polymerisation (RDRP) in air using oxygen tolerant polymerisation methods, such as Laccase and Glucose Oxidase (GOx) facilitating reactions,[20-28] in low volumes,[29] low temperatures,[30] and in non-chemistry laboratories,[25] has broadened the scope of possible applications. In contrast, the Fe ATRP experiments described in chapter 2, required deoxygenation procedures and the use of an anaerobic cabinet. In contrast, enzymes like GOx can be utilised to consume O_2 via catalysis with glucose to form H_2O_2, as part of a polymer initiation process, and in turn protect polymer chains from deactivation. Although extra additives such as glucose and GOx are required, this far outweighs the use of anaerobic cabinets to deoxygenate individual reaction components. Additionally, polymers generated using Fe ATRP had distributions that were reliant on the equilibrium between dormant and active Fe ATRP catalysts, which were difficult to control by the bacterial reduction pathways. It was hypothesised that rather than using a bacterial initiated Fe ATRP catalyst system, a RAFT polymerisation method facilitated by a bacterial induced Fe chemistry (Fenton) initiation system could be more effectively maintained.

An Fe-initiation system based on the Fenton reaction has previously been implemented into conventional radical and RAFT polymerisations. During this process, a RAFT polymerisation is initiated

by hydroxyl radicals produced upon the reaction of Fe^{2+} and H_2O_2.[31, 32] Such polymerisations were successful under benign reaction conditions (RT, aqueous solvent) with fast polymerisation kinetics and so it was hypothesised that this system might be suitable for bacterial mediated polymerisations. Moreover, Fenton-GOx (FG) cascade reactions have been employed in air tolerant free radical polymerisations (FRPs) towards various applications including;[31] hydrogels for implantable scaffold matrices, cellular encapsulation,[33] immuno-active coatings,[34] and biosensors.[35, 36] Indeed, these reactions have been applied to RAFT polymerisations,[31, 37] such as the incorporation of Haemoglobin (Hb) and blood as Fe catalysts in biological solvents (bovine, human serum).[38]

The biocompatibility, low cost and environmentally benign nature of FG-RAFT prompted the exploration of its marriage with bacterial redox systems in this chapter. Additionally, Fe^{2+} is known to be susceptible to oxidation under oxygenated conditions, which could reduce its effectiveness as a catalyst and cause difficulties with storage and handling. As demonstrated in chapter 2, AscA and bacteria can be used to activate Fe^{3+} to Fe^{2+} *in situ* and may therefore generate Fenton active Fe^{2+} in these studies. FG-RAFT may be implemented for i) potential biosensing applications, and ii) to assist bacteria facilitated polymerisations towards MIPs or ELM applications.

The role of GOx in the proposed polymerisation is to oxidise glucose to gluconic acid using O_2 to form H_2O_2. Once activated using bacteria or AscA, Fe^{2+} may react with H_2O_2 to form highly reactive hydroxyl radicals (OH), which can initiate a polymerisation (Figure 3. 1).

A biocompatible system in DPBS media was first established with the selected water-soluble monomer/CTA system and control experiments were carried out to ensure that i) Fe^{3+} cannot undergo Fenton chemistry to initiate the polymerisation under the reaction conditions, and ii) reduction of Fe^{3+} to Fe^{2+} with a reducing agent can initiate the FG-RAFT induced polymerisation. In consideration of toxicity studies, the monomer concentration was modified to ensure it would not compromise bacterial viability in subsequent bacterial experiments, and the effects of tailoring several reagent concentrations were explored. *C. met* was then used in place of AscA to initiate the polymerisation of several monomers. Living bacteria were essential to the reaction process. Fe concentrations as low as 7 μM were successful in driving the polymerisation which yielded polymers with acceptable M_n control and $Đ$s.

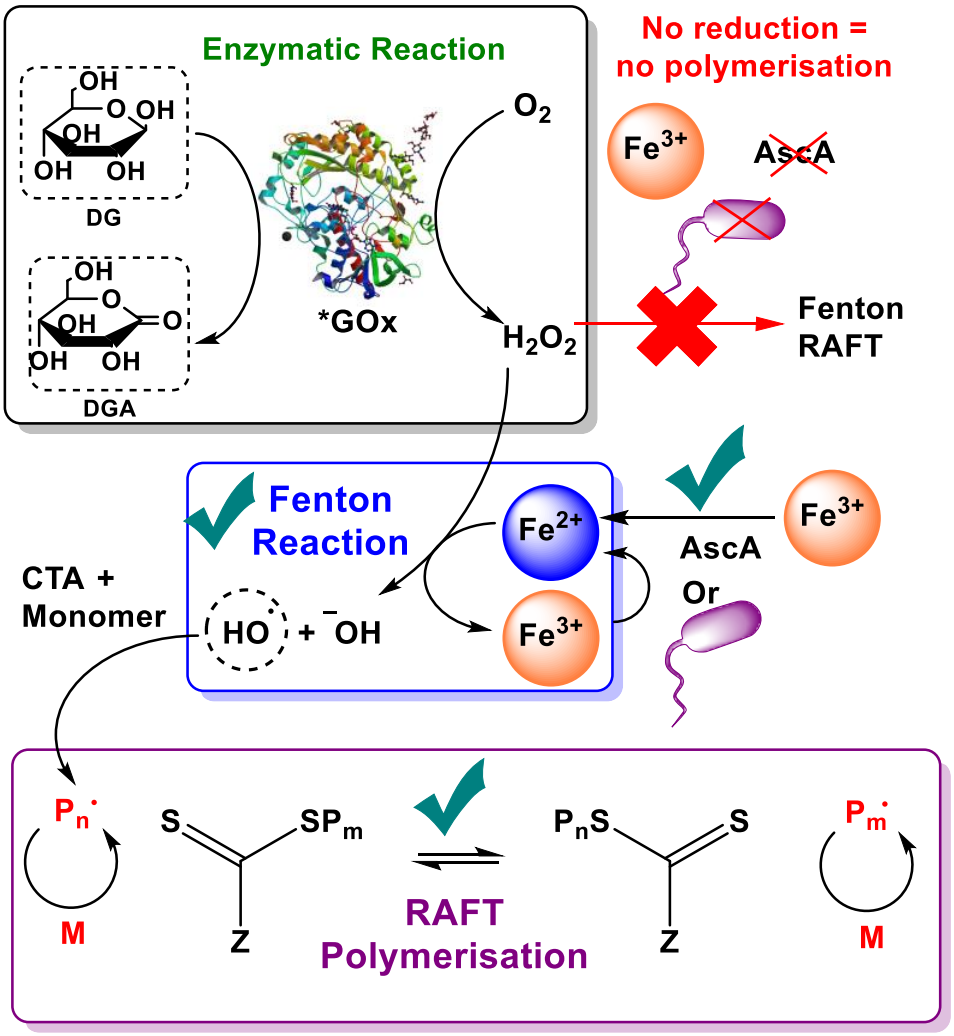

Figure 3. 1. Fenton GOx RAFT process initiated by reducing agents: ascorbic acid (AscA) or bacteria. D-Glucose (DG) is converted to D-Glucanolactate (DGA) by glucose oxidase (GOx) which consumes O_2 in the process to form H_2O_2. Without the presence of reducing agents, polymerisation should not take place. *GOx protein image from PBD ID: 3QVP.A.[39]

Results and Discussion

3.1.1 Establishing FG-RAFT under biocompatible conditions

3.1.1.1 Enzyme RAFT

Before attempting bacteria-initiated polymerisations *via* a modified FG-RAFT pathway it was first necessary to probe conditions in which i) FG-RAFT (starting from Fe^{3+}) could effectively take place, and ii) the polymerisation could take place without affecting bacterial metabolism. As discussed in Chapter 1, horseradish peroxidase (HRP) catalysed RAFT, developed by Zhang *et al,*[40] has been well studied and is carried out in the absence of oxygen. Hence, to test the commercially available, water soluble chain transfer agent (CTA), (2 - (2 – carboxyethylsulfanylthiocarbonyl-sulfanyl) propionic acid) for compatibility in enzyme cascade reactions, oxygen free HRP RAFT was first employed with a commonly used monomer, *N*,*N*-dimethylacrylamide (DMA), in DPBS at room temperature. Under these conditions acetylacetonate (ACAC) radicals were effectively produced through HRP catalysis and the reduction of H_2O_2 to form water. These radicals initiated the RAFT polymerisation which resulted in polymers with an M_n close to the theoretical value and $Đ$ ~ 1.10, (Figure S3. 1 and Table S3. 1).

It was then necessary to combine GOx and HRP enzymatic catalysis to test the efficacy of the biocompatible RAFT polymerization at room temperature in the presence of oxygen. It is important to note that similar experiments reported in prior literature require degassing of the solution

with N_2 for 30 minutes prior to the polymerisation reaction open to air.[41] In the experiments reported here external degassing was not required for the polymerization of DMA in air and good control of the resulting polymers was achieved (M_n^{sec} = 29 kDa, M_n^{th} = 20 kDa, $Đ$ ~ 1.10), with full conversion after 3 hours (Figure S3. 2 and Table S3. 1). The above reaction was repeated without glucose to prove the necessity of glucose to the reaction, where no polymer was formed (Figure S3. 3).

3.1.1.2 Fenton-GOx RAFT

A Fenton-GOx (FG) cascade was next implemented into the RAFT reaction, with reagent ratios modelled on previous reactions carried out by Reyhani *et al.*[37] Instead of directly initiating the reaction using air sensitive Fe^{2+}, it was envisioned that more air stable Fe^{3+} could be activated to Fe^{2+} *in situ* by ascorbic acid (AscA), the proposed mechanism is shown in Figure 3. 1. Indeed, the reaction of DMA in the presence of CTA, GOx, Glu, Fe^{3+} and AscA resulted in polymer formation after 20 hours (11%, Table 3. 1, Reaction A, Figure 3. 2, green). The negative controls C1; omitting AscA and C2; omitting both Fe and AscA gave no polymerisation (Table 3. 2, Figure S3. 4). Whereas the positive control C3; with Fe^{2+} and no ascorbic acid produced polymer as expected (Figure 3. 2, blue). These results confirm that under these conditions i) Fe^{2+} is Fenton active with H_2O_2, ii) Fe^{3+} is not Fenton active with H_2O_2, iii) AscA can reduce Fe^{3+} to Fe^{2+} which further reacts with H_2O_2 to begin a RAFT polymerization.

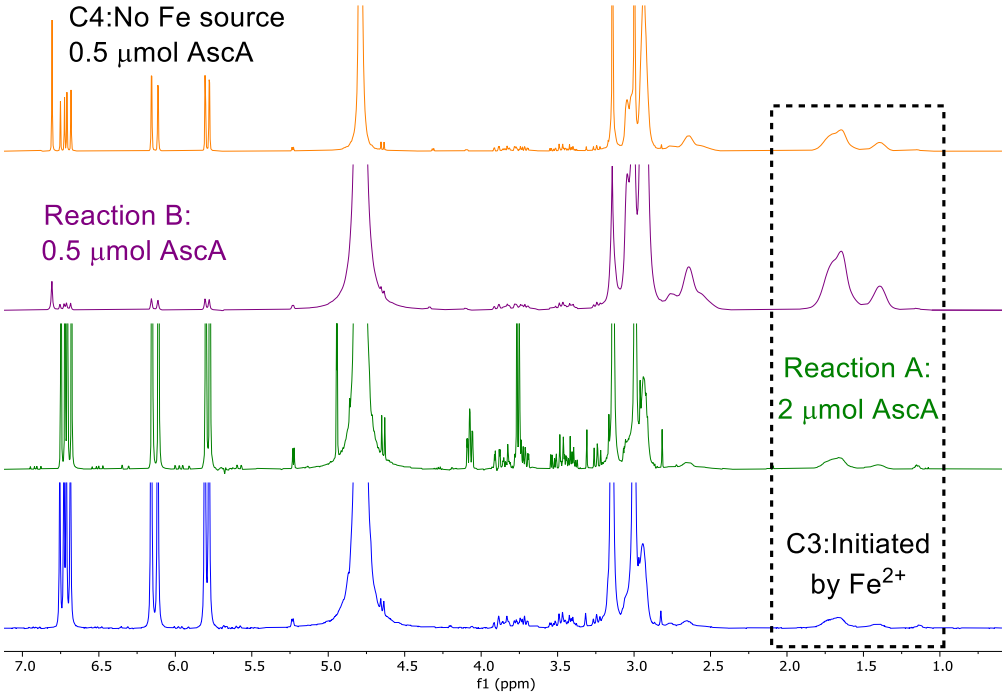

Figure 3. 2. ^{1}H NMR (400 MHz, D_2O) of final time point (20 hours) in Fenton-GOx-RAFT (FG RAFT) reactions of DMA with $FeCl_3.6H_2O$ of $FeCl_2.4H_2O$. C3 (Bottom, Blue): Positive control with Fe^{2+} initiated FG-RAFT without AscA. Reaction A (Green): Fe^{3+} and AscA (2 μmol) initiated FG-RAFT. Reaction B (Purple): Fe^{3+} and AscA initiated FG-RAFT with decreased AscA (0.5 μmol). C4 (Orange): AscA negative control using reagent ratios from reaction B but with no Fe source. Ratios are as follows: [DMA] : [CTA] : [GOx] : [Glu] : Fe source : AscA for Reaction A: 200 : 1 : 0.000025 : 10 : 0.07 : 1 and for Reaction B: 200 : 1 : 0.000025 : 10 : 0.07 : 0.22.

Table 3. 1 FG RAFT reactions of DMA initiated by AscA. Reactions A and B have different reagent ratios shown below with results of polymer conversions.

Reaction	Ratio: [DMA] : [CTA] : [GOx] : [Glu] : Fe source : AscA	Conv.[a]
A	200 : 1 : 0.000025 : 10 : 0.07 : 1	11%
B	200 : 1 : 0.000025 : 10 : 0.07 : 0.22	95%

[a] Estimated using of ^{1}H NMR from comparison of monomer (CH acrylate): polymer (CH_2 backbone) integrals.

Table 3. 2 Control reactions 1-4 and descriptions of each control element for FG-RAFT Polymerisations of DMA initiated by AscA.

Reaction	Control elements	Ratio	Conv. [a]
C1	Fe^{3+}, No AscA	A	0%
C2	No AscA, No Fe source	A	0%
C3	Fe^{2+}	A	12%
C4	AscA, No Fe source	B	64%

[a] Estimated using of ^{1}H NMR from a comparison of monomer (CH acrylate): polymer (CH_2 backbone) integrals integral. C1, C2 and C3 had reagent ratios: DMA: CTA: Glu: GOx: Fe: AscA = 200: 1: 10: 2.5 x 10^{-5} : 0.07: 1. C4 Had reagent ratios: Reagent ratios: DMA: CTA: Glu: GOx: Fe: AscA = 200: 1: 10: 2.5 x 10^{-5} : 0.07: 0.22.

It has previously been shown that AscA can interfere with some enzymatic reactions,[42] and can also act as an oxygen scavenger,[43] so it was hypothesized that high AscA concentrations might hinder the polymerisation. Indeed, when the AscA concentration was reduced, a large increase to 95% polymerisation was observed (Figure 3. 2, Reaction B, purple). A further control experiment (C4, Table 3. 2) was carried out to evaluate the effects of AscA on the reaction; where AscA was present, but Fe was completely omitted. The resulting polymer formation (64%) was likely due to the oxidisation of AscA by H_2O_2 (produced by GOx),[44] forming OH radicals which could initiate DMA polymerisation. However, there was still a substantial amount of monomer remaining in the ^{1}H NMR spectra (Figure 3. 2, orange) compared to that of Reaction B (Figure 3. 2, Reaction B, purple). Furthermore, the AscA induced polymer formation was not of concern as future experiments in this study required the use of bacterial redox chemistry to reduce Fe^{3+} instead of AscA.

The results presented thus far show that an FG cascade reaction could be used to drive a RAFT polymerisation. In these experiments Fe^{3+} and AscA were necessary to generate Fe^{2+} *in situ* which could subsequently react with H_2O_2 radicals in the Fenton reaction, forming OH initiating radicals to begin the RAFT polymerisation (Figure 3. 1). No polymer was formed when using Fe^{3+} without activation to Fe^{2+} by AscA as the Fenton reaction is much slower with Fe^{3+} compared to that with Fe^{2+}.[31] The results were in agreement with previous literature,[37] where interestingly, decreasing the concentration of AscA in these reactions improved polymer yields.

3.1.1.3 Investigating Monomer Concentration

The viability of microorganisms in applications towards biosensors and polymer-hybrids are extremely important. Before adding bacteria (*C. met*) into the reaction, *C. met* growth was monitored in the presence of several water soluble-monomers (DMA, *N*-acryloylmorpholine (NAM), and *N*-Hydroxyethyl acrylamide (NHEA)) at different concentrations (3.125 - 100 mM). Minimum inhibitory concentrations (MICs) were obtained from the results (Table 3. 3, Figure S3. 5). The polymerisations described thus far, contained DMA at concentrations of 2 M which according to the MIC results, would inhibit the growth of *C. met*. The total monomer concentration employed in further experiments was chosen to reflect the lowest MIC result obtained, 25 mM for NAM.

Table 3. 3 MICs of monomers, DMA, HEA and NAM, towards *C. met* metabolism.

MIC (mM)*		
DMA	**NHEA**	**NAM**
100	100	25

*Minimum inhibitory concentrations (MIC)s were calculated as the highest concentration of reagent that did not reduce the OD_{600} of culture at exponential phase by less than 30% than that of the wt.

The AscA initiated FG-RAFT experiment was carried out using DMA (25 mM) and the total reaction volume was increased to 1 mL, with all reagents adjusted to maintain the reagent ratios used previously. Unfortunately, no polymerisation was observed, likely because of the reduction in total GOx concentrations (2.50×10^{-4} mM to 3.10×10^{-6} mM) and glucose concentrations (100 mM to 1.25 mM) compared to the former experiments. It was postulated that this affected the efficiency of the *in-situ* solution degassing by GOx, particularly as the increased reaction volume (200 µL to 1 mL) would contain more terminating O_2 species. The overall GOx, Glu and $FeCl_3$ concentrations were next increased by i) reducing the reaction volume, and ii) directly increasing reagent concentrations in the same 1 mL volume. To observe whether reducing the reaction volume would assist the polymerisation of DMA (0.25 mM), the total reaction volume was decreased from 1 mL to 200 µL. Some polymerisation was observed (Figure 3.3: bottom, blue),

however a substantial monomer content was still evident by ^{1}H NMR spectroscopy at the end of the reaction.

In contrast, when the GOx concentration was increased to equal that of the original reaction (2.50 x 10^{-4} mM) along with Glu and Fe^{3+} reagents accordingly, full monomer conversion was observed after 24 hours (Figure 3.3: top, green). This observation suggests that the increase in GOx and Glu effectively deoxygenated the solution for the RAFT polymerisation to occur. Additionally, the 10 times rise in Fe concentration is likely to have increased the radical flux to facilitate the reaction further.

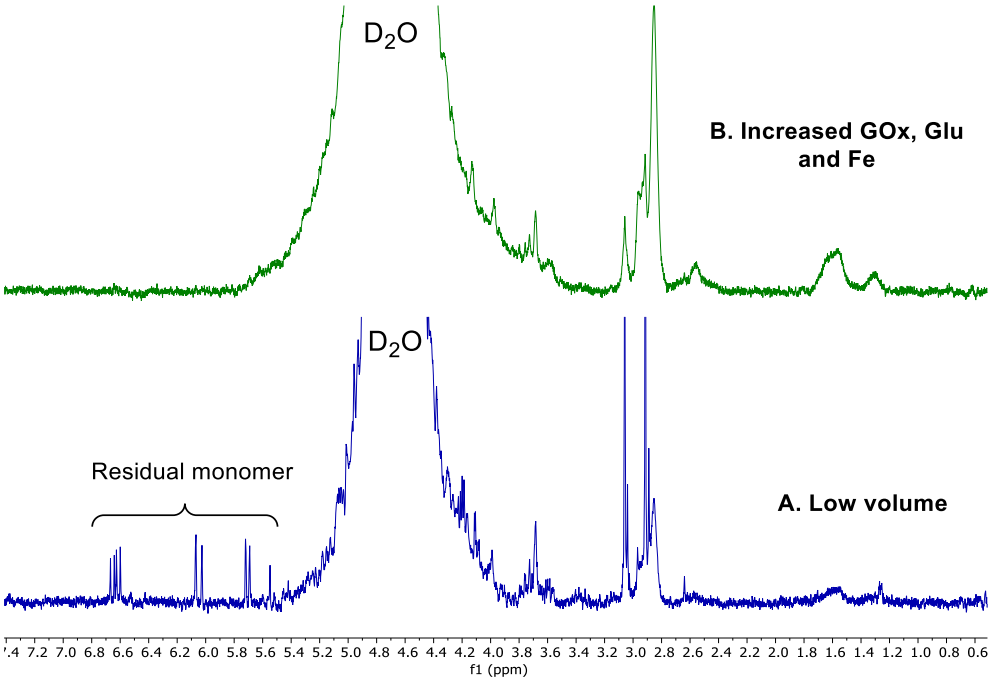

Figure 3.3 ^{1}H NMR (400 MHz, D_2O) of final time point (24 hours) for Fenton-GOx-RAFT reactions with 25 mM concentration of DMA monomer. The overall GOx, Glu and $FeCl_3$ concentrations were increased by A) (Bottom, blue) reducing the reaction volume, and B) (Top, green) directly increasing reagent concentrations in the same 1 mL volume. Reagent ratios of B: DMA: CTA: Glu: GOx: Fe: AscA = 200: 1: 800: 2 x 10^{-3} : 54 : 2.2. Note for B the $FeCl_3$ and AscA concentration was 10 times greater than that of A.

3.1.1.4 Ascorbic Acid Contribution

After establishing an FG-RAFT system under conditions that could be tolerable to bacteria, an investigation was carried out to verify the relationship between the concentration of the reducing agent used and the extent of monomer conversion to polymer. The results (Table 3.4, Figure S3. 6) showed that decreasing the AscA concentration increased the polymerisation yield, and it can be inferred that the rate of polymerisation was quicker, with satisfactory conversion (95%) reached using 2.2 µmol AscA. As discussed previously, the decreased reaction rates at higher AscA concentrations are likely due to the inhibitory effects that AscA may have on GOx and its O_2 consuming nature, which may have hindered the reaction.

Table 3.4 The affect of ascorbic acid concetration on Fenton-GOx-RAFT Polymerisations with DMA monomer.

AscA (µmol)	Conv. (%)[a]
2.2	95
22	22
44	14.5

[a] Estimated using of ^{1}H NMR from comparison of monomer (CH acrylate): polymer (CH_2 backbone) integrals. Reagent ratios: DMA: CTA: Glu: GOx: Fe: AscA (High) = 200: 1: 800: 2 x 10^{-3} : 54 : 17.6.

3.1.2 Tailoring reagent parameters in Fenton-GOx-RAFT Polymerisations

The scale of the established reaction mentioned was unfortunately too low to obtain sufficient sample mass for SEC analysis. For this reason, the total monomer concentration of DMA was increased from 25 mM to 100 mM (the maximum concentration that would not affect bacterial viability for DMA). The reaction was also scaled up and the degree of polymerisation (DP) was decreased from 200 to 100, as to maximise the polymer yield. Near quantitative conversion (>99 %) was achieved with 670 µM $FeCl_3.6H_2O$, and the resulting polymer was analysed by SEC revealing some molecular weight control (M_n^{SEC} ~ 16 kDa) (Table 3. 5, entry 1). The dispersity ($Đ$ ~ 1.58) indicated that the polymerisation was not 'living' but it was postulated that this could be attributed to high initial radical flux which can cause chain-chain coupling reactions.[45] During the polymerisation, H_2O_2 reacts with Fe^{2+} to form highly active OH radicals that subsequently initiate CTA molecules to begin the RAFT reaction. A large flux of OH radicals could lead to loss of initiating species through side-reactions, which would affect the resulting chain lengths of the polymers. Furthermore, high H_2O_2 concentrations can cause CTA oxidative degradation leading to poorly controlled polymerisations.[10, 45] The concentration of reagents that could influence the radical flux during FG-RAFT were therefore altered to investigate the effect on the resulting polymers (Table 3. 5).

3.1.2.1 Tailoring the radical flux in FG-RAFT

Firstly, the quantities of glucose and GOx, which control the generation of H_2O_2 from O_2 in the reaction, were i) individually, and ii) simultaneously decreased by half (Table 3. 5, entries 2-4). These had little effect on the conversion of the polymerisations but M_n^{SEC} of the resulting polymers were slightly closer to the M_n^{th} than that of the original polymerisation (Entry 1). The dispersities of these polymers also decreased slightly compared to that of the original reaction (Figure 3.4 (i)). This observation suggested that reducing Glu and GOx concentrations lowered the amount of H_2O_2 produced which decreased the radical flux generated upon reaction with Fe^{2+} to generate polymers with a slightly more uniform polymer dispersity with better M_n control.

Next, the quantities of Fe and AscA, which control the generation of Fe^{2+} to react with H_2O_2 and create OH radicals in the reaction, were decreased. Decreasing the Fe concentration by 50 % and 75 % consecutively lowered the dispersities (*Đ* ~ 1.53 and 1.49, respectively) of the resulting polymers and increased the M_n^{SEC} values obtained (20.1 and 21.9 kDa, respectively) closer to the theoretical values (Table 3. 5, entries 5 and 8). Lowering both the AscA and Fe concentration in the polymerisations further decreased the dispersity of the polymers generated (Figure 3.4 (ii)). However, the difference in dispersity was not substantial enough to pursue these conditions further.

Table 3. 5 Tailoring reagent parameters in Fenton-GOx-RAFT including Glucose, GOx, Fe, AscA and monomer type.

Entry	Monomer*	Reaction	Conv. (%)[a]	M_n^{th} (kDa)[b]	M_n^{SEC} (kDa)[c]	$Đ$[c]
1	DMA	Original	99.7	39.7	16.6	1.58
2	DMA	½ Glucose	99.6	39.7	18.9	1.49
3	DMA	½ GOx	99.1	39.5	18.2	1.45
4	DMA	½ Glucose and GOx	99.4	39.6	18.5	1.48
5	DMA	½ Fe	99.0	39.5	20.1	1.53
6	DMA	½ AscA	98.9	39.4	25.3	1.51
7	DMA	½ Fe and AscA	98.5	39.3	27.3	1.44
8	DMA	¼ Fe	99.4	39.6	21.9	1.49
9	DMA	¼ AscA	96.9	38.6	28.7	1.41
10	DMA	¼ Fe and AscA	96.6	38.5	29.7	1.35
11	HEA	Original	96.7	44.8	17.9	1.49
12	NAM	Original	99.1	56.2	14.0	1.91
13	NAM (25 mM)	Original	98.7	56.0	7.1	2.04
14	NAM (25 mM)	¼ Fe	96.9	55.0	14.6	1.74

[a] Estimated using of ^{1}H NMR from comparison of monomer (CH acrylate): polymer (CH_2 backbone) integrals. [b] M_n^{th} = ($Mr_{monomer}$)* 400* conversion) + 254 Da. [c]Calculated using SEC (DMF). *All monomer concentrations were set to 100 mM unless stated otherwise. Note: **Original** reagent ratio: Monomer: CTA: Glu: GOx: Fe: AscA = 400: 1: 400: 1 x 10^{-5}: 2.8: 8.8.

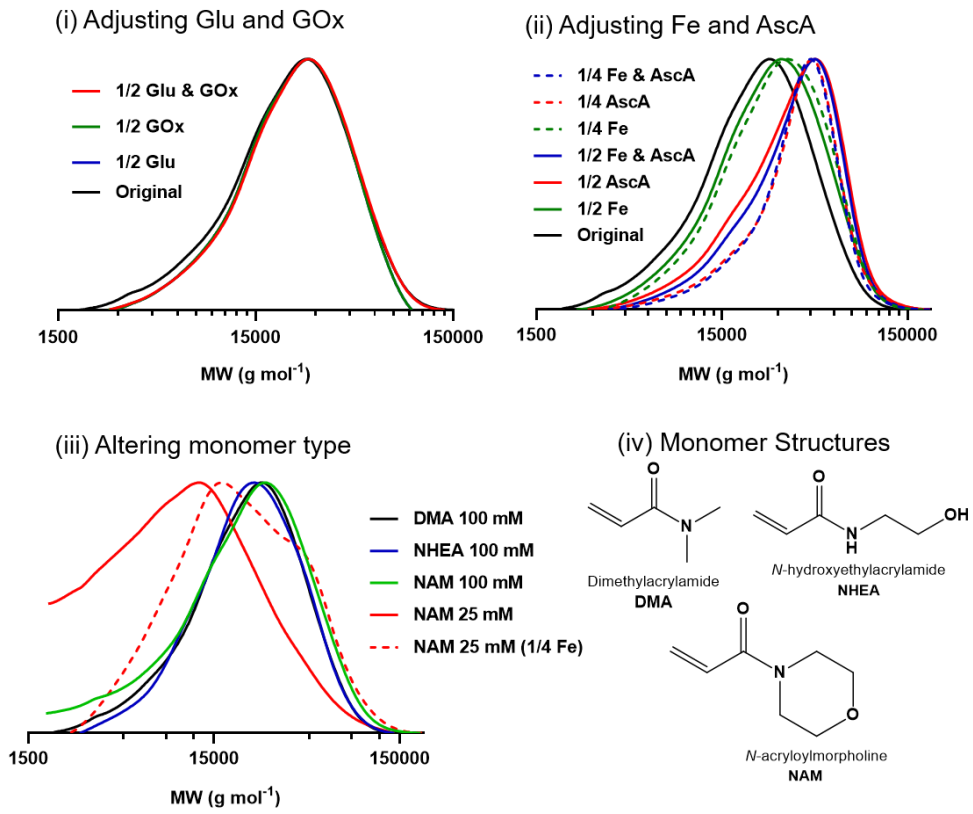

Figure 3. 4 SEC (DMF) graphs of polymers generated by Fenton-GOx-RAFT polymerisations with differing concentrations of (i) glucose (Glu) and GOx and (ii) Fe and AscA. SEC (DMF) graphs are also compared for differing monomer types (iii) and the monomer structures displayed (iv). Original reagent ratio: Monomer: CTA: Glu: GOx: Fe: AscA = 400: 1: 400: 1 x 10^{-5}: 2.8: 8.8.

3.1.2.2 Other Monomers

Additional monomers, NHEA and NAM (Figure 3.4 (iv)), were implemented into the polymerisation to demonstrate the versatility of the technique (Table 3. 5, entries 11-14). FG-RAFT polymerisations at 100 mM monomer concentrations were carried out and the ^{1}H NMR spectra (Figure S3. 7, Figure S3. 8) and GPC chromatograms (Figure 3.4 (iii)) of the polymers generated were analysed. Polymerisations with both NHEA and NAM monomers gave high conversions, 96.7% and 99.1%, respectively. Polymers resulting from the former were more controlled (***Đ*** ~ 1.49) compared to those of the latter (***Đ*** ~ 1.91), suggesting that the structure of the monomer is contributory to the homogeneous growth rate of polymer chains.

As the monomer NAM produced a lower MIC value (25 mM) towards C*. met*, the monomer concentration was reduced to be suitable for bacterial polymerisations later. The effect of this further increased the dispersity of the resulting polymers (***Đ*** ~ 2.04) and the SEC trace (Figure 3.4 (iii)) was not symmetrical. In efforts to improve the molecular weight control and dispersity control in polymerisations with NAM, the Fe concentration was decreased by 75 %, to ¼ of the original Fe concentration (Table 3. 5, entry 14). This effectively reduced the radical flux to generate a polymer with a lower dispersity (***Đ*** ~ 1.70) but the molecular weight (M_n^{SEC} = 14.6 kDa) remained far from the predicted values (M_n^{th} = 55.0 kDa). A slight shoulder was present in the SEC graph, typical of recombination termination events, which might be attributed to the lower monomer concentration compared to the 100 mM reaction.

3.1.3 Bacterial assisted Fenton-GOx-RAFT

3.1.3.1 Living vs Dead bacteria

The original hypothesis was that bacteria could be used to reduce Fe^{3+} and initiate the FG-RAFT polymerisation in the presence of air, analogous to using AscA in the above experiments. Bacterial assisted Fenton-GOx-RAFT (b-FG-RAFT) experiments were carried out using *Cupriavidus metallidurans* (*C. met*) as they were shown to successfully initiate Fe ATRP reactions in the previous chapter. Furthermore, disruptions to the reaction due to bacterial consumption of glucose are unlikely to occur with this bacteria type because *C. met* lacks the glucose transporter.[46] *C. met* were grown in LB, washed with PBS and re-suspended in PBS before being added to the reaction mixture.

To realise the significance of bacterial metabolism in the following reactions, b-FG-RAFT polymerisations were carried out using either i) living bacteria (1.7×10^{10} colony forming units (CFU)s mL^{-1}), or ii) heat killed bacteria (368 CFU mL^{-1}) in place of ascorbic acid. In the former case (i), 53% conversion was observed, and in the latter case (ii) no polymerisation was observed (Figure 3. 5). This indicated that living bacteria were essential to the redox process that converted Fe^{3+} to Fe^{2+} for the FG-RAFT polymerisation to take place. Omitting $FeCl_3$ from the polymerisation resulted in no conversion (Figure S3. 9) which revealed that the Fenton Reaction step plays a key role in the polymerisation process. Omitting bacteria (and AscA) from the reaction produced only minimal conversion (Figure S3. 9), highlighting its importance in the conversion of Fe^{3+} to Fe^{2+} for the FG-RAFT cascade to proceed.

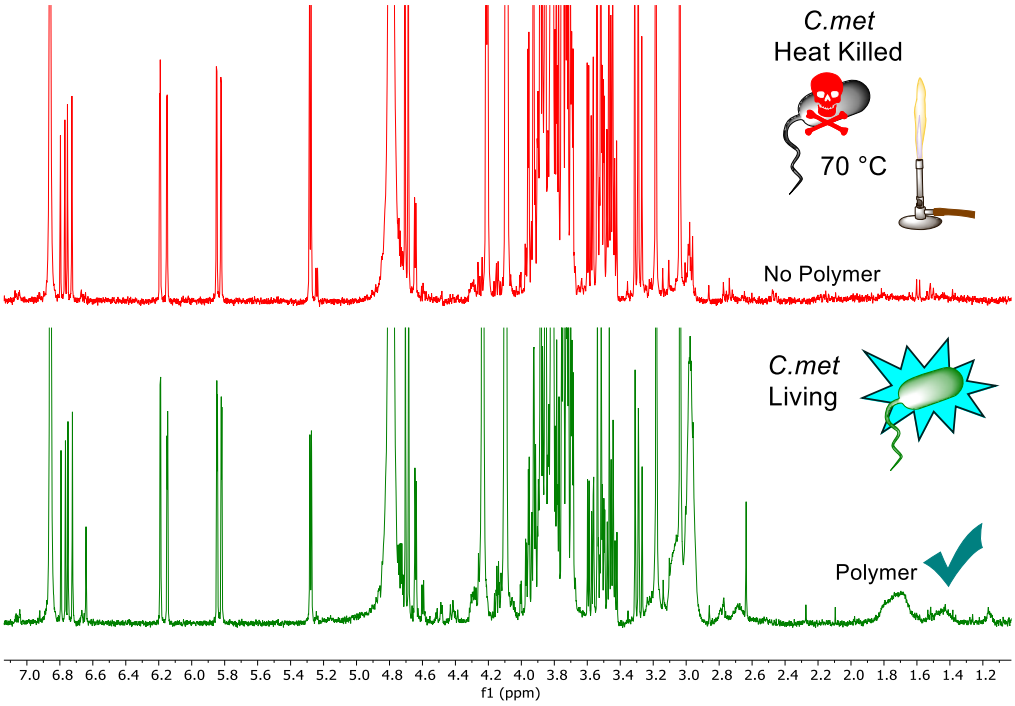

Figure 3. 5 ^{1}H NMR stacked spectra of Fenton-GOx-RAFT polymerisations in air at 30°C with living *C. met* (bottom, green) and heat-killed *C. met* (top, red). Reagent ratios: DMA: CTA: Glu: GOx: Fe = 200: 1: 800: 2 x 10^{-3} : 5.4.

3.1.3.2 Polymer Analysis

Polymerisations assisted by *C. met.*, utilising b-FG-RAFT, were then carried out at DP400 with different monomers to compare the conversion and M_n^{SEC} of the resulting polymers (Table 3. 6). The polymerisation with DMA achieved adequate conversion in 24 hours (62 %,^{1}H NMR: Figure S3. 10) to produce polymers with sufficiently controlled dispersities (***Đ*** ~ 1.12) and a symmetrical molecular weight distribution (Figure 3. 6, Black). Interestingly, polymers resulting from reactions with NHEA (^{1}H NMR: Figure S3. 11) had the broadest dispersity (***Đ*** ~ 2.4, Figure 3. 6) which were more uniform in analogous non-bacterial experiments with

NHEA (*Đ* ~ 1.91), suggesting an increased interference of bacterial components with this monomer structure.

Table 3. 6 Conversion and SEC results for Fenton-GOx-RAFT polymerisations of different monomers, initiated by *C. met* in air at 30°C, with varying reagent conditions.

Monomer	Total monomer conc. (mM)	Condition	Fe (μM)	Conv. (%)[a]	M_n^{th} (kDa) [b]	M_n^{SEC} (kDa) [c]	*Đ*[c]
DMA	100	Original	700	62.2	24.9	19.9	1.12
NHEA	100	Original	700	52.8	24.6	23.8	2.40
NAM	25	Original	700	60.8	34.6	50.0	1.70
NAM	25	25 % Fe	175	59.9	34.1	44.0	1.63
DMA	100	1 % Fe	7	44.3	17.8	20.7	1.28
DMA	100	No CTA	700	99.9	39.8	451.0	2.11

[a] Estimated using of ^{1}H NMR from comparison of monomer: polymer integral, time 24 h. [b] M_n^{th} = (Mr(monomer) * 400* conv.) + 254.3 Da. [c] SEC (DMF). *C. met* count in each reaction were 1.7 x10^{10} CFU mL^{-1} or 3.4 x10^{10} CFU in total reaction volume. Original reagent ratios: Monomer: CTA: Glu: GOx: Fe = 400: 1: 400: 1 x 10^{-5} : 2.8.

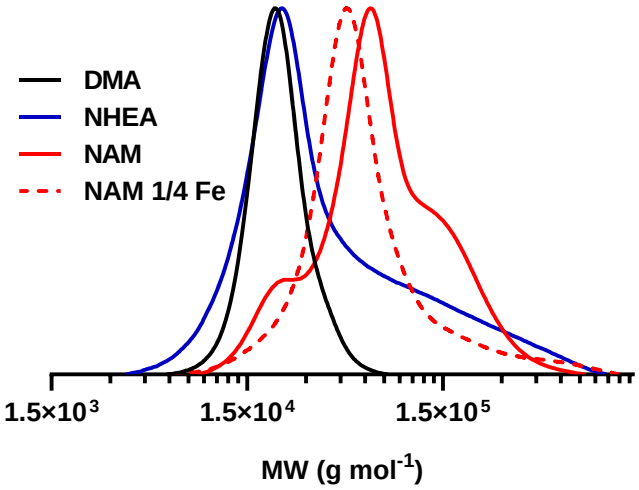

Figure 3. 6 SEC (DMF) of polymers resulting from bacterial-Fenton-GOx-RAFT of; DMA (Black), NHEA (Blue) at 100 mM monomer concentrations, and NAM (Red) at 25 mM monomer concentration. polymerisations carried out with ¼ the amount of Fe from the original are shown with NAM (Red Dotted). Original reagent ratios: Monomer: CTA: Glu: GOx: Fe = 400: 1: 400: 1 x 10^{-5} : 2.8.

To sustain the *C. met* metabolism in b-FG-RAFT polymerisations with NAM, experiments were carried out with lower NAM concentrations (25 mM, as per Table 3. 3). This resulted in polymers (^{1}H NMR: Figure S3. 12) with a relatively broad dispersity (***Đ*** ~ 1.70, Table 3. 6, Figure 3. 6) and a poorly controlled M_n^{SEC} (50.0 kDa) which was much higher than theoretical values (34.6 kDa). This might be explained by the more dilute solution (25 mM) in which CTA species may be subject to more degradation, effecting the initiation efficiency. The lack of control in M_n^{SEC} observed could alternatively be due to the presence of the bacteria or biological components (ECM) interfering with the polymerisation reagents. It is also important to highlight the absence of the AscA radical scavenger in b-FG-RAFT polymerisations which may protect the CTA from H_2O_2 degradation in analogous non-bacterial polymerisations. Conversely, b-FG-RAFT polymerisations with DMA and NHEA monomers resulted in polymers with significantly improved M_n control compared to the polymers produced by analogous AscA initiated polymerisations. This suggests that the structure of NAM may have contributed to the loss of M_n control seen in the b-FG-RAFT experiments described, likely due to its difference in reactivity.

To investigate whether control could be realised in b-FG-RAFT with NAM, the Fe concentration was reduced by 75% from 700 to 175 µM with efforts to decrease the initial flux of initiating radicals (OH). This resulted in polymers with slightly lower dispersity (***Đ*** ~ 1.63) and the M_n^{SEC} (44.0 kDa) was reduced slightly. However, NAM remained the monomer for which there was the least controlled polymerisation in the

study. Comparing the polymerisations of DMA, NHEA and NAM, the structure of the monomer strongly influenced the dispersity and the M_n control of the resulting polymers.

During the Fenton initiation of b-FG-RAFT, Fe^{3+} is regenerated in the reaction between Fe^{2+} and H_2O_2, which could then be re-catalysed by the bacteria back to the Fenton active Fe^{2+} in a continuous cycle. Due to this recycling effect of the Fe, it was hypothesised that Fe concentrations could be further decreased. Indeed, b-FG-RAFT experiments revealed that it was possible to reduce the Fe concentration to 7 µM whilst maintaining narrow dispersities (***Đ*** ~ 1.28, Table 3. 6, Figure 3. 7) in the resulting polymers. The M_n of the resulting polymers was close to theoretical values although the conversion was reduced to 44.3 %. A compromise between Fe concentration and polymerisation conversion must therefore be realised, but the ability to maintain adequate polymerisation control at low Fe concentrations using b-FG-RAFT under benign conditions was particularly encouraging towards progress in sustainable synthetic methods and green chemistry.[47, 48]

Lastly, polymerisations were carried out using DMA and omitting the CTA from the reaction, which resulted in polymers with extremely high and uncontrolled molecular weights (M_n^{SEC} = 451.3 kDa, Table 3. 6, Figure 3. 7), with a broad molecular weight distribution (***Đ*** ~ 2.11). These features are characteristic of radical polymerisation (RP) which is shown to take place in the absence of CTA.[49]

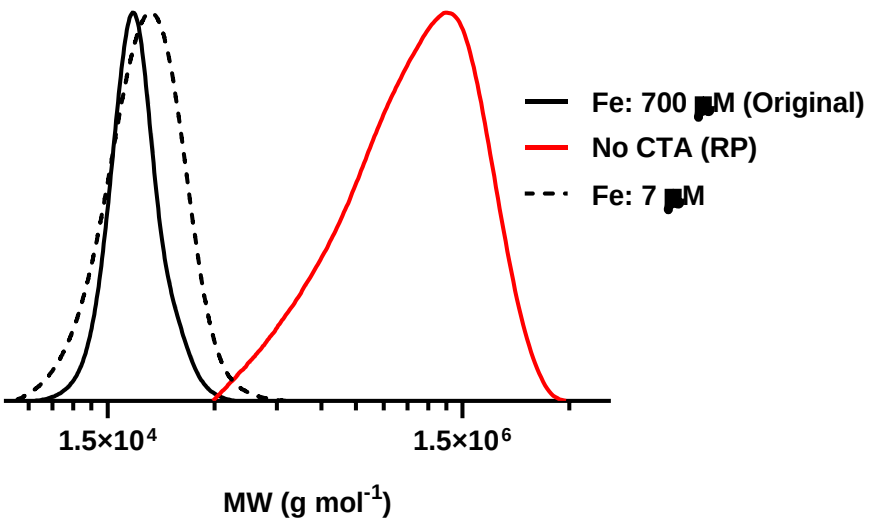

Figure 3. 7 SEC (DMF) of polymers resulting from bacterial-Fenton-GOx-RAFT of; DMA 100 mM monomer concentration with i) original Fe concentration (700 µM) (Black), ii) Fe concentration: 7 µM (Black, dotted), and iii) no chain transfer agent (CTA) i.e., Radical polymerisation (RP) (Red). Original reagent ratios: Monomer: CTA: Glu: GOx: Fe = 400: 1: 400: 1 x 10^{-5} : 2.8.

Conclusions

This chapter has demonstrated that bacterial Fe reduction can be used in FG-RAFT to generate uniform polymers with predictable molecular weights. The technique was first optimised in biological conditions using AscA in place of bacteria, during which, the reaction rate could be influenced by the AscA concentration. This new FG-RAFT reaction starting from Fe^{3+}, not only preserves the stability of the active Fe^{2+} catalyst, but also delivers an *in-situ* activation method which could be applied to future diagnostic applications. The radical flux was shown to be influenced by both Fe and AscA concentrations, but the control of the reaction was heavily monomer specific. Utilising *C. met.* in the place of AscA revealed well controlled polymerisations with DMA, in which living bacteria were necessary for the reaction to occur. Polymerisations were successful at Fe concentrations as low as 7 µM and experiments to reduce this further may be carried out in future work. The technique can be applied to a variety of monomer materials, but monomer-specific optimisation may be necessary to improve the quality of the resulting polymers. Overall, the technique presented offers a new way to fabricate polymers in virtually non-toxic environments with low catalyst concentrations and an *in-situ* initiation step upon activation by a living organism (bacteria). This combination of various chemistries with biology has enabled the emergence of b-FG-RAFT which may contribute towards developments in ELMs, biosensors or synthetic ECMs.

Materials and Methods

Materials

All chemicals were purchased from the supplier and used without further purification unless stated. N,N'-Dimethylacrylamide (DMA), N-acryloylmorpholine (NAM), and *N*-hydroxyethyl acrylate (NHEA), 2-(2-Carboxyethylsulfanylthiocarbonylsulfanyl)propionic acid) (CTA), Glucose, Glucose oxidase (GOx), Horse radish Peroxidase (HRP), Iron(II)chloride hydrate $FeCl_2.4H_2O$, Hydrogen peroxidase (H_2O_2), Acetylacetonate (ACAC), and Dulbecco's Phosphate Buffer Saline (DPBS) (without $CaCl_2$ and $MgCl_2$, filtered, suitable for cell culture) were purchased from Sigma Aldrich. Iron(III)chloride hexahydrate ($FeCl_3.6H_2O$) ≥98% was purchased from scientific laboratory supplies. Ascorbic acid (AscA) >99% was purchased from Alfa Aesar. For bacteria growth Lysogeny broth (LB) was used.

Methods

^1H NMR spectra were recorded at room temperature on a 400 MHz (Bruker DPX400 Ultrashield) using deuterated solvents (D_2O). NMR spectra were analysed using MestReNova 11.0.0-17609 2016 Mestrelab Research S.L.

DMF Size Exclusion Chromatography (SEC) was performed on Polymer Laboratories GPC 50 system fitted with refractive index (RI) detector, 2 x Agilent PLgel Mixed-D column and DMF + 0.1% LiBr eluent. Molecular weight (M_n) and polydispersity ($Đ$) were calculated according to PMMA narrow standards (1.5 - 1,000 kDa). Polymer samples were

made by dissolving 3 mg/mL pure polymer in 1 mL DMF + 0.1% LiBr followed by filtration.

Toxicity experiments - MICs of reagents were carried out using microplate reader (Infinite M Nano, TECAN) with 96-Well standard microplates (Costar 3363) measuring the $OD_{600\ nm}$ every 30 minutes for up to 24 hours. Detailed methods described in Chapter 2 (Section 2.6.6) of this thesis.

Experimental and Supplementary

Note: Due to COVID-19 restrictions some experimental work (Sections **3.1.9** and **3.1.11)** was carried out by **Cara Moloney** (Post Doctorial Fellow). Bacterial preparation was assisted by **Federico Turco** (PhD student) and **Francesco Catrambone** (PhD Student) (Sections **3.1.10** and **3.1.11**) due to building access restrictions. The author of experimental protocols and data analysis involved in this chapter was Mechelle Bennett. Experiments in all other sections were carried out by Mechelle Bennett.

3.1.4 Verification of Enzymatic Polymerisations

HRP Catalysed RAFT polymerisations

Stock solutions of reagents were prepared in deionised water and the required amounts were added according to the following reagent ratios:

[DMA] : [CTA] : [HRP] : [H_2O_2] : [ACAC] = 200 : 1 : 0.00054 : 0.2 : 4

DMA was de-inhibited using an aluminium oxide column before use. DMA (104 µL, 1 mmol), CTA (1.27 mg, $5x10^{-3}$ mmol) HRP (120 µg, $2.7x10^{-6}$ mmol), ACAC (2.05 µL, $2x10^{-2}$ mmol) and DPBS (800 µL) were added to a test tube and degassed with N_2 (g) for 10 minutes. H_2O_2 (34 µL of 30% solution) was added to begin the reaction and left stirring at room temperature for 90 minutes. Polymer $P(DMA)_{R1}$ was analysed by ^1H NMR (Figure S3.1) and SEC (Table S3.1).

GOx- HRP RAFT cascade validation

Stock solutions of reagents were prepared in deionised water and the required amounts were added according to the following reagent ratios:

[DMA] : [CTA] : [HRP] : [ACAC] : [GOx] : [Glu]

= 200 : 1 : 0.00054 : 4 : 0.0002 : 20

DMA was de-inhibited using an aluminium oxide column before use. DMA (104 µL, 1 mmol), CTA (1.27 mg, $5x10^{-3}$ mmol), ACAC (2.1 µL, $2x10^{-2}$ mmol), GOx (80 µg, $1x10^{-6}$ mmol), Glu (18 mg, 0.1 mmol) and DPBS (660 µL) were added to a test tube and left for 10 minutes to 'self-degas'. No external sources were used to degas the solution. After this HRP (120 µg, $2.7x10^{-6}$ mmol) was added to begin the reaction and left stirring at room temperature for 3 hours. Polymer $P(DMA)_{R2}$ was analysed by ^{1}H NMR (Figure S3.2) and SEC (Table S3.1). A control experiment without glucose was also carried out (Figure S3.3).

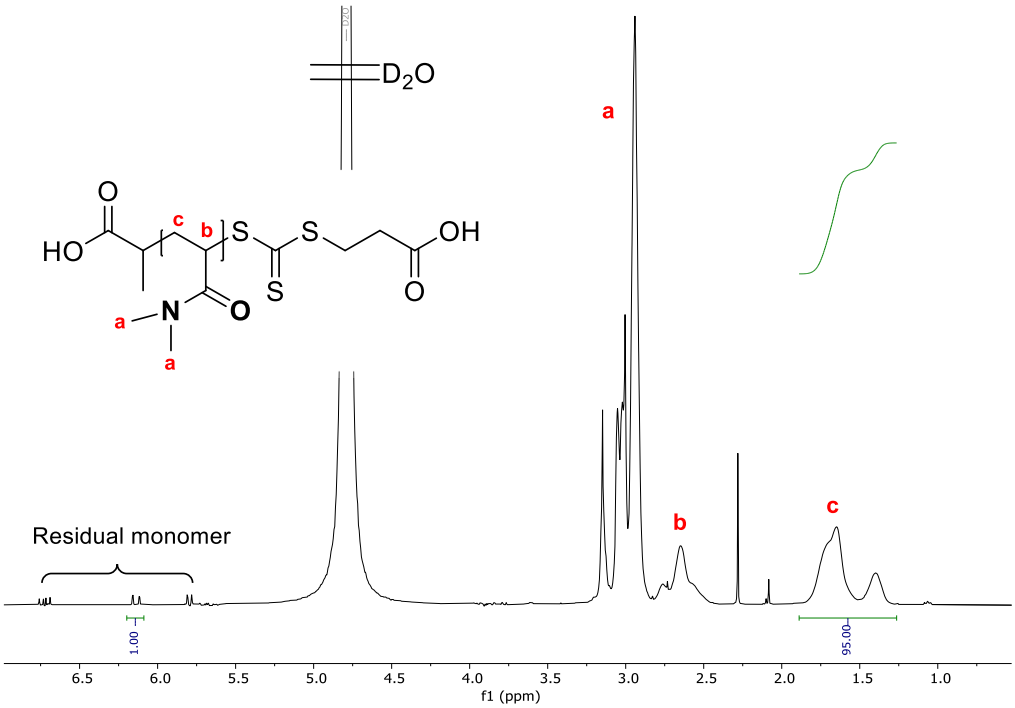

Figure S3. 1. ^{1}H (400 MHz, D_2O) of $P(DMA)_{R1}$ resulting from HRP initiated RAFT polymerisation.

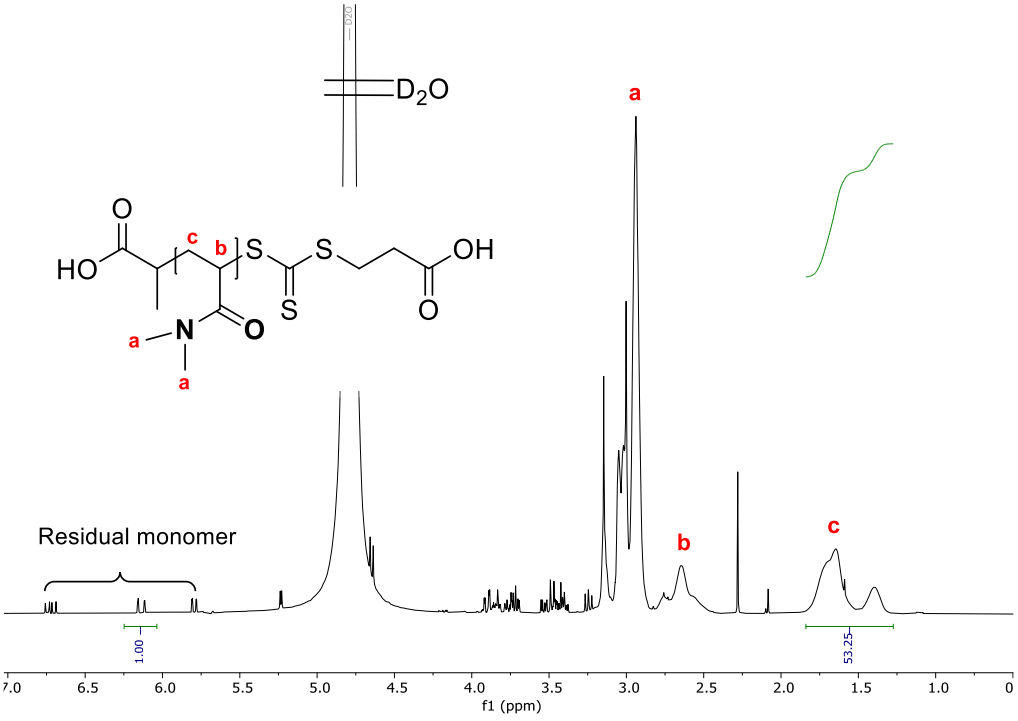

Figure S3. 2. ^{1}H (400 MHz, D_2O) of $P(DMA)_{R2}$ resulting from GOx-HRP initiated RAFT polymerisation in air.

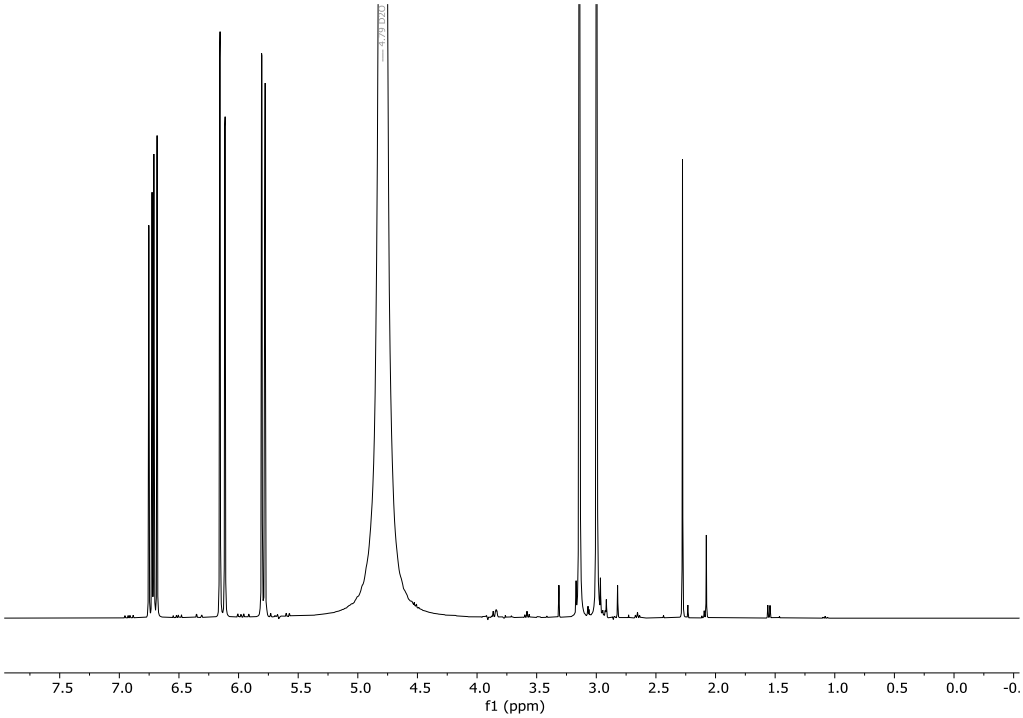

Figure S3. 3. ^{1}H NMR (400 MHz, D_2O) of no glucose control for HRP-GOx cascade reaction after 20 hours

Table S3. 1 SEC analysis of polymers formed in enzyme RAFT of DMA

Polymer	M_n^{SEC} (KDa)[a]	$Đ^{SEC}$ [b]	M_n^{th} (KDa)[b]
$P(DMA)_{R1}$	23	1.1	20
$P(DMA)_{R2}$	29	1.1	20

[a] M_n^{th} = (200* conversion) + 254.3 Da. [b] From SEC (DMF).

3.1.5 Establishing FG-RAFT under Biocompatible Conditions

Stock solutions of reagents were prepared in deionised water and the required amounts were added according to the following reagent ratios:

[DMA] : [CTA] : [GOx] : [Glu] : Fe source : AscA

= 200 : 1 : 0.000025 : 10 : 0.07 : 1

Reaction A; DMA was de-inhibited using an aluminium oxide column before use. DMA (42 µL, 0.41 mmol), CTA (0.508 mg, 0.002 mmol), GOx (4 µg, $5x10^{-8}$ mmol) Glu (3.6 mg, 0.02 mmol) $FeCl_3.6H_2O$ (38 µg, 1.4 x 10^{-4} mmol) and DPBS (to total volume 200 µL) were added to a test tube and left for 10 minutes to 'self-degas'. No external sources were used to degas the solution. Following this, AscA (0.35 mg, 0.002 mmol) was added to begin the reaction and left stirring at room temperature for 20 hours.

Reaction B; The protocol for Reaction A was used but the quantity of AscA was decreased. AscA (78 µg, 5 x 10^{-4} mmol).

Reagent ratios:

[DMA] : [CTA] : [GOx] : [Glu] : [Fe source] : [AscA]

= 200 : 1 : 0.000025 : 10 : 0.07 : 0.22

Table S3. 2 Control experiments carried out for Fenton-GOx-RAFT polymerisations.

Control	Protocol	AscA	Fe(II)	Fe(III)	Figure
C1	Reaction A	No	No	Yes	S3.4
C2	Reaction A	No	No	No	S3.4
C3	Reaction A	No	Yes	No	3.2
C4	Reaction B	Yes	No	No	3.2

* Reagent ratios for Reaction A: DMA: CTA: Glu: GOx: Fe: AscA = 200: 1: 10: 2.5 x 10-5 : 0.07: 1. Reaction B: Reagent ratios: DMA: CTA: Glu: GOx: Fe: AscA = 200: 1: 10: 2.5 x 10-5 : 0.07: 0.22

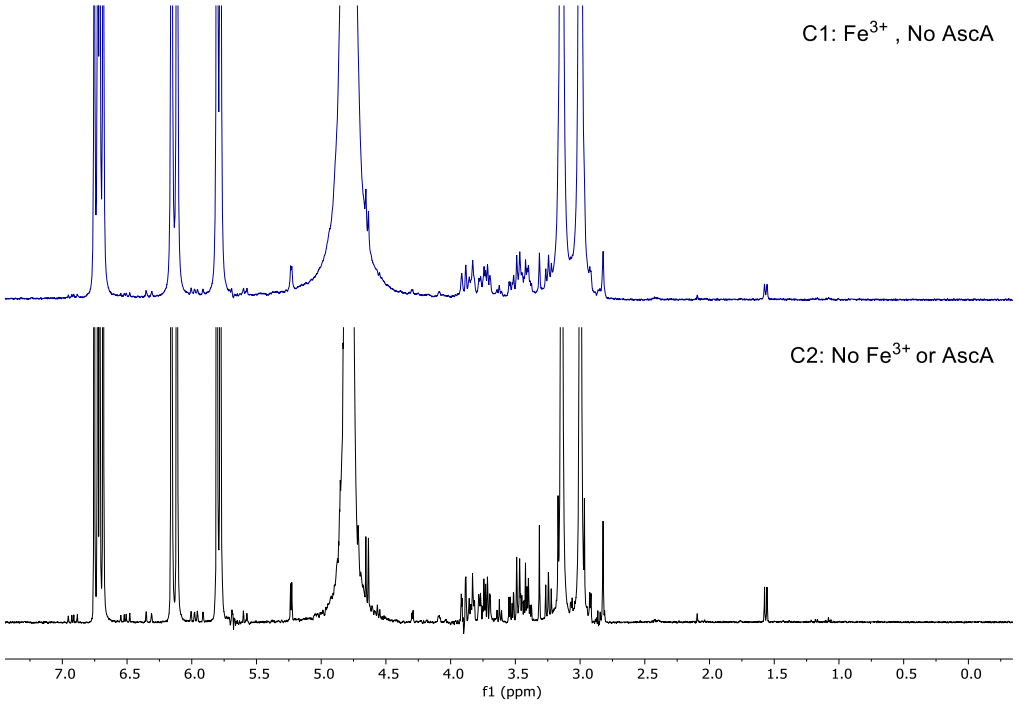

Figure S3. 4. ^{1}H NMR (400 MHz, D_2O) of Fenton-GOx-RAFT control reactions with $FeCl_3.6H_2O$. C1 (Top, blue): Reaction with Fe^{3+} omitting AscA from the reaction. C2 (Bottom, Black): Reaction omitting Fe source and AscA. Reagent ratios from Reaction A used: DMA: CTA: Glu: GOx: Fe: AscA = 200: 1: 10: 2.5 x 10-5 : 0.07: 1.

3.1.6 Toxicity studies of Monomers with *Cupriavidus metallidurans*

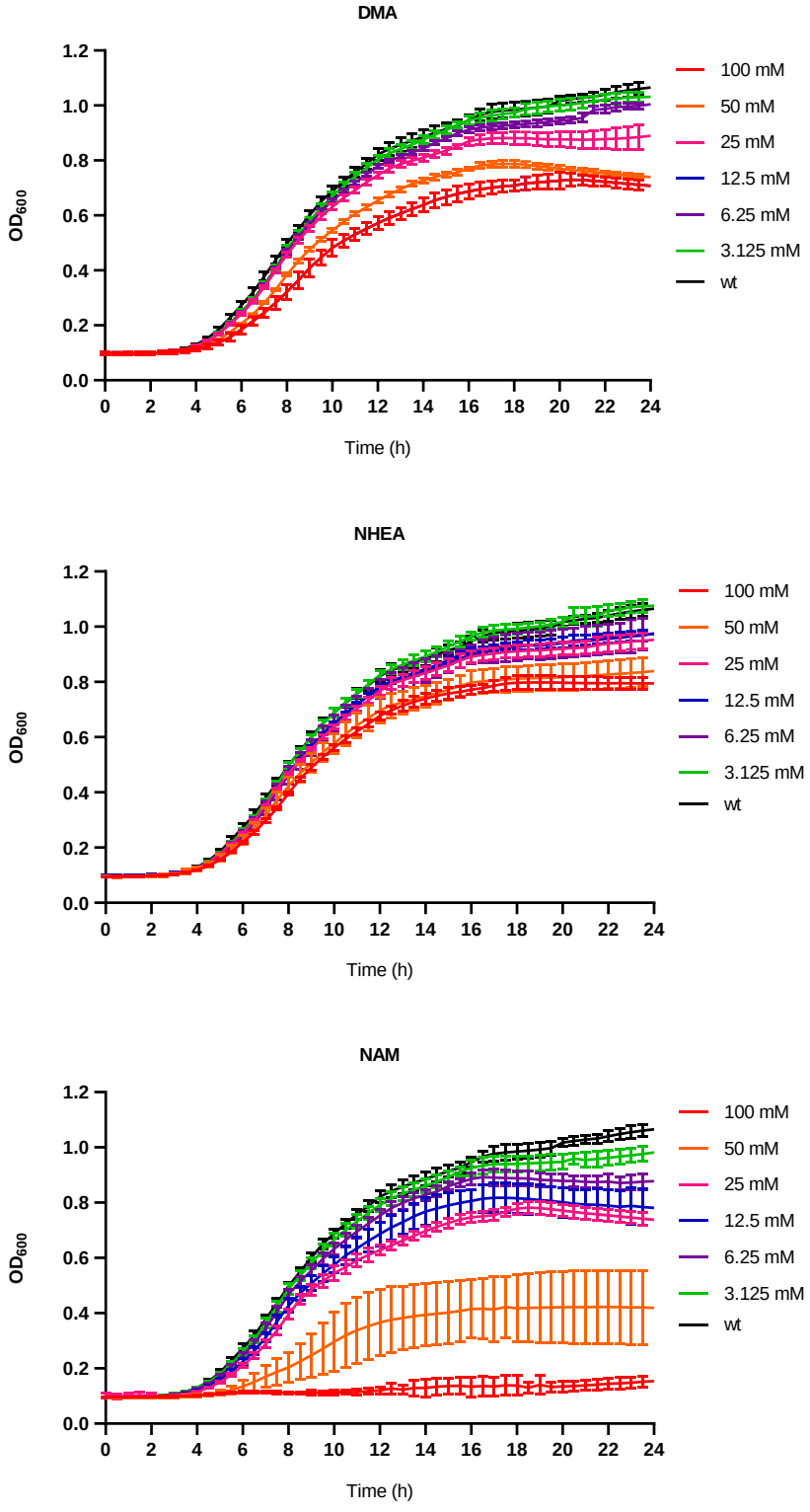

Figure S3. 5 Toxicity study to observe the effect of monomers DMA, NHEA and NAM on the growth of *C. met* at different concentrations (wt = wild type *C. met* in PBS only). Minimum inhibitory concentrations (MIC)s were calculated as the highest concentration

of reagent that did not reduce the OD_{600} of culture at exponential phase by less than 30% than that of the wt.

3.1.7 Optimising Monomer and GOx Concentrations for Bacterial Instructed FG-RAFT

Lower DMA concentration (25 mM) was necessary for bacterial survival. Stock solutions of reagents were prepared in deionised water and the required amounts were added according to reagent ratios in Table S3.3. ^{1}H NMR (400 MHz, D_2O) was used to monitor the reactions.

A. Original reagent ratios:

DMA (2.6 µL, 0.025 mmol), and CTA (31 µg, 0.125 µmol), $FeCl_3$ (2.4 µg, 8.7 $x10^{-3}$ µmol), GOx (0.25 µg, 3.1 $x10^{-9}$ mmol), Glucose (225 µg, 1.25 µmol) and PBS (to make final volume 1 mL) were added to a vial with AscA (22 µg, 0.125 µmol) and left rotating at 25 °C. No polymerisation occurred.

B. Lower Volume:

DMA (0.5 µL, 0.005 mmol), and CTA (6.36 µg, 0.025 µmol), $FeCl_3$ (36 µg, 0.133 µmol), GOx (4 µg, 5 $x10^{-8}$ mmol), Glucose (3.6 mg, 0.02 mmol) and PBS (to make final volume 200 µL) were added to a vial with AscA (7.8 µg, 0.044 µmol) and left rotating at 25 °C. No polymerisation occurred.

C. Increasing GOx and Glu was necessary:

Increase the concentration of GOx to 0.00025 mM. DMA (2.6 µL, 0.025 mmol) and CTA (31 µg, 0.125 µmol), $FeCl_3$ (180 µg, 0.67 µmol), GOx (20 µg, 2.5 x 10^{-7} mmol), Glucose (18 mg, 0.1 mmol) and PBS (to make final volume 1 mL) were added to a vial with AscA (390 µg, 2.2 x 10^{-3} mmol) and left rotating at 25 °C. ^{1}H NMR (400 MHz, D_2O) was used to monitor the reaction.

Table S3. 3 Optimising monomer and GOx concentrations for FG RAFT of DMA using different reagent ratios.

Reaction	DMA	CTA	GOx	Glu	Fe^{3+}	AscA	Vol (mL)	Conversion
A	200	1	0.000025	10	0.07	1	1	0%
B	200	1	0.002	800	5.4	1.8	0.2	~58%
C	200	1	0.002	800	54	17.6	1	>99%

3.1.8 Effect of AscA Concentration on FG-RAFT Polymerisations

DMA (2.6 µL, 0.025 mmol) and CTA (31 µg, 0.125 µmol), $FeCl_3$ (180 µg, 0.7 µmol), GOx (20 µg, 2.5 x 10^{-7} mmol), Glucose (18 mg, 0.1 mmol) and PBS (to make final volume 1 mL) were added to a vial with ascorbic acid and left rotating at 25 °C. ^{1}H NMR (400 MHz, D_2O) was used to monitor the reaction.

Table S3. 4 Ascorbic acid (AscA) mass and moles for Fenton-GOx-RAFT AscA study with reagent ratios: DMA: CTA: Glu: GOx: Fe: AscA (High) = 200: 1: 800: 2 x 10^{-3} : 54 : 17.6.

Reaction	Mass AscA	Moles AscA (µmol)
High	390 µg	222
Medium	3.9 mg	22
Low	7.8 mg	2.2

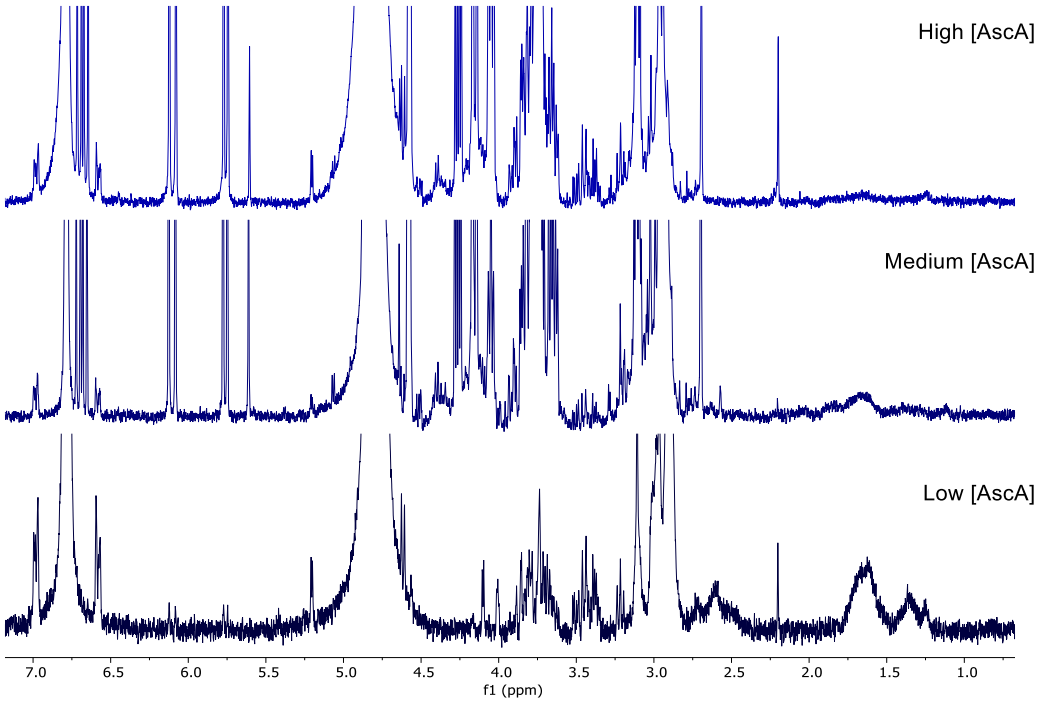

Figure S3. 6. ^{1}H NMR (400 MHz, D_2O) of Fenton-GOx-RAFT of DMA using different concentrations of AscA; Top = High (220 µmol), Middle = medium AscA (22 µmol),

Bottom = Low AscA (2.2 µmol). Reagent ratios: DMA: CTA: Glu: GOx: Fe: AscA = 200: 1: 800: 2 x 10^{-3} : 54 : 17.6.

3.1.9 Tailoring the Reagent Parameters in FG-RAFT Polymerisations

'Original' Conditions ref. Table 3.5 and S3.4:

DP400, 100 mM Reaction. DMA (41.1 µL, 0.4 mmol) **OR** HEA (46.4 µL, 0.4) **OR** NAM (56.0 µL, 0.4 mmol) was mixed with CTA (248 µg, 1 µmol), $FeCl_3$ (720 µg, 2.8 µmol), Glucose (72 mg, 0.4 mmol), GOx (80 µg, 1 x 10^{-8} mmol) and PBS (to make final volume 4 mL) in a vial with AscA (1.56 mg, 8.8 x 10^{-3} mmol) and left rotating at 30 °C. ^{1}H NMR (400 MHz, D_2O) was used to monitor the reaction.

DP400, 25 mM Reaction. NAM (14.0 µL, 0.1 mmol) was mixed with CTA (62 µg, 0.25 µmol), $FeCl_3$ (720 µg, 2.8 µmol), Glucose (72 mg, 0.4 mmol), GOx (80 µg, 1 x 10^{-8} mmol) and PBS (to make final volume 4 mL) in a vial with AscA (1.56 mg, 8.8 x 10^{-3} mmol) and left rotating at 30 °C. ^{1}H NMR (400 MHz, D_2O) was used to monitor the reaction.

Table S3. 5 Reagent parameters tailored to influence Fenton-GOx-RAFT polymerisations, including Glucose, GOx Fe and AscA. Monomers explored include DMA, HEA and NAM.

Entry	Monomer*	Reaction	Glucose (mmol)	GOx (mmol)	Fe (µmol)	AscA (µmol)
1	DMA	Original	0.4	$1x10^{-8}$	2.8	8.8
2	DMA	½ Glucose	0.2	$1x10^{-8}$	2.8	8.8
3	DMA	½ GOx	0.4	$0.5x10^{-8}$	2.8	8.8
4	DMA	½ Glucose and GOx	0.2	$0.5x10^{-8}$	2.8	8.8
5	DMA	½ Fe	0.4	$1x10^{-8}$	1.4	8.8
6	DMA	½ AscA	0.4	$1x10^{-8}$	2.8	4.4
7	DMA	½ Fe and AscA	0.4	$1x10^{-8}$	1.4	4.4
8	DMA	¼ Fe	0.4	$1x10^{-8}$	0.7	8.8
9	DMA	¼ AscA	0.4	$1x10^{-8}$	2.8	4.4
10	DMA	¼ Fe and AscA	0.4	$1x10^{-8}$	0.7	4.4
11	HEA	Original	0.4	$1x10^{-8}$	2.8	8.8
12	NAM	Original	0.4	$1x10^{-8}$	2.8	8.8
13	NAM (25 mM)	Original	0.4	$1x10^{-8}$	2.8	8.8
14	NAM (25 mM)	¼ Fe	0.4	$1x10^{-8}$	0.7	8.8

*Monomer concentration 100 mM unless otherwise stated. Original Reaction reagent ratio: Monomer: CTA: Glu: GOx: Fe: AscA = 400: 1: 400: 1 x 10^{-5} : 2.8 : 8.8.

^{1}H NMR spectra of polymers with labelled structures

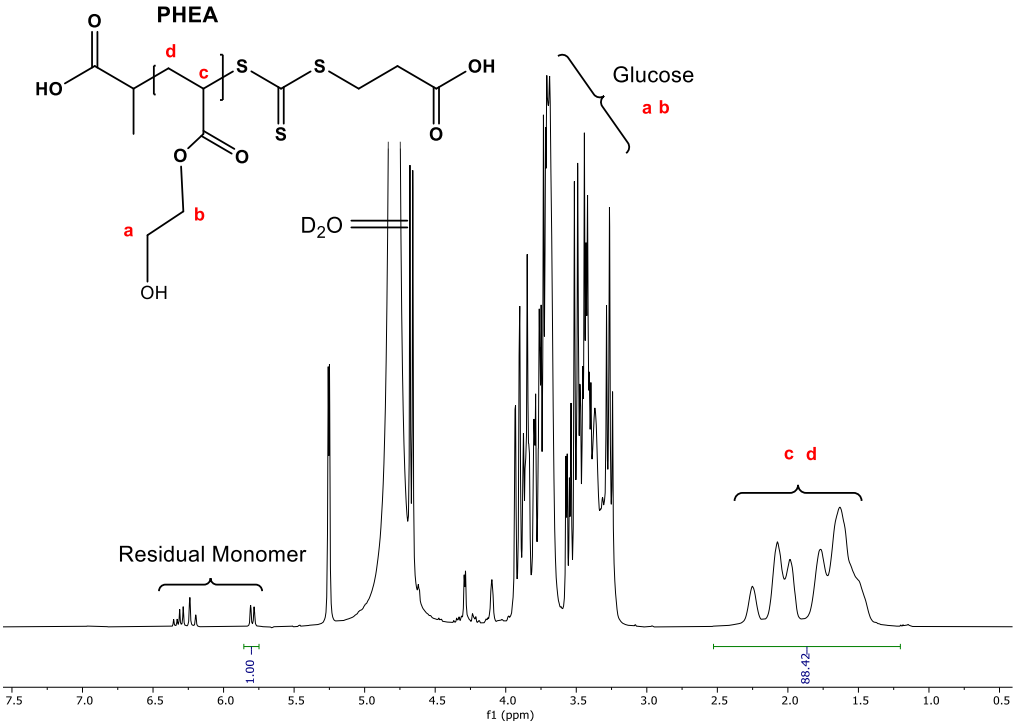

Figure S3. 7 ^{1}H NMR (400 MHz, D_2O) of P(NHEA) (100 mM) resulting from AscA initiated Fenton-GOx-RAFT polymerisation with Original Reaction reagent ratio: Monomer: CTA: Glu: GOx: Fe: AscA = 400: 1: 400: 1 x 10^{-5} : 2.8 : 8.8. (Table S3. 6, entry 11).

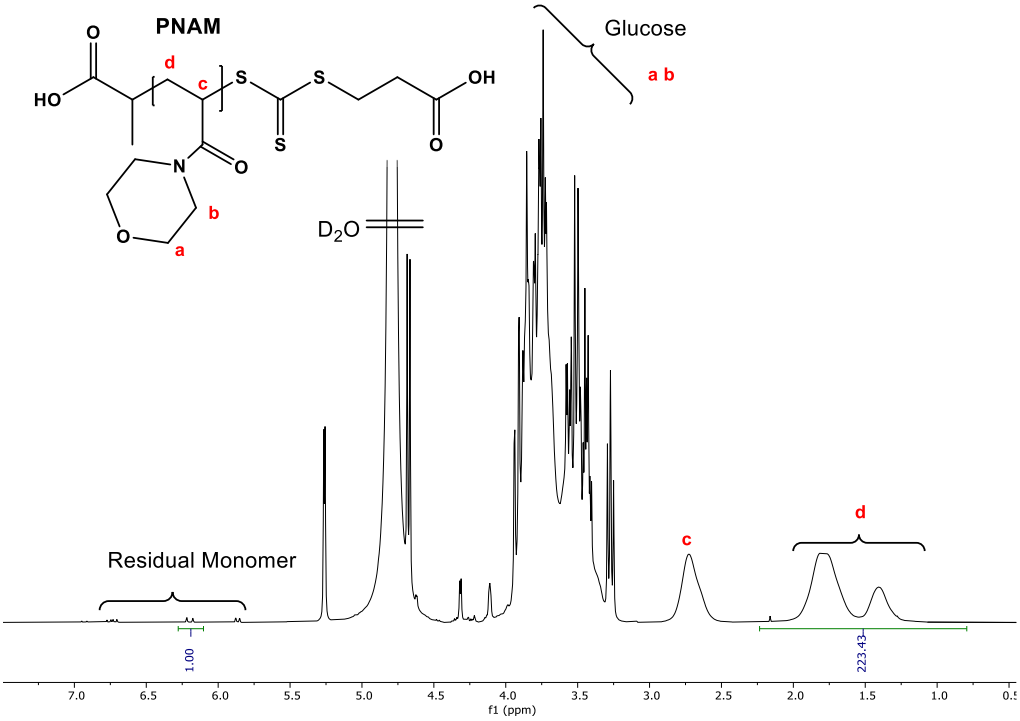

Figure S3. 8 ^{1}H NMR (400 MHz, D_2O) of P(NAM) (100 mM) resulting from AscA initiated Fenton-GOx-RAFT polymerisation with Original Reaction reagent ratio: Monomer: CTA: Glu: GOx: Fe: AscA = 400: 1: 400: 1 x 10^{-5} : 2.8 : 8.8. (Table S3. 7 entry 12).

3.1.10 Bacteria Assisted FG-RAFT Live/Dead Study

Bacteria Preparation

C. met was grown in 5 mL LB media for 18 hours. Solutions of 20 mL LB media were adjusted to OD_{600nm} = 0.1 and grown overnight at 30 °C shaking, to OD_{600nm} ~1. In preparation for the polymerisation the cultures were centrifuged (6000 rpm, 10 minutes) and the pellets washed twice with PBS (10 mL) via centrifugation. Each of the washed pellets were re-suspended in 4 mL PBS. 1 mL (3.4 x 10^{10} CFU ml^{-1}) was added to the FG-RAFT reaction mixture (1 mL) to give a total *C. met* count of ~3.4 x 10^{10} in the 2 mL volume, or 1.7 x 10^{10} CFU mL^{-1} (per mL).

Live and dead bacterial cultures

Live/Dead bacterial cultures were prepared as above. Live cultures were stored on ice until used in polymerisation. Dead bacterial cultures were heat treated (killed) by incubating at 70 °C for 20 minutes.

Table S3. 8 Colony forming units (CFU) in the 1 mL culture added at the beginning of each FG – RAFT polymerisation of DMA (DP200). Reagent ratios: DMA: CTA: Glu: GOx: Fe = 200: 1: 800: 2 x 10^{-3} : 5.4

Culture	Heat Treated	CFU (mL^{-1}) (n=3)
Live	No	$1.7x10^{10}$
Dead	Yes	368

Polymerisation Procedure

DP200 (25 mM) targeted. DMA (5.2 µL, 0.05 mmol), CTA (62 µg, 0.25 µmol), $FeCl_3$ (360 µg, 1.33 µmol), GOx (40 µg, 5 x 10^{-7} mmol), Glucose (36 mg, 0.2 mmol) were added to a vial with bacteria (1 mL). PBS was

added to make the final volume 2 mL and left rotating at 30 °C overnight. ^{1}H NMR (400 MHz, D_2O) was used to monitor the reaction.

Controls. Controls were carried out using the above method i) with bacteria but no $FeCl_3.6H_2O$ (Figure S3.10, top), and ii) without any bacteria (Figure S3.10, bottom).

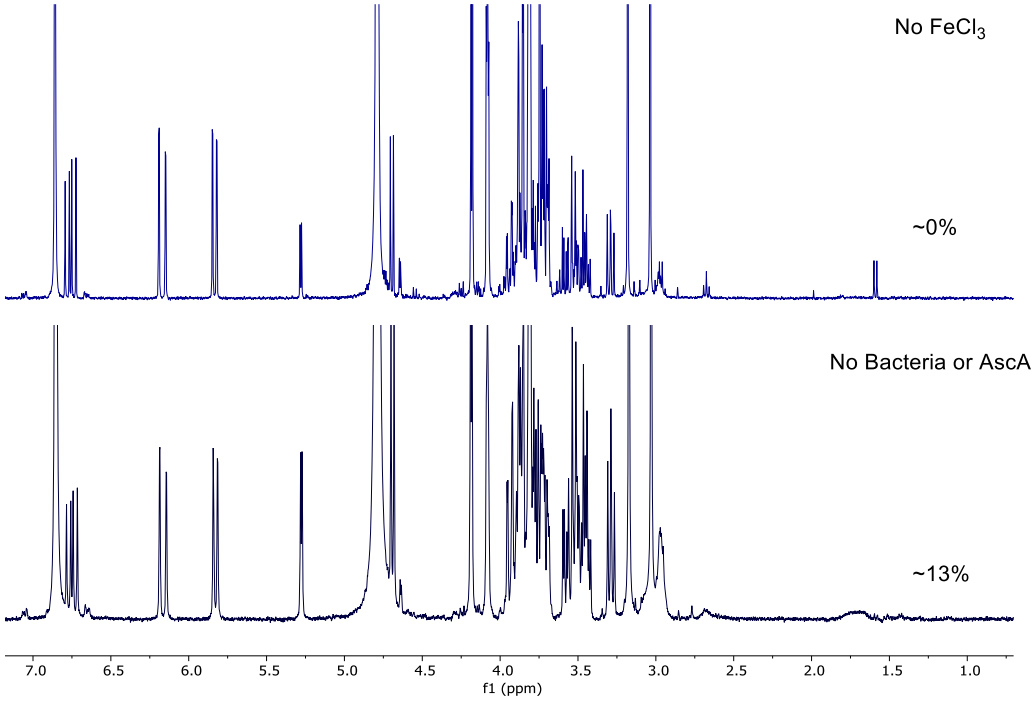

Figure S3. 9 ^{1}H NMR (400 MHz, D_2O) Time 24 hours after bacterial initiated FG-RAFT of DMA with control experiments: Top; without any Fe source, Bottom; without any bacteria. Reagent ratios: DMA: CTA: Glu: GOx: Fe = 200: 1: 800: 2 x 10^{-3} : 5.4.

3.1.11 Bacterial Driven FG-RAFT Polymerisation Scaled Up

Bacteria Preparation

C. met was grown in 5 mL LB media for 18 hours. Solutions of 20 mL LB media were adjusted to OD_{600nm} = 0.1 and grown overnight at 30 °C shaking, to OD_{600nm} ~1. In preparation for the polymerisation the cultures were centrifuged (6000 rpm, 10 minutes) and the pellets washed twice with PBS (10 mL) via centrifugation. Each of the washed pellets was re-suspended in 2 mL PBS. 1 mL was used in each FG-RAFT polymerisation to make approximately ~1.7 x 10^{10} CFU mL^{-1} *C. met*.

DP400 targeted. *Monomer/CTA stock mixture (Table S3.8), $FeCl_3$ (720 µg, 2.8 µmol), Glucose (72 mg, 0.4 mmol), GOx (80 µg, 1 x 10^{-8} mmol) and bacteria (1 mL) (to make final volume 4 mL) were added to a vial and left rotating at 30 °C overnight. ^{1}H NMR (400 MHz, D_2O) was used to monitor the reaction.

Table S3. 9 Details of Scaled up bacterial initiated FG-RAFT polymerisations. Monomer and chain transfer agent (CTA) stock solution details are listed according to final monomer concentrations required in the polymerisation. Reagent ratios: Monomer: CTA: Glu: GOx: Fe: = 400: 1: 400: 1 x 10^{-5} : 2.8.

Monomer	Final conc. (mM)	Monomer Quantity	CTA quantity
DMA	100	41.12 µL, 0.4 mmol	248 µg, 1 µmol
HEA	100	46.4 L, 0.4 mmol	248 µg, 1 µmol
NAM	100	56 µL, 0.4 mmol	248 µg, 1 µmol
NAM	25	14 µL, 0.1 mmol	62 ug, 0.25 µmol

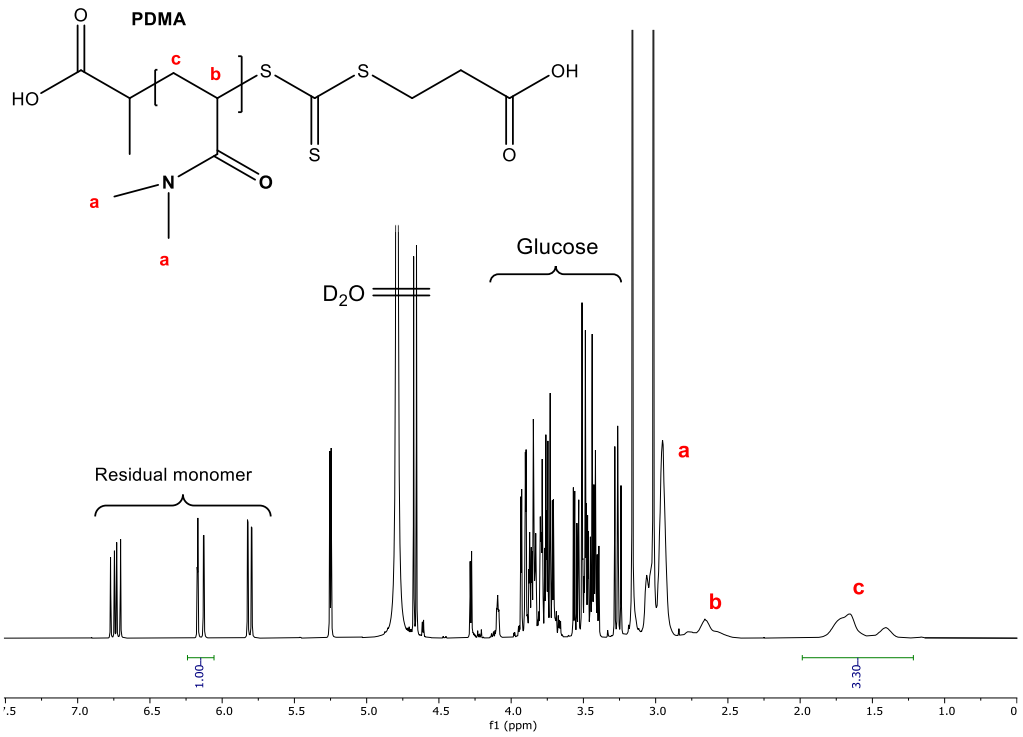

Figure S3. 10 ^{1}H NMR (400 MHz D_2O) spectra for b-FG-RAFT polymerisation of DMA (100 mM) with reagent ratios: Monomer: CTA: Glu: GOx: Fe = 400: 1: 400: 1 x 10^{-5} : 2.8.

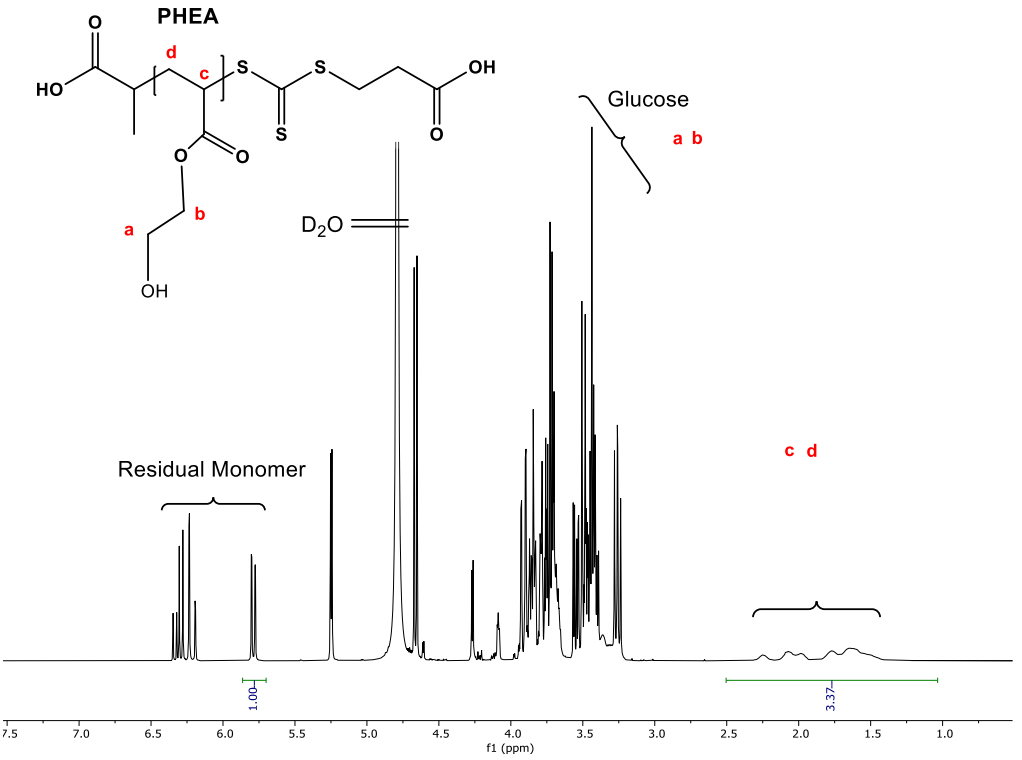

Figure S3. 11 ^{1}H NMR (400 MHz D_2O) spectra for b-FG-RAFT polymerisation of NHEA (100 mM) with reagent ratios: Monomer: CTA: Glu: GOx: Fe = 400: 1: 400: 1 x 10^{-5} : 2.8.

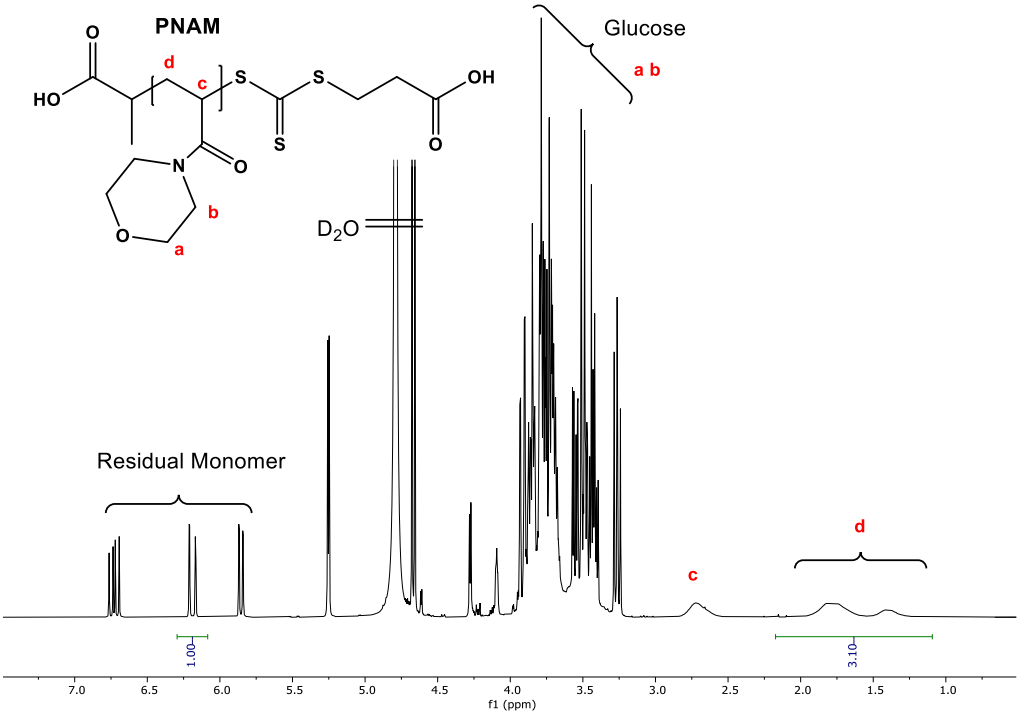

Figure S3. 12 ^{1}H NMR (400 MHz D_2O) spectra for b-FG-RAFT polymerisation of NAM (25 mM) with reagent ratios: Monomer: CTA: Glu: GOx: Fe = 400: 1: 400: 1 x 10^{-5} : 2.8.

References

1. N. Schuergers, C. Werlang, C. M. Ajo-Franklin and A. A. Boghossian, *Energy Environ Sci*, 2017, **10**, 1102-1115.
2. A. M. Duraj-Thatte, N. D. Courchesne, P. Praveschotinunt, J. Rutledge, Y. Lee, J. M. Karp and N. S. Joshi, *Adv. Mater.*, 2019, **31**, e1901826.
3. C. A. Custodio, R. L. Reis and J. F. Mano, *Adv Healthc Mater*, 2014, **3**, 797-810.
4. E. Andriukonis, A. Stirke, A. Garbaras, L. Mikoliunaite, A. Ramanaviciene, V. Remeikis, B. Thornton and A. Ramanavicius, *Colloids Surf B Biointerfaces*, 2018, **164**, 224-231.
5. J. Niu, D. J. Lunn, A. Pusuluri, J. I. Yoo, M. A. O'Malley, S. Mitragotri, H. T. Soh and C. J. Hawker, *Nat Chem*, 2017, **9**, 537-545.
6. A. Ramanavicius, E. Andriukonis, A. Stirke, L. Mikoliunaite, Z. Balevicius and A. Ramanaviciene, *Enzyme Microb. Technol.*, 2016, **83**, 40-47.
7. H. G. Sherman, J. M. Hicks, A. Jain, J. J. Titman, C. Alexander, S. Stolnik and F. J. Rawson, *Chembiochem*, 2019, **20**, 1008-1013.
8. M. D. Nothling, H. Cao, T. G. McKenzie, D. M. Hocking, R. A. Strugnell and G. G. Qiao, *J. Am. Chem. Soc.*, 2020, DOI: 10.1021/jacs.0c10673.
9. M. R. Bennett, P. Gurnani, P. J. Hill, C. Alexander and F. J. Rawson, *Angew. Chem. Int. Ed. Engl.*, 2020, **59**, 4750-4755.

10. M. Dietrich, M. Glassner, T. Gruendling, C. Schmid, J. Falkenhagen and C. Barner-Kowollik, *Polymer Chemistry*, 2010, **1**, 634-644.
11. K. Matyjaszewski, *Macromolecules*, 2020, **53**, 495-497.
12. L. Martin, G. Gody and S. Perrier, *Polymer Chemistry*, 2015, **6**, 4875-4886.
13. P. A. J. M. De Jongh, A. Mortiboy, G. S. Sulley, M. R. Bennett, A. Anastasaki, P. Wilson, D. M. Haddleton and K. Kempe, *ACS Macro Letters*, 2016, **5**, 321-325.
14. A. Reyhani, T. G. McKenzie, Q. Fu and G. G. Qiao, *Aust. J. Chem.*, 2019, **72**, 479-489.
15. C. Bray, G. Li, A. Postma, L. T. Strover, J. Wang and G. Moad, *Aust. J. Chem.*, 2021, **74**, 56-64.
16. J. Yeow, S. Shanmugam, N. Corrigan, R. P. Kuchel, J. Xu and C. Boyer, *Macromolecules*, 2016, **49**, 7277-7285.
17. C. A. Figg, J. D. Hickman, G. M. Scheutz, S. Shanmugam, R. N. Carmean, B. S. Tucker, C. Boyer and B. S. Sumerlin, *Macromolecules*, 2018, **51**, 1370-1376.
18. L. D. Blackman, K. E. B. Doncom, M. I. Gibson and R. K. O'Reilly, *Polym Chem*, 2017, **8**, 2860-2871.
19. C. L. McCormick and A. B. Lowe, *Acc. Chem. Res.*, 2004, **37**, 312-325.
20. X. Wang, S. Chen, D. Wu, Q. Wu, Q. Wei, B. He, Q. Lu and Q. Wang, *Adv. Mater.*, 2018, **30**, e1705668.
21. R. Chapman, A. J. Gormley, K.-L. Herpoldt and M. M. Stevens, *Macromolecules*, 2014, **47**, 8541-8547.
22. F. Oytun, M. U. Kahveci and Y. Yagci, *J. Polym. Sci., Part A: Polym. Chem.*, 2013, **51**, 1685-1689.
23. A. E. Enciso, L. Fu, A. J. Russell and K. Matyjaszewski, *Angew. Chem. Int. Ed. Engl.*, 2018, **57**, 933-936.
24. A. E. Enciso, L. Fu, S. Lathwal, M. Olszewski, Z. Wang, S. R. Das, A. J. Russell and K. Matyjaszewski, *Angew. Chem. Int. Ed. Engl.*, 2018, **57**, 16157-16161.
25. J. Yeow, R. Chapman, A. J. Gormley and C. Boyer, *Chem. Soc. Rev.*, 2018, **47**, 4357-4387.
26. Y. Lv, Z. Liu, A. Zhu and Z. An, *J. Polym. Sci., Part A: Polym. Chem.*, 2017, **55**, 164-174.
27. D. K. Schneiderman, J. M. Ting, A. A. Purchel, R. Miranda, M. V. Tirrell, T. M. Reineke and S. J. Rowan, *ACS Macro Letters*, 2018, **7**, 406-411.
28. A. Reyhani, H. Ranji-Burachaloo, T. G. McKenzie, Q. Fu and G. G. Qiao, *Macromolecules*, 2019, **52**, 3278-3287.
29. R. Chapman, A. J. Gormley, M. H. Stenzel and M. M. Stevens, *Angew. Chem. Int. Ed. Engl.*, 2016, **55**, 4500-4503.
30. J. Tan, X. Dai, Y. Zhang, L. Yu, H. Sun and L. Zhang, *ACS Macro Letters*, 2019, **8**, 205-212.
31. A. Reyhani, T. G. McKenzie, Q. Fu and G. G. Qiao, *Macromol. Rapid Commun.*, 2019, **40**, e1900220.
32. A. Reyhani, T. G. McKenzie, H. Ranji-Burachaloo, Q. Fu and G. G. Qiao, *Chemistry*, 2017, **23**, 7221-7226.

33. L. M. Johnson, B. D. Fairbanks, K. S. Anseth and C. N. Bowman, *Biomacromolecules*, 2009, **10**, 3114-3121.
34. P. S. Hume, C. N. Bowman and K. S. Anseth, *Biomaterials*, 2011, **32**, 6204-6212.
35. B. J. Berron, A. M. May, Z. Zheng, V. Balasubramaniam and C. N. Bowman, *Lab Chip*, 2012, **12**, 708-710.
36. L. C. Recco, I. Tokarev, S. Minko and V. A. Pedrosa, *Chemistry*, 2014, **20**, 1226-1230.
37. A. Reyhani, S. Allison‐Logan, H. Ranji‐Burachaloo, T. G. McKenzie, G. Bryant and G. G. Qiao, *J. Polym. Sci., Part A: Polym. Chem.*, 2019, **57**, 1922-1930.
38. A. Reyhani, M. D. Nothling, H. Ranji-Burachaloo, T. G. McKenzie, Q. Fu, S. Tan, G. Bryant and G. G. Qiao, *Angew. Chem. Int. Ed. Engl.*, 2018, **57**, 10288-10292.
39. P. R. Kommoju, Z. W. Chen, R. C. Bruckner, F. S. Mathews and M. S. Jorns, *Biochemistry*, 2011, **50**, 5521-5534.
40. B. Zhang, X. Wang, A. Zhu, K. Ma, Y. Lv, X. Wang and Z. An, *Macromolecules*, 2015, **48**, 7792-7802.
41. J. Tan, Q. Xu, X. Li, J. He, Y. Zhang, X. Dai, L. Yu, R. Zeng and L. Zhang, *Macromol. Rapid Commun.*, 2018, **39**, e1700871.
42. F. Martinello and E. L. da Silva, *Clin. Biochem.*, 2006, **39**, 396-403.
43. J. S. Lee, Y. Chang, E. S. Lee, H. G. Song, P. S. Chang and J. Han, *J. Food Sci.*, 2018, **83**, 682-688.
44. J. C. Deutsch, *Anal. Biochem.*, 1998, **255**, 1-7.
45. M. D. Nothling, T. G. McKenzie, A. Reyhani and G. G. Qiao, *Macromol. Rapid Commun.*, 2018, **39**, e1800179.
46. P. J. Janssen, R. Van Houdt, H. Moors, P. Monsieurs, N. Morin, A. Michaux, M. A. Benotmane, N. Leys, T. Vallaeys, A. Lapidus, S. Monchy, C. Medigue, S. Taghavi, S. McCorkle, J. Dunn, D. van der Lelie and M. Mergeay, *PLoS One*, 2010, **5**, e10433.
47. M. Bystrzanowska, P. Petkov and M. Tobiszewski, *ACS Sustainable Chemistry & Engineering*, 2019, **7**, 18434-18443.
48. P. Anastas and N. Eghbali, *Chem. Soc. Rev.*, 2010, **39**, 301-312.
49. W.-F. Su, in *Principles of Polymer Design and Synthesis*, Springer Berlin Heidelberg, Berlin, Heidelberg, 2013, DOI: 10.1007/978-3-642-38730-2_7, ch. Chapter 7, pp. 137-183.

Chapter 4. Up-Regulation of Cytochrome-C Protein, NapC, in *E. coli*

Abstract

Iron (Fe) reduction and related cellular metabolic processes are essential to biological activity.[1, 2] Fe reduction by bacteria is facilitated by extracellular electron transfer (EET) and control or modulation of EET may be used not only to influence bacterial activity but might also be exploited in biosynthetic technologies or biosensors.[3-5] The periplasmic cytochrome C protein, NapC in *Escherichia coli (E. coli),* plays a role in cellular Fe reduction or metabolism and is explored in these studies. Three plasmid constructs were created with different promoters to upregulate NapC protein generation in *E. coli*. Of these, the plasmids with arabinose inducible P_{BAD} promoters were able to upregulate NapC protein upon arabinose induction at total arabinose concentrations of 0.0018% and 0.18%. These clones (*E. coli*$_{(IP\_0.0018\%)}$ and *E. coli*$_{(IP\_0.18\%)}$,

respectively) were used in Fe atom transfer radical polymerisation (ATRP), revealing faster polymerisation rates than cultures containing suppressed or empty plasmids (*E. coli*$_{(IP\_S)}$ and *E. coli*$_{(E)}$, respectively). Electrochemical studies were carried out to further probe the Fe reduction capabilities of the clones, but a complete set of results were not obtained due to lab closures following COVID-19. The preliminary results lead to the hypothesis that EET mechanisms are up regulated in times of environmental stress, but more work is necessary to fully conclude this observation.

Introduction

Microbial electrochemistry concerns the investigation of interactions between microorganisms and electrodes.[6] Microbial technologies utilise electroactive microorganisms possessing extracellular electron transfer (EET) capabilities for applications such as bioenergy, biosensing or biocomputing.[3, 7-9] However, limitations such as poor energy output and expensive materials restrict scalability and industrial uses surrounding these applications.[8] The study of the electron transport chain in bacteria is therefore important, particularly for microbial fuel cells (MFC)s,[10-13] biosensors,[7, 11, 14-17] electrobiosynthesis[18-20] and bioremediation technologies,[21-24] as discussed in Chapter 1. Various research groups have explored methods to improve the efficiency of EET and to increase the understanding of the biological pathways involved, such as, anodic

materials development,[25-32] bacterial membrane manipulation,[33, 34] and genetic engineering techniques,[3, 35, 36] but only for a limited selection of bacteria types, and much still remains to be discovered.

The previous chapters of this thesis focussed on harnessing microbial EET to convert an inactive catalyst to an active form and drive a synthetic polymerisation. It was shown that electrogenic *Cupriavidus metallidurans (C. met),*[37-40] and model microbe *Escherichia coli (E. coli)* were able to initiate Iron (Fe) Atom Transfer Radical Polymerisation (ATRP) reactions and *C. met* could also drive Fenton Glucose Oxidase - Reversible Deactivation Chain-transfer (FG-RAFT) polymerisations. It was hypothesised that the metal reduction took place via microbial EET involving membrane bound C type Cytochrome (C-Cyt) proteins, possibly in combination with synergistic Fe homeostasis efflux pumps.[39] To further understand the role of microbial EET in Fe catalysis, a particular C-Cyt (NapC of *E. coli*) was investigated in this chapter.

C-Cyts are enzymes that contribute to bacterial EET for the production of energy, particularly involving the reduction of metals.[41-44] They also exist in the mitochondria of eukaryotic cells where they play a significant part in apoptosis,[45-48] making them useful for cancer therapies and understanding the underlying biological redox mechanisms.[16, 49-52] The study in less complex organisms (i.e. bacteria) may later shed light on such oncological mechanisms. C-Cyts of the NapC/NirT family exist in the periplasmic membrane of Gram-negative bacteria and are responsible for transferring electrons from the quinone pool to periplasmic oxidoreductases.[53, 54] The electron transport chain of *S.*

oneidensis MR1 contain well researched C-Cyts, able to contribute to metal reduction,[18, 55] with protein CymA showing particular value.[56] Indeed, when *cymA* encoding genes were upregulated in *Shewanella* MR1,[57] or inserted into the genome of *E. coli,*[43, 58] an increase in Fe^{3+} reduction was observed, indicating that the CymA enzyme is integral to the reduction of metals.

NapC is also a member of the NapC/NirT family of C-Cyts, existing in the periplasmic membrane of *E. coli*.[53] NapC showed ferric reductase activity like its homologue, CymA, with the ability to substitute for CymA when inserted into *Shewanella* strains.[58] *E.coli* K12 top 10 is often used in microbiology laboratory studies due to its low pathogenicity, hardiness, and susceptibility to keeping cloned plasmids.[59] *E. coli* are less well known for metal reduction than other types of bacteria, but given the success previously shown with Cu catalysts for ATRP,[60] and Fe catalysts in the second chapter of this thesis,[5] it was sought to explore its EET chain further.

Electrochemical methods such as cyclic voltammetry (CV) and linear sweep voltammetry (LSV) have been used to investigate intracellular and extracellular electron transfer systems in yeast.[61, 62] Recently, Sherman *et al* advanced the application of such methods to examine EET by trans plasma electron transport systems (tPMET)s in cancer cells.[52, 63] LSV was used to shed light on these mechanisms by observing cell assisted Fe reduction by direct electron transfer via cytochrome DcytB and by shuttling mechanisms through tPMETS. By probing the Fe reduction capabilities of NapC (encoded by *E. coli*), a better understanding of

periplasmic proteins in EET chains might be realised and further translated to other bacteria types or mammalian cells. Increasing Fe reduction capabilities could also help to improve bacterial assisted Fe ATRP or FG-RAFT methods towards MFCs or biosensor applications.

Investigations were carried out in this chapter to determine whether the upregulation of the NapC protein in *E. coli* could increase the metal reduction efficiency of the bacteria. These investigations aimed to shed light on Fe reduction pathways, particularly relating to bacterial-initiated polymerisation experiments in chapters 2 and 3 of this thesis. It was sought to probe the role and limitations of NapC in the EET pathway of the bacteria.

Plasmids were constructed in *E. coli* strains containing *napC* with different promoters and high copy number replicon *colE1*. The constitutive (always active) promoter from *Clostridium sporogenes* ferredoxin (P_{fdx}) was shown to be detrimental to the host,[64] resulting in loss of plasmid, cell death, or incomplete transcription. The cloning of *napC* into plasmids containing the weaker native *napC* promoter (P_{Nat}) or arabinose-inducible promoter (P_{BAD}) were shown by DNA sequencing to be achieved successfully. Constructs based on P_{BAD} were able to regulate the quantity of NapC protein expressed by changing the concentration of arabinose inducer. When applied to Fe ATRP reactions these clones were able to activate the polymerisation with slightly elevated reaction rates. Studies using LSV were carried out to further probe the effect of NapC upregulation on bacterial Fe reduction. Unfortunately, the interruption of lab experiments due to the COVID-19

pandemic prevented conclusive results but the continuation of LSV studies in the future will enable a progression of understanding into the role of NapC towards EET and Fe regulation.

Results and Discussion

4.1.1 Cloning of napC into pMTL83153; Ferredoxin Promoter

Plasmids are circular pieces of DNA that exist naturally in bacteria and can be edited and inserted into strains to control desired functions.[65] Restriction enzymes can be used in this process to cut pieces of DNA at specific sites (restriction sites), whilst the enzyme ligase joins matching ends of DNA strands together. This method of cloning was used to insert *napC* into the plasmid pMTL83153, immediately downstream from the constitutive P_{fdx} promoter (Figure 4. 1, purple) which allows continual transcription of the associated gene, *napC.* In theory, this would lead to

high levels of the corresponding NapC protein and facilitate investigations into the effects of NapC on iron reduction.

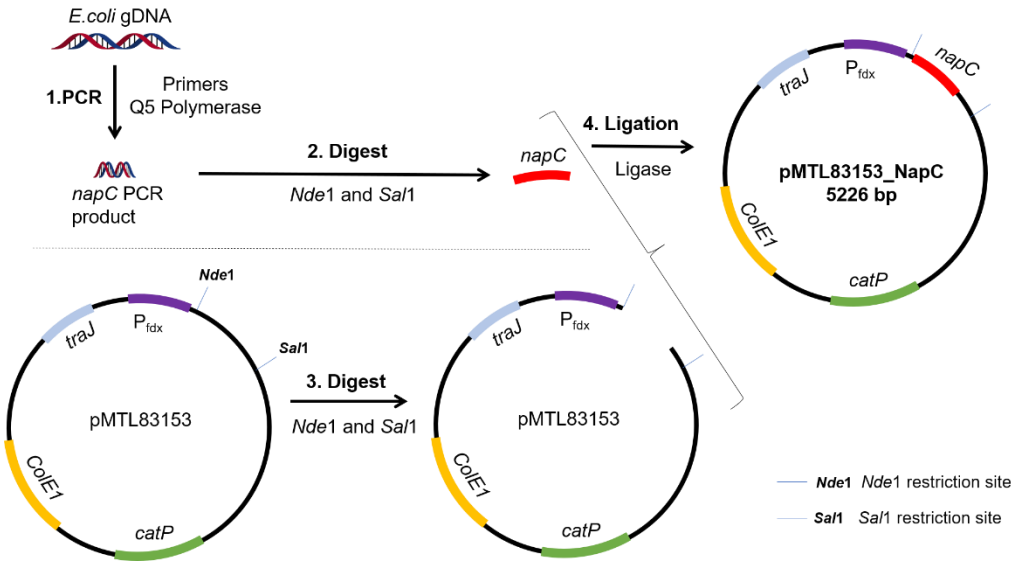

Figure 4. 1 Diagram to show the cloning process of *napC* gene into PMTL83153 plasmid. 1; PCR of *napC* gene region. 2; Digest of PCR product with restriction enzymes Nde1 and Sal1. 3; Digest of pMTL83153 with Nde1 and Sal1. 4; Ligation of digested *napC* region and digested pMTL83153.

The pMTL8000 modular plasmid collection was designed for ease of component selection during cloning and can be useful for tuning; plasmid replicons (controls replication efficiency), markers (antibiotic resistance selection), promoters (drives the transcription of the target gene), and multiple cloning sites (MCSs) (containing restriction sites (RS) for restriction enzyme (RE) cloning).[66] Although these were created to aid cloning in *Clostridium* cultures, they are hosted in *E. coli* and so were convenient in the cloning of *napC* into *E. coli*. The plasmid used, pMTL83153 (Figure 4. 1), contains a chloramphenicol acetyltransferase (*catP*) gene (Figure 4. 1, green), with resistance to chloramphenicol (Cm) antibiotics. This allows for the selection of colonies containing the plasmid, differentiating from those that may lose the plasmid and

therefore die. The gene, *colE1* (Figure 4. 1, yellow) is a Gram-negative replicon which allows the plasmid to replicate in *E. coli*.[67] The transfer (*traJ*) gene (Figure 4. 1, pale blue) activates bacterial conjugation for plasmid DNA transfer.

Firstly, the *napC* gene in *E. coli* was identified using the NCIB (Gene ID: 946706) and Kegg databases, and DNA genomic extraction was carried out to purify the DNA. Polymerase Chain Reaction (PCR) was used to amplify the *napC* section of DNA from *E. coli* with forward and reverse primers containing RSs, *Nde*I and *Sal*I respectively. The amplified DNA and the plasmid pMTL83153 vector (isolated using plasmid prep and purification) were digested with *Nde*I and *Sal*I REs, and gel electrophoresis analysis (Figure 4. 2) revealed expected bands, corresponding to *napC* DNA digest (~ 603 bps) and plasmid digest (~ 4620 bps).

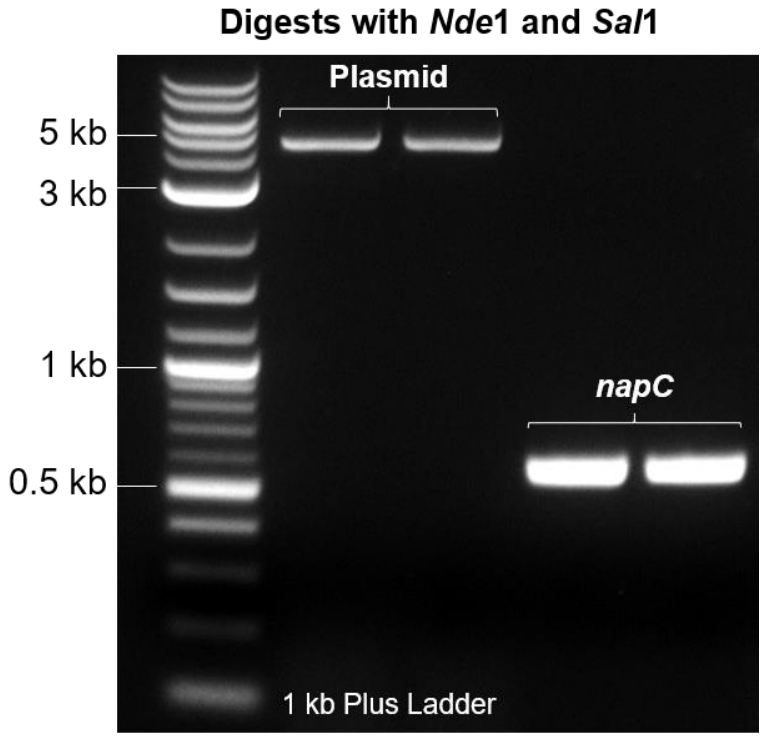

Figure 4. 2 Gel electrophoresis of components digested with *Nde*I and *Sal*I enzymes, against 1kb plus NEB ladder. Left; pMTL83151 (expected ~ 4620 bps), and Right; *napC* DNA (expected 603 bps).

Ligation was carried out using T4 DNA ligase enzyme, joining the compatible cohesive ends of the *napC* amplicon into the plasmid vector. After this, a transformation took place to insert the complete plasmid into *E. coli* chemically competent cells. The bacteria were then grown on agar plates (with Cm selection), but very few colonies were able to grow, suggesting significant loss of plasmid, poor cell growth or cell death from stress due to excess NapC protein.[64, 68] After several cloning attempts, few colonies were obtained, screened using colony PCR with primers (ColE1+tra_F2 and pCB102_R1) and Gel electrophoresis was used to identify whether *napC* insertion was successful (Figure 4. 3). Only one colony showed to have the correct band size (~1.3 kb), but after sequencing the clone was not found to be correct (Figure 4. 4). The lack of colonies suggests that *napC* is toxic in this construct, possibly due to its constant overproduction by a strong promoter.[64, 68] A new strategy was therefore necessary, where i) the promoter was not as strong, or ii) NapC expression could be controlled.

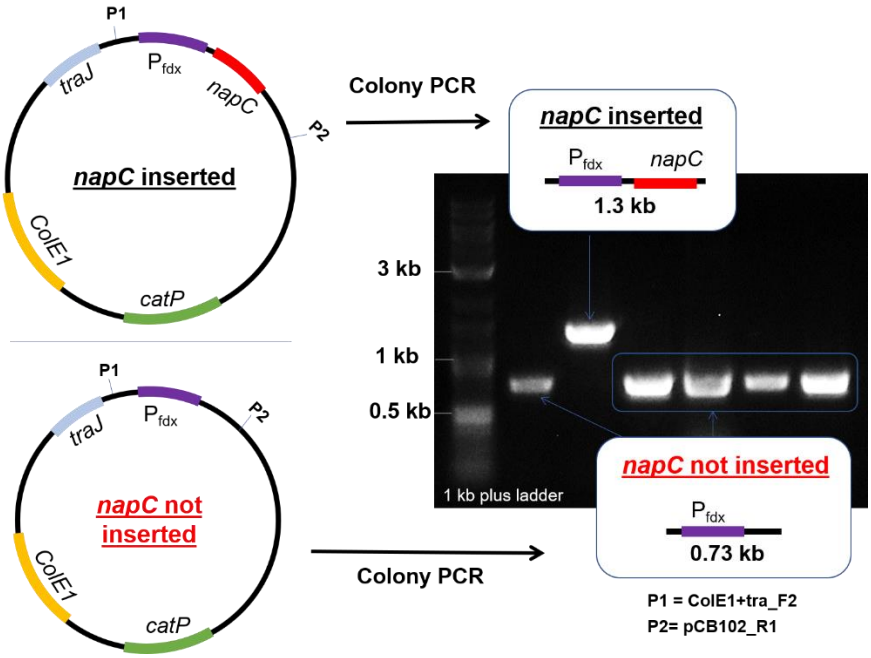

Figure 4. 3 Colony PCR (Primers: ColE1+tra_F2 and pCB102_R1) process to determine the success of *napC* insertion into a vector containing P_{fdx}. Gel electrophoresis showing vector products of different colonies, with one band the correct size.

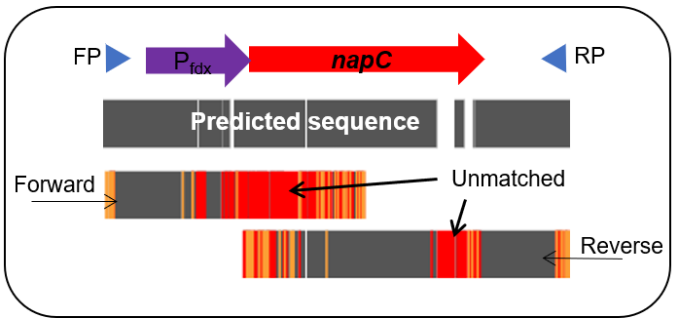

Figure 4. 4 Sanger sequencing diagram showing mismatched parts of the DNA sequence.

4.1.2 Cloning using a Native Promoter and an Inducible Promoter

The binding of RNA polymerase and transcription factors of a target gene is controlled by the promoter, influencing the amount of protein expressed. Due to the difficulties that arose with the strong

constitutive P_{fdx} promoter, cloning using i) the native promoter for *napC* (P_{Nat}), and ii) a non-constitutive inducible promoter (P_{BAD}), were carried out. The native promoter is weaker than P_{fdx} and therefore should cause less toxicity, but still be effective at overexpressing the NapC protein. Similarly, the P_{BAD} promoter activity can be regulated by the concentration of inducer (arabinose) added and therefore any toxicity to excess transcribed protein (NapC) can be controlled. Three different components of DNA make up both vectors and so NEBuilder® HiFi DNA Assembly was used over conventional ligation methods as it is advantageous for cloning multiple fragments of DNA efficiently whilst avoiding cloning errors.

Native promoter vector design

The NEBuilder® online tool was used to design the vector containing the native promoter for *napC* which was identified using BPROM promoter predictor. Forward and reverse primers were designed (NEBuilder®) and PCR was carried out to extract and amplify i) the native promoter region and ii) the *napC* region from the gDNA of *E. coli*. The regions of DNA were purified, and correct band sizes were confirmed using Gel Electrophoresis (Figure S4. 1). The PMTL83153 plasmid was then digested using *Not*1 and *Sal*1, removing the P_{fdx} section (Figure 4.5), and sizes verified using gel electrophoresis (Figure S4. 2). Hifi ligation Assembly was then carried out to obtain the completed vector which was transformed (heat shock) into chemically competent cells. After this, the bacteria were grown on agar plates (with Cm selection).

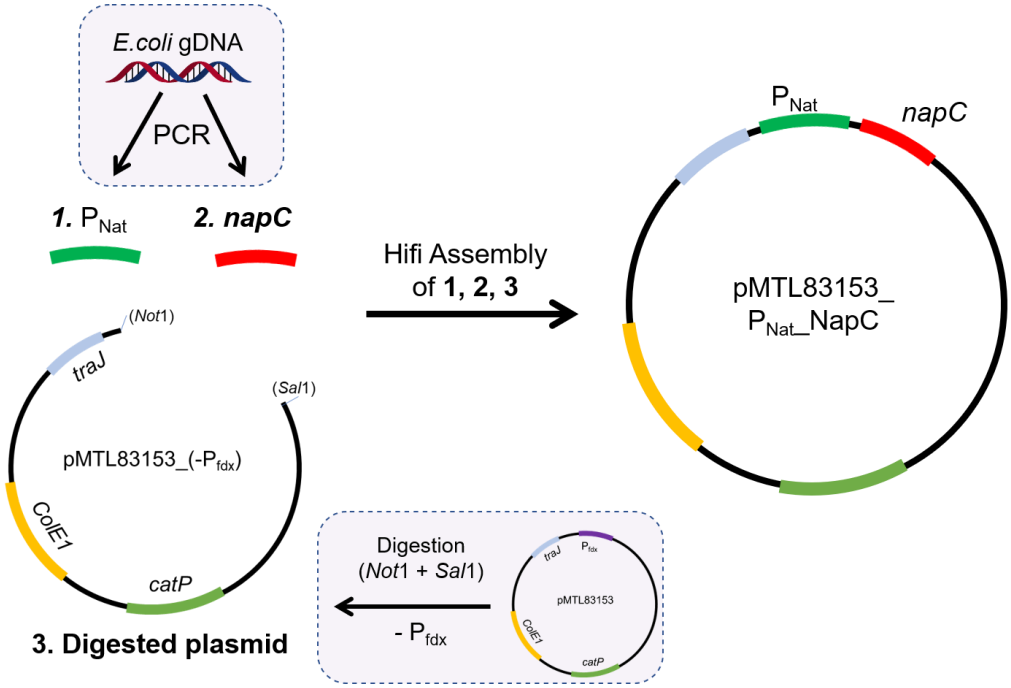

Figure 4. 5 Assembly of Native Promoter Vector containing P_{Nat} for NapC overexpression. PCR of *E. coli* gDNA was carried out with specific primers to extract 1, P_{Nat} region and 2, *napC* region of DNA. Plasmid pMTL83153 was digested with REs Not1 and Sal1 to remove the P_{fdx} promoter, resulting in region 3, digested plasmid. The three regions were ligated using Hifi Assembly to create to completed vector.

Inducible promoter vector Design

NEBuilder® online tool was also used to design the vector containing P_{BAD}. It was necessary to extract and amplify the promoter (P_{BAD}) region from a plasmid (pMTL71101_P_{BAD}_araC) using PCR (Figure 4. 6). The DNA region also contained *araC* which represses P_{BAD} *activity* in the absence of the arabinose inducer. PCR was also used to amplify and extract the *napC DNA* region of *E. coli* gDNA (Figure 4. 6). After purification, gel electrophoresis confirmed the expected band sizes of the PCR products (Figure S4. 1). The PMTL83153 plasmid was digested with REs (*Not*1 and *Sal*1) sizes verified using gel electrophoresis (Figure S4. 2). Hifi ligation Assembly was carried out to

obtain the completed vector which was transformed (Heat shock) into chemically competent cells. After this, the bacteria were grown on agar plates (with Cm selection).

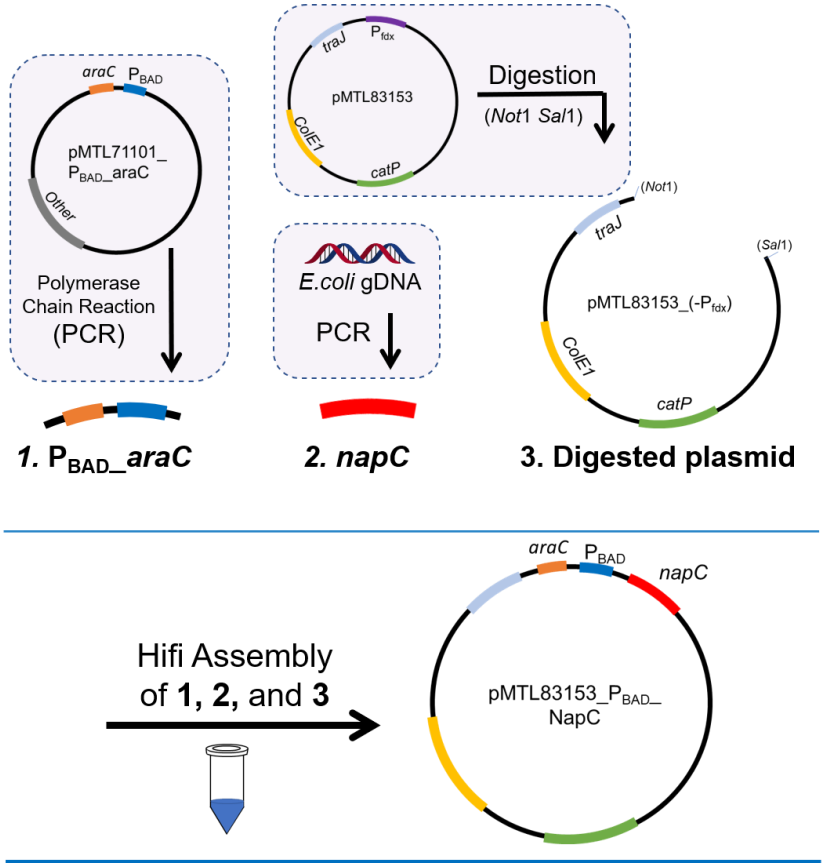

Figure 4. 6 Assembly of Inducible Promoter Vector containing promoter P_{BAD} for NapC overexpression and control. PCR was carried out with specific primers to extract and amplify regions 1, P_{BAD}_araC and 2, *napC*. Region 1 was obtained from the plasmid pMTL71101_P_{BAD}_araC and region 2 was obtained from *E. coli* gDNA. The plasmid pMTL83153 was digested with REs Not1 and Sal1 to remove the P_{fdx} promoter, resulting in region 3, digested plasmid. The three regions were ligated together with Hifi Assembly to create to the completed vector.

Colony PCR and Sequencing

The transformation of the cloned vectors led to the growth of colonies that were selected on Cm plates for Colony PCR (Primers: ColE1+tra_F2 and pCB102_R1). Gel electrophoresis was used to inspect the purified PCR products (Figure S4. 3) and determine the success of the Hifi assemblies. Sequencing of colonies containing the Native promoter vector (*E. coli*$_{(NP)}$) (expected ~1207 bps) and colonies containing the Inducible promoter vector (*E. coli*$_{(IP)}$) (expected ~ 2340 bps) were as anticipated. The sequencing revealed the successful insertion of *napC* into both vectors (Figure 4. 7).

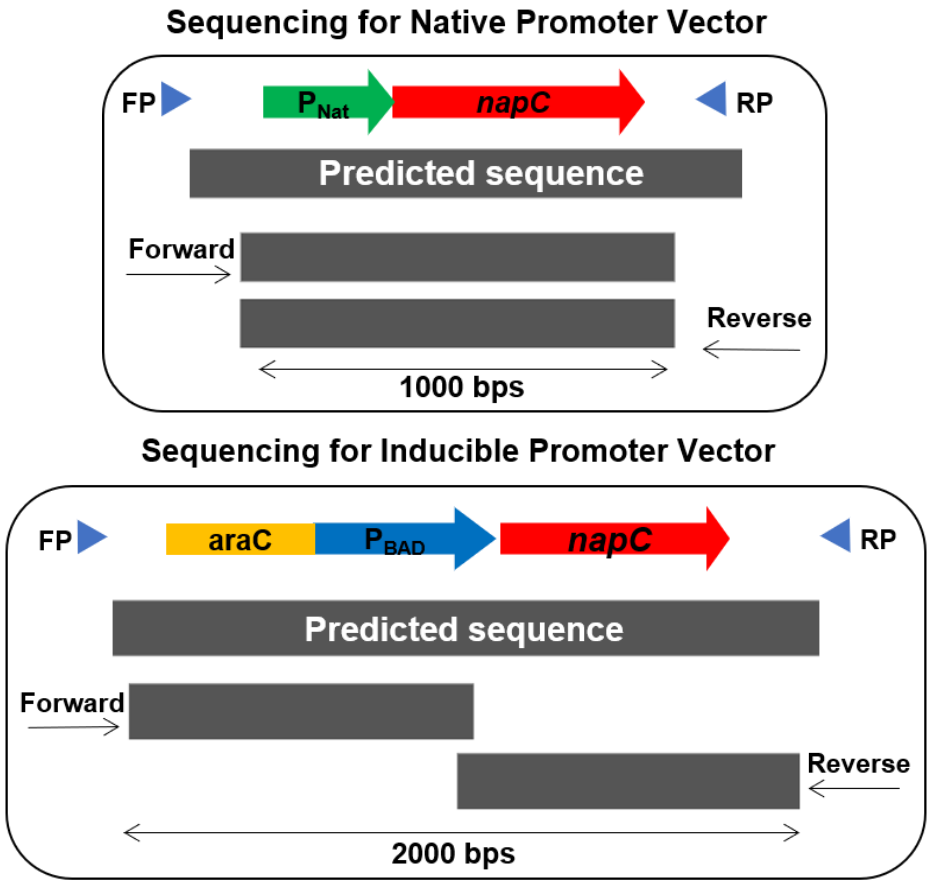

Figure 4. 7 Sanger sequencing diagrams for Native promoter Vector (Top) and Inducible promoter vector (Bottom). Both showing matching DNA regions of sequencing with forward and reverse primers compared to a model sequence.

4.1.3 NapC Protein Expression Analysis

Given the successful HiFi cloning of the *napC* gene into the vectors containing native and inducible promoters, it was necessary to examine the resulting NapC protein expression in *E. coli* cultures containing the vectors. Protein expression of bacteria containing each vector was studied alongside clones harbouring a control plasmid, pMTL83151, referred to as the 'Empty Plasmid' (*E. coli*$_{(E)}$) (without *napC* but containing Cm resistance) which would show typical background NapC expression without the overexpression vectors. High quantities of NapC expression were desired for further studies into NapC Fe reduction, but too much protein would cause toxic effects to the bacteria. Bacteria containing the Native Promoter Vector (*E. coli*$_{(NP)}$) are likely to continuously produce NapC, whereas, NapC expression in bacteria containing the Inducible promoter Vector (*E. coli*$_{(IP)}$) must be 'switched on' by the presence of inducer, arabinose, which binds to *araC* activating the P_{BAD} promoter and initiating P_{BAD} transcription of the desired protein. This expression can be tuned by arabinose concentration and so *E. coli*$_{(IP)}$ was induced with different arabinose quantities to examine the effect on NapC protein content.

E. coli$_{(IP)}$ were exposed to a final arabinose concentration of; 0% (band I_0), 0.000018% (band I_1), 0.0018% (band I_2), and 0.18% (band I_3). As a control measure, arabinose was also added to *E. coli*$_{(E)}$ (band E) and *E. coli*$_{(NP)}$ (band N), permitting a consistent comparison between protein expression levels. Toxicity studies were also carried out to ensure that the metabolism of the bacteria was not negatively affected by the

arabinose (Figure S4. 4). After arabinose induction, cell lysates were prepared using protease Inhibitor, which helps to preserve the function and stability of metal dependant proteins. Total protein quantification was carried out using bicinchoninic acid (BCA) protein assay, with Bovine serum Albumin (BSA) standard curve (Figure S4. 5) to determine total protein concentration in each sample (Table S4. 13).

The total protein concentration was standardised for each sample and SDS-PAGE Gel Electrophoresis was used to analyse each sample (loading 23 µg protein). SDS PAGE is governed by the assumption that the relative mobility of proteins complexed to SDS is dependent on the molecular weight (Mr) of that protein. However, in reality, not all proteins have identical mass/charge ratio or the same shape when complexed to SDS, meaning that the relative mobility of the same size proteins can differ.[69] A certain band of interest (Figure 4. 8, circled green area) was identified in the resulting protein gel. Although the band was calculated by protein migration analysis (Figure S4. 6) to be higher (~34 kDa) than the expected molecular weight for NapC (~24 kDa),[53] it is likely to be the correct protein from the observed increase in intensity of bands for higher arabinose inductions (I_2 and I_3), and due to its low intensity in bands not induced (I_0) or *E. coli*$_{(E)}$ (Band E).

The intensity of this band for *E. coli*$_{(NP)}$ cultures is similar to *E. coli*$_{(E)}$, suggesting that P_{Nat} is not particularly effective at overexpressing NapC. The promoter (P_{Nat}) chosen was upstream of *napB* and could potentially be part of an operon, which is a cluster of genes controlled by the same promoter. Gene organization within an operon can affect expression and

may explain the lack of overexpression.[70] Other explanations could be due to gene alteration responses by the bacteria, causing down regulation of other pathways to compensate for the NapC increase (e.g. down regulation of the NapC expression on the chromosomal DNA).

The intensity of bands I_0 and I_1 show similar intensities but increase for I_2 and I_3 suggesting that a certain amount of arabinose induction (0.0018%) is necessary for P_{BAD} to actively promote NapC overexpression. Increasing this further (0.18%) only increases the intensity slightly indicating a limit of expression.

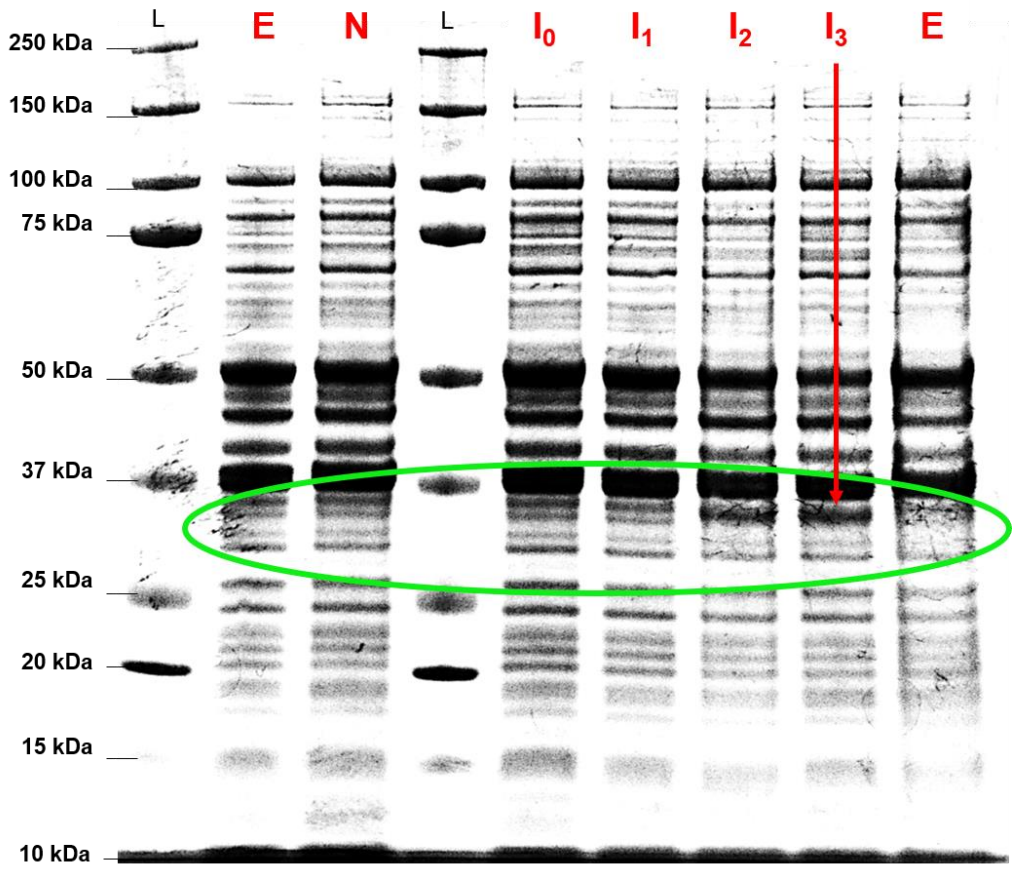

Figure 4. 8 SDS PAGE Gel for lysates of bacteria containing empty plasmid (E), Native promoter vector (N), and Inducible promoter vector with 0% (I_0), 0.000018% (I_1), 0.0018% (I_2) and 0.18% (I_3) total arabinose concentration induction. Protein Gel against Precision Plus Protein™ Kaleidoscope ladder (L).

4.1.4 Applications of Inducible Promoter Vector

4.1.4.1 Fe ATRP Initiated by *E. coli* Clones

In the previous section, the upregulation of NapC was shown to be achieved using the inducible promoter vector in *E. coli*. In this section, the use of the *E. coli* clones harbouring this vector were explored towards an increased Fe reduction capability. As shown in Chapter 2, Fe ATRP can be activated by bacteria including *E. coli*. To investigate the effects of NapC upregulation on Fe reduction rates, *E. coli*$_{(IP)}$ were used in Fe ATRP reactions alongside *E. coli*$_{(E)}$. Cultures of *E. coli*$_{(IP)}$ were either i) suppressed by addition of glucose *E. coli*$_{(IP\_S)}$, ii) activated by 0.0018% total arabinose concentration *E. coli*$_{(IP\_0.0018\%)}$, or ii) activated by 0.18% total arabinose concentration *E. coli*$_{(IP\_0.18\%)}$. These arabinose concentrations were chosen as they produced the highest NapC protein overexpression according to SDS PAGE analysis shown previously. *E. coli*$_{(IP\_S)}$ was suppressed by glucose addition to inhibit P_{BAD} activation of NapC expression.[71] As glucose is a reducing agent, the bacterial suspension were centrifuged and the supernatant was discarded to remove glucose before the pellet was resuspended in PBS for Fe ATRP reactions. Similarly, centrifugation was also used to remove arabinose from the arabinose induced *E. coli*$_{(IP)}$ cultures prior to polymerisations.

The kinetics of each reaction were monitored by ^{1}H NMR and the resulting polymers were analysed by SEC (Figure 4. 9, Table 4. 1). A small increase in the rate of polymerisation was observed by the larger polymer yield for *E. coli*$_{(IP\_0.0018\%)}$ and *E. coli*$_{(IP\_0.18\%)}$ activated reactions, compared to those activated by *E. coli*$_{(E)}$ or *E. coli*$_{(IP\_S)}$ cultures. This

suggested that the upregulation of the NapC protein could have had some effect on the rates of Fe^{3+} reduction to Fe^{2+}. As this difference is small, repeats should be carried out to determine the rate of error before a conclusion can be draw. Other rate limiting steps are likely to effect the EET rate from the bacteria to the Fe catalyst; these might include (electron transfer) ET across the periplasm via other cascade proteins in the electron transport chain, or EET between shuttle molecules and the Fe catalyst (Figure 4. 10).

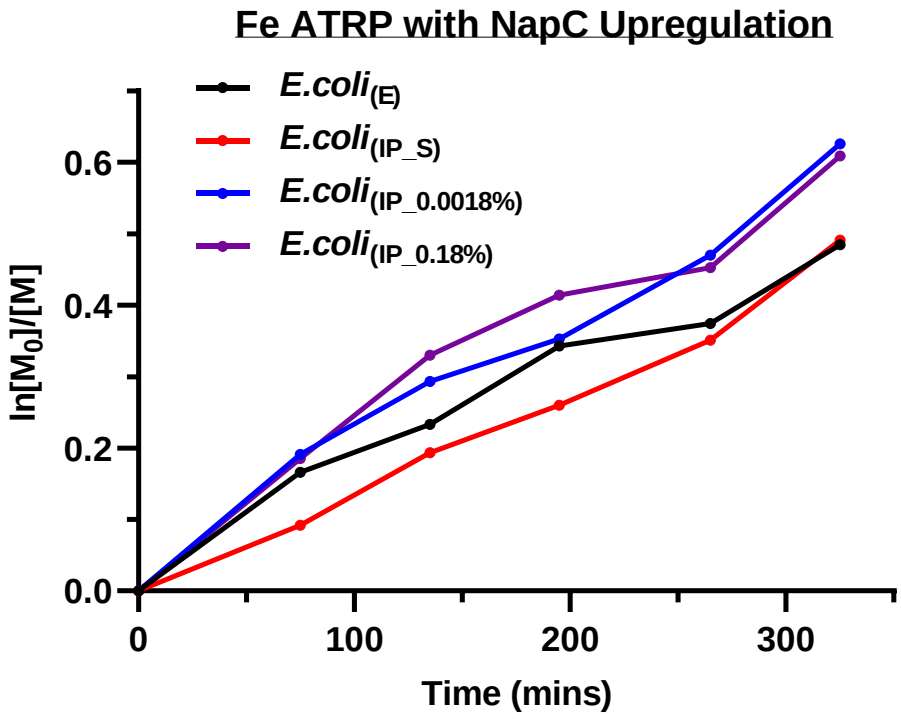

Figure 4. 9 ^{1}H NMR kinetics of Fe ATRP activated by *E. coli* harbouring empty plasmids, *E. coli*$_{(E)}$ (black), or inducible promoter plasmids, *E. coli*$_{(IP)}$ either i) suppressed by addition of glucose *E. coli*$_{(IP\_S)}$ (red), ii) activated by 0.0018% total arabinose concentration *E. coli*$_{(IP\_0.0018\%)}$ (blue) or ii) activated by 0.18% total arabinose concentration *E. coli*$_{(IP\_0.18\%)}$ (purple).

Table 4. 1 Displaying the results of Fe ATRP polymerisations of PEGMA activated by *E. coli* cultures harbouring different plasmids to compare the effects of NapC protein upregulation.

Culture	Conv.[a]	M_n^{th} (kDa)[b]	M_n^{SEC} (kDa)[c]	$Đ$[c]
E. coli$_{(E)}$	38.4%	23.3	251.9	3.0
E. coli$_{(IP\_S)}$	38.8%	23.5	237.4	2.9
E. coli$_{(IP\_0.0018\%)}$	46.5%	28.1	228.0	2.7
E. coli$_{(IP\_0.18\%)}$	45.6%	27.6	230.0	3.0

[a] Estimated from ^{1}H NMR monomer: polymer integrals. [b] M_n^{th} = (300 * 200* conversion) + 211 Da. [c] From SEC (THF).

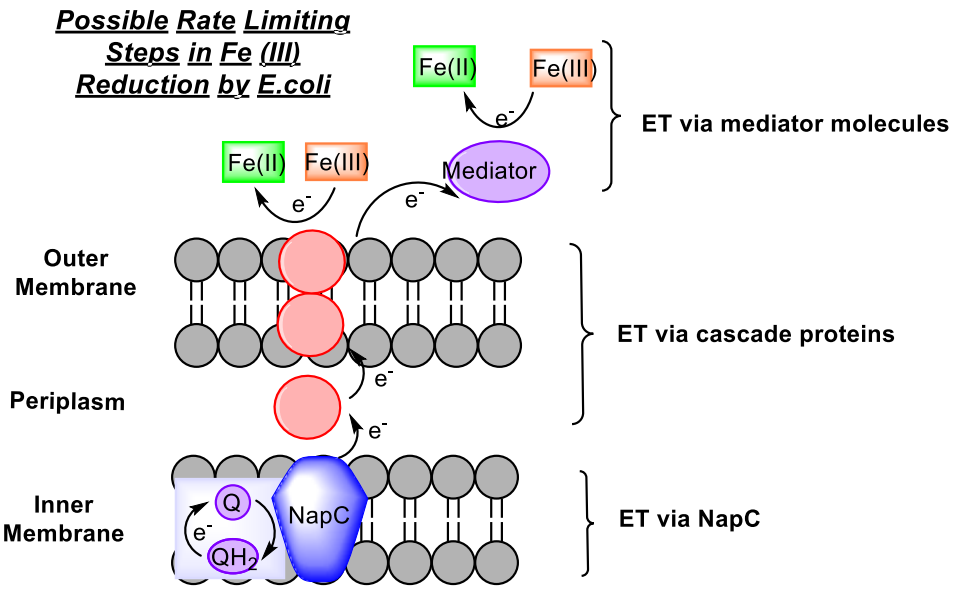

Figure 4. 10 Possible Rate limiting steps in Fe(III) reduction including electron transfer (ET) via NapC, ET via cascade proteins and ET via mediator molecules.

The SEC results show that initiator efficiency is extremely poor, likely due to the loss of initiator species as discussed in chapter 2. The dispersity of the resulting polymers is also rather broad, again indicating inefficient halogen exchange from the catalyst to growing polymer chains. There was little difference between the Fe ATRP reaction rates

catalysed by *E. coli*$_{(IP\_0.0018\%)}$ (46.5% conversion) and *E. coli*$_{(IP\_0.18\%)}$ (45.6% conversion) (Table 4. 1). In light of the factors that could contribute to Fe reduction and the rate of Fe ATRP, other techniques were necessary to evaluate the effectiveness of Fe reduction by the *E. coli*$_{(IP)}$ clones.

4.1.4.2 Electrochemical Methods to Probe Fe Reduction by Clones

Electrochemical methods such as LSV can be used to observe oxidation and reduction reactions by sweeping through a voltage and measuring the current of an electrochemical system (see methodology (section 4.6) for detailed description). LSV is a sensitive technique that has been used previously to detect concentration changes corresponding to EET in cells.[52, 61, 62] During LSV, a potential is applied in one direction and the current is measured. The resulting voltammogram of current against potential enables the determination of reducing or oxidising species. During this process, the concentration of reduced or oxidised species can be determined by the steady state current values (I_{ss}). As mentioned in the methodology section, the Randles-Sevcik equation shows that the concentration of analyte is directly proportional to the I_{ss}, meaning that the concentration of redox species in a solution can be monitored by LSV.

Calibration Graph

To analyse the Fe reduction capabilities of *E. coli*$_{(IP)}$ clones, a calibration graph was first created. The Ferricyanide and ferrocyanide redox couple was used in this experiment due to its well-known redox profile and for ease of comparison to similar Fe reduction studies by Sherman *et al*.[52] A three electrode system including a carbon fibre microelectrode (33 µM) was used in the following experiments, resulting in linear sweep voltammograms which could be used to probe Fe concentrations (Figure 4. 11).

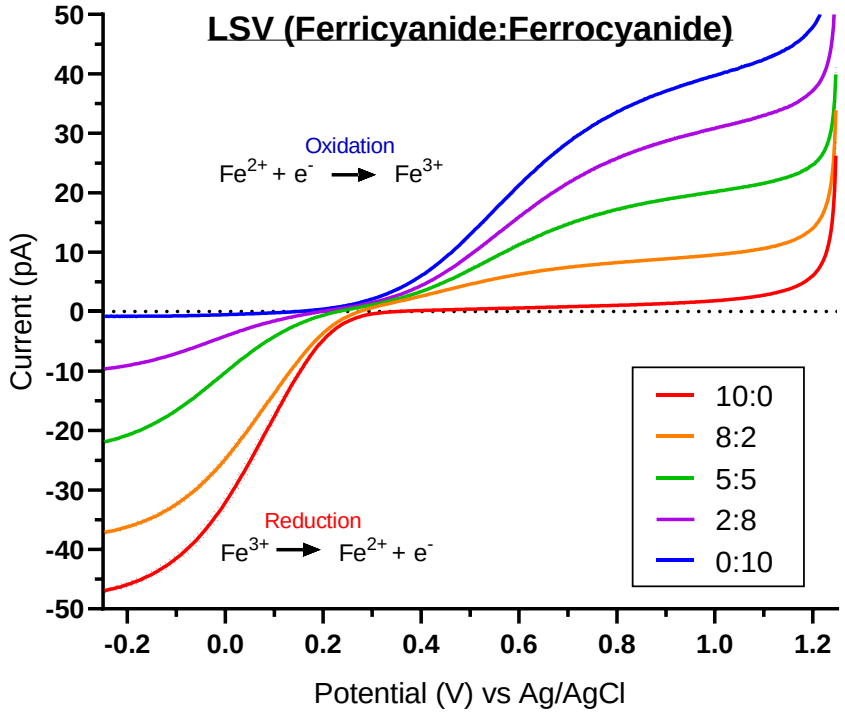

Figure 4. 11 Linear sweep voltammogram of Current Vs Potential curried out using 3 electrode system with carbon fibre micro-disk electrode (33 µm), Ag/AgCl reference electrode and Pt counter electrode in 1X PBS electrolyte. Scans were carried out at 100 mV/s from 1.25 V to -0.25 V. 1 mM potassium ferricyanide and ferrocyanide were made in PBS (1X) and mixed in ratios (10:0, 8:2, 5:5, 2:8, 0:10) and voltammograms observed (n=3, error = SD) for each sample, where electrode was polished between each scan.

The negative (reduction) current corresponds to the presence of ferricyanide (Fe^{3+}) in the sample whilst the positive (oxidation) current

corresponds to ferrocyanide (Fe^{2+}) in the sample. Changing the concentration ratios of ferricyanide to ferrocyanide from 10:0 to 0:10 caused a decrease in negative current and an increase in positive current. To more accurately determine the steady state reduction $I_{ss,red,}$ and steady state oxidation $I_{ss,ox}$ peaks, the first derivative function can be applied to the graph to extract the rate of change ($d(I_{ss})/dt$) (Figure 4. 12). A calibration graph was created by plotting the $d(I_{ss})/dt$ peak values against ferricyanide or ferrocyanide concentrations (Figure 4. 13). The lines of best fit could then be compared to first derivative values of LSV graphs for samples reduced by bacterial clones to provide the corresponding Fe concentrations.

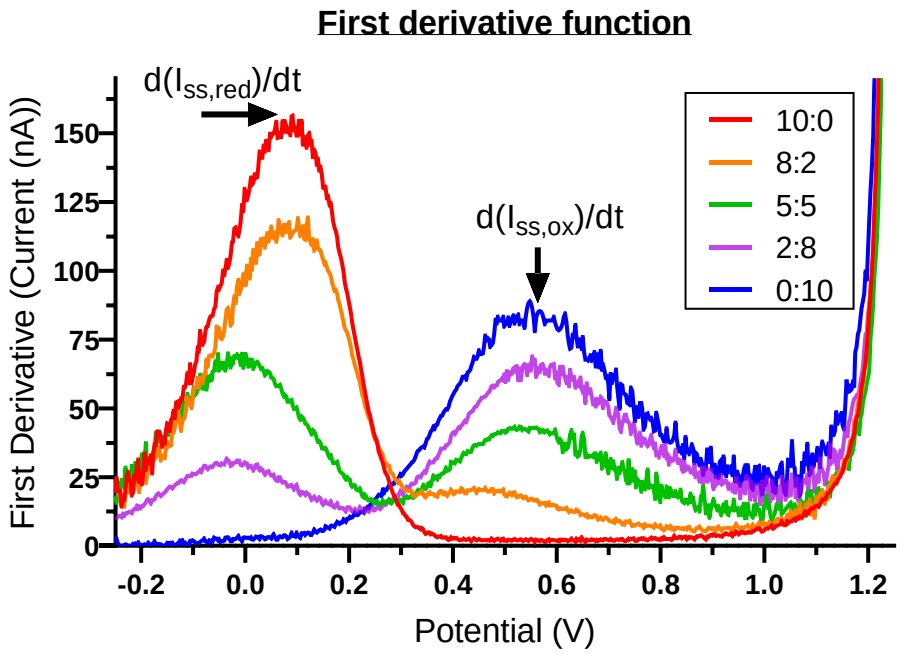

Figure 4. 12 First derivative function applied to Linear sweep voltammogram from Figure 4.10 to determine $d(I_{ss})/dt$ values. Fe^{3+} reduction peaks occur < 0 V and Fe^{2+} oxidation peaks occur > 0 V (Using GraphPad prism).

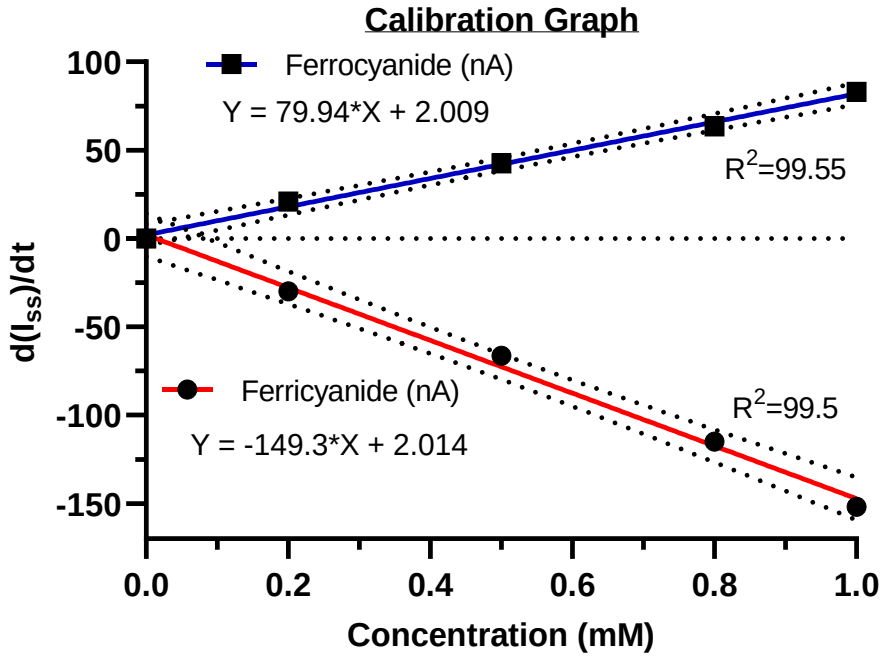

Figure 4. 13 First derivative peaks from graphs in figures 4.10 and 4.11 against Ferricyanide or ferrocyanide concentration with line of best fit and 95% confidence bands (Using GraphPad prism).

Electrochemical determination of Fe^{3+} reduction

Experiments were carried out to determine whether *E. coli*$_{(IP)}$ clones with upregulated NapC protein could reduce more Fe^{3+} in the form of ferricyanide. The previous sections showed that *E. coli*$_{(IP\_0.0018\%)}$ and *E. coli*$_{(IP\_0.18\%)}$ upregulated NapC expression and slightly increased the rate of ATRP reactions compared to suppressed cultures or those containing an empty plasmid. Samples of *E. coli*; *E. coli*$_{(E)}$, *E. coli*$_{(IP\_S)}$, *E. coli*$_{(IP\_0.0018\%)}$, and *E. coli*$_{(IP\_0.18\%)}$ were incubated with ferricyanide (1 mM) for 1 hour at 37 °C, after which the bacteria were removed by centrifugation and the supernatant was taken. Three aliquots of each supernatant sample were scanned (n=3) using LSV and the working electrode was polished between scans. The average current was taken

for each sample and the first derivative graph was plotted to determine $d(I_{ss})/dt$ values. The whole experiment was repeated with new biological samples (N=2). These experiments were carried out before the COVID-19 pandemic so unfortunately a third biological repeat was not possible and therefore statistical tests cannot be carried out, however the results obtained can be analysed as preliminary data sets. The $d(I_{ss})/dt$ values of each sample were compared to the calibration graph and the concentration of Fe^{2+} in solution was plotted as a percentage of total Fe concentration (Figure 4. 14).

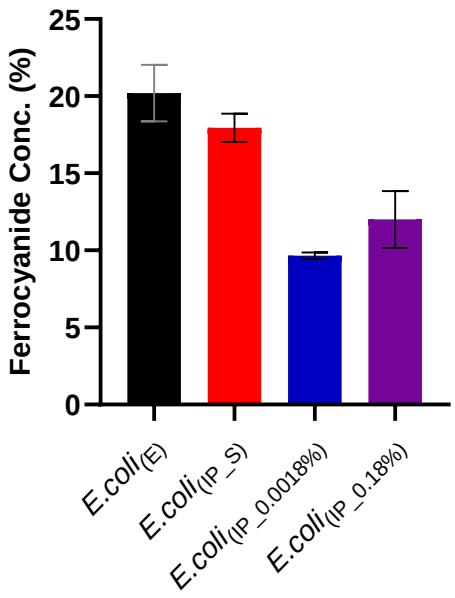

Figure 4. 14 Percentage concentrations of ferrocyanide detected in the supernatant of samples (starting concentration 1 mM ferricyanide) incubated for 1 hour with *E. coli*$_{(IP)}$ or *E. coli*$_{(E)}$. Prior to incubation with ferricyanide clones were either i) suppressed by addition of glucose *E. coli*$_{(IP\_S)}$ (red), ii) activated by 0.0018% total arabinose concentration *E.coli*$_{(IP\_0.0018\%)}$ (blue) or ii) activated by 0.18% total arabinose concentration *E. coli*$_{(IP\_0.18\%)}$ (purple). LSV was used to analyse the supernatant of incubated samples (N=2, n=6) and the first derivative function was applied to resulting voltammograms. The concentrations were determined using the calibration graph (Figure 4.12).

From the preliminary results shown above, it is indicated that *E. coli*$_{(E)}$ and *E. coli*$_{(IP\_S)}$ cultures reduced more ferricyanide to ferrocyanide than the clones that were induced with arabinose to overexpress NapC. This suggests that a shift in the bioenergetics of the bacteria may have been triggered in *E. coli*$_{(IP\_0.0018\%)}$ and *E. coli*$_{(IP\_0.18\%)}$ cultures, whereby EET reduction pathways were stunted due to the use of excess energy required for the over-production of the NapC protein. Interestingly, there was a slight increase in the ferricyanide reduction with *E. coli*$_{(IP\_0.18\%)}$ cultures compared to *E. coli*$_{(IP\_0.0018\%)}$ cultures. Previous MIC studies revealed that increasing total arabinose concentrations to 0.18% induced detrimental effects on the metabolism of *E. coli*$_{(IP)}$ (Figure S4. 4). The increased stress in *E. coli*$_{(IP\_0.18\%)}$ cultures may have triggered EET systems (such as NapC) resulting in an increase in ferricyanide reduction. Stress induced tPMET upregulation pathways were also observed in analogous experiments with cancer cells,[63] suggesting that cells utilise EET systems to balance bioenergetic requirements. Although the bioenergetics of Fe metabolism in living organisms remains challenging to study,[72] it might be possible to gain more insights through monitoring Fe reducing behaviour in stress induced environments, such as temperature, pH and chemical treatments.

Evaluation of preliminary findings

It would be expected that the cultures shown by LSV to reduce the highest percentage of ferricyanide to ferrocyanide (*E. coli*$_{(E)}$ or *E. coli*$_{(S)}$) would provide faster polymerisation kinetics in Fe ATRP experiments,

however this was not observed in polymerisation experiments with *E. coli* cultures. The behaviour observed could be attributed to use of ferricyanide in LSV experiments compared to $FeCl_3$/Me_6TREN complexes in ATRP reactions. As ferricyanide is extremely stable unless under acidic (pH <5.2) or extremely basic (pH~14) conditions,[73, 74] it is likely that the two different forms of Fe are reduced/captured by different pathways and in different quantities. $FeCl_3$/Me_6TREN complex is more susceptible to hydrolysis and capture by Fur proteins which regulate Fe homeostasis.[75]

Future LSV experiments with $FeCl_3$/Me_6TREN might provide further insight into these observations.

Secondly, the Fe ATRP polymerisations were carried out under anaerobic conditions whereas the *E. coli* cultures incubated with ferricyanide before LSV experiments were in the presence of air. The differences observed could be attributed to the regulation of bacterial metabolism under aerobic vs anaerobic conditions. These could be investigated by carrying out Fe reduction experiments with the clones under i) aerobic conditions and ii) anaerobic conditions. It is also important to reiterate that there are many components of the EET chain that might be rate limiting (Figure 4. 10) such as shuttle molecules, and investigations into these will contribute to the knowledge of EET pathways.

Conclusions

The cloning of *napC* gene into *E. coli* for subsequent overexpression of NapC protein was carried out to aid future investigations into the role of NapC in Fe reduction. Several promoters were applied to regulate *napC* expression, including P_{fdx}, P_{Nat} and P_{BAD}. Of these, P_{fdx} proved too strong, producing only a few colonies after translation into *E. coli* cells, and many deformities were observed upon sequencing. Vectors containing P_{Nat} and P_{BAD} were more successful, producing colonies after translation which showed correct construction by sequencing, confirming *napC* insertion into the vectors. NapC protein expression was then examined, revealing that *E. coli*$_{(NP)}$ clones were not effective at overexpressing the protein, whereas *E. coli*$_{(IP\_0.0018\%)}$ and *E. coli*$_{(IP\_0.18\%)}$ clones produced more intense NapC bands in SDS PAGE, revealing successful overexpression. P_{BAD} was the most effective promoter, allowing tailored expression of NapC and so *E. coli*$_{(IP)}$ clones were then used to catalyse Fe ATRP reactions. The polymerisation rates for ATRP catalysed by *E. coli*$_{(IP\_0.0018\%)}$ and *E. coli*$_{(IP\_0.0018\%)}$ were faster than those of *E. coli*$_{(IP\_0.0018\%)}$ and *E. coli*$_{(IP\_0.0018\%)}$, suggesting than NapC upregulation has some effect on the Fe^{3+} reduction system. However repeats should be carried out in order to confirm this observation.

To investigate these mechanisms in more depth LSV was employed, implicating the hypothesis that *E. coli*$_{(IP\_0.0018\%)}$ clones upregulate EET pathways in response to stress. However, more experiments must be carried out to validate the statistical significance of this observation. As

E. coli is simple to culture, recognizing proteins such as NapC as CymA homologues might contribute to understanding C-Cyts in many other bacteria, or even human cells.

Experimental and Supplementary

4.1.5 Materials

All chemicals were purchased from the supplier and used without further purification unless stated. Iron(II)chloride hydrate $FeCl_2.4H_2O$ and L-Arabinose were purchased from sigma Aldrich. Iron(III)chloride hexahydrate ($FeCl_3.6H_2O$) ≥98% was purchased from scientific laboratory supplies. Ascorbic acid (AscA) >99% was purchased from Alfa Aesar. For bacteria growth Lysogeny broth (LB) was used.

Kits used: GenElute™ Bacterial Genomic DNA Kit was purchased from Sigma-Aldrich. Monarch® Plasmid Miniprep Kit, Monarch® DNA Gel Extraction kit and Monarch® PCR & DNA Cleanup kit were purchased from New England Biolabs (NEB). Pierce™ BCA Protein Assay Kit was purchased from Thermo Fisher Scientific.

Table S4. 1 Medias and Buffers.

Medium/Buffer	Components	Quantity (g/l)
Lysogeny Broth (LB)*	Tryptone	10
	Yeast Extract	5
	Sodium Chloride	10
Phosphate Buffered Saline (PBS), pH 7.4	NaCl	8
	KCl	0.2
	Na_2HPO_4	1.44
	KH_2PO_4	0.24

*Agar plates were prepared using 1.5% w/v No. 1 Bacteriological Agar (Oxoid)

Antibiotics. Chloramphenicol (Cm) (25 mg/mL) stock solution was made up in 100% Ethanol solution where 2.5 µL was added for each 5 mL LB culture (62.5 µg) and 200 µL to each 200 mL agar.

napC oligonucleotide sequence

ATGGGAAATTCTGACCGTAAGCCTGGTCTGATTAAGCGCCTGTGGAAATGGTGGCGTACC
CCCAGCCGTCTGGCGCTGGGGACGCTGCTGTTGATCGGTTTTGTTGGCGGCATCGTCTTC
TGGGGTGGCTTTAACACCGGGATGGAAAAAGCCAATACCGAAGAGTTCTGCATTAGCTGC
CACGAAATGCGCAACACGGTGTATCAGGAATACATGGATTCCGTGCACTACAACAACCGTA
GCGGCGTCCGTGCGACCTGTCCGGATTGTCACGTTCCGCACGAGTTTGTGCCGAAGATGA
TACGCAAGCTCAAAGCAAGTAAAGAGCTGTATGGTAAAATTTTTGGCGTTATTGACACGCC
GCAGAAATTTGAAGCTCATCGTCTGACGATGGCACAGAATGAGTGGCGGCGCATGAAGGA
CAATAACTCGCAGGAGTGCCGTAACTGTCACAACTTCGAGTATATGGATACAACCGCCCAG
AAATCGGTTGCCGCGAAGATGCATGACCAGGCGGTGAAAGATGGGCAAACCTGTATTGAT
TGCCATAAAGGGATAGCGCACAAGCTGCCCGATATGCGTGAAGTCGAGCCAGGTTTTTAA

(Sourced using Kegg genome database for Escherichia coli K-12 MG1655: b2202, https://www.genome.jp/dbget-bin/www_bget?eco:b2202)

Table S4. 2 Bacteria and Plasmid Strains.

Strain/Plasmid	Description	Source/Reference
Escherichia coli wild type	Plasmid Storage Strain (K12 Top 10)	Invitrogen
PMTL_83153	Modular plasmid containing pCB102, catP, ColE1 + tra, P_{fdx}+ MCS	http://www.clostron.com/pMTL80000.php
PMTL_83151	Modular plasmid containing pCB102, catP, ColE1 + tra, MCS	http://www.clostron.com/pMTL80000.php

Table S4. 3 Oligonucleotide Primers used for PCR of DNA regions.

Primers	Sequence (5'-3')	Tm (°C)	Function
NapC_fwd_fdx	ATATATCATATGGGAAATTC TGACCGTAAG	61.7	To amplify *napC* in cloning with **P_{fdx} promoter**
NapC_rev_fdx	GAAGTCGAGCCAGGTTTTT AAGTCGACATATAT	62.1	To amplify *napC* in cloning with **P_{fdx} promoter**
NapC_fwd_hifi	GAGCGAAATCATGGGAAAT TCTGACCGTAAG	61.8	To amplify *napC* in cloning with **P_{BAD} and P_{Nat} promoter**
NapC_rev_hifi	ATCTCCATGGACGCGTGAC GTTAAAAACCTGGCTCGAC	59.3	To amplify *napC* in cloning with **P_{BAD} and P_{Nat} promoter**
115usNapB_fwd	CAGGAAACAGCTATGACCG CAACAAAGCCCGGTGCAGG	69.2	Amplify **P_{Nat} promoter**
115usNapB_rev	AATTTCCCATGATTTCGCTC CCGAACTCC	65.8	Amplify **P_{Nat} promoter**
P_{BAD}_araC-fwd	CAGGAAACAGCTATGACCG CTTATGACAACTTGACGGC	59.3	Amplify **P_{BAD} promoter**
P_{BAD}_araC_rev	AATTTCCCATTTTCTCCTCT TTAATCTAGAGAATTC	58.9	Amplify **P_{BAD} promoter**
ColE + *tra*_F2*	CCATCAAGAAGA GCGAC	56.7	**Colony PCR**
pCB102_R1*	GATAGTCAAAAGGCATAAC AG	55.4	**Colony PCR**

All Primers used for PCR with **Q5 ® Polymerase**. *Exceptions used for Colony PCR with **Green DreamTaq.**

4.1.6 Experimental

4.1.6.1 Microbiology

Storage and growth conditions of bacteria

Bacterial cultures were stored at - 80 °C on beads from Microbank™ Long term Bacterial storage system (Prolabs Diagnostics). For recovery of cultures, *E. coli* Top 10 wild type were grown from beads at 37°C overnight (18 hours) in LB (5 mL) with agitation. *E. coli* harbouring pMTL8000 series plasmids with Cm resistance gene (*catP*) were grown from beads at 30°C overnight (18 hours) in LB (5 mL) and 2.5 µL Cm stock solution with agitation.

Genomic and Plasmid DNA extraction and quantification

Genomic DNA (gDNA) was extracted from cultures using GenElute™ Bacterial Genomic DNA Kit, following the manufacturer's instructions and eluted in nuclease free water (Thermo scientific). Plasmid DNA was extracted from overnight cultures using Monarch® Plasmid Miniprep Kit, following manufacturer's instructions and eluted in nuclease free water.

DNA concentrations were quantified using NanoDrop Light Spectrophotometer (Thermo scientific) at 260 nm against dH_2O blanks.

Polymerase Chain Reaction (PCR) of gDNA

Forward and reverse primers in Table 4.S2 were synthesized by Sigma and used to amplify regions of gDNA during PCR. PCR was performed using Q5® high fidelity DNA Polymerase (NEB) according to the manufacturer's instructions. Table 4.S4 describes the reagent

quantities involved. Annealing temperatures (Table 4.S5) were chosen according to melting temperatures (Tm)s of primer sets, using NEB online Tm calculator. If all the PCR product was visualised using Gel electrophoresis, DNA was purified from the gel using Monarch® DNA Gel Extraction kit (following manufacturer's instructions). If only a sample of the PCR product was visualised using Gel electrophoresis, then the remainder of the PCR product was purified using Monarch® PCR & DNA Cleanup kit (following manufacturer's instructions).

Table S4. 4 Components used for Q5® PCR reactions to amplify gDNA.

Reaction component	Volume of Component (µL)
gDNA	1
Q5 ® Reaction master mix	10
dH_2O	7
Forward Primer (10 µM)	1
Reverse Primer (10 µM)	1

Table S4. 5 PCR Cycle steps used with Q5® Polymerase reactions.

PCR Step	Temperature (°C)	Time	Cycles
Initial denaturation	98	30 s	1
Denaturation	98	10 s	30
Annealing	60	30 s	
Extension	72	30 s per kb	
Final Extension	72	2 mins	1
Hold	10	-	-

Colony Polymerase Chain Reaction (PCR)

Green DreamTaq Polymerase (Promega) was used according to the manufacturer's instructions to screen colonies in the desired *napC* insertion region. Reaction components (Table S4.6) were used via PCR protocol (Table S4.7) with annealing temperatures chosen according to Tm of primers.

Table S4. 6 Components used for DreamTaq PCR reactions to amplify gDNA.

Reaction Component	Volume (µl)
Template DNA*	1
Green DreamTaq MasterMix	10
ColEI+tra_F2 primer (10 uM)	1
pCB102_R1 primer (10 uM)	1
Water	7

* Colony resuspended in dH_2O

Table S4. 7 PCR Cycle steps used with DreamTaq Polymerase reactions.

PCR Step	Temperature (°C)	Time	Cycles
Initial denaturation	94	30 s	1
Denaturation	94	10 s	30
Annealing	55	30 s	
Extension	72	30 s per kb	
Final Extension	72	2 mins	1
Hold	10	-	-

Agarose Gel Electrophoresis

DNA fragments, amplified by PCR or generated during Colony PCR, were analysed by agarose gel electrophoresis. Gels were made up of 1% w/v agarose in 1 x Tris acetate EDTA (TAE) buffer (VWR International Ltd.) with SYBR™ safe (Thermo Fisher Scientific) staining gel (1:10,000 final concentration). 6X purple loading dye (NEB) was added to DNA samples before loading (1:5, dye: sample) and 1 kb Plus (NEB) DNA ladder was used. Once the gel had set the comb was removed, immersed in 1X TAE buffer and samples loaded in the empty wells. The gels were run at 100 V for 40-60 minutes and visualised in a Gel Doc™ XR+ imaging system (Bio-Rad). DNA bands were extracted when necessary, under ultraviolet light using sterile scalpel and purified using Monarch® DNA Gel Extraction kit using manufacturer's instructions.

4.1.6.2 Cloning Methods

Restriction Enzyme digestion of DNA and plasmids

Restriction enzymes (RE) and corresponding buffers were supplied by NEB and digests carried out according to the manufacturer's instructions. DNA fragments or plasmids were digested using REs for 1-2 hours at 37°C and purified using Monarch® PCR & DNA Cleanup kit (following manufacturer's instructions).

Table S4. 8 Restriction enzyme digestion components.

Reaction components	Amount (µL)
RE 1	1
RE 2	1
Cutsmart® buffer	2
dH2O	20 – (x+3)
DNA or plasmid	X* = 1000/n

*Where n = concentration of DNA (ng/µL)

Standard Ligation of vector components

The clone pMTL83153_NapC is made of two vector components and so standard ligation was used to combine them. Ligations were set up using T4 DNA ligase (Promega) with 100 ng of digested plasmid according to the manufacturer's instructions. A molar ratio of 1:3, vector (digested plasmid): insert (*napC*-DNA), was used. The reaction was carried out at room temperature for 3 hours.

$$\text{ng of insert} = \frac{\text{vector (ng)} \times \text{size of insert (kb)}}{\text{size of vector (kb)}} \times \text{ molar ratio of } \left(\frac{\text{insert}}{\text{vector}}\right)$$

$$\text{ng of insert} = \frac{100\ \text{(ng)} \times\ 0.6\ \text{kb}}{4.67\ \text{kb}} \times\ \frac{3}{1} = 39\ \text{ng}$$

Table S4. 9 Standard ligation components used for cloning of pMTL83153_NapC.

Component	Quantity (uL)
Insert (*napC*-DNA)	X (39 ng)
Vector (Digested Plasmid)	Y (100 ng)
T4 DNA ligase	1
Ligase 10X Buffer	2
Nuclease free H_2O	17 – (X+Y)

Hi Fi assembly Ligation

Instead of standard ligation, HiFi assembly was used to construct plasmids for clones containing P_{Nat} and P_{BAD} promoters. NEB online calculator was used to calculate reagent ratios of components and reactions carried out according to manufacturer's instructions. For each reaction, the required components were mixed in an Eppendorf and incubated at 50°C for 50 minutes, then stored at -20°C or transformed immediately.

Table S4. 10 Reaction components for Hifi cloning of plasmid with * P_{Nat} promoter or **P_{BAD} promoter.

Component	**Quantity**
NapC-DNA	28.7 ng
pMTL83153 digest	100 ng
NEBuilder Hifi DNA assembly mastermix	10 µL
Plus the addition of:	
115usNapB*	6.6 ng
OR	
P_{BAD}_araC**	58 ng

*Hifi cloning for P_{Nat} promoter plasmid. **Hifi cloning reaction for P_{BAD} promoter plasmid. H_2O added to make total reaction volume 20 µL.

Chemical Transformation of complete plasmids into competent cells

The chemical transformation was carried out according to the NEB chemical transformation protocol. Chemically competent cells were thawed for 10 minutes on ice then 15 µL of plasmid DNA was added. The mixture was incubated on ice for 30 minutes before being heat shocked at 42 °C for exactly 30 seconds. It was placed on ice for a further 5

minutes, then 500 µL SOC (Super Optimal broth with Catabolite repression) media (NEB) was added before incubating at 37 °C for 60 minutes. After this, the cells were streaked on agar plates (with Cm) and left to grow at 24 °C for 4 days.

Preparation of Chemically competent cells.

Pre-warmed LB broth (200 ml, 37°C) was inoculated with an overnight culture of *E. coli* top 10 (2 mL) and grown to an OD_{600} of 0.5 - 0.7. 40 mL of the culture was added to falcon tubes (2 x 40 mL) and left on ice for 15 minutes. The tubes were centrifuged (4,000 rpm, 10 minutes, 4°C) and the supernatant discarded. The pellets were gently resuspended and combined an in ice cold CaCl solution (20 mL, 100 mM). The culture was placed on ice for 30 minutes, then centrifuged (4,000 rpm, 10 minutes, 4°C) before discarding the supernatant. The pellet was resuspended in 2 mL ice cold CaCl (100 mM) + 15 % glycerol solution. 100 µL aliquots were added to centrifugation tubes and stored at -80°C.

Sequencing of plasmids

Colony PCR amplified DNA regions were sequenced using sanger sequencing (Source Bioscience service) and results analysed using Benchling sequence alignment tool.

4.1.6.3 Evaluation of Protein Expression

Induction of P_{BAD} cultures

Clones containing the P_{BAD} promoter were induced using L-arabinose according to protocol in manual 'pBAD/His A, B, and C pBAD/Myc-His A, B, and C' (Invitrogen™). Briefly, a culture of the clone was grown in 5 mL LB with 2.5 µL Cm stock at 30 °C overnight. 3 tubes containing 10 mL LB with 5 µL were labelled and culture was added to achieve OD_{600nm} 0.05. These were grown to OD_{600nm} 0.5 and arabinose (0.1 mL, X stock, Figure S4.11) was added to each. After 8 hours (or stationary phase achieved), 2 mL of each culture was harvested by centrifugation (8000 rpm, 10 minutes, 4 °C) and stored at -20 °C overnight before total protein content was evaluated.

Table S4. 11 Arabinose induction concentrations for *E. coli* containing Inducible Promoter Vector.

Sample	Stock arabinose, X (w/v)	Final arabinose Concentration
E. coli$_{(IP\_0\%)}$	0	0
E. coli$_{(IP\_0.000018\%)}$	0.0018%	0.000018%
E. coli$_{(IP\_0.0018\%)}$	0.18%	0.0018%
E. coli$_{(IP\_0.18\%)}$	18%	0.18%

Cell lysate preparation

Overnight cultures were diluted to OD_{600} of 0.05 (10 mL LB + 5 µL Cm), grown for 8 hours (stationary phase) and 2 mL harvested by centrifugation (10000 rpm, 10 mins, 4°C) and stored overnight at -20°C. Pellets were thawed on ice and cells were lysed using Bugbuster® Master Mix and ROCHE cOmplete™ EDTA-free protease Inhibitor

Cocktail (according to manufacturer's instructions). Briefly, 300 µL of a 1X Bugbuster® Master mix/protease inhibitor solution was added to each pellet and vortexed gently until homogeneous. These were mixed gently at RT for 30 minutes on a plate shaker and then centrifuged (100000 rpm, 20 mins, 4°C). The soluble fraction was transferred to a fresh tube and kept on ice.

BCA Assay

Total protein concentration in each cell lysate sample was analysed using Pierce™ BCA Protein Assay Kit (Thermo Scientific™) according to the manufacturer's instructions (microplate procedure) using flat bottom 96-well plates (Costar, Corning®). CLARIOstar® microplate reader (BMG LABTECH) was used to measure the absorbance of samples at 562 nm against D_2O blank and compared to that of albumin standard curves.

A BSA standard sample was analysed for protein content using the BCA assay at different concentrations to create a standard curve. A standard curve was used to compare the absorbance of protein from cell lysates to calculate total protein concentration in each sample (Table S4.11).

Sodium dodecyl sulfate - polyacrylamide gel electrophoresis (SDS PAGE)

The total protein content of cell lysates was analysed using BCA assay and standardised to the lowest concentration (1.75 mg/µL) using dH_2O. 25 µL of each standardised cell lysate was mixed with 6 µL NuPAGE® LDS Reducing sample buffer (thermo fisher) and boiled at 100°C for 5 minutes to denature. Samples were loaded in equal volumes onto 1.0 mm precast Bolt™ 4-12% Bis-Tris Protein Gels (Invitrogen™) against Precision Plus Protein™ Keleidoscope (Bio-Rad) protein ladder. Electrophoresis was carried out using XCell SureLock™ Mini-Cell Electrophoresis System (Thermo Scientific) at 150 Volts, 75 mins, in 1 x NuPAGE® SDS buffer solution.

Gel Staining and detaining

After SDS PAGE gels were rinsed gently with water and stained using Coomassie brilliant blue solution (0.25% Coomassie Brilliant Blue R-250, 50% methanol, 10% acetic acid (w/v)) for 1 hour gently shaking on plate shaker. De-staining was carried out overnight using solution of 30% methanol and 10% acetic acid (w/v). Gel Doc™ XR+ imaging system (Bio-Rad) was used to image the resulting gels.

4.1.6.4 Applications with Clones

Fe Atom Transfer Radical Polymerisation (ATRP)

E.coli$_{IP}$ cultures were grown and induced according to protocol mentioned previously (4.4.2.2). The induced clones were grown to OD_{600} ~1.1 (20 mL LB + 10 µL Cm), centrifuged (6000 rpm, 20 mins), washed (PBS, 10 mL and 5 mL) then re-suspend in degassed PBS (1.5 mL, approximately 1.35 x 10^{10} CFU ml^{-1} in final reaction volume (4 mL)) before being used in the Fe ATRP reactions.

The reagent quantities are shown in table S4.12. Stock solutions were made for $FeCl_3.6H_2O$ and HEBIB. Appropriate volumes of $FeCl_3.6H_2O$ stock and Me_6TREN were added to a 5mL Eppendorf for each reaction with a stir bar and PBS. In separate tubes, PEGMA and HEBIB were dissolved in PBS. These were placed in the anaerobic cabinet for a minimum 1 hour to degas. The total amount PBS (including bacteria equalled 4 mL) in each reaction. After degassing, bacteria were added to $FeCl_3$/Me_6TREN mix and pre-mixed for 15 minutes before adding a monomer/initiator mixture where the reaction began. The reaction was left overnight and terminated by exposure to air.

Table S4. 12 Reagent ratios for *E. coli$_{IP}$* initiated Fe ATRP.

Reagent	Ratio	mmol	Mass (mg)	Vol (uL)
PEGMA	100	0.052	17	16.2
$FeCl_3.6H_20$	4.65	0.0024	0.65	-
Me_6TREN	13.95	0.0072	1.7	1.9
HEBIB	2	0.0010	0.22	0.15

Linear Sweep Voltammetry (LSV)

LSV was carried out using a 3-electrode system: carbon fibre micro-disk working electrode (33 µm), Ag/AgCl reference electrode and platinum wire counter electrode from ALS Co. Ltd., Japan. Experiments were conducted using potentiostat 'Autolab PGStat302A' with low current module (EDC). Measurements and analysis were carried out using NOVA 2.1 software. All electrochemical experiments were carried out in 1X phosphate buffer saline solution (PBS) supporting electrolyte, at current range 100 pA, scan rate 100 mV/s from 1.25 V to -0.25 V at room temperature. For the calibration curve 1 mM potassium ferricyanide and ferrocyanide were made up in PBS (1X) mixed in ratios (10:0, 8:2, 5:5, 2:8, 0:10). A sample of PBS was applied to all measurements as a control baseline subtraction. A PK-3 electrode polishing kit (ALS Co. Ltd.) was used to polish the working electrode between measurements. The first derivative functions of the calibration voltammograms were taken to create a cross-referencing tool to determine steady state peak currents (I_{ss}) of the bacterial reduction experiments. First derivative functions were applied using GraphPad Prism 8.1.2.

Bacteria were prepared by inducing where necessary according to previous protocols in this thesis. Bacteria were induced/grown overnight (10 mL, LB +cm) and pellets were resuspended in potassium ferricyanide (5 ml, 1 mM) for 1 hour at 37 °C. Bacteria were removed by centrifugation (5000 g, 10 minutes) and the supernatant was analysed by LSV. The first derivative of the voltammograms was taken and Fe concentrations were calculated using the calibration graph.

4.1.7 Supplementary

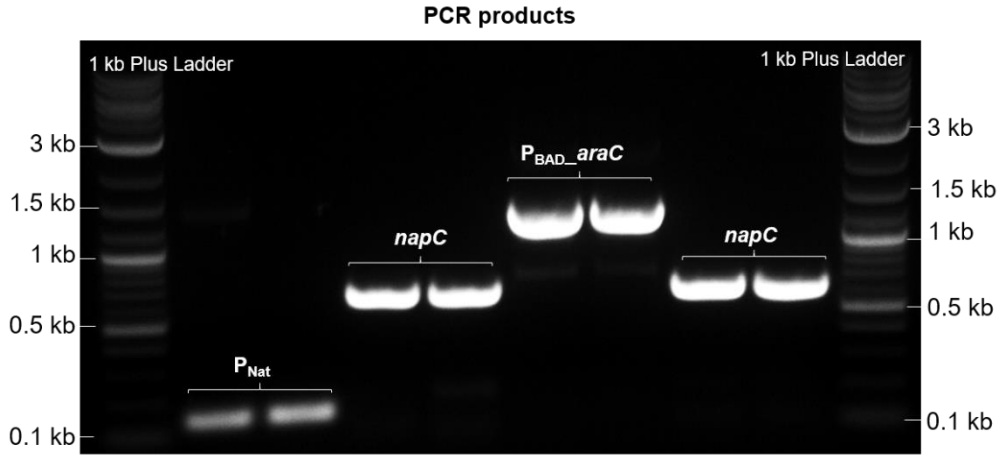

Figure S4. 1 Gel electrophoresis of PCR products for DNA regions making up the Native promoter vector and the Inducible promoter vector, against 1 KB Plus DNA ladder (Left and Right edges). For the Native promoter vector: P_{Nat} DNA region (145 bps), and *napC* DNA region (633 bps) are as expected. For the Inducible promoter vector: P_{BAD}_*araC* DNA region (1278 bps) and *napC* DNA region (633 bps) are as expected.

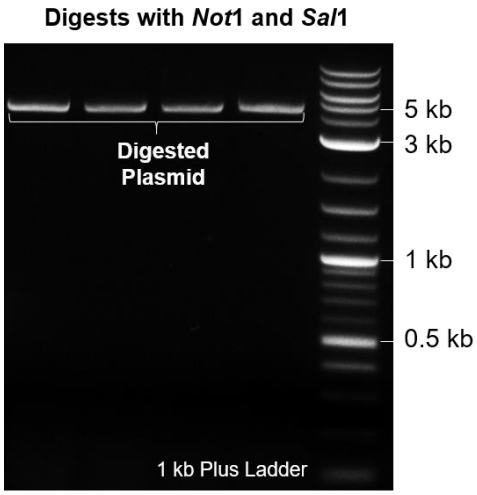

Figure S4. 2 Gel electrophoresis of digested pMTL83153 plasmid (Not 1 and Sal1 REs) component for the Native promoter vector and the Inducible promoter vector. (Against 1 KB Plus DNA ladder - Left and Right edges).

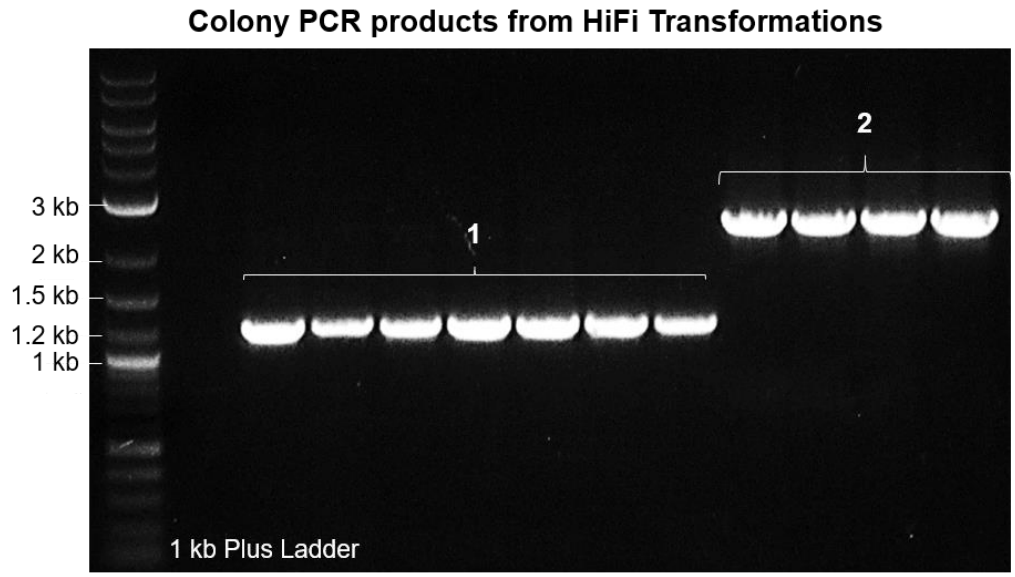

Figure S4. 3 Colony PCR (Primers: ColE1+tra_F2 and pCB102_R1) products to determine the success of *napC* insertion into 1: Native Promoter Vector and 2: Inducible Promoter Vector. Gel electrophoresis shows vector products of colonies from transformation of 1 (expected ~1207 bps) and 2 (expected ~ 2340 bps). All bands show expected sizes.

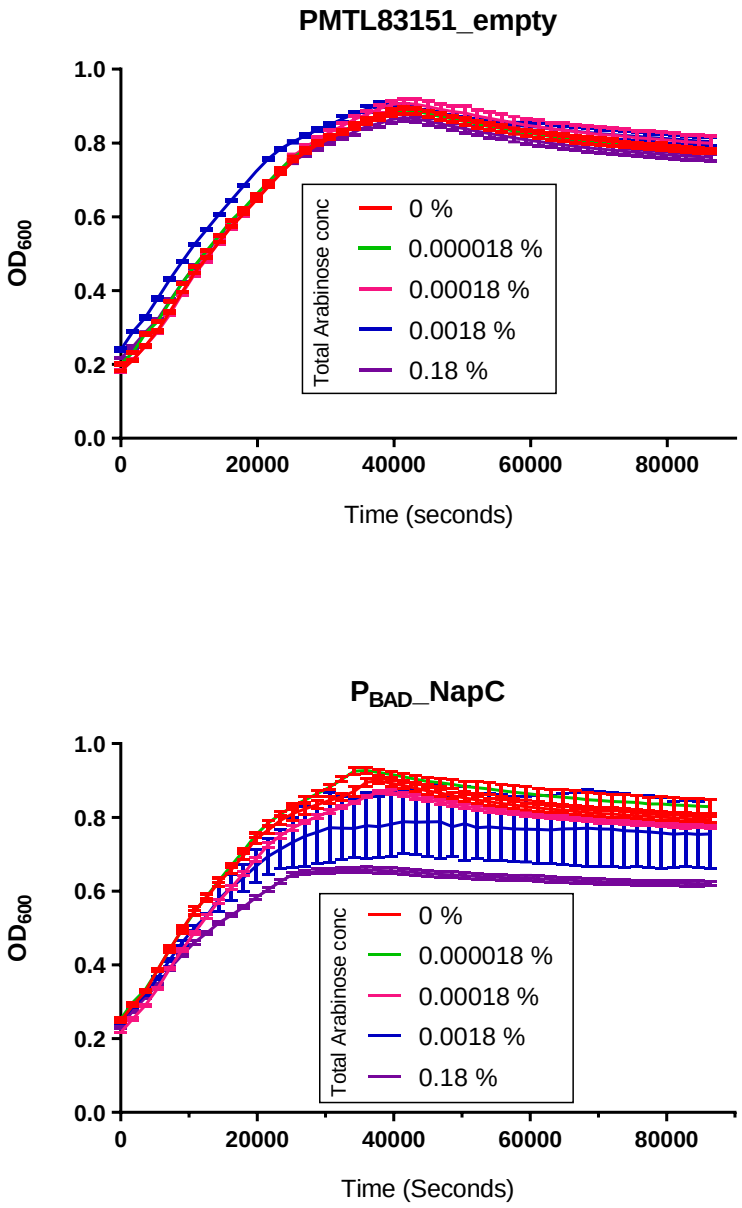

Figure S4. 4 Arabinose toxicity study for, Top: *E. coli* containing empty plasmid and Bottom: *E. coli* containing Inducible vector Plasmid at different arabinose concentrations.

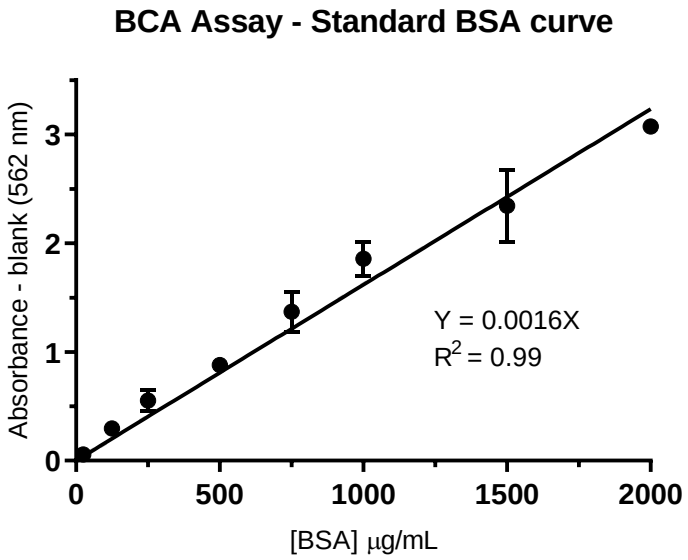

Figure S4. 5 BCA Standard curve for BSA (Bovine Serum albumin).

Table S4. 13 Protein standardisation calculations using BCA assay.

Vector	Abs_{562nm} (av)	Sample conc. (µg/mL)*	Original conc. (µg/mL)**	mg/ml
Empty Plasmid	1.57	982.7	1965	1.97
Native Promoter	1.63	1020	2040	2.04
E. coli$_{(IP\_0\%)}$	1.63	1019	2038	2.04
E. coli$_{(IP\_0.000018\%)}$	1.69	1053	2106	2.11
E. coli$_{(IP\_0.0018\%)}$	1.65	1029	2058	2.06
E. coli$_{(IP\_0.18\%)}$	1.40	873	1746	1.75

*Calculated using BSA equation (y=0.0016x). **Note samples were diluted by 2 so concentrations doubled to obtain original solution concentrations.

Arabinose toxicity

Overnights were growth in 5 mL LB + 2.5 µl chloramphenicol (Cm) where appropriate. These were adjusted to 0.05 OD in 2 mL LB (+Cm) and grown to OD_{600} 0.4. They were then induced with arabinose if necessary.

Protein Migration Analysis

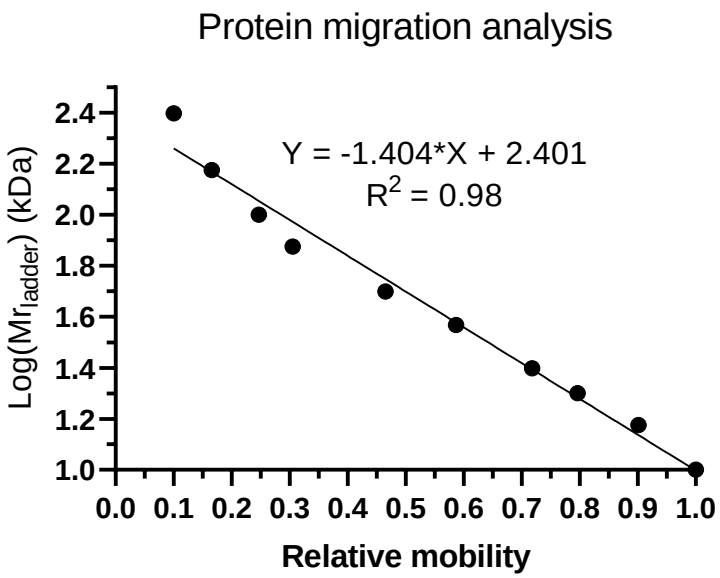

Figure S4. 6 Protein migration analysis of protein ladder Log(Mr) against relative mobility on SDS PAGE Gel.

Migration (NapC) = 10.7 cm

Dye front = 17.2 cm

$$\text{Relative mobility (X)} = \frac{\text{migration}}{\text{dye front}} = \frac{10.7}{17.2} = 0.622$$

$$Log\left(Mr_{NapC}\right) = [-(1.404 * X) + 2.401]$$

$$Log\left(Mr_{NapC}\right) = \ (-1.404 * 0.622) + 2.401$$

$$Mr_{NapC} = 10^{((-1.404*0.622)+2.401)} \ = \ 33.7\ kDa$$

4.1.8 Molecular Cloning Techniques

Polymerase chain Reaction (PCR)

PCR is used to amplify target regions of DNA.[76] The process (Figure S4.7) begins with denaturation where the heating of a piece of DNA (94 - 98°C) physically separates the strands of the DNA double helix. The temperature is then lowered (50-65°C) in the annealing stage, and the primers (short single stranded oligonucleotides with a complementary sequence to the target DNA region) bind to the target DNA, which becomes a template for the new DNA strand. With a slight temperature increase (~72°C) DNA polymerase (an enzyme which catalyses the synthesis of DNA molecules) can then assemble the new DNA from free nucleotides in the extension stage. Denaturation, annealing, and extension are repeated for ~30 cycles to produces millions of target DNA copies. A final extension cycle is then carried out before the reaction is cooled to ~10°C before use of amplified DNA or short-term storage.

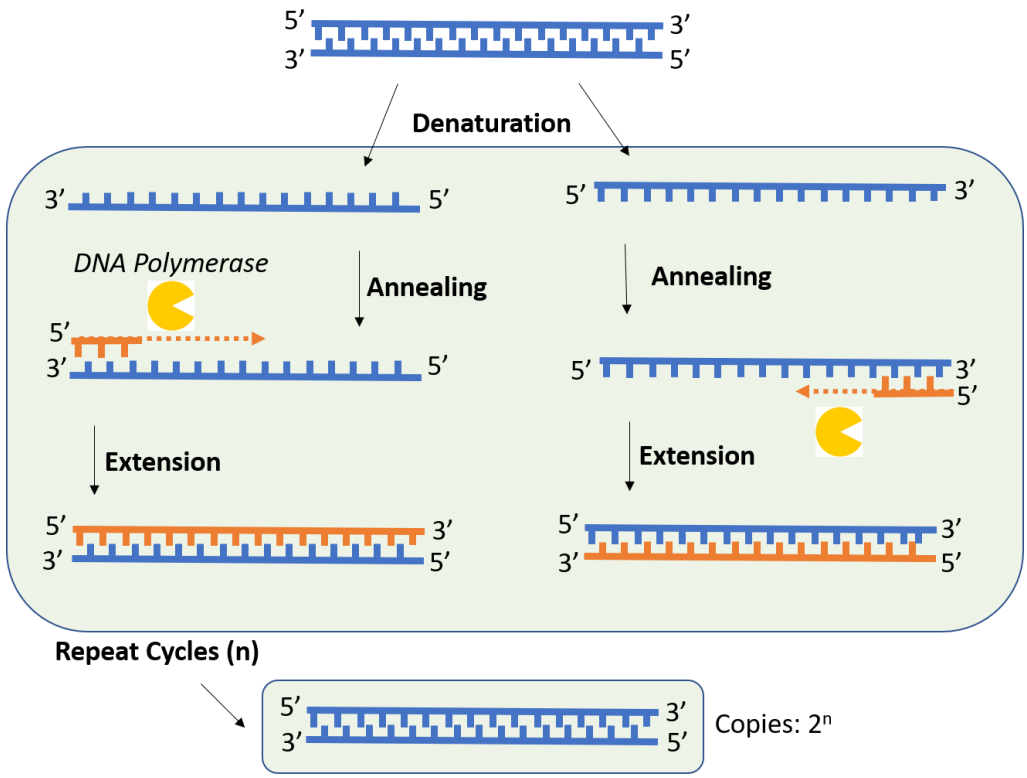

Figure S4. 7 Polymerase Chain Reaction (PCR) Cartoon to show denaturation, annealing and extension steps of DNA amplification.

Agarose Gel Electrophoresis

This technique permits the separation of DNA by loading samples with a dye in a pre-set gel and applying a voltage.[77] The highly cross-linked agarose gel matrix contains a network of pores that are capable of molecular sieving (higher agarose concentration decreases the size of the pores). DNA fragments are negatively charged so they are forced to migrate through the matrix to the anode in response to the electric current. UV light is used for visualisation and extraction of DNA fragments that have migrated through the gel. Shorter DNA fragments move faster than longer fragment and a DNA ladder of known molecular weights can be used to determine the molecular weight of a DNA fragment.

Sodium dodecyl sulphate – polyacrylamide gel electrophoresis (SDS-PAGE)

SDS-PAGE allows proteins to be separated by molecular weight, but electrophoretic mobility is governed by the length, conformation and charge of a molecule.[78] Proteins are structurally diverse compared to DNA molecules as they have folded tertiary structures, and therefore have differing charge to mass ratios. This means that they need to be denatured and linearised before SDS-PAGE analysis. This can be achieved by heating a protein with anionic detergent (SDS buffer) to disrupt ionic inter or intramolecular interactions, whilst providing an overall negative charge to the molecules.

A pre-set polyacrylamide gel is made by radical polymerisation with a crosslinker (*N*,*N*'methylene bisacrylamide), and the ratio and final percentage of acrylamide to crosslinker determine the pore size of the gel. The samples are loaded into wells of the pre-set gel, placed in an SDS running buffer, and a voltage is applied, causing the negatively charged molecules to migrate to the anode. A reference ladder of a known molecular weight is run alongside the proteins to aid molecular weight determination - smaller proteins migrate more quickly than larger ones. Once the gel has run to completion, staining with Coomassie solution allows the dye to bind tightly to protein molecules. The dye also stains the whole gel so a de-staining step is used to resolve the dye-bound protein bands. The molecular weights of the proteins can then be resolved by observing the migration of the bands. Some proteins,

however, resolve at higher molecular weights due to excess positive charge or incomplete denaturation.[69]

4.1.9 Electrochemical Methodology

Fundamentals

Electrochemical methods are often used to investigate electron transfer processes (reduction or oxidation) in chemical reactions or biological reactions. Such redox events at an electrode surface can be monitored by applying a voltage (potential) and measuring the current (flow of electrons), known as voltammetry. An electrolytic cell is used for such experiments (Figure S4.8), consisting of a working electrode (WE), reference electrode (RE) and a counter electrode (CE). The reaction must take place in an ionic conductor solution (electrolyte), and a potentiostat is used to apply potential and measure the current. Redox events occur at the WE which is set to a given potential. The RE has a known potential and is used as a reference by the potentiostat to apply the correct voltage to the WE. The CE is where the complementary oxidation or reduction reaction to that at the WE takes place, it also completes the circuit and allows current to flow through the system. The current measured is reflective of the rate at which electrons transfer across the electrode-solution interface and so electrolysis can measure electroactive chemical species through redox these reactions.[79]

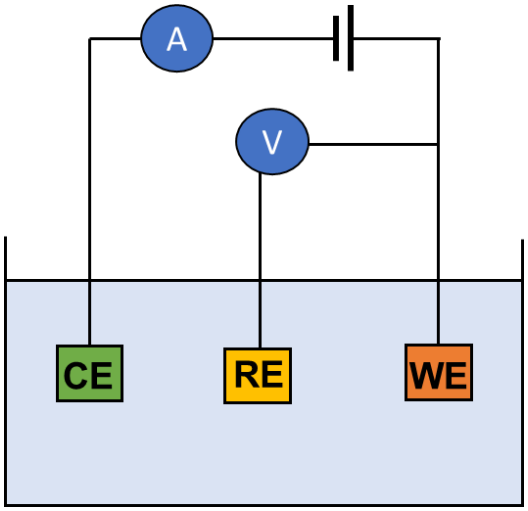

Figure S4. 8 A 3 electrode electrochemical cell complete with a working electrode (WE), reference electrode (RE) and counter electrode (CE). Current flows through the circuit from the working electrode to the counter electrode. The voltage of the system is regulated using the reference electrode of known electrode potential.

Linear Sweep Voltammetry (LSV)

In linear sweep voltammetry (LSV) the potential is swept linearly at the WE and the corresponding current is measured with time. When using a microelectrode, the peak current (I_p) obtained can be described by the Randles-Sevcik equation:

$$I_p = 2.69x10^5\, n^{\frac{3}{2}}\, A\, D^{\frac{1}{2}} C\, v^{\frac{1}{2}}$$

Where, n = number of electrons, A = electrode area (cm^2) C = concentration of analyte (mol/cm^3), v = scan rate (V/s) and D = Diffusion coefficient (cm^2/s).[79, 80] The flow of current in an electrochemical cell is a direct measure of the rate of the electrochemical reaction taking place at the electrode surface. The rate of reaction is influenced by the movement of reactants from the bulk solution to the electrode surface, known as mass transport or flux (J). Diffusional flux (J_D) is the main contributing

factor effecting mass transport and is dependent on the size and shape of the electrode surface.

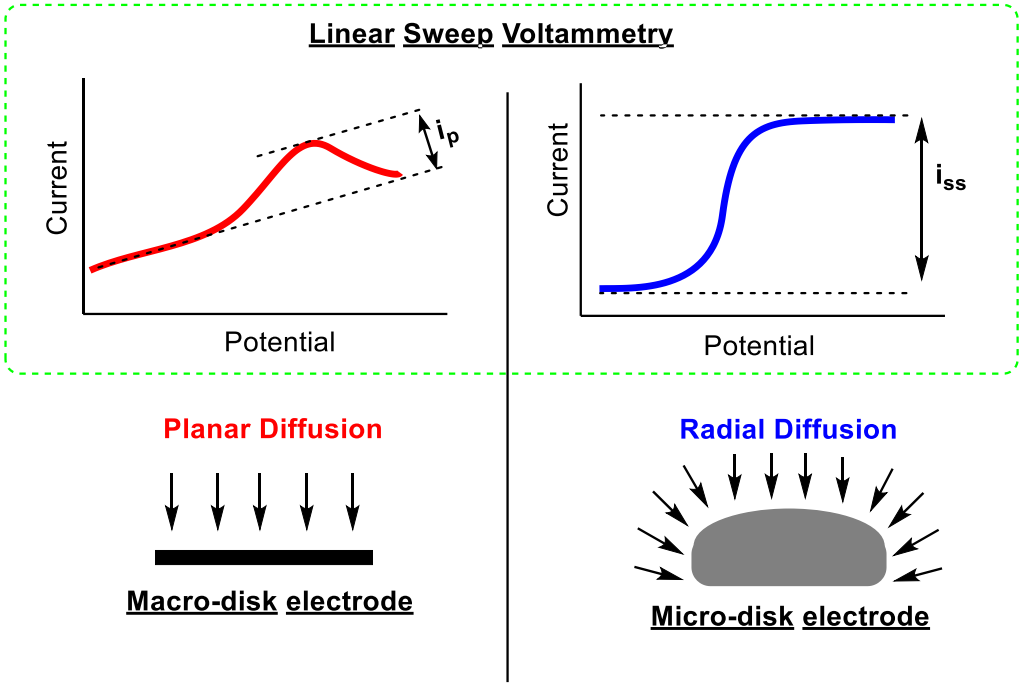

Figure S4. 9 Linear Sweep Voltammetry showing voltammograms of positive (oxidative current) produced using a three electrode system with; a macroelectrode (Top, left, red) and a microelectrode (Top, right, blue). Illustrations comparing diffusion of macroelectrode (Bottom left, red) to microelectrode (Nottom, right, blue)

Microelectrodes

Macroelectrodes, with sizes < mm, are subject to planar diffusion (Figure S4.9) of electroactive species to the electrode. At the point where the peak plateaus (red) the reaction becomes diffusion limited and the rate of electron transfer is hindered by mass transport of species to and from the electrode surface. Whereas microelectrodes, with sizes < µM, experience radial diffusion (Figure S4.9) with substantially increased flux of species to the electrode surface, this creates a steady state peak

(blue) which is time independent.[81] The Randles-Sevcik equation can be simplified in this instance, and the steady state current (I_{ss}) is measured:

$$I_{ss} = 4nFDCr$$

Where, n = number of electrons, F = faradays constant (6,485.3 C/mol), D = Diffusion coefficient (cm^2/s), C = analyte concentration (mol/cm^3) and r = radius of micro-electrode (cm).[82]

Microelectrodes are advantageous as faster electron transfer kinetics can be studied due to the steady state current behaviour, resulting from faster mass transport. They also produce lower capacitance levels and reduced ohmic drop which is observed at macroelectrodes.

References

1. J. L. Pierre, M. Fontecave and R. R. Crichton, *Biometals*, 2002, **15**, 341-346.
2. N. C. Andrews and P. J. Schmidt, *Annu Rev Physiol*, 2007, **69**, 69-85.
3. M. A. TerAvest and C. M. Ajo-Franklin, *Biotechnol. Bioeng.*, 2016, **113**, 687-697.
4. M. Kaneko, K. Ishihara and S. Nakanishi, *Small*, 2020, **16**, e2001849.
5. M. R. Bennett, P. Gurnani, P. J. Hill, C. Alexander and F. J. Rawson, *Angew. Chem. Int. Ed. Engl.*, 2020, **59**, 4750-4755.
6. U. Schröder, F. Harnisch and L. T. Angenent, *Energy & Environmental Science*, 2015, **8**, 513-519.
7. Y. Cui, B. Lai and X. Tang, *Biosensors (Basel)*, 2019, **9**, 92.
8. A. J. Slate, K. A. Whitehead, D. A. C. Brownson and C. E. Banks, *Renewable and Sustainable Energy Reviews*, 2019, **101**, 60-81.
9. Y. Hu, Y. Yang, E. Katz and H. Song, *Chem Commun (Camb)*, 2015, **51**, 4184-4187.
10. C. Santoro, C. Arbizzani, B. Erable and I. Ieropoulos, *J. Power Sources*, 2017, **356**, 225-244.
11. A. Kisieliute, A. Popov, R.-M. Apetrei, G. Cârâc, I. Morkvenaite-Vilkonciene, A. Ramanaviciene and A. Ramanavicius, *Chem. Eng. J.*, 2019, **356**, 1014-1021.
12. Y. L. Kang, S. Pichiah and S. Ibrahim, *Int. J. Hydrogen Energy*, 2017, **42**, 1661-1671.
13. W. Wang, S. You, X. Gong, D. Qi, B. K. Chandran, L. Bi, F. Cui and X. Chen, *Adv. Mater.*, 2016, **28**, 270-275.
14. R.-M. Apetrei, G. Cârâc, G. Bahrim and P. Camurlu, *International Journal of Polymeric Materials and Polymeric Biomaterials*, 2018, **68**, 1058-1067.
15. A. Kausaite-Minkstimiene, V. Mazeiko, A. Ramanaviciene and A. Ramanavicius, *Sensors and Actuators B: Chemical*, 2011, **158**, 278-285.
16. H. G. Sherman, J. M. Hicks, A. Jain, J. J. Titman, C. Alexander, S. Stolnik and F. J. Rawson, *Chembiochem*, 2019, **20**, 1008-1013.
17. N. Idil and B. Mattiasson, *Sensors (Basel)*, 2017, **17**, 708.
18. M. Shi, Y. Jiang and L. Shi, *Science China Technological Sciences*, 2019, **62**, 1670-1678.
19. Y. Wang, Y. Tashiro and K. Sonomoto, *J Biosci Bioeng*, 2015, **119**, 10-18.
20. S. Kato, *Microbes Environ*, 2015, **30**, 133-139.
21. N. Bansal, J. J. Coetzee and E. M. N. Chirwa, *Ecotoxicol. Environ. Saf.*, 2019, **172**, 281-289.
22. J. Yang, M. Zhou, Y. Zhao, C. Zhang and Y. Hu, *Bioresour. Technol.*, 2013, **150**, 271-277.
23. T. R. Sandrin and D. R. Hoffman, in *Environmental Bioremediation Technologies*, eds. S. N. Singh and R. D. Tripathi, Springer Berlin Heidelberg, Berlin, Heidelberg, 2007, DOI: 10.1007/978-3-540-34793-4_1, ch. Chapter 1, pp. 1-34.

24. D. R. Lovley, *ASM News*, 2002, **68**, 231-237.
25. H. Hou, X. Chen, A. W. Thomas, C. Catania, N. D. Kirchhofer, L. E. Garner, A. Han and G. C. Bazan, *Adv. Mater.*, 2013, **25**, 1593-1597.
26. L. Hao, B. Zhang, M. Cheng and C. Feng, *Bioresour. Technol.*, 2016, **201**, 105-110.
27. Y. S. Xu, T. Zheng, X. Y. Yong, D. D. Zhai, R. W. Si, B. Li, Y. Y. Yu and Y. C. Yong, *Bioresour. Technol.*, 2016, **211**, 542-547.
28. R. B. Song, Y. Wu, Z. Q. Lin, J. Xie, C. H. Tan, J. S. C. Loo, B. Cao, J. R. Zhang, J. J. Zhu and Q. Zhang, *Angew. Chem. Int. Ed. Engl.*, 2017, **56**, 10516-10520.
29. R.-B. Song, K. Yan, Z.-Q. Lin, J. S. Chye Loo, L.-J. Pan, Q. Zhang, J.-R. Zhang and J.-J. Zhu, *Journal of Materials Chemistry A*, 2016, **4**, 14555-14559.
30. N. Thepsuparungsikul, T. C. Ng, O. Lefebvre and H. Y. Ng, *Water Sci. Technol.*, 2014, **69**, 1900-1910.
31. Y. Hindatu, M. S. M. Annuar and A. M. Gumel, *Renewable and Sustainable Energy Reviews*, 2017, **73**, 236-248.
32. A. Stephenson-Brown, S. Yong, M. H. Mansor, Z. Hussein, N. C. Yip, P. M. Mendes, J. S. Fossey and F. J. Rawson, *Chem Commun (Camb)*, 2015, **51**, 17213-17216.
33. J. Liu, Y. Qiao, Z. S. Lu, H. Song and C. M. Li, *Electrochem. Commun.*, 2012, **15**, 50-53.
34. M. J. Angelaalincy, R. Navanietha Krishnaraj, G. Shakambari, B. Ashokkumar, S. Kathiresan and P. Varalakshmi, *Frontiers in Energy Research*, 2018, **6**.
35. X. Y. Yong, D. Y. Shi, Y. L. Chen, J. Feng, L. Xu, J. Zhou, S. Y. Wang, Y. C. Yong, Y. M. Sun, P. K. OuYang and T. Zheng, *Bioresour. Technol.*, 2014, **152**, 220-224.
36. M. Li, M. Zhou, X. Tian, C. Tan, C. T. McDaniel, D. J. Hassett and T. Gu, *Biotechnol. Adv.*, 2018, **36**, 1316-1327.
37. M. J. Colombo, J. Ha, J. R. Reinfelder, T. Barkay and N. Yee, *Chem. Geol.*, 2014, **363**, 334-340.
38. N. Wiesemann, L. Butof, M. Herzberg, G. Hause, L. Berthold, B. Etschmann, J. Brugger, G. Martinez-Criado, D. Dobritzsch, S. Baginsky, F. Reith and D. H. Nies, *Appl. Environ. Microbiol.*, 2017, **83**, e01679-01617.
39. F. Reith, B. Etschmann, C. Grosse, H. Moors, M. A. Benotmane, P. Monsieurs, G. Grass, C. Doonan, S. Vogt, B. Lai, G. Martinez-Criado, G. N. George, D. H. Nies, M. Mergeay, A. Pring, G. Southam and J. Brugger, *Proc Natl Acad Sci U S A*, 2009, **106**, 17757-17762.
40. A. Espinoza Tofalos, M. Daghio, M. Gonzalez, M. Papacchini, A. Franzetti and M. Seeger, *FEMS Microbiol. Lett.*, 2018, **365**.
41. K. Tanaka, S. Yokoe, K. Igarashi, M. Takashino, M. Ishikawa, K. Hori, S. Nakanishi and S. Kato, *Front Microbiol*, 2018, **9**, 2905.
42. M. J. Edwards, G. F. White, C. W. Lockwood, M. C. Lawes, A. Martel, G. Harris, D. J. Scott, D. J. Richardson, J. N. Butt and T. A. Clarke, *J. Biol. Chem.*, 2018, **293**, 8103-8112.

43. H. M. Jensen, M. A. TerAvest, M. G. Kokish and C. M. Ajo-Franklin, *ACS Synth Biol*, 2016, **5**, 679-688.
44. G. F. White, M. J. Edwards, L. Gomez-Perez, D. J. Richardson, J. N. Butt and T. A. Clarke, in *Advances in Microbial Physiology*, ed. R. K. Poole, Academic Press, 2016, vol. 68, pp. 87-138.
45. O.-M. H. Richter and B. Ludwig, in *Reviews of Physiology, Biochemistry and Pharmacology*, Springer Berlin Heidelberg, Berlin, Heidelberg, 2003, DOI: 10.1007/s10254-003-0006-0, pp. 47-74.
46. J. Cai, J. Yang and D. P. Jones, *Biochim. Biophys. Acta*, 1998, **1366**, 139-149.
47. M. Huttemann, P. Pecina, M. Rainbolt, T. H. Sanderson, V. E. Kagan, L. Samavati, J. W. Doan and I. Lee, *Mitochondrion*, 2011, **11**, 369-381.
48. G. C. Brown and V. Borutaite, *Biochim. Biophys. Acta*, 2008, **1777**, 877-881.
49. S. Santra, C. Kaittanis and J. M. Perez, *Mol Pharm*, 2010, **7**, 1209-1222.
50. J. Mendez, M. Morales Cruz, Y. Delgado, C. M. Figueroa, E. A. Orellano, M. Morales, A. Monteagudo and K. Griebenow, *Mol Pharm*, 2014, **11**, 102-111.
51. A. Macone, S. Masciarelli, F. Palombarini, D. Quaglio, A. Boffi, M. C. Trabuco, P. Baiocco, F. Fazi and A. Bonamore, *Sci Rep*, 2019, **9**, 11749.
52. H. G. Sherman, C. Jovanovic, S. Stolnik and F. J. Rawson, *Anal. Chem.*, 2018, **90**, 2780-2786.
53. M. L. Cartron, M. D. Roldan, S. J. Ferguson, B. C. Berks and D. J. Richardson, *Biochem. J*, 2002, **368**, 425-432.
54. M. D. Roldán, H. J. Sears, M. R. Cheesman, S. J. Ferguson, A. J. Thomson, B. C. Berks and D. J. Richardson, *J. Biol. Chem.*, 1998, **273**, 28785-28790.
55. H. M. Jensen, A. E. Albers, K. R. Malley, Y. Y. Londer, B. E. Cohen, B. A. Helms, P. Weigele, J. T. Groves and C. M. Ajo-Franklin, *Proc Natl Acad Sci U S A*, 2010, **107**, 19213-19218.
56. C. R. Myers and J. M. Myers, *J. Bacteriol.*, 1997, **179**, 1143-1152.
57. A. Vellingiri, Y. E. Song, G. Munussami, C. Kim, C. Park, B.-H. Jeon, S.-G. Lee and J. R. Kim, *Journal of Chemical Technology & Biotechnology*, 2019, **94**, 2115-2122.
58. J. S. Gescher, C. D. Cordova and A. M. Spormann, *Mol. Microbiol.*, 2008, **68**, 706-719.
59. S. V. Rajagopala, N. Yamamoto, A. E. Zweifel, T. Nakamichi, H. K. Huang, J. D. Mendez-Rios, J. Franca-Koh, M. P. Boorgula, K. Fujita, K. Suzuki, J. C. Hu, B. L. Wanner, H. Mori and P. Uetz, *BMC Genomics*, 2010, **11**, 470.
60. E. P. Magennis, F. Fernandez-Trillo, C. Sui, S. G. Spain, D. J. Bradshaw, D. Churchley, G. Mantovani, K. Winzer and C. Alexander, *Nat Mater*, 2014, **13**, 748-755.
61. F. J. Rawson, A. J. Downard and K. H. Baronian, *Sci Rep*, 2014, **4**, 5216.
62. F. J. Rawson, A. J. Gross, D. J. Garrett, A. J. Downard and K. H. R. Baronian, *Electrochem. Commun.*, 2012, **15**, 85-87.
63. H. G. Sherman, C. Jovanovic, A. Abuawad, D. H. Kim, H. Collins, J. E. Dixon, R. Cavanagh, R. Markus, S. Stolnik and F. J. Rawson, *Biochim Biophys Acta Bioenerg*, 2019, **1860**, 628-639.

64. M. Fakruddin, R. Mohammad Mazumdar, K. S. Bin Mannan, A. Chowdhury and M. N. Hossain, *ISRN Biotechnol*, 2013, **2013**, 590587.
65. H. Lodish, A. Berk, S. L. Zipursky, P. Matsudaira, D. Baltimore and J. Darnell, in *Molecular Cell Biology. 4th edition*, WH Freeman, New YOrk, 2000.
66. J. T. Heap, O. J. Pennington, S. T. Cartman and N. P. Minton, *J. Microbiol. Methods*, 2009, **78**, 79-85.
67. V. Hershfield, H. W. Boyer, C. Yanofsky, M. A. Lovett and D. R. Helinski, *Proc Natl Acad Sci U S A*, 1974, **71**, 3455-3459.
68. M. J. Carrier, M. E. Nugent, W. C. A. Tacon and S. B. Primrose, *Trends Biotechnol.*, 1983, **1**, 109-113.
69. A. Matagne, B. Joris and J. M. Frere, *Biochem. J*, 1991, **280 (Pt 2)**, 553-556.
70. H. N. Lim, Y. Lee and R. Hussein, *Proc Natl Acad Sci U S A*, 2011, **108**, 10626-10631.
71. A. Roux, C. Beloin and J. M. Ghigo, *J. Bacteriol.*, 2005, **187**, 1001-1013.
72. L. J. Bird, V. Bonnefoy and D. K. Newman, *Trends Microbiol*, 2011, **19**, 330-340.
73. I. M. Kolthoff and E. A. Pearson, *Industrial & Engineering Chemistry Analytical Edition*, 1931, **3**, 381-382.
74. J. Luo, A. Sam, B. Hu, C. DeBruler, X. Wei, W. Wang and T. L. Liu, *Nano Energy*, 2017, **42**, 215-221.
75. S. C. Andrews, A. K. Robinson and F. Rodriguez-Quinones, *FEMS Microbiol. Rev.*, 2003, **27**, 215-237.
76. L. Garibyan and N. Avashia, *J Invest Dermatol*, 2013, **133**, 1-4.
77. P. Y. Lee, J. Costumbrado, C. Y. Hsu and Y. H. Kim, *J Vis Exp*, 2012, DOI: 10.3791/3923, 3923.
78. U. Laemmli and M. Favre, *Nature*, 1970, **227**, 680-682.
79. J. Wang, *Analytical Electrochemistry*, John Wiley & Sons, Incorporated, Hoboken, UNITED STATES, 2006.
80. M. A. Brett Christopher and M. Oliveira Brett Ana, *Journal*, 1993, 1-1.
81. R. J. Forster, *Chem. Soc. Rev.*, 1994, **23**, 289-297.
82. J. T. Cox, J. P. Guerrette and B. Zhang, *Anal. Chem.*, 2012, **84**, 8797-8804.

Chapter 5. Conclusions and Future Work

Conclusions

A thorough review of existing literature in the first chapter of this thesis highlighted the necessity to broaden the current understanding of polymer synthesis in combination with biotic redox chemistries. Reversible Deactivation Radical Polymerisation (RDRP) methods known as Atom Transfer Radical Polymerisation (ATRP) and Reversible Addition-fragmentation chain-transfer (RAFT) were discussed in several redox driven polymerisation systems, including those catalysed by enzymes, bacteria, and yeast. Although whole cell catalysis has been briefly explored with such systems, the research area remains relatively novel and more experiments were necessary to expand the scope of hybrid 'polymer-biomachinery'. The research presented in this thesis explored the development of novel RDRP systems initiated by bacterial redox mechanisms, resulting in the development of two polymerisation methods adapted for bacterial redox initiation. The upregulation of a gene of interest encoding a Cytochrome C (C-Cyt) periplasmic protein (NapC) was also carried out and probed for its Fe reducing abilities. The research presented aims to broaden the scope of living biomaterials towards a variety of applications and to progress the understanding of Fe reduction systems in bacteria.

Firstly, it was envisioned that Fe ATRP systems might be applicable in biological environments for whole cell polymerisation catalysis. As concluded from the first chapter, previous research regarding Fe ATRP had not been carried out under biological conditions. The second chapter

of this thesis consequently explored Fe ATRP methods which could be compatible with bacterial systems. Ascorbic acid (AscA) initiated polymerisations were firstly tested under these conditions for a selection of monomers (Poly(ethylene glycol) methyl ether methacrylate (PEGMA), 2-(Methacryloyloxy) ethyl dimethyl-(3-sulfopropyl) ammonium hydroxide (MEDSA), N-Hydroxyethyl acrylamide (NHEA), Hydroxyethyl methacrylate (HEMA), and Sodium-2-Acrylamido-2-methyl-1-propanesulfonic (Na-AMPS)) and catalysts (Tris[2-(2-methoxyethoxy)ethyl]amine (TDA-1), Tris(2-dimethylaminoethyl)amine (Me_6TREN), Tris(N-methyl-2-aminoethyl)amine (Me_3TREN), 2, 2 – Bipyridine (Bpy)). Bacteria cultures (*Cupriavidus metallidurans* (*C. met*), *Escherichia coli* (*E. coli*) and *Clostridium sporogenes* (*C. spor*)) were subsequently implemented into these polymerisation systems where *C. met* were able to initiate Fe ATRP polymerisations whilst maintaining viability, and living bacteria were found to be essential to catalyse the reaction. Different components of the bacterial polymerisation were explored (Monomer, bacteria type, bacteria concentration, catalyst concentration, DP, Initiator type) and were found to alter the polymerisation kinetics, conversion, and the dispersity (*Đ*) and molecular weight (M_n) control of the resulting polymers. Although changing the parameters of the system had some effect on the polymers generated, the M_n remained a challenge to control. Nonetheless, not all applications require well defined polymers, for example, high molecular weight polymers produced by this method could be of interest for high wear resistance applications.[1, 2] Literature reported prior to this work focussed

on methods catalysed by Cu and were not optimised to maintain bacterial viability. This work is the first reported Fe ATRP system that was carried out in biological conditions, catalysed by 3 types of whole living cells.[3] The findings signify the requirement of living cells to the polymerisation and indicate substantial participation of bacterial EET redox metabolism.

The Fe ATRP polymerisations described were extremely sensitive to air which required careful deoxygenation of all reaction components, making the set up difficult and costly. This also confined future applications to anaerobic environments because the polymerisation could not be carried out in air. Considering the challenges encountered in the second chapter, an alternative RDRP method, which did not rely on a complex metal catalyst to maintain polymerisation control and could withstand aerobic conditions, was introduced in chapter 3. Fenton Glucose Oxidase (FG) RAFT techniques discussed in chapter 1 that could be carried out in the presence of air were advanced to be compatible with whole bacteria cells. Firstly, the reaction cascade was developed with *in situ* activation of air stable Fe^{3+} to Fenton active Fe^{2+} by AscA in air without the need for prior degassing. Reaction components (Glucose, GOx, Fe and AscA) were adjusted to tailor the radical flux and the effects on the M_n and $Đ$ control of the resulting polymers were observed, with Fe and AscA showing the most profound effects. *C. met* were effectively able to replace AscA and living bacteria were shown to be essential to the polymerisation, implicating the importance of cell metabolism in the polymerisation redox initiation. Several monomers (Dimethylacrylamide (DMA), N-Hydroxyethyl acrylamide (NHEA) and N-

acryloylmorpholine (NAM)) were compatible with the system, but the M_n control of the resulting polymers was dependant on the monomer type, with DMA being the most controllable ($Đ$ = 1.12). In chapter 2 high Fe concentrations (>700 µM) were required for fast Fe ATRP reaction rates which were greatly dependent on the metal catalyst structure and stability. As b-FG-RAFT only depends on the Fe concentration as a radical source, lower Fe concentrations could be utilised in chapter 3 with better control over the resulting polymers. In this chapter, b-FG-RAFT could be carried out with Fe concentrations as low as 7 µM whilst maintaining acceptable M_n control and narrow $Đ$ ($Đ$ = 1.28). The polymerisations described could be carried out in air without the need for degassing which greatly reduced set up time, costs, and broadens the range of possible applications. Here, a novel technique to generate polymers under aerobic conditions is presented, generating polymers with improved M_n and $Đ$ control compared to bacterial initiated Fe ATRP polymerisations shown in chapter 2. The method has significantly advanced the current literature to hybridise synthetic chemistry with biological redox chemistry, to generate well defined polymers under benign conditions. Beyond the scope of this work, potential remains for additional optimisation by further lowering Fe concentrations, trialling other monomer materials and different living organisms, to tailor the technique towards specific applications.

Lastly, the aims of chapter 4 were to improve the understanding of C-Cyts in *E. coli* by investigating the significance of NapC. Previous research indicated the importance of NapC in bacterial Fe reduction, and

consequently upregulation of this protein in *E. coli* was carried out. Several gene promoters, P_{fdx}, P_{Nat} and P_{BAD}, were used to drive expression of *napC*. Once transformed into *E. coli,* the resulting vectors containing the latter two promoters (*E. coli*$_{(N)}$ and *E. coli*$_{(IP)}$, respectively) gave rise to colonies which showed correct construction by genetic sequencing. Upon sodium dodecyl sulphate-polyacrylamide gel electrophoresis (SDS PAGE) protein studies, *E. coli*$_{(IP)}$ clones were shown to over express the NapC protein with arabinose induction. To test the effect of NapC upregulation had on bacterial Fe reduction, *E. coli*$_{(IP)}$ were incorporated into Fe ATRP polymerisations. This gave rise to reaction rates higher than that of *E. coli* without NapC upregulation, suggesting that NapC helped to improve Fe^{3+} reduction. LSV studies were carried out to gain a better understanding of the Fe^{3+} reduction capabilities of *E. coli*$_{(IP)}$. However, a global pandemic (COVID-19) caused interruptions with these experiments. Further investigations of these clones will enable light to be shed on the role of NapC in bacterial Fe reduction and help to improve our understanding of C-Cyt mechanisms in bacteria.

Overall, this thesis conveys the importance of bacterial redox chemistry, demonstrating that the synergy between biological and chemical disciplines can be used to develop new techniques (Figure 5. 1). Indeed, two of the most common RDRP methods, ATRP and RAFT were adapted to perform under benign conditions, whereby bacterial viability could be maintained and living bacteria were shown to be essential to the polymerisation methods. The challenges of poor control

seen with Fe ATRP bacterial polymerisation methods might be improved by using different metal catalysts that are less susceptible to ligand dissociation or bacterial interference. This could be carried out by screening various metal and ligand combinations. The application of b-FG-RAFT overcame the challenges of poor control seen with ATRP methods but was shown to be monomer specific and could be improved by altering the Fe concentrations. Further screening of different monomers, chain transfer agents (CTA)s and creating co-polymers would broaden this field of research by providing a tool to create polymers with different properties using a sustainable polymer synthesis method under benign conditions. Upregulation of NapC was found to have some effects on bacterial Fe reduction and shows that EET is not just confined to Dissimilatory Iron Reducing Bacteria (DIRB). The work presented in this thesis highlights the complexity of bacterial redox mechanisms, showing that continual research is necessary to further probe and improve EET machinery. As this new field of research matures, reactions such as step growth polymerisations,[4, 5] conducting polymer synthesis,[6] other metal catalysed reactions,[7] or biocatalytic processes,[8] could be envisioned. Research in these areas may contribute to new opportunities for greener synthesis methods or new technologies such as biosensors, MFCs, or living materials.

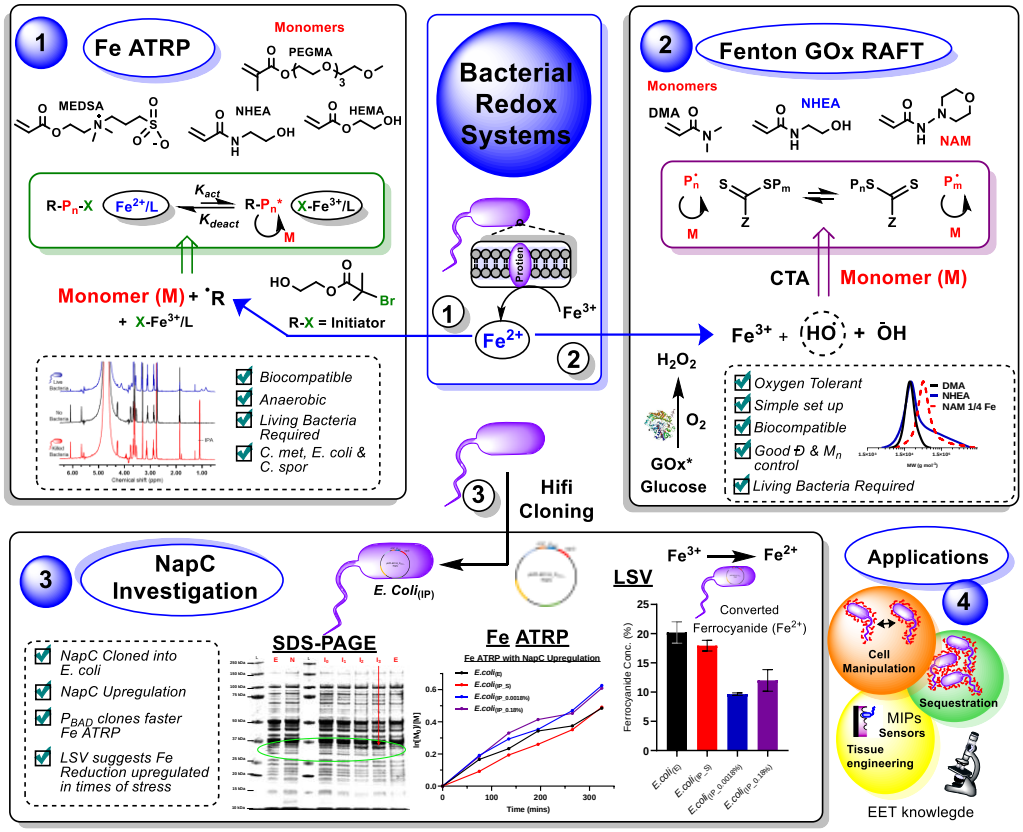

Figure 5. 1. Summary illustration of results from thesis chapters 2-4 exploring bacterial redox systems. Depiction of bacterial reduction of Fe^{3+} to Fe^{2+} and subsequent reaction with 1, Atom Transfer Radical Polymerisation (ATRP) components and 2; Fenton Glucose Oxidase (GOx) Reversible Addition Fragmentation chain-Transfer (RAFT) polymerisation components. 1; Fe ATRP initiated by bacteria with different monomers (Poly(ethylene glycol) methyl ether methacrylate (PEGMA), 2-(Methacryloyloxy) ethyl dimethyl-(3-sulfopropyl) ammonium hydroxide (MEDSA), *N*-Hydroxyethyl acrylamide (NHEA) and Hydroxyethyl methacrylate (HEMA)) and bacteria types (*Escherichia coli* (*E. coli*), *Cupriavidus metallidurans* (*C. met*), *Clostridium sporogenes* (*C. spor*)). ^{1}H NMRs are presented, indicating the necessity of live bacteria to polymer formation. 2; Fenton GOx RAFT initiated by bacteria with monomers (Dimethylacrylamide (DMA), N-acryloylmorpholine (NAM) and NHEA) and size exclusion chromatography (SEC) graphs of resulting polymers. 3; Hifi-Cloning of Vector with *napC* gene for NapC protein upregulation, using inducible promoter (P_{BAD}) transformed into *E. coli* cells to *E. coli*$_{(IP)}$. Sodium dodecyl sulphate – polyacrylamide gel electrophoresis (SDS-PAGE) showing upregulation of NapC protein. Fe ATRP results showing faster reaction kinetics for *E. coli*$_{(IP)}$ and linear sweep voltammetry (LSV) study summary. 4. Possible applications for the work presented in thesis.

Future Work

As discussed, growing synthetic polymers in the presence of bacteria might not only provide novel ECM mimics,[9, 10] but also bacterial-specific sequestrants and sensors.[11, 12] Whilst the aims set out at the beginning of this thesis have been achieved, several challenges and research ideas to purse in the future have arisen accordingly. Although the field could be used to greatly enhance the sustainability of catalysis by harnessing bacterial EET, scale up issues may arise in the industry and these would need to be specifically optimised to each system. Furthermore, deeper research into EET, different cells types and a broadening of materials development is required before applications can be fully developed. Both short term and long-term goals could be considered to aid the development of the field.

5.1.1 Short Term Considerations

5.1.1.1 Cell Type Investigations

In this thesis, three bacteria types were used to explore the redox capabilities of Fe reduction to initiate polymerisations. One might consider the next step in these investigations to be the exploration of different bacteria types and different cell types (Figure 5. 2 A). To conduct such experiments, it would be beneficial to perform and analyse Fe ATRP or FG-RAFT polymerisations using an array of bacteria to observe whether any differences might be correlated to Gram type, oxygen tolerance, or membrane structure (e.g., pili), which might shed light on

different EET mechanisms. Secondly, human cell types could be integrated into these systems as a means to tissue engineering, ELMs, or to increase the knowledge of EET in human systems, particularly as studies have shown that different cancer cell types to have different Fe reduction pathways and capabilities.[13] It might also be beneficial to explore the use of viruses in the polymerisation systems presented to shed light on how they exploit EET pathways or for MIP biosensors, towards infection prevention and virus detection.[14] By expanding the scope of cells that are compatible with these methods, more information could be gathered on EET mechanisms, and applications towards multiple targets might be fulfilled.

5.1.1.2 Materials Development

The second and third chapters of this thesis described novel polymerisation methods, Fe ATRP and FG-RAFT, respectively, which could be used to create homopolymers of different materials. To further develop these methods, polymerisations using monomers that could form block co-polymers,[15] functional polymers,[15, 16] or stimuli-responsive polymers,[17-19] could be pursued towards applications surrounding molecularly imprinted polymers (MIP)s, sensors and tissue engineering or cell manipulation.[10, 11] The fabrication of block co-polymers would enable the physical properties of the resulting polymers to be specifically tailored to control factors such as cell adhesion,[15] proliferation,[10] or sequestration,[20] by altering the monomer types and their ratios. Whilst functional monomers might provide a means to chemically attach

fluorescent dyes to directly image polymer formation around cells, [15, 16, 21] or provide crosslinking opportunities to create hydrogels towards ELMs.[10] Indeed, anthracene methacrylamide (AnMA) (Figure 5. 2, B) is not fluorescent in its monomer form, but upon polymerisation the acrylate bond becomes saturated and fluorescence is activated. This provides a means to image the polymer formed as recently demonstrated in the literature.[21] Furthermore stimuli-responsive polymers might be incorporated into the polymer structures to target visualisation of changes in temperature, pH, redox, or light.[22] Lastly, as demonstrated by Hawker *et al*,[16] it might be beneficial to perform the polymerisation methods described whilst employing cell-surface bound RAFT or ATRP initiators towards cell surface modification applications, which would prevent initiator loss observed with the Fe ATRP system and alleviate the poor M_n control of the resulting polymers.

5.1.1.3 Bacteria as Recycled 'Immortal' Catalysts

Both polymerisation methods described in Chapters 2 and 3 utilised Fe^{3+} activation by living bacterial redox metabolism. A fresh set of cultured bacteria for every polymerisation batch was used throughout. The extra steps required to culture these each time could be eliminated by re-using the same cultured bacteria as a recycled 'Immortal catalyst' (Figure 5. 2, C). To investigate this, a bacterial catalysed polymerisation would be carried out as described in chapters 2 and 3, and the bacteria removed via gentle centrifugation. This bacterial pellet could be re-suspended in PBS buffer and added to a new reaction, with the process

continuing over and over. The pellet could also be re-suspended and stored in LB for several hours to replenish nutrients to the culture if necessary. This would decrease the time and steps used in the reactions to culture and wash the bacteria, saving time and money, which is of great importance to industrial applications.

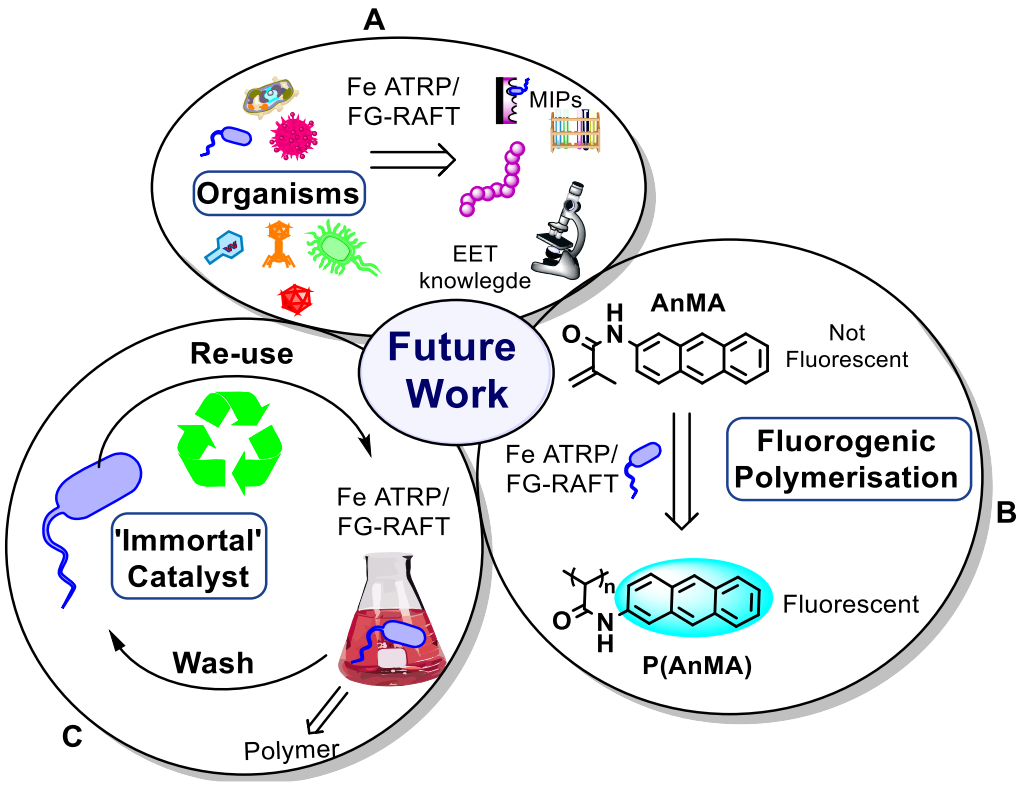

Figure 5. 2 Future work depicting A; the use of various organisms in (Iron) Fe Atom Transfer Radical Polymerisation (ATRP) and Fenton Glucose Oxidase (FG) Reversible Activation Fragmentation chain-Transfer (RAFT) polymerisations towards Molecularly Imprinted Polymers (MIP) applications and knowledge of extracellular electron transfer (EET) mechanisms in living cells, B; the application of non-fluorescent monomer (AnMA) in fluorogenic Fe ATRP and FG-RAFT polymerisations, resulting in fluorescent polymer P(AnMA) that could be used to visualise polymer upon UV irradiation, C; the re-use of bacteria in Fe ATRP and FG-RAFT polymerisations as an 'Immortal catalyst'.

5.1.2 Long Term Considerations

5.1.2.1 LPS Mimics from Glycopolymers

Lipopolysaccharides (LPS)s are a component of a Gram - negative bacterial cell wall that are recognised by the immune system using pattern recognition receptors such as Toll-like receptors (TLR)s.[23] TLRs on an immune cell bind to pathogenic LPS sites to initiate defensive responses such as apoptosis.[24] The polymerisation methods developed in Chapters 2 and 3 could be used to produce glycopolymers or LPS mimics on the surface of harmful cancer cells to signal an immune response which would otherwise be 'hidden.' The altered Fe metabolism of cancer cells[25] could be used to target LPS formation upon cancer cell detection commencing an immune response. Steps towards this long-term vision could be taken by firstly producing glycopolymers from an RDRP method, then advancing to cancer cell initiation. The initiators of the system would need to target the cancer cells exclusively so the main challenge would be to prevent healthy cells from being targeted. However, small steps towards this long-term goal may be beneficial to cancer research in broadening the knowledge of cancer redox mechanisms,[25] somewhat explored by Sherman *et al*.[13, 26]

5.1.2.2 Iron Oxide Nanoparticles for Tumour Suppression

Polymerisations in Chapter 3 were carried out using Iron (III) Chloride as a catalyst. To broaden the scope of this technique further, studies incorporating Iron oxide (FeO) nanoparticles, which are capable of the Fenton reaction, may be carried out. FeO nanoparticles are non-

toxic to cells and are much more stable than Fe^{3+} or Fe^{2+} ions, so they are less likely to be up taken by bacterial regulation proteins (i.e., siderophores). The use of FeO nanoparticles would sustain the concentration of Fe at the site of polymerisation to maintain a constant radical flux, and possibly aid the polymerisation control further. In addition, an even lower starting concentration of FeO would be needed compared to $FeCl_3$ which would i) be more cost effective and ii) further prevent uncontrolled radical flux. FeO nanoparticles have shown efficacy in preventing tumour growth,[27] and so this work could directly translate to mechanistic investigations or diagnostics for cancer research.

5.1.2.3 Cloning and Electrochemical methods

Experiments in chapter 4 revealed that the periplasmic protein NapC in *E. coli* could be upregulated by molecular cloning. Preliminary Linear sweep voltammetry (LSV) studies suggested that environmental stress could induce Fe reduction upregulation pathways. Future work could be carried out to confirm this hypothesis. Additionally, other C-Cyt proteins could be upregulated or removed (knocked out) by molecular cloning to further probe the EET mechanisms involved in metal reduction and broaden the knowledge of the rate limiting steps in EET. This research would help to improve knowledge in the field of bacterial reduction, particularly important to microbial fuel cells (MFC)s, biosensors, and the new field of hybrid bacterial-synthetic polymerisation methods.

In summary, a plethora of research paths have arisen from the research in this thesis, creating a novel platform for the investigation of

bacterial redox systems. In Chapter 2 a bacterial driven Fe ATRP method is presented which may be useful in anaerobic environments for high molecular weight polymer applications and may have potential in other areas with more optimisation studies. Chapter 3 reveals a versatile b-FG-RAFT technique with opportunities to expand the scope of biomedical applications including tumour suppression. The 4th chapter of this thesis provides an insight into C-Cyt mechanisms but also highlights the complexity of bacterial redox chemistry. Further research into these mechanisms may enable a better understanding of bacterial hybrid technologies such as MFCs and biosensors.

References

1. A. Reyhani, S. Allison‐Logan, H. Ranji‐Burachaloo, T. G. McKenzie, G. Bryant and G. G. Qiao, *J. Polym. Sci., Part A: Polym. Chem.*, 2019, **57**, 1922-1930.
2. M. Hussain, R. A. Naqvi, N. Abbas, S. M. Khan, S. Nawaz, A. Hussain, N. Zahra and M. W. Khalid, *Polymers*, 2020, **12**, 323.
3. M. R. Bennett, P. Gurnani, P. J. Hill, C. Alexander and F. J. Rawson, *Angew. Chem. Int. Ed. Engl.*, 2020, **59**, 4750-4755.
4. T. Yokozawa and Y. Ohta, *Chem Rev*, 2016, **116**, 1950-1968.
5. A. Poater, E. Pump, S. V. C. Vummaleti and L. Cavallo, *Chem. Phys. Lett.*, 2014, **610-611**, 29-32.
6. S. Ramanavicius and A. Ramanavicius, *Nanomaterials (Basel)*, 2021, **11**, 371.
7. Y. M. Zhao, P. C. Zhang, C. Xu, X. Y. Zhou, L. M. Liao, P. J. Wei, E. Liu, H. Chen, Q. He and J. G. Liu, *ACS Appl Mater Interfaces*, 2020, **12**, 17334-17342.
8. S. Kato, *Microbes Environ*, 2015, **30**, 133-139.
9. Y. Zhao, X. Zhang, Y. Wang, Z. Wu, J. An, Z. Lu, L. Mei and C. Li, *Carbohydr. Polym.*, 2014, **105**, 63-69.
10. A. M. Duraj-Thatte, N. D. Courchesne, P. Praveschotinunt, J. Rutledge, Y. Lee, J. M. Karp and N. S. Joshi, *Adv. Mater.*, 2019, **31**, e1901826.
11. S. Piletsky, F. Canfarotta, A. Poma, A. M. Bossi and S. Piletsky, *Trends Biotechnol.*, 2020, **38**, 368-387.
12. S. A. Zaidi, *Crit. Rev. Anal. Chem.*, 2020, DOI: 10.1080/10408347.2020.1755822, 1-10.
13. H. G. Sherman, C. Jovanovic, A. Abuawad, D. H. Kim, H. Collins, J. E. Dixon, R. Cavanagh, R. Markus, S. Stolnik and F. J. Rawson, *Biochim Biophys Acta Bioenerg*, 2019, **1860**, 628-639.
14. M. Dan, A. L. Wang and C. C. Wang, *Mol. Microbiol.*, 2000, **36**, 447-456.
15. E. P. Magennis, F. Fernandez-Trillo, C. Sui, S. G. Spain, D. J. Bradshaw, D. Churchley, G. Mantovani, K. Winzer and C. Alexander, *Nat Mater*, 2014, **13**, 748-755.
16. J. Niu, D. J. Lunn, A. Pusuluri, J. I. Yoo, M. A. O'Malley, S. Mitragotri, H. T. Soh and C. J. Hawker, *Nat Chem*, 2017, **9**, 537-545.
17. C. G. Palivan, R. Goers, A. Najer, X. Zhang, A. Car and W. Meier, *Chem. Soc. Rev.*, 2016, **45**, 377-411.
18. A. Bordat, T. Boissenot, J. Nicolas and N. Tsapis, *Adv Drug Deliv Rev*, 2019, **138**, 167-192.
19. M. P. Robin and R. K. O'Reilly, *Chemical Science*, 2014, **5**, 2717-2723.
20. L. T. Lui, X. Xue, C. Sui, A. Brown, D. I. Pritchard, N. Halliday, K. Winzer, S. M. Howdle, F. Fernandez-Trillo, N. Krasnogor and C. Alexander, *Nat Chem*, 2013, **5**, 1058-1065.
21. M. D. Nothling, H. Cao, T. G. McKenzie, D. M. Hocking, R. A. Strugnell and G. G. Qiao, *J. Am. Chem. Soc.*, 2020, DOI: 10.1021/jacs.0c10673.
22. T. M. Reineke, *ACS Macro Letters*, 2016, **5**, 14-18.

23. S. Fried, S. Tosun, G. Troost, S. Keil, K. S. Zaenker and T. Dittmar, *PLoS One*, 2016, **11**, e0148438.
24. M. Triantafilou and K. Triantafilou, *J. Endotoxin Res.*, 2005, **11**, 5-11.
25. R. A. M. Brown, K. L. Richardson, T. D. Kabir, D. Trinder, R. Ganss and P. J. Leedman, *Front Oncol*, 2020, **10**, 476.
26. H. G. Sherman, J. M. Hicks, A. Jain, J. J. Titman, C. Alexander, S. Stolnik and F. J. Rawson, *Chembiochem*, 2019, **20**, 1008-1013.
27. S. Zanganeh, G. Hutter, R. Spitler, O. Lenkov, M. Mahmoudi, A. Shaw, J. S. Pajarinen, H. Nejadnik, S. Goodman, M. Moseley, L. M. Coussens and H. E. Daldrup-Link, *Nat Nanotechnol*, 2016, **11**, 986-994.